DESIGN AND CONTROL STUDIES ON THE FLUID CATALYTIC CRACKING PROCESS

Thesis by

Iftikhar Huq

In Partial Fulfillment of the Requirements

for the Degree of

Doctor of Philosophy

California Institute of Technology

Pasadena, California

1998

(Submitted October 13, 1997)

Acknowledgements

I am truly indebted to the Caltech community for creating an unparalleled and unique environment which fosters not only academic excellence, but also personal growth. I am honored to have been a part of this environment, and hope that in some way I have made some contribution to this legacy.

Two people have influenced this thesis work greatly. First and foremost, my thesis advisor - Manfred Morari. Manfred's continuously critical, prodding and skeptical approach towards science has been a source of inspiration and encouragement to reach for heights that would otherwise have seemed impossible to attain. Secondly, the many interesting discussions related to the Fluid Catalytic Cracking operation with Ronald C. Sorensen of the Chevron Research and Technology Company were critical in formulating and analyzing the many aspects of this fascinating process. Thanks Ron for your unique and practical perspective!

The long years of Graduate school have been made a lot more enjoyable because of the friendship and camaraderie of many talented and unique individuals with whom I have had the pleasure to interact with, on both a technical and personal level. In particular, I would like to thank all the past and present students of the Morari group, and specially Mayuresh Kothare, Simone Oliveria, Carl Rhodes and Matthew Tyler. The time in Zurich was significantly more enjoyable thanks to you. Special thanks also go out to Richard Braatz and Mayuresh for the many interesting and informative technical discussions that we have had over the years.

I will forever be grateful to my parents for instilling in me those traits, without which I would not be where I am today. Thank you Mom and Dad! I am also very lucky to have a wonderful and fully supportive brother and sister-in-law. The many weekly phone conversations we have had over the years has been a bottomless well for mental rejuvenation and focus. Although my family is scattered over the globe, we are still, and will always be a single strong unit in spirit. Thank you!

Finally, no note of thanks can be complete without acknowledging the enormous support, encouragement and friendship that I have received from Lisa, my soulmate and trusted companion. You have always been there, holding me up in times of need, gently encouraging me along and always believing in me. Thank you!

Iftikhar

Abstract

Fluid Catalytic Cracking (FCC) units are widely used in the oil refining industry to crack low value hydrocarbons into a range of higher value hydrocarbons including gasoline. Because of its feed processing flexibility, the FCC process is considered a primary conversion unit in an integrated refinery and optimal FCC operation can have a significant impact on the refinery profitability. Because of its important role in the refinery, the FCC process has recently attracted renewed interest both from academia and industry, with the main emphasis on better understanding and operating the process.

In general, several possible alternatives can usually be postulated or envisioned to realize operational improvements, and the critical task is then to rank order these alternatives. Rank ordering the available alternatives requires the utilization of suitable:

1. process models describing each alternative,

2. tools to quantitatively assess the operational performance achievable with each alternative. "Operational performance" here refers to the quality of closed loop process response.

The different alternatives have often been analyzed and compared through extensive simulations. However, because of stringent environmental and economic requirements, most industrial plants, including the FCC process have evolved into highly complex and integrated processes and ranking through simulation might be infeasible. In ranking design alternatives through simulation, two crucial factors must be considered if the conclusions drawn from such studies are to be reasonably reliable:

- Detailed case studies need to be conducted for all the alternatives. These case studies typically require considering the effect of a wide range of disturbances, inputs, operating conditions, model structures and parameters, control structures and parameters. It might be necessary to examine many hundreds if not thousands of possible alternatives. Moreover, the effect of many other aspects of practical operation such as plant/model mismatch, process constraints, sensor/actuator failures, etc. on the operational performance must also be considered for each case, and makes the assessment significantly more involved.

- While qualitative "good/bad" indicators might have been sufficient in the past, it is becoming more important to quantitatively rank order the available alternatives in todays highly competitive environment. Indeed, choosing a "slightly better" alternative over a "good" alternative can have a significant impact on the sustained profitability of the process.

Because of the large number of possible cases that must be considered, contradictory conclusions can often be drawn when using such an approach to rank the available alternatives. Such a simulation approach is therefore infeasible except possibly for the simplest of cases. This suggests the utilization of more efficient screening tools to effectively assess the many design alternatives possible for improved process operation while accounting for the practical considerations just discussed. With respect to the requirements (1) and (2) above for ranking the possible alternatives, we note that:

1. *FCC models:* The renewed interest in improved FCC operation is partially reflected by the recent publication in the open literature of two first principles models claiming to describe the essential features of the FCC process dynamics (Arbel, Huang, Rinard, Shinnar and Sapre 1995, McFarlane, Reineman, Bartee and Georgakis 1993) .

2. *Tools for operational performance assessment:* The structured singular value (SSV) framework introduced by Doyle (1982) provides a quantitative measure of the achievable operational performance, explicitly accounts for plant/model mismatch, and also permits the approximate incorporation of many of the practical requirements indicated above into the analysis.

Utilizing the two first principles FCC models and the structured singular value framework, several aspects of the design and control of FCC processes have been addressed in this thesis, with special emphasis on quantitatively ranking possible design/control options from an operational performance improvement viewpoint:

1. Model IV FCC units differ from other cracking units in that model IV FCC units do not have slide valves in the catalyst circulation lines to enable direct control of catalyst circulation rate through the unit. Reducing fluctuations in catalyst circulation rate is found to significantly improve closed loop performance of this FCC unit. Based on this process insight: (1) an operational modification: operating the regenerator with the catalyst overflow weir always flooded, and (2) a design modification: installing slide valves in the catalyst circulation U-tubes are studied and shown to reduce catalyst flow fluctuations and improve the operational performance of the FCC unit. It is interesting to note that essentially all new FCC units and revamped older FCC units typically include both the above two modifications. To reflect this current FCC operation it is assumed for all the subsequent analysis in this thesis that the above two modifications are already incorporated into the FCC design.

2. A quantitative rank ordering of possible control structures for FCC operation in both partial combustion (PC) mode and complete combustion (CC) mode operation is undertaken. It is argued that intentional transitions between the PC and CC modes is rare. For FCC units operated within design specifications, 2×2 control structures are found to be sufficient for effective regulatory control. In particular, it is found that high coking feeds cannot be processed in CC mode operation as the safe upper limit on regenerator temperature can be

violated. For PC mode regulation, riser temperature (T_r) and regenerator dense bed temperature (T_{rgn}) - $[T_r, T_{rgn}]$ are the most suitable choice for controlled variables. For CC mode regulation, $[T_r, C_{O_2,fg}]$ are the most suitable choice for controlled variables, where $C_{O_2,fg}$ is the flue gas O_2 molar concentration. If higher coking feeds are to be processed, the FCC would need to be refitted with additional process units, as discussed in Point 4 below. For both PC and CC modes, using feed temperature (T_{feed}) and combustion air rate (F_{air}) as manipulated variables is found to provide operational performance levels comparable to those achieved with more conventional control structures typically used in industry (using catalyst circulation rate (F_{cat}) and combustion air rate). That feed temperature can be an effective manipulated variable can have significant implications for the improved operation of older FCCs (*e.g.* the Model IV) where catalyst circulation rate cannot be directly manipulated.

3. Decentralized regulatory control of the FCC unit operating in PC mode is examined in detail. Decentralized PI controllers are considered, as they are most often used in the industrial setting. It is found that (1) Decentralized PI controllers can provide satisfactory regulation over the normal FCC operating range. (2) A common regulatory control strategy for PC mode operation is to use decentralized PI controllers for the pairing T_r/F_{cat} and T_{rgn}/F_{air} (notation in Point 2). It is shown that "tightening" the two PI controllers in fact reduces the process interactions and improves operational performance. This is counterintuitive - typically, detuning the controllers is expected to reduce process interactions and improve performance. (3) Certain FCC operating points are unstable. In the absence of control action, the FCC process would either drift to a stable operating point at a higher regenerator temperature or wind down to the cold state (negligible regenerator combustion and reactor cracking). It is shown that reasonable transitions to unstable operating points can be effectively handled with an appropriately tuned decentralized PI controller. (4) A theoretical development that provides insight into possible changes in the sign of the steady–state and infinite frequency relative gain array (RGA) elements is also presented. It is found to be related to the non–minimal phase behavior of one or more of the following (a) the overall plant, (b) the individual loop transfer functions, (c) the remaining system if some controlled variable and the associated manipulated variable is removed. Stable plants for which pairing for performance can correspond to negative steady–state RGA pairings are thus identified.

4. There is a growing need in the oil refining industry to process higher coking feeds in FCC units. However, FCC units operated in the CC mode might not be able to process sufficiently high coking feeds (as discussed in Point 2 above), and would have to be refitted to accommodate this greater feed processing flexibility. The most significant operating limitation is found to be the upper limit on regenerator temperature. The two possible refitting options considered here to alleviate the impact of this constraint are: (1) converting to partial combustion mode (PC mode) operation by installing a CO boiler and (2) extending com-

plete combustion mode (CCE mode) operation by installing a catalyst cooler. The main objective is to compare the steady–state and dynamic characteristics of these two refitting options. From a steady state viewpoint, it is found that installing the catalyst cooler has a distinct advantage over installing the *CO* boiler when processing high coking feeds - because the regenerated catalyst is always clean burned. In particular, the product yields as well as overall conversions are typically higher. A comparison of dynamic characteristics suggests that while a simple decentralized control strategy provides satisfactory performance over a wide operating regime in PC mode, a more sophisticated control strategy might be required to achieve tight control over a comparable operating range in CCE mode with the catalyst cooler.

Contents

List of Figures

List of Tables

Chapter 1 Introduction

In the present highly competitive global environment, there is an ever increasing customer expectation for consistent high quality products. At the same time, safety and environmental regulatory agencies have been imposing stricter safety limits and tighter restrictions on emission of pollutants. In order to meet these numerous stringent limits on product specifications and plant operations, while maintaining a profitable enterprise through reduced energy and raw material costs, industrial processes over the last two decades have been forced to evolve into highly integrated and complex processes. In general, several possible alternatives can usually be postulated or envisioned to realize operational improvements, and the critical task is then to rank order these alternatives. However, even when design and/or operational changes are implemented to enhance process performance and operation, it might be difficult to assess the level of performance improvement realized. Carrying out such an assessment based on only approximate process information and knowledge is even more difficult. Several design and process operation issues related to the Fluid Catalytic Cracking (FCC) process, which is widely used in the oil refining industry to upgrade the value of low value hydrocarbons will be discussed in detail in this thesis. The primary focus is on better understanding the FCC operation and investigating alternatives for improving the FCC operability and controllability.

1.1 Motivation

In considering improved process operation, several possible alternatives can usually be postulated or envisioned to realize operational improvements, and the critical task is then to rank order these alternatives. Rank ordering the available alternatives requires the utilization of suitable:

1. process models describing each alternative,

2. tools to assess the operational performance achievable with each alternative. "Operational performance" here refers to the quality of closed loop process response.

The different alternatives have often been analyzed and compared through extensive simulations. However, because of stringent environmental and economic requirements, most industrial plants, including the FCC process have evolved into highly complex and integrated processes. In ranking design alternatives through simulation, two crucial factors must be considered if the conclusions drawn from such studies are to be reasonably reliable:

- Detailed case studies need to be conducted for all the alternatives. These case studies typically require considering the effect of a wide range of disturbances, inputs, operating conditions, model structures and parameters, control structures and parameters. It might be necessary to examine many hundreds if not thousands of possible alternatives. Moreover, the effect of many other aspects of practical operation such as plant/model mismatch, process constraints, sensor/actuator failures, etc. must also be considered for each case, and makes the assessment significantly more involved.

- While qualitative "good/bad" indicators might have been sufficient in the past, it is becoming more important to quantitatively rank order the available alternatives in todays highly competitive environment. Indeed, choosing a "slightly better" alternative over a "good" alternative can have a significant impact on the sustained profitability of the process.

Because of the large number of possible cases that must be considered, contradictory conclusions can often be drawn when using such an approach to rank the available alternatives. Such a simulation approach is therefore infeasible except possibly for the simplest of cases. This suggests the utilization of more efficient screening tools to effectively assess the many design alternatives possible for improved FCC operation while accounting for the practical considerations just discussed. With respect to the requirements (1) and (2) above for ranking the possible alternatives, we note that:

1. *FCC models:* The renewed interest in improved FCC operation is partially reflected by the recent publication in the open literature of two first principles models claiming to describe the essential features of the FCC process (Arbel et al. 1995, McFarlane et al. 1993) .

2. *Tools for operational performance assessment:* The structured singular value (SSV) framework introduced by Doyle (1982) provides a quantitative measure of the achievable operational performance, explicitly accounts for plant/model mismatch, and also permits the approximate incorporation of many of the practical requirements indicated above into the analysis.

Each of the above two issues will be discussed in some detail next.

1.1.1 FCC Models

Industrial processes are often characterized by

- large dimensionality,
- non–linearity,
- strong interactions among process variables,
- uncharacterized and often unknown process disturbances,
- limited process measurements. Most process variables besides pressure, temperature and flow rates are typically not easily measurable.

Thus, in most cases, the underlying physics of the process are not fully understood. The effort to understand the steady–state and dynamic characteristics of the many industrial processes currently in operation is an ongoing long term effort, drawing on both on–site, hands–on experience and increasingly on process models of various levels of complexity. Furthermore, it has been recognized for some time that for many integrated plants, the optimal operation of certain specific subprocesses is particularly crucial for the profitability and success of the overall plant.

In the oil refinery, one such critical process is the Fluid Catalytic Cracking (FCC) unit which catalytically cracks a wide range of low value hydrocarbons into a range of more valuable products including gasoline. Because of its impact on overall refinery economics, the FCC unit is often one of the first units considered for the application of advanced control and optimization strategies, and various aspects of the modeling, optimization and control of this important process has attracted renewed interest both in industry and academia in the recent past (McFarlane et al. 1993). In particular, within the industrial setting, Chevron Oil Company is one of several that has successfully implemented advanced control strategies (for example Dynamic Matrix Control (DMC)) to attempt optimal operation and control of some of their FCC units (*e.g.* a Model IV FCC unit located at El Segundo, California) (Sorensen 1993). Secondly, from a more fundamental operations viewpoint, there have been two recent non–confidential collaborations between industry and academia that resulted in detailed first principles models that are purported to describe the essential features of the FCC operation. These are the Amoco/Lehigh effort (McFarlane et al. 1993), and the Mobil/CCNY effort (Arbel et al. 1995). These two models are discussed in detail in Chapter 2, Section 2.7 and Section 2.8 respectively. Therefore, while efforts to study alternatives for improved FCC operation might have been limited by the lack of realistic process models in the past, the recent availability of the above two first principles models permits renewed efforts to analyze alternatives for improved FCC process operation. The major emphasis of this thesis is to understand various design and operational issues involved in the optimal operation of the FCC process, including:

- investigating design features of the older Model IV FCC units that limit the achievable performance of that unit and analyzing physically motivated design and operational changes that can be expected to improve the process operation.
- investigating different control structures and control strategies for improved regulatory control and operation of the FCC process.
- investigating the impact of higher coking feeds processing on the current FCC

units. Heavier feed processing is becoming an increasingly more economically significant operational requirement for many refineries.

1.1.2 Tools for Operational Performance Assessment

In general, several possible alternatives can usually be postulated or envisioned to realize operational improvements, and the critical task is then to rank order these alternatives. Several practically relevant issues must be addressed for successfully ranking these alternatives, including:

- *Practical operational considerations:* Most modern strategies for improved operation are based on some model of the process. Such models can range from "black box" (low effort, high uncertainty) type models to models based on rigorous mathematical and physical principles (significant effort, lower uncertainty). However, regardless of the model used for design, optimization and analysis, plant/model mismatch will always be present because the available model essentially never represents the true physical system exactly. For low–order, linear models that are often used for the control system design, this "plant/model mismatch" or "model uncertainty" can be quite significant. The consequences of process constraints, sensor/actuator failures, etc. must also be considered.

- *Process performance quantification:* In order to evaluate whether process design or process control changes are required to improve process performance, one must quantify the current performance level of the process, and additionally quantify the best performance possible. These are crucial steps, the determination of which can be made particularly difficult by the ever present plant/model mismatch just discussed in the previous step. While qualitative "good/bad" indicators might have been sufficient in the past, it is becoming more important to quantitatively rank order the available alternatives in todays highly competitive environment. Indeed, choosing a "slightly better" alternative over a "good" alternative can have a significant impact on the sustained profitability of the process.

The Past:

In the past, the different alternatives were often analyzed and compared through extensive simulation. However, because of stringent environmental and economic requirements, most industrial plants, including the FCC process have evolved into highly complex and integrated processes and the number of simulation case studies that must be carried out to arrive at a reliable ranking is typically prohibitive. Ranking design alternatives through simulation involving detailed case studies, which typically require considering the effect of a wide range of disturbances, inputs, operating conditions, model structures and parameters, control structures and parameters, can require examining many hundreds if not thousands of possible alternatives. Moreover, each of these case studies will have to address at least approximately the practical operational considerations mentioned above if the conclusions drawn from such studies are to be reasonably reliable. Contradictory conclusions may arise when such aspects are considered in ranking the available alternatives.

Thus the simulation approach is generally infeasible except possibly for the simplest of cases. This suggests the utilization of more efficient screening tools to effectively assess the many design alternatives possible for improved FCC operation while accounting for the practical operational considerations just discussed, and more efficient tools need to be utilized for ranking design/operational alternatives.

The Present: - and Future ?

The structured singular value (SSV) framework introduced by Doyle (1982) provides a quantitative measure of the achievable operational performance, while (i) explicitly accounting for plant/model mismatch, (ii) partially or completely incorporating the practical operational requirements indicated above into the analysis. The SSV framework is used to throughout this work. In the SSV framework, the plant/model mismatch is described mathematically as a set of norm bounded perturbations to the nominal model. These perturbations capture either partially or entirely:

- the possible discrepancies between the nominal model and the real system,

- the effect of process constraints
- the effect of actuator/sensor failures
- the effect of process dead times
- etc.

In the industrial process community, the SSV framework has already been successfully used for performance assessment and dynamic analysis of several aspects of distillation column operation in the research groups of Professor Skogestad (Norwegian University of Science and Technology) and Professor Morari (Caltech, Swiss Federal Institute of Technology). The theoretical basis for the SSV framework is now well established, and software is available for its efficient utilization. The SSV framework is therefore a powerful, readily usable tool for *quantitative* and practical performance assessment.

1.1.3 Motivation - Summary

In summary, it is fair to say that despite the renewed emphasis on understanding and improving FCC operation, there appears to be little effort at utilizing the theoretical and computational tools from the area of robust control for efficiently ranking the many alternatives that can be postulated for improved operation. Moreover, these tools allow for an efficient screening of these alternatives without sacrificing the practically relevant issues. Utilizing the two first principles FCC models and the structured singular value framework, several aspects of the design and control of FCC processes have been addressed in this thesis, with special emphasis on quantitatively ranking possible design/control options from an operational performance improvement viewpoint.

1.2 Thesis Outline

This thesis is organized as follows:

1.2.1 The Fluid Catalytic Cracking Process

In Chapter 2 an overview of the FCC process is provided, with special emphasis on understanding the dynamic process characteristics.

1.2.2 The Significance of Control Studies during Process Design

In some operations, the achieved operational performance level might be less than satisfactory. Specifically, the poor performance could be due to one (or both) of the following two causes:

1. control system deficiencies
2. plant design deficiencies

Control system deficiencies might be solved by an array of methods including:

- better tuning the available controllers,
- changing the manipulated variables and controlled variables,
- applying different control strategies.

However, in some operations it is the plant design deficiencies that make overall process control difficult - regardless of the controllers used. Such plants are said to possess poor controllability or operability (Skogestad and Postlethwaite 1996). Identifying those physical process attributes that limit the realizable performance, and redesigning (or changing the operating characteristics) of the plant to improve operability is often termed debottlenecking.

In general it is difficult to determine which one of the above two cases is the primary cause of the poor plant performance, and this assessment is made even more difficult because of the inherent plant/model mismatch and the other practical operating considerations discussed in Section 1.1.2.

It has been known for some time that the Model IV FCC unit is difficult to control (McFarlane et al. 1993, Sorensen 1993), and the reported performance has been less than satisfactory (poor controllability). However, a thorough understanding and analysis of this observed inferior performance does not seem to have been reported in the open literature. In Chapter 3, the SSV framework as well as several other controllability indicators are used to quantify the design deficiencies of the Model IV FCC unit, and rank order different physically motivated design and operational changes to improve the process controllability and operability.

1.2.3 Control Structure Selection for Optimal Regulatory Control of the FCC Process

As mentioned in Section 1.1, the incorrect selection of controlled variables and manipulated variables can lead to control structures that limit the achievable operational performance. It is therefore critical to rank order control structures from a performance and operational viewpoint. The recent work by Arbel, Rinard and Shinnar (1996) presents some qualitative criteria for control structure selection including:

- *Modelability:* Select inputs and outputs for which the transfer matrix can be relatively easily determined.

- *Dominance:* Select controlled variables that have a significant effect on several other process variables. For example, in the FCC unit, the riser temperature has a significant impact on all the cracking reactions, and should therefore be selected as a controlled variable.

- *Sufficiency:* Select control structures that can satisfy a significant fraction of the required operational performance objectives.

The critical deficiencies of such qualitative criteria include:

- despite the qualitative nature of the criteria, detailed process understanding and a process model is required for effective utilization of the above criteria.

At best, the criteria above allow for a preliminary screening of possible control structure selection for engineers intimately familiar with the specific process under consideration. Moreover, with the detailed process model, a more quantitative ranking can be undertaken.

- the inherently qualitative nature of such criteria does not permit rank ordering of control structures that might perform comparably, yet such small operational differences might have significant effects on the process profitability.

Another recent work to rank order control structures for the FCC process was the work of Hovd and Skogestad (1993), and is one of the first to address the control structure selection problem for the FCC in a quantitative manner. Hovd and Skogestad (1993) base their work on the FCC dynamic model of Kurihara (1967). However, the Kurihara model has several structural assumptions which are no longer representative of the operating conditions and catalyst flow mechanisms currently prevalent in FCC operation. Some of the parameters of the Kurihara model have been updated by ?, and these updated parameters were used by Hovd and Skogestad (1993).

Neither of the two approaches above accounts for plant/model mismatch, and a more detailed, yet systematic approach is required. On the other hand, the SSV framework explicitly incorporates plant/model mismatch and allows for a quantitative assessment of the achievable performance of different control structures, and therefore allows ranking of these control structures for effective process control.

In Chapter 4 the problem of determining the best control structures for FCC regulatory control is formulated, and analyzed in detail. An in depth comparison with the recent work of Arbel et al. (1996) and Hovd and Skogestad (1993) is also conducted. The operability and controllability aspects of some control strategies that are commonly used are analyzed.

1.2.4 Decentralized Regulatory Control of the FCC Process in Partial Combustion Mode

Decentralized control is the most commonly used strategy in industry. Several control structures and associated pairings have been used so frequently that they are now referred to as the "conventional pairings" for FCC regulatory control. However, there is no guarantee that these control structures are optimal in any sense, and a thorough analysis of the process characteristics under decentralized control needs to be undertaken.

In Chapter 5, decentralized control of the FCC unit is examined. Several FCC operating phenomena reported in the literature are explained through the analysis presented.

1.2.5 Options for Heavier Feed Processing in FCC Units

Because of economic considerations, there is a growing need in the oil refining industry to process higher coking feeds in the available FCC units. However, FCC units operated in the complete combustion mode might not be able to process sufficiently high coking feeds, and design modifications could be necessary to permit greater feed processing flexibility. Some design alternatives have been briefly discussed recently in Upson, Hemler and Lomas (1993) but no analysis or relative comparison is provided.

In Chapter 6, two possible refitting options to alleviate the impact of the constraint on regenerator temperature are considered: (1) converting to partial combustion mode operation by installing a CO boiler and (2) extending complete combustion mode operation by installing a catalyst cooler. The main objective is to compare the steady–state and dynamic characteristics of these two refitting options.

1.2.6 Conclusions

In Chapter 7, the most significant contributions of this thesis are summarized.

Chapter 2 The Fluid Catalytic Cracking Process

Summary

The Fluid Catalytic Cracking (FCC) process is described. Particular emphasis is placed on gaining insights into the steady–state and dynamic characteristics of the FCC process through the analysis of several different mathematical models available to describe the FCC operations.

2.1 Background

The Fluid Catalytic Cracking (FCC) process is considered the primary conversion unit in an integrated refinery. For many refiners optimal steady–state and dynamic operation of their FCC units is the key to profitability and success in the currently competitive environment. There are approximately four hundred (400) FCC units operating worldwide, with a total processing capacity of over twelve million barrels per day (12 MMbbl/day). Several oil companies, such as Exxon, Shell, and TOTAL have their own FCC designs. However, most of the current operating units have been designed and/or revamped by three engineering companies: Universal Oil Products (UOP), M. W. Kellogg and Stone & Weber. Although the mechanical configuration of the FCC unit may be arranged differently, they all share a common objective: To upgrade low–value feedstocks into more valuable products.

2.2 Process Description

An universal characteristic of the FCCU is the continuous circulation of catalyst between the two integral parts of the FCC process - the reactor section and the regenerator section. A short description of the catalyst flow cycle is given next.

Fresh feed is contacted with hot catalyst at the base of the riser (Figure 2.1) and travels rapidly up the riser where the cracking reactions occur. The desirable products of reaction are gaseous hydrocarbons which are separated from the catalyst particles and passed to a fractionator and subsequently to separation units for recovery and purification. An undesirable byproduct of cracking is coke which is deposited on the catalyst particles, reducing their activity significantly. Catalyst coated with coke is called *spent catalyst* and is transported to the regenerator section where the coke is burned off in a stream of air thereby restoring catalytic activity and raising catalyst temperature. The regenerated catalyst is transported back to the riser base where it is contacted with more fresh feed. The regenerated catalyst at the elevated temperature provides the enthalpy required to vaporize the fresh feed as well as the energy required

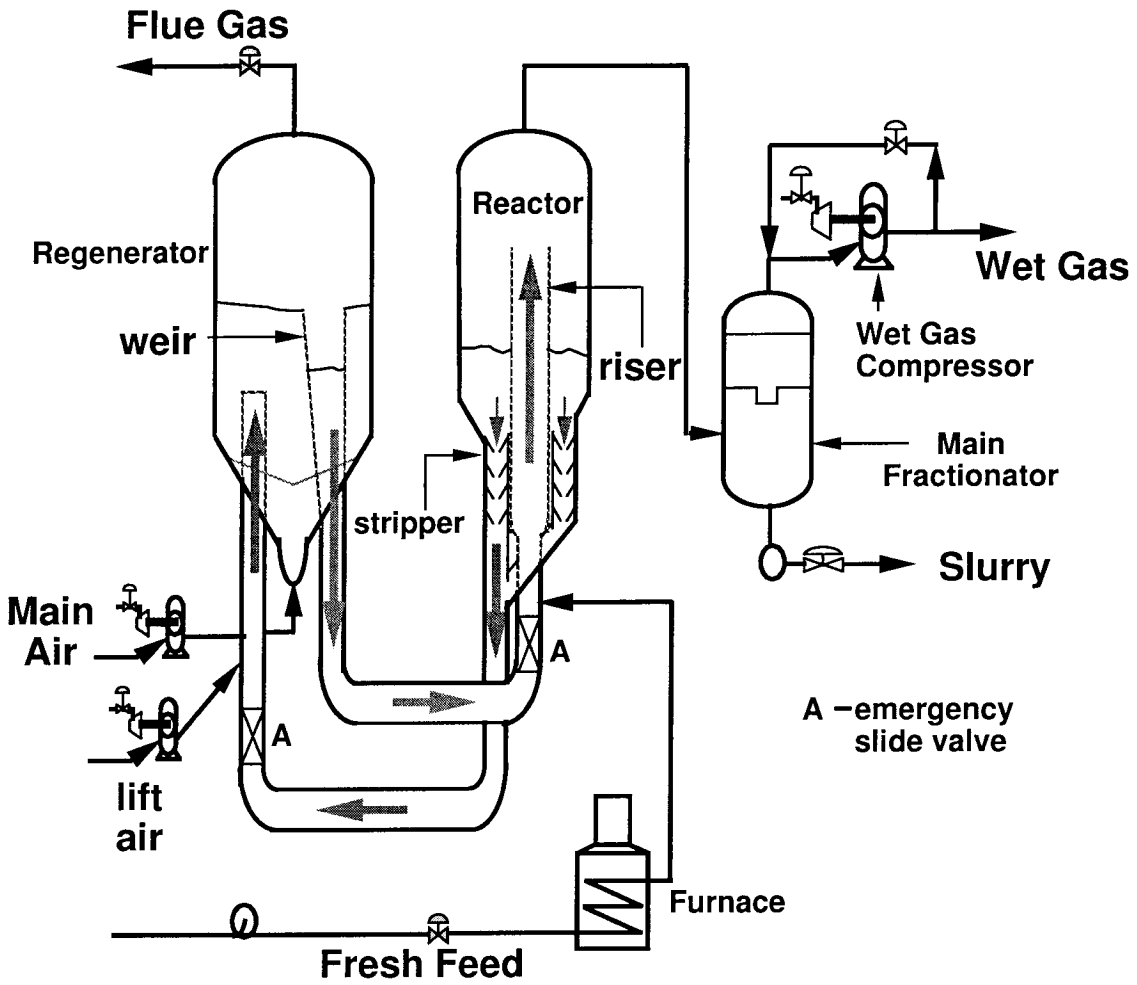

Figure 2.1: Model IV FCCU schematic

for the endothermic cracking reaction.

An important component of the FCCU is a *slide valve* which permits the direct control of catalyst flow rate from the regenerator to the reactor and back from the reactor to the regenerator (Figure 2.2). However, a unique feature of the older Model IV FCCU depicted in Figure 2.1 is the absence of slide valves in the catalyst circulation lines. The ability to directly affect the catalyst circulation rate between the regenerator and reactor section is therefore limited. These slide valves have been reintroduced in subsequent FCCU designs and a typical schematic is shown in Figure 2.2. The absence of slide valves can significantly affect the process controllability. This issue is discussed in detail in Chapter 3.

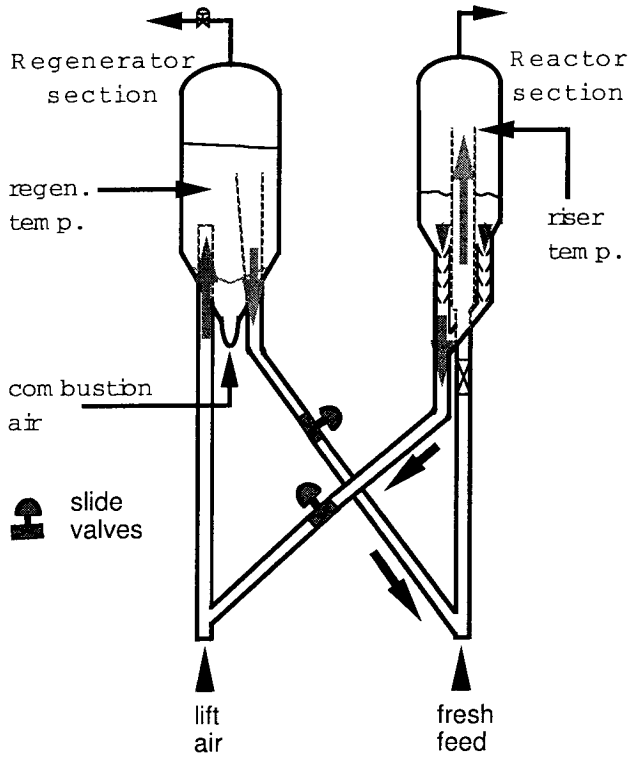

Figure 2.2: FCCU schematic. Slide valves installed.

2.3 Modes of FCCU Operation

Catalyst regeneration in the regenerator proceeds through two combustion reactions:

$$C + O_2 \rightarrow CO_2 \qquad \Delta H_{comb} = 169.3 KJ/mol \tag{2.1}$$

$$C + \frac{1}{2}O_2 \rightarrow CO \qquad \Delta H_{comb} = 47.5 KJ/mol \tag{2.2}$$

The coke on the spent catalyst will be combusted to both CO and CO_2 in the regenerator. However, the relative quantities of CO and CO_2 will depend strongly on the actual regenerator conditions - in particular the regenerator temperature and the available oxygen concentration. If significant quantities of both CO and CO_2 are produced, the regenerator is characterized as operating in *partial combustion mode* **(PC mode)**, because the coke is only partially combusted to CO_2. However, if only

trace amounts of CO (ppm levels) is present, then the regenerator is characterized as operating in *complete combustion mode* **(CC mode)**, because the coke is essentially completely combusted to CO_2. This apparently minor difference in the regenerator operating conditions has several far reaching consequences including:

- different dynamic characteristics
- different product yield levels

The issue of operating in different combustion modes will be examined in detail in Chapter 4 and Chapter 6.

Some operational characteristics of each of these two modes include:

- A wider range of feed qualities can typically be processed in PC mode operation. This is because the coke is burned partially to CO (ΔH_{comb}= 47.5 KJ/mol) and partially to CO_2 (ΔH_{comb} = 169.3 KJ/mol). The total enthalpy release is therefore lower than in CC mode but enough to maintain acceptable regenerator temperatures at steady-state.
- In PC mode operation, the catalyst is not typically clean burned as the regeneration conditions are not severe enough to ensure essentially complete coke combustion.
- In PC mode operation, there is an appreciable quantity of CO in the disengaging zone and the flue gas line. If there is sufficient O_2 and CO in the disengaging zone between the top of the bed and the cyclones in the regenerator, significant conversion of CO to CO_2 will occur with evolution of heat. This process is called *afterburn*. It is therefore important to monitor the temperatures of the cyclone banks as well as downstream piping so that the metallurgic limit is not exceeded.
- In the CC mode operation, essentially all the CO formed in the dense bed is converted to CO_2 within the dense bed owing to excess air (oxygen) flow through the system. There is typically negligible afterburn in the disengaging section

of the regenerator and therefore little possibility of the cyclone temperatures exceeding the metallurgic limits. Cyclone temperature is sometimes controlled, and the advantages and disadvantages of this operating strategy is discussed in detail in Chapter 4.

- Because of the more severe regeneration conditions typically associated with CC mode operation, the regenerated catalyst is typically clean burned. However because of the large enthalpy released during complete $C \rightarrow CO_2$ combustion only high quality feeds (low coking tendency) can be processed, and the physical restrictions on regenerator temperature as well as possible catalyst deactivation limits the amount of coke that can be combusted, and therefore the range of feed qualities that can be processed.

- During CC mode operation, a large excess of O_2 in the flue gas is economically wasteful, since energy is needed to provide the additional air supply. However, a large excess of O_2 is indicative of sub–optimal operation:

  - the fresh feed throughput is too low - a significantly higher throughput could be processed with the available equipment without violating constraints.
  - the combustion air compressor is significantly over designed for the specific unit.

  Neither of these possibilities is desirable. However, a minimum excess is generally recommended to ensure complete combustion operation.

2.4 Significant Process Variables

Different studies published in the literature (Arbel et al. 1995, Grosdidier, Mason, Aitolahti, Heinonen and Vanhamåki 1993, Hovd and Skogestad 1993, Monge and Georgakis 1987) suggest that the following variables are important to FCCU operation. We categorize them as measured (controlled) variables, manipulated variables

and disturbances.

2.4.1 Measured Variables

- riser temperature
- regenerator temperature
- reactor pressure
- regenerator pressure
- wet gas compressor suction pressure
- reactor stripper catalyst level
- total air flow to the regenerator
- reactor/regenerator differential pressure
- flue gas O_2 concentration
- flue gas CO concentration
- regenerator cyclone temperatures

2.4.2 Manipulated Variables

- total feed rate
- feed preheat temperature
- catalyst circulation rates (when control slide valves are available)
- combustion air flow rate
- stack gas flow rate
- lift air blower throughput
- wet gas compressor throughput

2.4.3 Disturbances

- variations in feed coking characteristics
- feed temperature changes
- ambient temperature changes
- fluctuations in reactor pressure
- main fractionator and downstream separation unit pressure changes

A number of process disturbances (including changes in feed quality) eventually affect reactor pressure. Of particular significance for the Model IV FCCU are fluctuations in main fractionator pressure that directly affect reactor pressure. Upon consultations with Ron Sorensen (Sorensen 1993), variations in the pressure drop between the main fractionator and the reactor (ΔP_{frac}) was included as a disturbance to the system. This was done to study the effect of upsets in the fractionator unit (which is not modeled) on the performance of the regenerator/reactor system. Changes in main fractionator pressure can arise when vapor flow rate is altered (*e.g.* as a result of changes in wet gas compressor suction flow rate). Variations in internal vapor and liquid traffic in the main fractionator (due to changes in condenser/reboiler duty) can also lead to changes in main fractionator pressure. In the original model a constant pressure drop between the main fractionator and reactor section of 9.5psi (ΔP_{frac}) was assumed. Fluctuations in fractionator pressure can be effectively modeled as variations in ΔP_{frac}. Pressure disturbances in down-stream recovery units (down-stream from wet gas compressor) can also be effectively modeled as changes in ΔP_{frac}. ΔP_{frac} is therefore taken to be a disturbance for the Model IV FCCU studied in Chapter 3.

The feed temperature was originally considered to be a disturbance. It was noted from the CLDG analysis of the Model IV FCCU (Chapter 3) that feed temperature was in fact the most significant disturbance for those systems that did not have fuel flow rate to the feed pre–heat furnace as a manipulated variable. It is clear

that feed pre–heater has a direct influence on the feed temperature and should be used to control that temperature only. Thus, the feed temperature was removed from the set of disturbances, and the fuel rate to the feed pre–heater furnace was removed from the set of free manipulated variables, the implicit assumption being that the feed temperature will be controlled by an independent control loop using as the manipulated variable, Figure 2.3.

2.5 Operating Constraints for Model IV FCCUs

As stated previously the FCCU is used to convert high boiling gas oil to more useful lighter hydrocarbons. From an economic standpoint, the primary objective for the operation of the FCCU would be to maximize feed throughput at a given riser temperature. However there are numerous operating constraints in the physical process which cannot be violated in trying to achieve this goal. The constraints specified in the original AMOCO problem are listed in Table 2.1 for reference. Most of the constraints are self explanatory *e.g.* valves fully open or fully closed *etc.*. However specific comments regarding some of the other constraints provide additional insights into FCCU operation.

2.5.1 Regenerator Operating Mode

The Amoco/Lehigh FCCU model claims to capture the operating characteristics of the model IV FCCU in complete combustion mode operation.

2.5.2 Limits on Air Supply Rate

The amount of coke that can be burned off from the catalyst in the regenerator is limited by the combustion air compressor capacity. However, combustion air blower capacity may be indirectly limited by the maximum allowable gas superficial velocity through the regenerator - since it is undesirable to have excessive entrainment of catalyst from the regenerator dense bed as:

Constrained Variable	Units	Lower Bound	Upper Bound
Flow Rates:			
wash oil (F_1)	lb/s	0	17
diesel (F_2)	lb/s	0	16
total feed (F_3)	lb/s	0	144
slurry recycle (F_4)	lb/s	0	10
furnace fuel (F_5)	scf/s	0	40
All Valves	%	0	100
Vessel Pressures			
Reactor	psig	–	49.2
Regenerator	psig	–	39.7
Main Fractionator	psig	–	39.7
Reactor P. - Reg. P	psia	-5	2
Compressor Surge	$F_{sucn} > F_{surge}$		
Total Comb. Oper.			
Flue Gas O_2 conc.	mol%	1.5	–
Regenerator T.	$°F$	1265	–
Flue Gas CO conc.	ppm	–	350
Metallurgical Temp.			
Reactor T.	$°F$	–	995
Cyclone T.	$°F$	–	1310
Furnace Firebox T.	$°F$	–	1700

Table 2.1: Process constraints and limits for the Amoco/Lehigh Model IV FCCU

- this can lead to unnecessarily high catalyst loss as fines in the flue gas line
- reduce the regeneration efficiency in the dense bed (DeLasa and Grace 1979, Errazu, DeLasa and Sarti 1979).

2.5.3 Regenerator Bed Temperature

Regenerator dense bed temperature varies slightly along the height of the bed (Felipe 1992), being lowest at the bottom and highest at the top. If regenerator bed temperature is too low there is insufficient combustion of coke leading to coke buildup on catalyst which will reduce overall cracking efficiency. On the other hand, excessive regenerator temperature will result in rapid thermal deactivation of the catalyst

(Wrench and Glasgow 1992).

2.5.4 Metallurgical Limits

For economic reasons, the FCCU is typically operated at a high riser temperature, as the product yield and conversion is then high (Arbel et al. 1995). The operating temperature is therefore often close to the metallurgical limit of the riser construction material. Clearly, extended operation at a higher temperature is unacceptable.

In the regenerator section, most of the CO is converted to CO_2 in the dense bed, although some CO is still present in the disengaging zone. The gas phase reaction of CO with O_2 to form CO_2 is exothermic and the enthalpy of combustion is transferred to the cyclones. It is therefore important to monitor cyclone temperature to prevent possible melt downs. Possible overheating of the cyclones is an important concern if the FCCU is operated in partial combustion mode.

2.6 Mathematical Models describing FCC Operation

2.6.1 Regenerator Models and Reactor Models

Numerous models are available in the literature for the regenerator section of the FCCU (DeLasa and Grace 1979, DeLasa, Errazu, Barreiro and Solioz 1981, Elnashaie and Elshishini 1992, Falti-Saravelou, Vasalos and Dimogiorgas 1991). For control purposes, a reasonable regenerator model must be able to predict the following information:

- regenerator dense bed temperature
- flue gas concentrations of O_2, CO_2, and CO
- concentration of carbon on regenerated catalyst

Errazu et al. (1979) found that a grid model for the regenerator fluidized bed provides good estimates for all the above information. They did not however consider the regenerator disengaging section in their analysis resulting in some discrepancy with experimentally observed data. They do however emphasize the importance of taking into account the disengaging section of the regenerator.

The reactor riser model must be able to predict the following information :

- amount of wet gas produced at given operating conditions
- amount of coke deposited on catalyst
- riser exit temperature

The reactor riser model should be detailed enough to capture the dependence of production rates of wet gas and coke on the following factors which are known to influence these rates (McFarlane et al. 1993, Shah, Huling, Paraskos and McKinney 1977):

- catalyst to oil ratio in the riser
- hot regenerated catalyst temperature
- residence time of feed oil in the riser
- the state of activation of regenerated catalyst (coke content)
- coking characteristics of the feed (affects coke production)
- weight hourly space velocity in the riser (WHSV)

2.6.2 Models for Combined Reactor/Regenerator Section

A few models exist to predict the overall dynamics for the reactor/regenerator section of the FCCU (Elnashaie and Elshishini 1992, Felipe 1992, Kurihara 1967, Lee and Groves Jr. 1985). A brief description of the more common FCCU models will be given emphasizing modeling assumptions and shortcomings:

1. *Kurihara Model (1967)*

   The Kurihara model (Kurihara 1967) was widely accepted in the refining industry (at the time it was published) as it was one of the first to predict the dynamic characteristics of the FCC operation. Assumptions in this model include (Denn 1986):

   - There is no hydrocarbon carryover on spent catalyst into the regenerator.
   - The spent catalyst flow rate always equals the regenerated catalyst flow rate, but the actual catalyst circulation rate can be independently specified. Because spent catalyst flow rate always equals regenerated catalyst flow rate, the regenerator and reactor catalyst inventories are constant.
   - It was originally assumed that the cracking reaction occurred in the fluidized bed of the reactor, and this was the assumption in this model. Early measurements with older silica–alumina and alumina catalysts indicated that a significant part of the cracking process in fact occurred in the riser itself (Avidan and Shinnar 1990), and only a smaller fraction occurred in the reactor fluidized bed. Subsequently, with the newer zeolite catalysts currently used in FCCs, it is reported that the cracking reaction is essentially complete in the riser (Lee and Weekman 1976), and such findings led to the removal of the riser fluidized bed altogether. Thus the assumption of the cracking reaction occurring in the fluidized reactor bed is no longer even partially valid.
   - Catalyst residence time in the regenerator (5 min) is large compared to reactor hold up time (1.5 min) and a pseudo steady–state assumption was made for reactor dynamics. Thus rate of coke deposition on catalyst, riser temperature and total carbon on spent catalyst is described by algebraic relations.

2. *Lee and Groves Model (1985)*

Following is a list of some aspects of the Lee and Groves model (Lee and Groves Jr. 1985) including benefits and assumptions:

- The gas oil cracking model takes into account catalyst to oil ratio, residence time of oil in the riser and level of activation of catalyst coming from the regenerator section. Gasoline yield from the cracking reaction products is also modeled.
- There is no hydrocarbon carryover on spent catalyst from the stripper to the regenerator.
- As in the Kurihara model, flow rates of spent and regenerated catalyst are assumed constant and inventories in the reactor stripper and regenerator are also constant.
- A distinction is made between the activity of coke that is freshly deposited on catalyst in the riser and activity of coke that was already on the catalyst from the regenerator.

3. *Amoco/Lehigh Model (1993)*

This is one of the models (McFarlane et al. 1993) adopted for this project. Some features of this model are:

- The regenerator is empirically modeled to account for the freeboard region above the dense bed.
- The reactor model is very simple - production rate of wet gas is assumed to depend only on riser temperature (linear dependence).
- Friction factors in the catalyst flow lines are assumed constant but catalyst flow rates are independently accounted for and not assumed constant.
- A constant hydrocarbon fraction is assumed for spent catalyst flowing into the regenerator but the effect of steam in the stripper is not modeled.

4. *Mobil/CCNY Model (1995)*

This recently published model (Arbel et al. 1995) is another model adopted for this project. Some features of this model are:

- A ten lump kinetic model describing the cracking reactions is utilized
- Operation in both the PC mode and CC mode as well as the transition between these two modes is described. This is one of the first mathematical models of the FCC to describe operation in both modes.
- The spent catalyst flow rate always equals the regenerated catalyst flow rate, but the actual catalyst circulation rate can be independently specified. Because spent catalyst flow rate always equals regenerated catalyst flow rate, the regenerator and reactor catalyst inventories are constant.
- This model predicts multiple steady–states within the normal operating regime.

The Amoco/Lehigh model as well as the Mobil/CCNY model will be described in detail next.

2.7 The Amoco/Lehigh Model IV FCCU Dynamic Model

The essential process units in the model IV FCCU (McFarlane et al. 1993) can be divided into seven groups:

- Feed system
- Reactor and Main Fractionator
- Wet Gas Compressor
- U-bends
- Regenerator

- Air blowers

The model is claimed to describe the dynamics of the process accurately enough to test control performance but is not intended to predict product compositions. Each of the FCCU operating sections will now be described:

2.7.1 Feed System

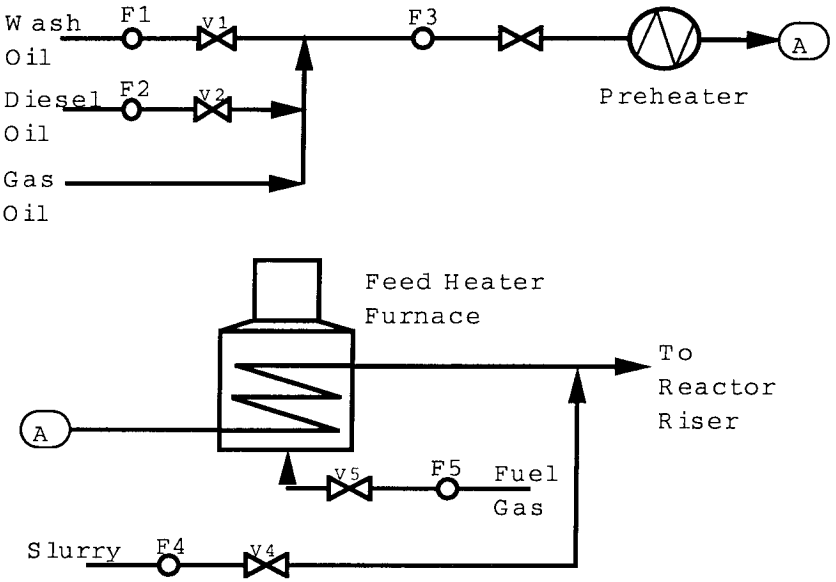

Figure 2.3: Feed system schematic

Figure 2.3 is a schematic of the feed train to the FCCU. The AMOCO model does not include a detailed product distribution model. Therefore the feed streams are characterized by their tendency to form and deposit coke on catalyst particles. There are three feed components - wash-oil, gas-oil, and diesel. For the same amount of each feed, wash-oil deposits more coke on the catalyst after cracking than gas-oil and diesel deposits less coke than gas-oil. The three streams are mixed in-line and passed to a feed heating furnace. The feed system is assumed to be totally controlled. Flow controllers manipulate wash-oil, diesel-oil, total fresh feed, and slurry recycle flow rates in a manner that keeps these flows constant at their set point values. The

heated fresh feed stream is mixed in-line with a slurry recycle stream from the bottom of the main fractionator and passed to the base of the reactor riser.

The feed preheater in Figure 2.3 is not modeled. However, the model contains dynamic energy balances for the furnace firebox and coil. The fuel supply to the furnace can be regulated to control feed temperature. It is assumed that the feed enters the furnace with a specified temperature (460.9° F) and is then heated up by passage through the furnace.

2.7.2 Reactor and Main Fractionator

The cracking reaction is assumed to occur only in the riser. The sequential steps of evaporation, adsorption (on the catalyst granules), reaction, and desorption are not modeled. Catalyst deactivation is not taken into account either. The model of the riser and reactor is based on the catalyst material balances, energy balances, and impulse balances (for pressure). The reactor riser model predicts cracking temperature, pressure drop across the riser, the yield of wet gas and the amount of deposited coke. The main fractionator and associated piping is assumed to be a single volume and is not considered to work as a separator, because no attempt is made to calculate the reactor product composition. All the wet gas produced in the riser is assumed to pass through the fractionator overhead to the wet gas compressor and subsequently to the downstream vapor recovery units. A constant pressure drop between the main fractionator and the reactor was originally assumed.

2.7.3 Wet Gas Compressor

The wet gas compressor is modeled as a single stage centrifugal compressor operated far from surge conditions. The wet gas compressor model includes an operating curve in equation form and a single surge point specification. The flow rate through the compressor is also modeled.

2.7.4 Catalyst Circulation Through U-bends

Circulation of spent and regenerated catalyst is assumed to be governed by force balances. The friction factor in each catalyst flow line is assumed constant. There is a strong interdependence among the pressures in the reactor and regenerator, catalyst flows, catalyst inventory distribution, temperatures, and kinetics of the reactions.

2.7.5 Regenerator

As a result of the cracking reaction in the riser, coke is deposited on the catalyst particles, greatly reducing catalyst activity. Catalytic activity is restored in the regenerator section. The regenerator catalyst is fluidized by the passage of air through it. The air is supplied primarily by the combustion air compressor and partly by the lift air compressor. The burning of coke and hydrogen is described by kinetic equations integrated along the regenerator height. The results of the simulation showed profiles similar to the compositions presented in the literature (Falti-Saravelou et al. 1991). The model contains total mass and energy balances, a standpipe inventory balance, species balances (C, CO, CO_2, O_2), and impulse equations. It describes catalyst entrainment and includes airlift calculations.

2.7.6 Air Blowers

There are two air blowers: the lift air blower, a single stage centrifugal compressor driven by a variable speed steam turbine; and the combustion air blower, driven by a constant speed electric motor. The model of the compressor contains performance equations related to polytropic head and suction volume. Air flow rates are computed, taking into account ambient temperature and pressure.

2.8 The Mobil/CCNY FCC Dynamic Model

The Mobil/CCNY model (Arbel et al. 1995) operation is divided into the following component parts:

- Feed system
- Reactor section
- Regenerator section
- Combustion air blower

Since these component parts have been described in detail in Section 2.7, they will not be discussed here. The focus here is on understanding the regenerator combustion mechanism as well as the reactor cracking mechanism. The Mobil/CCNY model describes the operation of the FCCU in both partial combustion mode and complete combustion mode. Furthermore, the transition between these two modes is also described.

2.8.1 Regenerator Section

Combustion kinetics

The primary objective in the regenerator section of the FCC is to burn off the coke deposited on the catalyst particles to restore the catalyst activity. The term *coke* is generally applied to a combustible carbonaceous material that contains appreciable amounts of hydrogen. Coke is reported to have a composition ranging from $CH_{0.5}$ to $CH_{1.0}$ (Weisz and Goodwin 1966). The primary combustion reactions in the regenerator are the following:

I	$C + \frac{1}{2}O_2 \xrightarrow{k_1} CO$
II	$C + O_2 \xrightarrow{k_2} CO_2$
III$_c$	$CO + \frac{1}{2}O_2 \xrightarrow{k_{3c}} CO_2$
III$_h$	$CO + \frac{1}{2}O_2 \xrightarrow{k_{3h}} CO_2$
IV	$2H + \frac{1}{2}O_2 \xrightarrow{k_4} H_2O$

The production of trace quantities of NO_x and SO_x are significant from an environmental viewpoint (Evans and Quinn 1993), but are not considered in the model of Arbel et al. (1995), and not considered in this thesis. Note the following:

- **Reaction IV:** The combustion of H carried over to the regenerator on the spent catalyst proceeds very fast. H combustion is reported to proceed significantly faster than the carbon combustion (Avidan and Shinnar 1990). For modeling purposes, it is assumed that the reaction IV occurs instantaneously and proceeds to completion. Thus, the incoming combustion O_2 supply rate is reduced by the amount of O_2 required for the stoichiometric completion of reaction IV. The enthalpy change of combustion is however included in the energy conservation equation for the overall regenerator.

- **Reactions I and II** the combustion of the carbon component of coke proceeds either to CO or CO_2. The rate of reaction I (r_1) is given in Arbel et al. (1995) by:

$$r_1 = (1-\epsilon)\rho_c k_1 \frac{C_{rgc}}{MW_c} P_{O_2} \tag{2.3}$$

where:

ϵ	= regenerator dense bed void fraction
ρ_c	= settled catalyst density (68 lb_m/ft^3)
C_{rgc}	= coke fraction (of catalyst mass) on regenerated catalyst
MW_c	= molecular weight of carbon (12 $lb_m/lbmol$)
P_{O_2}	= O_2 partial pressure

and the rate of reaction II (r_2) is given as:

$$r_2 = (1-\epsilon)\rho_c k_2 \frac{C_{rgc}}{MW_c} P_{O_2} \tag{2.4}$$

The critical parameter is the relative ratio of conversion to CO_2 *vs.* conversion to CO *i.e.* the CO_2/CO product ratio. This is because the heat of combustion

for carbon to CO_2 is almost three times as large as the heat of combustion to CO. We note from Equation 2.3 and Equation 2.4 above that steady–state CO_2/CO product ratio equals k_2/k_1. Arbel et al. (1995) report the temperature dependence of k_2/k_1 as:

$$\frac{k_2}{k_1} = 3.981 \times 10^{-4} \exp\left[\frac{11232}{T_{rgn} + 460}\right] \tag{2.5}$$

where T_{rgn} ($^\circ F$) is the regenerator dense bed temperature. In investigating this phenomenon, Weisz (1966) reported that the initial CO_2/CO product ratio is a function of the temperature only. This intrinsic ratio is sometimes referred to as the *Aurthur ratio*. Moreover, the CO_2/CO product ratio was found to display an Arrhenius type dependence on temperature. The rate constant for the overall coke combustion ($k_1 + k_2$) was reported by Weisz and Goodwin (1966):

$$k_1 + k_2 = 7.275 \times 10^6 \exp\left[\frac{-34000}{T_{rgn} + 460}\right] \tag{2.6}$$

and knowing k_2/k_1 (Equation 2.5) and $k_1 + k_2$ (Equation 2.6), the individual rate constants k_1 and k_2 can be determined.

- **Reactions III_c and III_h:** Once CO is produced, it undergoes subsequent combustion to CO_2, and this enthalpy change of combustion also contributes to the overall regenerator energy conservation equation. There are two distinct regions where the gas phase CO to CO_2 conversion occurs, and the mechanisms for these two regions is thought to be different:

  1. The catalyst particles are porous, typically having an internal surface area on the order of $300 m^2/g$ catalyst (Weisz and Goodwin 1966). Since the cracking reaction occurs within the catalyst particles, coke is deposited within the catalyst particles as well. After the initial $C \rightarrow CO$ conversion at the catalyst surface, the CO diffuses through the catalyst particle pores to the surface of the particle. Weisz (1966) reported that the observed CO_2/CO product ratio at the surface was often significantly different from

that predicted by the intrinsic CO_2/CO ratio of Aurthur. He found that:

- the larger the catalyst particle, the higher the CO_2/CO product ratio at the surface, at a given catalyst temperature.
- the CO_2/CO product ratio depends on the catalyst surface properties. In particular, the CO_2/CO product ratio was higher for catalyst particles coated with oxides of transitions metals than the base catalyst with no such coating.

These observations can be explained by the following mechanism:

- the initial CO_2/CO product ratio at the catalyst (internal) surface is still determined by the Aurthur ratio, and depends on catalyst temperature only.
- as the CO diffuses through the catalyst pores to the catalyst surface, the combustion of CO continues. The rate depends on (1) the catalyst size. The larger the particle, the longer the diffusion path, and the greater the extent of reaction and (2) the catalyst surface properties. The presence of oxides of transition metals appears to increase the extent of reaction, and therefore *promotes* the $CO \rightarrow CO_2$ combustion. These oxides of transition metals (most often Pt_2O_3 and Cr_2O_3) are therefore referred to as *combustion promoters.*

k_{3c} is therefore the rate constant for the $CO \rightarrow CO_2$ reaction within the catalyst particle itself, and accounts for the effect of different catalyst additives. The rate of this intra–particle reaction (r_{3c}) is given by:

$$r_{3c} = x_{pt}(1-\epsilon)\rho_c k_{3c} P_{O_2} P_{CO} \tag{2.7}$$

where additionally,

x_{pt} = factor accounting for contribution of combustion promoters

P_{CO} = CO partial pressure

2. Once the CO molecules are in the void space of the bulk catalyst, $CO \rightarrow CO_2$ conversion still proceeds, but by a different mechanism. It is reported that this homogeneous phase reaction is a thermal free–radical reaction which is inhibited by the presence of solids (Avidan and Shinnar 1990). This homogeneous phase reaction is accounted for using the rate constant k_{3h}. The rate of inter–particle reaction (r_{3h}) is given by:

$$r_{3h} = \epsilon k_{3h} P_{O_2} P_{CO} \tag{2.8}$$

The overall conversion of the $CO \rightarrow CO_2$ (r_3) is the sum of the intra–particle $CO \rightarrow CO_2$ conversion and the inter–particle $CO \rightarrow CO_2$ conversion:

$$r_3 = r_{3c} + r_{3h} \tag{2.9}$$

The Arbel et al. (1995) model is the first that we are aware of that attempts to account for the impact of CO combustion promoters on the overall regenerator combustion kinetics.

Regenerator modeling

Since the seminal work of Ford, Reineman, Vasalos and Fahrig (1976) detailing the regenerator combustion reactions and reaction zones, the following modeling assumptions have generally been made (also in the Amoco/Lehigh model):

- the the regenerator dense phase solids are described by a perfectly mixed stirred tank model. The consequences of this assumption are that:

  1. regenerator dense bed temperature
  2. the coke fraction on regenerated catalyst (C_{rgc})

  are uniform throughout the regenerator dense bed. Sadeghbeigi (1995) indicates that these assumptions indeed reflect actual regenerator operation closely.

- the gas flow through the regenerator is modeled by a series of three CSTRs.

Note that this series of CSTRs assumption for the gas phase is in contrast to the assumption in Errazu et al. (1979) who assumed a uniform O_2 concentration throughout the dense bed. While this might have been justified for the rather "shallow" regenerator bed Errazu et al. (1979) analyzed (16.4ft high, 45.9ft diameter), this assumption is found not to be valid for the "deep" regenerator beds currently used in the regenerator section (Sadeghbeigi 1995). For example, the Arbel et al. (1995) model assumes a regenerator 45ft high and 27ft diameter.

Thus, for each of the three CSTRs in series, the following conditions hold:

- constant temperature = T_{rgn} (isothermal reaction)
- constant coke on catalyst = C_{rgc}
- uniform CO, CO_2 and O_2 concentration in each CSTR

A steady–state mass balance of each of the three CSTRs leads to the following equations describing the O_2, CO and CO_2 exit flow rate from each CSTR:

$$f_{O_2} = f_{O_2,in} - V_{CSTR}\left[(1-\epsilon)\rho_c\left(\frac{1}{2}k_1 + k_2\right)\frac{C_{rgc}}{MW_c}\frac{f_{O_2}}{f_{tot}}P_{rgn} + \frac{1}{2}k_3\frac{f_{O_2}}{f_{tot}}\frac{f_{CO}}{f_{tot}}P_{rgn}^2\right] \quad (2.10)$$

$$f_{CO} = f_{CO,in} + V_{CSTR}\left[(1-\epsilon)\rho_c k_1\frac{C_{rgc}}{MW_c}\frac{f_{O_2}}{f_{tot}}P_{rgn} - k_3\frac{f_{O_2}}{f_{tot}}\frac{f_{CO}}{f_{tot}}P_{rgn}^2\right] \quad (2.11)$$

$$f_{CO_2} = f_{CO_2,in} + V_{CSTR}\left[(1-\epsilon)\rho_c k_2\frac{C_{rgc}}{MW_c}\frac{f_{O_2}}{f_{tot}}P_{rgn} + k_3\frac{f_{O_2}}{f_{tot}}\frac{f_{CO}}{f_{tot}}P_{rgn}^2\right] \quad (2.12)$$

where:

f_i = exit molar flow rate of component i from CSTR

$f_{i,in}$ = inlet molar flow rate of component i into CSTR $(lbmol/s)$

V_{CSTR} = volume of each CSTR (ft^3)

f_{tot} = total molar flow rate through CSTR $(lbmol/s)$

P_{rgn} = regenerator pressure (psia)

Note that:

$$k_3 = x_{pt}(1-\epsilon)\rho_c k_{3c} + \epsilon k_{3h} \tag{2.13}$$

Equation 2.10 and Equation 2.11 are solved numerically to determine f_{O_2} and f_{CO} at the exit of each CSTR. A numerical solution is required as f_{tot} contains f_{CO} and f_{O_2}. f_{CO_2} can then be determined by substitution. Note that a steady–state mass balance is used, and justified as the gas flows up the length of the regenerator rapidly (within seconds), and a pseudo steady–state assumption can be made to simplify the dynamic analysis.

2.8.2 Reactor Section

The incoming fresh feed is contacted with hot regenerated catalyst at the bottom of the reactor riser. The feed is vaporized (almost instantaneously) and the catalyst/oil mixture is transported in a dilute phase up the reactor riser. The feed is cracked during this dilute phase transport. The currently used zeolite based catalysts are highly active and the required riser residence time is therefore very short ($< 10s$). The feed cracking reaction proceeds very fast, and is essentially complete within the reactor riser section.

Moreover, since the time scale for the cracking reactions (5s–10s) is significantly shorter than the overall process dynamics (20–50 min.) a pseudo steady–state assumption is made for the cracking reactions to simplify the overall dynamic model. The main impact of the riser on the overall steady–state and dynamic FCC operations is through:

- the product yield and distribution,

- the coke production rate,
- energy transfer due to the endothermic cracking reaction.

For steady–state optimization the prediction of the product stream properties is critical. However, it is difficult to accurately predict the product yield and distribution and account for all the factors that can affect the yield and distribution including catalyst properties, feed composition (which often changes in normal FCC operation), etc.. For this reason, we have not focused on steady–state control and optimization studies for the FCC as we feel that conclusions that can be applied to a wider range of FCC units cannot be derived. However, from a dynamic operations viewpoint, the critical aspects are the coke production rate and the energy transfer rate due to the endothermic cracking reaction, and these can be predicted with a greater degree of certainty:

1. The coke production rate is a function of:
    - feed coking quality
    - catalyst/oil ratio
    - residence time in riser
    - catalyst activity
    - reactor temperature
2. The heat of endothermic cracking reaction is a function of:
    - catalyst/oil ratio
    - residence time in riser
    - catalyst activity
    - reactor temperature

The most significant characteristics of the incoming feed from a process dynamics viewpoint will be described in Section 2.8.2, the cracking kinetics and reaction scheme will be described in Section 2.8.2 and the assumptions made for the reactor riser model itself will be described in Section 2.8.2.

Fresh feed characteristics

Two characteristics of the fresh feed are considered critical for the dynamic modeling and analysis of the FCC. These are

1. *Feed composition:* The incoming feed to the FCC is generally a mixture of many different hydrocarbons *e.g.* normal gas oil, diesel oil etc. that are piped in from different parts of the oil refinery. Considering the properties of each pure hydrocarbon is infeasible. A practical ten lump model used to characterize the feed and products is described in Section 2.8.2. Feeds of different compositions have varying effects on FCC operation, most significantly through the feed coking characteristics, which is described next.

2. *Feed coking characteristics:* Quantifying the feed coking characteristics is still an active area of research (Sadeghbeigi 1995). The FCC feed typically consists of a mixture of a number of different hydrocarbon sources each with different feed coking characteristics. For example, it is reported (McFarlane et al. 1993) that many slurries (typically bottoms product from distillation units) produce more coke on cracking that normal gas oil, while diesel oil produces less coke than normal gas oil. A relative coking factor (γ) is therefore often used to rank order the relative coking characteristics of different feed components. For example, if normal gas oil has $\gamma_{gasoil} = 1$, then the slurry has $\gamma_{slurry} > 1$ and diesel oil has $\gamma_{diesel} < 1$. The actual coking characteristic of the feed will obviously depend on the fractional contributions from each feed component type. The contribution of each feed component can be accounted for by using a weighted relative coking rate - the weight being the mass fraction (for example) of each feed component. Such a weighted sum of relative feed coking characteristics to quantify the feed coking characteristics of the overall incoming feed is used in (Arbel et al. 1995, McFarlane et al. 1993) and modeled as in Equation 2.14.

$$\Psi = \sum_i \gamma_i y_i(0) \tag{2.14}$$

where γ_i indicates the relative coking tendency of feed component i and $y_i(0)$ is the weight fraction of feed component i in the incoming fresh feed stream.

Cracking kinetics

A ten lump model is used to describe the cracking reactions occurring in the reactor riser. These ten lumps are given in Table 2.2.

Lump #	Symbol	Description
1	Ph	heavy paraffins
2	Nh	heavy naphthenes
3	Ah	heavy aromatics
4	Rh	heavy aromatic rings
5	Pl	light paraffins
6	Nl	light naphthenes
7	Al	light aromatics
8	Rl	light aromatic rings
9	G	gasoline
10	C	coke

Table 2.2: Components of the ten lump kinetic model.

It is assumed that the cracking reaction proceed through nine primary reactions. These are tabulated in Table 2.3 using the terminology for the lumps indicated in Table 2.2.

Index #	Cracking Reaction (symbolic)
1	$\mathrm{Ph} \rightarrow \mathrm{Pl} + \mathrm{G} + \mathrm{C}$
2	$\mathrm{Nh} \rightarrow \mathrm{Nl} + \mathrm{G} + \mathrm{C}$
3	$\mathrm{Ah} \rightarrow \mathrm{Al} + \mathrm{Rl} + \mathrm{G} + \mathrm{C}$
4	$\mathrm{Rh} \rightarrow \mathrm{Rl} + \mathrm{C}$
5	$\mathrm{Pl} \rightarrow \mathrm{G} + \mathrm{C}$
6	$\mathrm{Nl} \rightarrow \mathrm{G} + \mathrm{C}$
7	$\mathrm{Al} \rightarrow \mathrm{G} + \mathrm{C}$
8	$\mathrm{Rl} \rightarrow \mathrm{C}$
9	$\mathrm{G} \rightarrow \mathrm{C}$

Table 2.3: Symbolic representation of the cracking reactions for each lump. Note that the stoichiometric coefficients are *not necessarily* one.

From:

- the reaction rates at $1000°F$
- the activation energies for each reaction

which are provided in Arbel et al. (1995), the pre–exponential factor for each of the nine reactions in Table 2.3 can be calculated. It is also assumed that each cracking reaction is described by an elementary first order reaction. Thus, for example in Reaction # 1 in Table 2.3, where Ph is catalytically decomposed into Pl, G and C, each individual decomposition Ph→Pl, Ph→G, and Ph→C are assumed to be described by an elementary first order reaction.

Reactor riser model

The reactor riser is assumed to be an adiabatic plug flow reactor, with a radially uniform temperature distribution. Assuming a radially uniform temperature distribution can be an unrealistic assumption especially in the region around the feed and catalyst entrance where the intense solids/liquid/gas mixing makes this assumption difficult to justify. However, in practice, a significant effort has been undertaken to ensure that the mixing occurs as rapidly as possible, and the region where the radially uniform temperature distribution assumption is only partially valid is therefore small (Sadeghbeigi 1995). Thermal reactions which can become significant at higher riser temperatures are not considered.

Chapter 3 The Significance of Control Studies during Process Design

Summary

Model IV Fluid Catalytic Cracking Units (FCCUs) differ from other cracking units in that model IV FCCUs do not have slide valves in the catalyst circulation lines to enable direct control of catalyst circulation rate through the unit. Reducing fluctuations in catalyst circulation rate is found to significantly improve closed loop performance of the FCCU. Some design and operational modifications that can be made to model IV FCCUs to improve closed loop performance at the regulatory level based on this insight are mathematically modeled and compared. Closed loop performance of a model IV FCCU operated with the weir and standpipe always flooded is examined. The achievable performance is significantly better than that of the standard model IV FCCU. The closed loop performance of the model IV FCCU modified to incorporate slide valves in the catalyst circulation lines is also examined. The performance of the FCCU with slide valves is better than the performance achievable by the FCCU with the weir flooded. It is found that model IV FCCUs are ill-conditioned owing to the use of the weir and standpipe arrangement in the regenerator section. Both the operational and design modifications studied reduce plant ill-conditioning appreciably.

3.1 Motivation

The economically optimal and safe operation of a processing unit requires that the unit is designed appropriately:

- from a steady–state point of view, and
- from a dynamic point of view, i.e. that it is possible to run the unit at the desirable operating conditions despite dynamic variations in the environment, e.g. disturbances, feedstock changes, drifts in the parameters defining the operation of the unit, *etc.*

The work described in this Chapter is focused on this second aspect of the design process. The observed closed loop response of any given processing unit might be acceptable or unacceptable when evaluated by appropriate criteria. If the performance is acceptable then there might be little incentive to improve the overall process. However, if the observed performance is unacceptable, then a natural question is whether one can obtain better performance. Note that the dynamic operability of the plant depends on two factors: the design of the unit itself and the design of the associated control system. Thus, the poor performance must be due to one (or both) of the following two causes:

- control system deficiencies:
  - the controller might be poorly tuned.
  - the controller structure is inappropriate for the process under study. An example might be if single loop controllers are used when multivariable controllers might provide significantly better control (*e.g.* for ill-conditioned plants).
- plant design deficiencies:
  - the physical design or setup of some part of the overall plant prevents one achieving better closed loop performance.

Clearly if it can be shown that regardless of the controller chosen, one cannot achieve acceptable closed loop performance, then there must be some feature of the plant design itself that limits the achievable performance. In general, it is not easy to rigorously establish that no controller will improve the observed performance of the process under study. A simplified approach that utilizes currently available theory has to be undertaken to assess the best closed loop performance achievable from a given plant.

The following measures have been used in this Chapter to examine *qualitatively* possible physical design limitations of the plant itself:

- Right half plane transmission zeros (RHPT zeros) within the desired bandwidth will limit achievable closed loop performance of the process regardless of the controller type used (Holt and Morari 1985b, Morari, Zafiriou and Holt 1987). Several of the control structures analyzed have significant RHPT zeros *i.e.* RHPT zeros within the desired bandwidth.

- The model by (McFarlane et al. 1993) indicates that the model IV FCCU is ill-conditioned *i.e.* the plant gain is strongly dependent on the input direction. Ill-conditioned plants are characterized by strong directionality *i.e.* inputs in the direction of high plant gain are strongly amplified while inputs in the direction of low plant gain are not (Morari and Zafiriou 1989, Skogestad, Morari and Doyle 1988).

To obtain a more *quantitative* measure of achievable performance, we will use the structured singular value (commonly referred to as μ). The properties of μ-synthesis (μ-optimal controller design) and μ-analysis that we will appeal to are the following:

- Model uncertainty is always present in practice. μ-synthesis explicitly accounts for model uncertainty during controller synthesis. Model uncertainty is also explicitly accounted for during the subsequent analysis.

- No restrictions are imposed on controller structure during μ-synthesis. In general the μ-optimal controller is multivariable. Note that it is most common to

use single loop PI(or PID) controllers at the regulatory level. Therefore, using PI(or PID) controllers restricts controller structure. However, the major goal in this Chapter is to determine the best possible performance regardless of what controller is used. Thus the best achievable performance with any controller would be just as good or better than that achievable with PI(or PID) controllers.

- A wide range of disturbance signals are considered in designing the μ-optimal controller. For an appropriately scaled system (Equation 3.1, 3.2, 3.3) all disturbances satisfying $\|\hat{d}\|_2 \leq 1$ are considered. The μ-optimal controller minimizes the largest possible gain $\|\hat{y}\|_2/\|\hat{d}\|_2$ which can result from any $\hat{d}$ satisfying $\|\hat{d}\|_2 \leq 1$.

- Robust stability and robust performance can be addressed in a rigorous and consistent manner.

- For a fixed uncertainty and performance specification (to be discussed shortly),

$$\text{Robust Performance Guaranteed} \Leftrightarrow \mu_{RP}(\omega) < 1 \quad \text{for all } \omega$$

- In comparing different designs using a fixed uncertainty and performance specification, the lower the $\mu_{RP}(\omega)$ for a given design, the better the design is.

In this Chapter the best possible performance of the Model IV FCCU is assessed. Subsequently, design and operational modifications that can be implemented on the Model IV FCCU to improve dynamic performance are proposed. The best closed loop performance attainable *after* implementing these modifications is compared to the best performance obtained from the original model IV FCCU to assess whether the proposed modifications in fact result in better plant designs.

3.2 Preliminaries

The operating points used for the simulations are tabulated in Appendix A. In order to facilitate easy comparisons of different inputs, outputs and disturbances, the system was made dimensionless as follows:

$$\hat{y} = {y_{scale}}^{-1}(y_{\text{dim}} - y_{\text{ss}}) \tag{3.1}$$

$$\hat{u} = {u_{scale}}^{-1}(u_{\text{dim}} - u_{\text{ss}}) \tag{3.2}$$

$$\hat{d} = {d_{scale}}^{-1}(d_{\text{dim}} - d_{\text{ss}}) \tag{3.3}$$

The scaling factors used to scale the inputs and outputs are tabulated in Appendix A as well. Note that $\hat{u}$, $\hat{y}$, and $\hat{d}$ are vectors since we have a MIMO system and at the *nominal* operating point the inputs, disturbances and outputs are all zero vectors. Furthermore $\hat{y}$ is the output error vector. Each element of the input vector $\hat{u}$ is scaled so that all physically implementable manipulated variable inputs are of magnitude less than one. The output error vector is scaled to make each error element equally significant to the process. The modeled disturbances to the system are:

1. d_1 - variations in ambient temperature
2. d_2 - changes in feed coking characteristics resulting from variations in feed quality
3. d_3 - pressure fluctuations propagating back from the main fractionator to the reactor section of the FCCU

An additional disturbance often cited in the literature (Hovd and Skogestad 1993, Lee and Groves Jr. 1985) is variations in inlet feed temperature. In this Chapter it is assumed that feed temperature is maintained at a pre-specified setpoint by a local temperature controller and is therefore not considered a disturbance to the system.

Variations in ambient temperature affect the combustion air compressor throughput and therefore the ability to burn off coke deposited on the catalyst particles. High

ambient temperatures lead to lower oxygen supply to the regenerator and reduce the amount of coke that can be burnt off (and therefore the maximum fresh feed rate that can be processed). Feed quality refers to the coking characteristics of incoming feed *i.e.* how much coke will be deposited on the catalyst particles as a result of the cracking reaction. Changes in feed quality are reported to be a significant process disturbance (Grosdidier et al. 1993, Hovd and Skogestad 1993, McFarlane et al. 1993) as it directly affects the coke deposition rate on the catalyst and therefore the feed processing rate. A number of process disturbances (including changes in feed quality) eventually affect reactor pressure. Of significance are fluctuations in main fractionator pressure that affect reactor pressure. Changes in main fractionator pressure can arise when vapor flow rate is altered (*e.g.* as a result of changes in wet gas compressor suction flow rate). Variations in internal vapor and liquid traffic in the main fractionator (due to changes in condenser/reboiler duty) can also lead to changes in main fractionator pressure. In the original model a constant pressure drop between the main fractionator and reactor section of 9.5psi (ΔP_{frac}) was assumed. Fluctuations in fractionator pressure can be effectively modeled as variations in ΔP_{frac}. Pressure disturbances in down-stream recovery units (down-stream from wet gas compressor) can also be effectively modeled as changes in ΔP_{frac}.

Variations in ambient temperature (which affects compressor throughput) were modeled as ramps with a period of 24 hours. The designed controllers were capable of rejecting disturbances in ambient temperature rapidly. Fluctuations in feed quality (disturbance d_2) were modeled as steps because the fresh feed composition in the feed holdup tank changes rapidly when heavy oil cuts of different compositions are added. Since pressure fluctuations in the reactor are expected to occur on time scales of tens of seconds, the fluctuations were modeled as steps. The 'typical' peak deviation assumed for changes in ΔP_{frac} is tabulated in Appendix A. Each disturbance is scaled by its maximum expected deviation from steady–state. Thus any disturbance input vector element of magnitude one represents the largest (smallest) expected disturbance. Nominal values for the disturbances and corresponding scaling factors are tabulated in Appendix A.

Notation	Controlled Variables	Manipulated Variables
SI	$C_{O_2,fg}$, T_r	V_{lift}, F_3
SII	$C_{O_2,fg}$, T_r	V_{lift}, V_{14}
SIII	$C_{O_2,fg}$, T_r	V_{lift}, T_2

Table 3.1: Notation for different control schemes

In this Chapter both design and operational modifications to model IV FCCUs are studied. For notational convenience different modifications to the original model are referred to as model B and model C (this notation will be explicitly stated as required). Model A refers to the original model IV FCCU. The control schemes considered in this study are listed in Table 3.1. The notation used in this Chapter is the same as that used in (McFarlane et al. 1993) for ease of comparison with that work.

The output variables are the same for all control schemes. Maintaining riser temperature (T_r) at a pre-determined setpoint is critical to overall process economics as it strongly affects product yield. It is necessary to maintain flue gas oxygen concentration ($C_{O_2,fg}$) above some safe pre-specified minimum to prevent operation in the transitional zone between total combustion and partial combustion modes which is reported to be unstable (Arbel et al. 1995, Grosdidier et al. 1993). Lift air supply (determined by V_{lift}) is always a manipulated variable as it is the only source of additional air supply to the regenerator - the combustion air blower is assumed to operate at full capacity in this study. Other available manipulated variables such as fresh feed rate (F_3), flue gas valve opening (V_{14}) and feed temperature (T_2) are examined in conjunction with V_{lift}. There are several other manipulated variables and many other possible output variables and the most common of these will be discussed.

- Combustion air supply is sometimes used as a manipulated variable. However, for maximum economic benefit of the investment made in the blower, the combustion air blower is operated close to maximum capacity. Therefore, changing the compressor speed does not result in appreciable changes in air flow rate. Combustion air supply is thus not used as a manipulated variable. This is

consistent with industrial practice where the combustion air blower is operated close to maximum capacity with the blower speed regulator operated manually.

- Wet gas compressor throughput is often used to regulate reactor pressure. Since it was intended to examine the effect of variations in reactor pressure on overall FCCU operation, the wet gas compressor throughput was not used as a manipulated variable. The wet gas compressor is also operated near maximum capacity.

- Regenerator dense bed temperature, regenerator cyclone temperature and flue gas CO concentration are sometimes used as controlled variables (Hovd and Skogestad 1993, Lee and Groves Jr. 1985, McFarlane et al. 1993). Owing to the strong interaction between the reactor and regenerator sections, regenerator temperature and reactor riser temperature are closely related. Recall that riser temperature influences product yield and distribution and therefore plant economics. Regenerator temperature responds relatively slowly to process changes owing to the large thermal inertia of the regenerator section (Hovd and Skogestad 1993). Therefore riser temperature is generally the controlled variable.

- Low concentrations of CO (ppm range) or excess O_2 in the flue gas line indicates total combustion operation. However, energy is required to provide O_2 (air) and it is economically beneficial to have just enough excess of O_2 to ensure operation in the total combustion mode. Controlling CO concentration in the flue gas line would not guarantee minimal excess O_2 in the flue gas line. Therefore O_2 concentration is the controlled variable.

- In total combustion operation with sufficient CO combustion promoter, there is relatively little afterburn in the regenerator catalyst disengaging zone and cyclone temperatures are typically below the metallurgical limits. This is not the case for partial combustion operation where afterburn can raise cyclone temperatures close to the metallurgical limits. In partial combustion mode,

cyclone temperatures must be monitored to prevent meltdowns. It is assumed that cyclone temperatures are well below the metallurgical limit since the FCCU is operated in total combustion mode.

3.2.1 Uncertainty and Performance Description

Our analysis is based on linear models derived by linearizing the nonlinear model around the operating point tabulated in Appendix A. The open loop step responses to a 0.2 (scaled) step in feed coking characteristic for the linear and nonlinear models are compared in Appendix A. The frequency range of interest (expected closed loop bandwidth) was taken to be 10^{-4}rad/s to 10^{-2}rad/s which corresponds to process variations on time scales of minutes to hours. Note that for these time scales, the dynamic response of the linear and nonlinear models are close (Appendix A, Figure A.1). Unless otherwise stated, the response plots are those observed with the linear model. The state space models for several selected control schemes are listed in Appendix B.

Since our control objective is effective disturbance rejection, the μ-optimal controllers were designed to minimize the ∞-norm of the weighted sensitivity function. Thus for each control scheme an optimal controller was synthesized and the closed loop performance achievable with this controller examined. The controllers were synthesized using software available in the μ - Analysis and Synthesis Toolbox (Balas, Doyle, Glover, Packard and Smith 1991) in MATLAB. Excellent descriptions of the calculation, interpretation and use of μ are given in Balas et al. (1991) and Morari and Zafiriou (1989). A reasonable representation of model uncertainty is needed before the controllers can be synthesized. The uncertainty description adopted for this study will be discussed next. Note that unless explicitly stated, the analysis is carried out on the linearized models.

The model adopted for this study is only an approximate description of the actual FCCU process. In practice, model uncertainty is always present. An uncertainty model based on heuristic arguments has been adopted for this study. The formulation

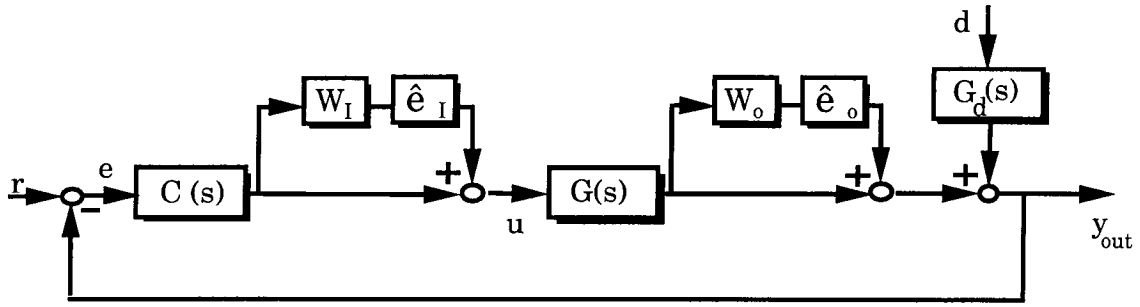

Figure 3.1: Closed loop system. Δ_I - complex, diagonal, Δ_O - complex, full block. $\bar{\sigma}(\Delta_I) \leq 1$, $\bar{\sigma}(\Delta_O) \leq 1$

of the uncertainty model closely follows the procedure described in the μ - Analysis and Synthesis Toolbox (Balas et al. 1991) as well as the guidelines specified in Lundström, Skogestad and Wang (1991). The uncertainty description postulated includes plant input and plant output uncertainty. The physical interpretation of these uncertainties are actuator uncertainty and measurement uncertainty respectively. Clearly, the uncertainty level is dependent on frequency - it is difficult to accurately follow a rapidly changing signal while a slowly varying signal can be tracked relatively accurately. The block diagram used for closed loop analysis is shown in Figure 3.1. At any frequency, the actual uncertainty level is given by $|W_I|$ and $|W_O|$. The blocks Δ_I and Δ_O are transfer matrices. The structures of Δ_I and Δ_O are pre-specified but the actual transfer functions are unknown except that they are norm bounded:

$$\bar{\sigma}(\Delta_I) \leq 1 \qquad\qquad \bar{\sigma}(\Delta_O) \leq 1 \tag{3.4}$$

The unknown transfer matrices Δ_I and Δ_O are used to parameterize the difference between the nominal plant $G(s)$ and the real plant *i.e.* the model uncertainty. The actual uncertainty level assumed is described below.

- *Input (Actuator) Uncertainty* - The inability of the process actuators to exactly follow the controller signal is accounted for explicitly. As mentioned before, actuators will be able to follow rapidly varying control signals only approximately while slowly varying signals will be tracked relatively accurately. A low

frequency ($\omega < 10^{-3}$ rad/s) uncertainty of 5% was assumed in each input signal increasing to 50% uncertainty at high frequency ($\omega > 10^{-1}$ rad/s). At even higher frequencies ($\omega \gg 10^{-1}$ rad/s) one can expect complete phase uncertainty (uncertainty > 100%). Closed loop robust performance analysis indicates that all the results hold even with more conservative uncertainty bounds (*i.e.* uncertainty level > 50% for $\omega > 10^{-1}$ rad/s). It is assumed that the actuators are independent of each other. The uncertainty in each input signal is therefore expected to be independent and Δ_{I} is assumed diagonal (no manipulated variable interactions). A magnitude/frequency plot for the uncertainty model in each input variable is shown in Figure 3. The transfer function used for the uncertainty description is:

$$w_{\mathrm{o}} = w_{\mathrm{i}} = 0.05\frac{129.515s + 1}{12.952s + 1} \tag{3.5}$$

$$W_{\mathrm{I}} = w_{\mathrm{i}} I \tag{3.6}$$

$$W_{\mathrm{O}} = w_{\mathrm{o}} I \tag{3.7}$$

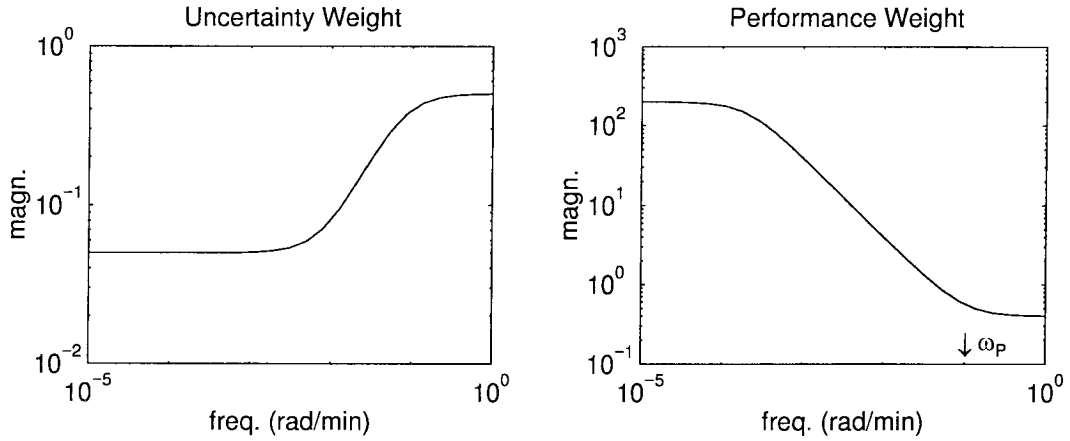

Figure 3.2: Uncertainty and performance specifications. $\omega_p = 0.1$ rad/s.

- *Output (Measurement) Uncertainty* - Owing to sensor limitations, the actual plant output may differ from what is measured. Uncertainty in each output sig-

nal was modeled in the same manner as input uncertainty and W_O is assumed diagonal. It is more difficult to ascribe output uncertainty to sensor error only. Other factors including unmodeled plant dynamics may also contribute to output uncertainty. Such possible interactions between different output signals are accounted for by making Δ_O full block.

- *Performance Specification* - The control objective for all cases in this paper is effective disturbance rejection. The performance requirements are:

  1. high frequency disturbance amplification by a factor of at most 2.5
  2. steady–state offset of at most 0.5 %

  The transfer function for the performance weights is :

$$w_P = 200 \frac{\frac{1}{\omega_p} s + 1}{\frac{500}{\omega_p} s + 1} \tag{3.8}$$

$$W_P = w_P I \tag{3.9}$$

  The performance requirement for each output variable was assumed to be the same. This is justified since the output variables were scaled so that any output error was equally significant. A magnitude/frequency plot for the performance weight is plotted in Figure 3.2. The 'corner frequency' ω_p (Equation 3.8) is used as an adjustable parameter to quantify the best achievable performance for a given control scheme. Higher ω_p (Figure 3.2) implies faster closed loop response (Lundström et al. 1991).

3.3 Analysis of Model A (Original Model IV FCCU)

3.3.1 Open Loop Analysis of Model A

Figure 3.3 is a plot of the maximum and minimum singular values of the plants corresponding to control schemes SI, SII and SIII as a function of frequency. The maximum singular value of the disturbance transfer function matrix ($\bar{\sigma}(G_d)$) is also plotted.

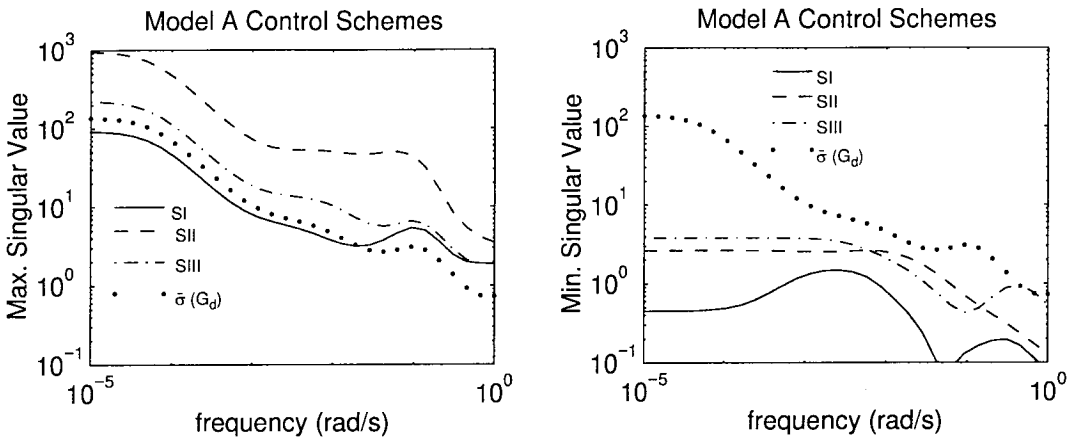

Figure 3.3: Frequency response plots for disturbance model and schemes SI, SII & SIII, Model A

Note that the maximum plant gain for scheme SI is smaller than the maximum disturbance gain suggesting that the available control action might be insufficient to reject expected disturbances.

The catalyst flow behavior between the reactor and regenerator section is an important operational parameter in FCCU operation. Figure 3.4 shows the change in catalyst circulation rate at steady–state as a function of change in reactor pressure (in open loop). The nonlinear model was used to obtain the data in Figure 3.4. ΔP_{frac} was stepped up and the system allowed to attain steady–state. The changes in catalyst circulation rate and reactor pressure were noted. Clearly increased reactor pressure leads to increased catalyst circulation rate at steady–state *i.e.* there is a positive gain between changes in catalyst circulation rate and changes in reactor pressure.

The steady–state effect of a step increase in reactor pressure (ΔP_r) on catalyst circulation rate is examined for model A. In particular we want to determine if the positive gain is generic for systems of this type or a consequence of the particular parameter choices. It is expected and our simulations show that positive ΔP_r results in a shift of catalyst from the reactor to the regenerator section. To explain the positive gain, the following question is posed for each catalyst U-bend: *How much catalyst must be transferred from the reactor to regenerator to exactly counter balance*

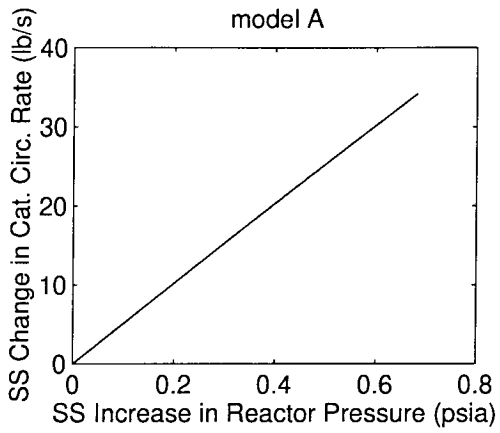

Figure 3.4: Model A dependence of catalyst circulation rate on changes in reactor pressure (ΔP_r) at steady–state

the increased reactor pressure so that there is no change in catalyst driving force in that U-bend at steady–state? The independent variable is clearly ΔP_r and the dependent variable is taken to be the decrease in catalyst level in the reactor (ΔH_{str}) which is a measure of how much catalyst has been transferred. By deriving the requisite relations for the regenerated and spent catalyst U-bends it is possible to determine conditions under which the steady–state catalyst circulation rate will increase or decrease for a ΔP_r increase in reactor pressure. These bounds are derived below for model A.

Of the total amount of catalyst shifted from the reactor to the regenerator section (ΔW_{str}), a fraction ends up in the standpipe (ΔW_{sp}) and the remainder in the regenerator dense bed (ΔW_{reg}) at steady–state. This split is accounted for by defining a parameter α as follows:

$$\alpha = \frac{\Delta W_{sp}}{\Delta W_{str}} \tag{3.10}$$

We address the above question for each catalyst U-bend separately, and consider the steady–state condition after a ΔP_r increase in reactor pressure:

Regenerated catalyst U-bend: To exactly counter balance the increased reactor pressure so that there is no change in catalyst driving force in the regenerated catalyst

U-bend, it is required that:

$$144 \times \Delta P_r = \frac{\Delta W_{sp} \frac{g}{g_c}}{A_{sp}} = \frac{\alpha \Delta W_{str} \frac{g}{g_c}}{A_{sp}} \tag{3.11}$$

the second relation is from the definition of α in Equation 3.10. Note that $\Delta W_{str} = \Delta H_{str} A_{str} \rho_c$, and so

$$144 \times \Delta P_r = \frac{\alpha \Delta H_{str} A_{str} \rho_c \frac{g}{g_c}}{A_{sp}} \tag{3.12}$$

However, if:

$$144 \times \Delta P_r < \frac{\alpha \Delta H_{str} A_{str} \rho_c \frac{g}{g_c}}{A_{sp}} \tag{3.13}$$

then the regenerated catalyst flow rate *increases*. Therefore, the condition for a net increase in regenerated catalyst flow rate at steady–state for step increase in ΔP_r is given by:

$$\frac{\Delta H_{str}}{\Delta P_r} > \frac{1}{\alpha} \frac{A_{sp}}{A_{str}} \frac{1}{\rho_c} \frac{144}{g/g_c} \tag{3.14}$$

Spent catalyst U-bend: To exactly counter balance the increased reactor pressure so that there is no change in catalyst driving force in the spent catalyst U-bend, it is required that the increase in the catalyst head in the regenerator and the stripper balance the increased reactor pressure:

$$144 \times \Delta P_r = \frac{\Delta W_{reg} \frac{g}{g_c}}{A_{reg}} + \frac{\Delta W_{str} \frac{g}{g_c}}{A_{str}} \tag{3.15}$$

Note that $\Delta W_{reg} = (1-\alpha)\Delta W_{str} = (1-\alpha)\Delta H_{str} A_{str} \rho_c$, and substituting into Equation 3.15, we get:

$$144 \times \Delta P_r = \frac{\Delta H_{str} \rho_c}{A_{reg}} \left[A_{reg} + (1-\alpha) A_{str} \right] \frac{g}{g_c} \tag{3.16}$$

However if:

$$144 \times \Delta P_r > \frac{\Delta H_{str} \rho_c}{A_{reg}} \left[A_{reg} + (1-\alpha) A_{str} \right] \frac{g}{g_c} \tag{3.17}$$

then the spent catalyst flow rate *increases*. Therefore, the condition for a net increase

in spent catalyst flow rate at steady–state for a step increase in ΔP_r is given by:

$$\frac{\Delta H_{str}}{\Delta P_r} < \frac{A_{reg}}{A_{reg} + (1-\alpha)A_{str}} \frac{1}{\rho_c} \frac{144}{g/g_c} \tag{3.18}$$

Therefore bounds on $\Delta H_{str}/\Delta P_r$ for which there will be a net *increase* in the overall catalyst circulation rate at steady–state for an increase in reactor pressure are obtained by combining the two conditions (Equation 3.14 and Equation 3.18) above to yield:

$$\frac{1}{\alpha} \frac{A_{sp}}{A_{str}} \frac{1}{\rho_c} < \frac{\Delta H_{str}}{\Delta P_r} < \frac{A_{reg}}{A_{reg} + (1-\alpha)A_{str}} \frac{1}{\rho_c} \tag{3.19}$$

For model A α is close to one for all observed cases ($\alpha > 0.9$ typically). Thus after a process upset essentially all the catalyst shifted from the reactor to the regenerator section ends up in the standpipe once the system settles. Substituting $\alpha = 1$ in Equation 3.19 yields:

$$\frac{A_{sp}}{A_{str}} \frac{1}{\rho_c} < \frac{\Delta H_{str}}{\Delta P_r} < \frac{1}{\rho_c} \tag{3.20}$$

Note that for $A_{sp} < A_{str}$ (as in Model A) there will be an increase in catalyst circulation rate at steady–state for an increase in reactor pressure. $A_{sp} < A_{str}$ is typically the case in Model IV FCCUs.

3.3.2 Closed Loop Analysis of Model A

The steady–state plant condition numbers as well as any RHPT zeros for model A schemes SI, SII and SIII are summarized in Table 3.2. All three schemes are ill-conditioned indicating that while nominal performance and robust stability might be satisfied, robust performance could be unsatisfactory (Morari and Zafiriou 1989, Skogestad et al. 1988).

Figure 3.5 is a plot of the robust performance μ, (μ_{RP}) for model A control schemes SI, SII and SIII. For all three cases $\mu_{RP} > 1$ over the frequency range of interest indicating that there are plants in the uncertainty set for which the designed controllers would be unable to provide the requisite performance. However in all three cases, robust stability was achieved (plot not shown) and the closed loop system would

Scheme	Condition #	RHPT zero
SI	207	none
SII	363	0.273
SIII	59.4	none

Table 3.2: Steady–state plant condition number and location of RHPT zero for Model A control schemes

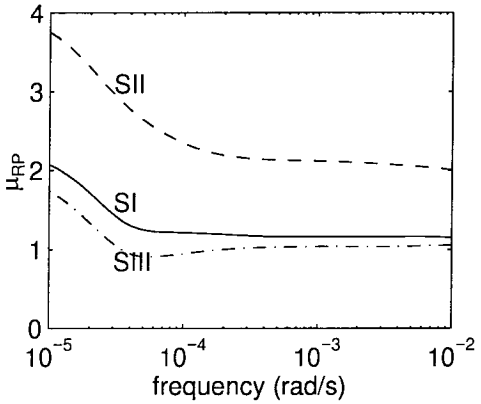

Figure 3.5: Robust performance comparison for Model A, schemes SI, SII & SIII, $\omega_p = 0.01$

be stable for all allowable perturbations.

The time responses of model A schemes (nominal plants) to a unit step in ΔP_{frac} (disturbance d_3) are shown in Figure 3.6. Pressure upsets in down stream units propagating back to the FCC section are the most severe disturbances for this system. The other significant disturbance is variations in feed quality, but this disturbance eventually affects reactor pressure as well. In practice it is desirable to reject disturbances within about ten to fifteen minutes from the onset and therefore $\omega_p = 0.01$ for all cases considered in model A. The controlled variables (Figure 3.6) display relatively large deviations from their steady–state values during the disturbance transient period. In addition it is not possible to reject a unit step disturbance in d_3 using scheme SI (more control action required than is available). Note that the transient deviations of the controlled variables from steady–state are largest for scheme SII (largest μ_{RP} over frequency) and smallest for scheme SIII (smallest μ_{RP} over frequency).

Catalyst circulation rates are also observed to undergo large fluctuations (Fig-

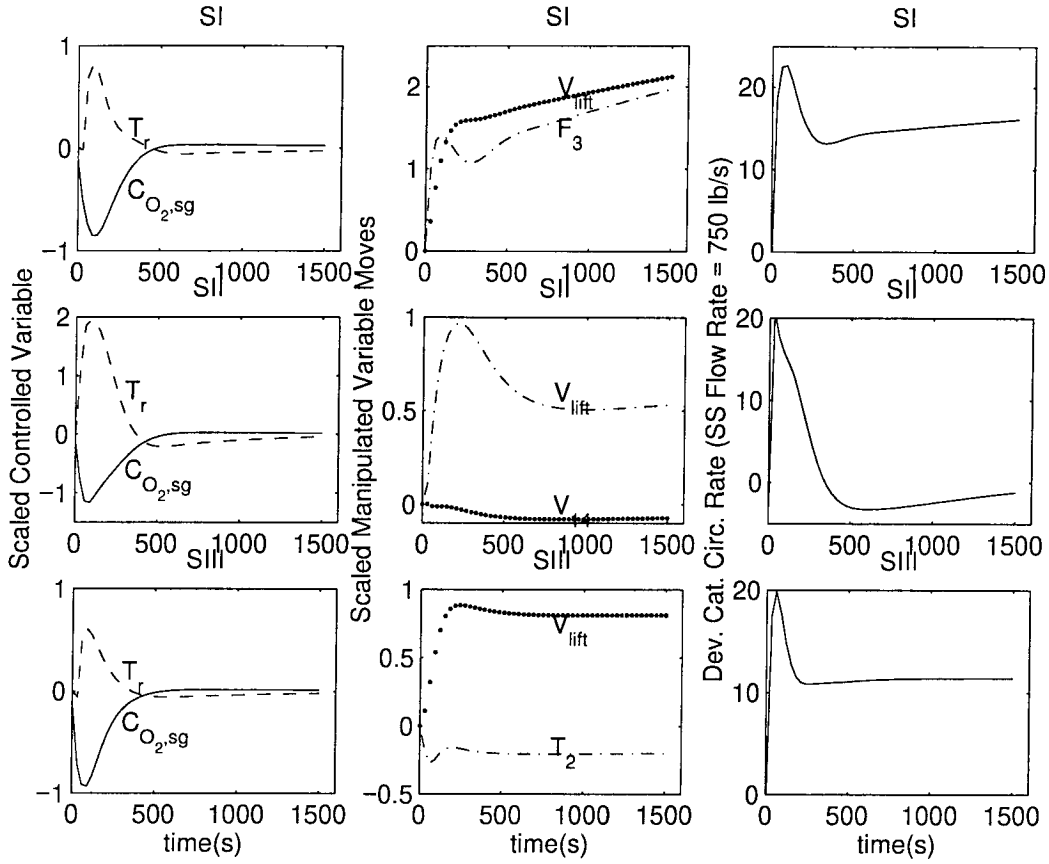

Figure 3.6: Closed loop time response to unit step in fractionator pressure for Model A schemes, $\omega_p = 0.01$ rad/s

ure 3.6). It is shown later that in open loop the deviation of output variables from steady–state is directly related to the deviation of catalyst flow rate from steady–state. Large fluctuations in controlled variables and catalyst flow rate are expected for model A owing to the use of an overflow weir and standpipe setup in the regenerator section which serves to convey regenerated catalyst to the riser. Regenerator dense bed catalyst is fluidized by passage of combustion air through it and flows over the weir into the standpipe (Figure 1). Since catalyst particles are small and the bed is fluidized, slight variations in regenerator bed height cause relatively large variations in catalyst flow rate over the weir. Furthermore, since the cross-sectional area of the standpipe is small compared to the cross-sectional area of the regenerator ($7ft^2$ vs 590 ft^2) small variations in regenerator bed height will result in significant variations in

standpipe inventory level and therefore regenerated catalyst flow rate. The equation governing catalyst flow over the weir is given by:

$$F_{sp} = f_{of}\sqrt{A_{sp}}(z_{bed} - 13) + \beta \tag{3.21}$$

where f_{of} is the overflow factor. For a given standpipe area, f_{of} measures sensitivity of catalyst flow over the weir to changes in dense bed height. In the original problem formulation, this factor was 424. Small changes in dense bed height therefore result in relatively large changes in catalyst flow over the weir - leading to large changes in regenerated catalyst flow rate to the riser. Lowering f_{of} would be expected to reduce changes in flow rate over the weir and minimize variations in catalyst flow rate.

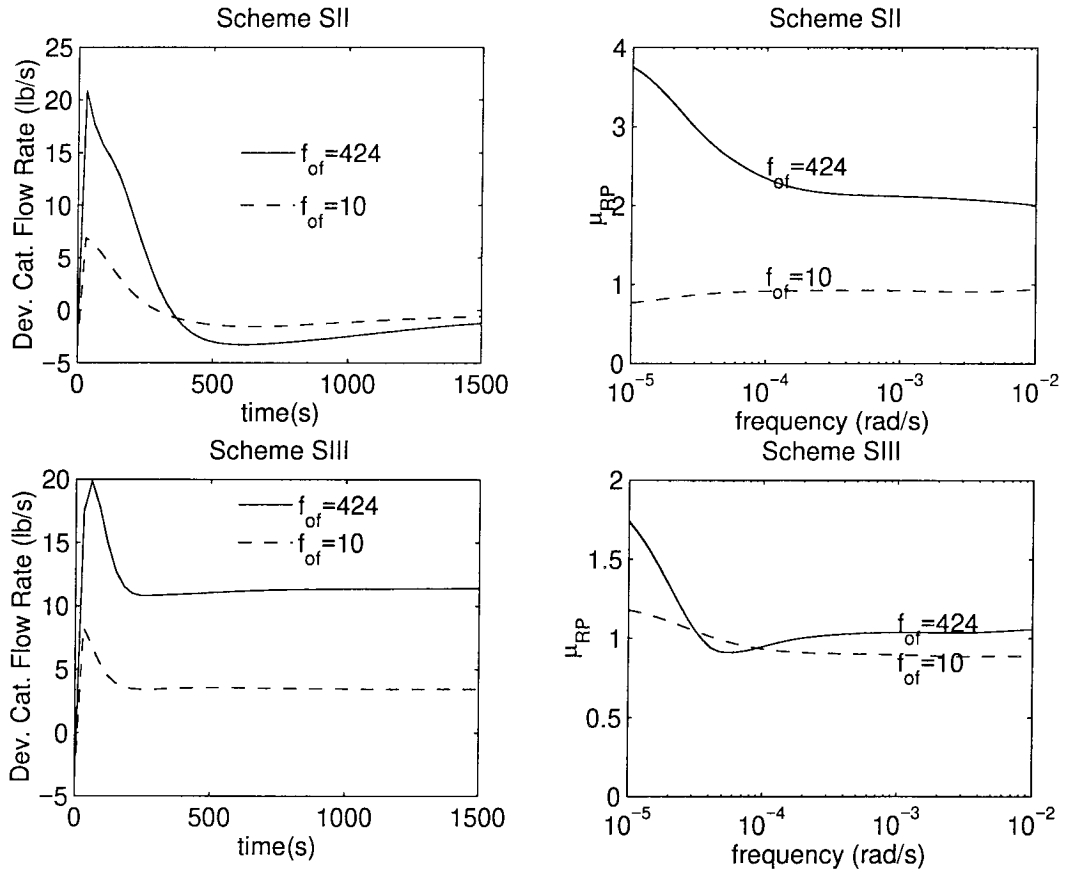

Figure 3.7: Comparison of time response and μ_{RP} for f_{of}=424 & f_{of}=10, Model A, schemes SII & SIII, $\omega_p = 0.01$

	SII		SIII	
f_{of}	Condition #	RHPT zero	Condition #	RHPT zero
424	363	0.273	59.4	none
10	6.54	9.96×10^{-3}	4.23	none

Table 3.3: Steady-state condition # and location of plant RHPT zero(s) for model A schemes SII & SIII, for $f_{of} = 10$ and $f_{of} = 424$.

Figure 3.7 shows the closed loop response of catalyst circulation rate to a unit step in fractionator pressure (disturbance d_3) for two different values of f_{of} as well as a μ_{RP} comparison for the two cases ($f_{of} = 424$ and $f_{of} = 10$). Two control schemes are considered - SII & SIII. The plant condition number as well as any RHPT zeros for schemes SII and SIII are tabulated in Table 3.3 for $f_{of} = 10$ and $f_{of} = 424$. Fluctuations in catalyst circulation rate are reduced by lowering f_{of}. Robust performance is also improved. To accomplish the reduction in f_{of} the constant factor β was adjusted to maintain F_{sp} constant for both runs while f_{of} was changed.

It is evident that design or operational modifications made to model A to damp out fluctuations in catalyst flow rate are expected to improve closed loop performance of the unit and reduce disturbance sensitivity. It is difficult to reliably alter the overflow factor to reduce fluctuations in catalyst flow rate in model A. Two physically implementable modifications to model A are considered next.

3.4 Flooding the Weir and Standpipe in Regenerator Section

The operational modification implemented in this study was to increase catalyst inventory and operate the regenerator section with catalyst level above the standpipe, thereby ensuring that the standpipe is always full, Figure 3.8. The operation of the rest of the unit remains unchanged. This operational modification could be implemented in practice by adding catalyst to the unit and then maintaining total catalyst inventory at the requisite level. We will refer to this unit as **model B**.

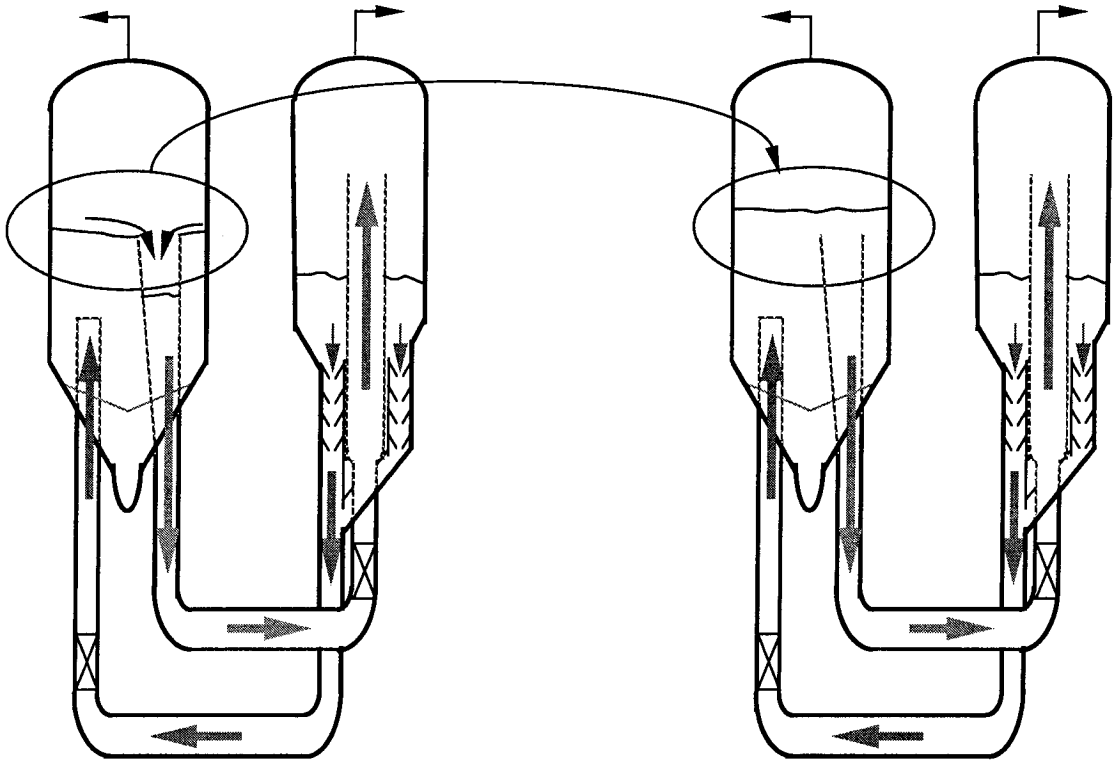

Figure 3.8: Operational modification to Model A - weir flooded

The primary difference between model A and model B is that model B is operated with the weir flooded and the standpipe always full. Therefore the component of driving force due to catalyst level in the standpipe in model A is replaced with regenerator dense bed height in model B. Several alternatives are available to compensate for the increased driving force due to additional catalyst head in the filled standpipe. For this study we reduced regenerator pressure and incorporated restrictions in the catalyst U-bends to generate additional pressure drop. The equation used to model the additional pressure drop is of the form:

$$\Delta P = \frac{1}{2} N \rho_c \frac{v^2}{g_c} \tag{3.22}$$

N = N_{rgc} = 26 for regenerated catalyst line

N = N_{sc} = 22 for spent catalyst line

The additional pressure drop reduces overall driving force for both the regenerated catalyst flow and spent catalyst flow. N was used as an adjustable parameter to attain the desired pressure drop to maintain model B operating conditions within acceptable limits and close to the operating conditions in Model A. Note the use of specific values for the number of velocity heads in the regenerated and spent catalyst lines in model B (Equation 3.22). While actual quantitative results will vary somewhat with the selected values for N_{rgc} and N_{sc}, the observations and conclusions are unaffected by the selection. Figure 3.9 shows flow characteristic plots for different values of N_{rgc} and N_{sc} including the case $N_{rgc} = N_{sc} = 0$ which corresponds to merely flooding the standpipe. In all cases the important flow characteristic, namely a negative gain between changes in reactor pressure and changes in catalyst circulation rate, is preserved.

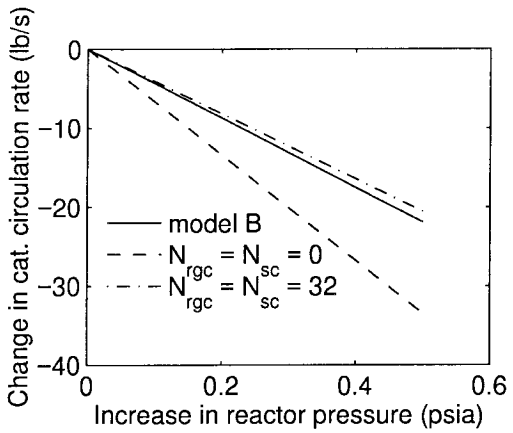

Figure 3.9: Catalyst flow sensitivity to reactor pressure for different N_{rgc} and N_{sc} in Model B type setup. For Model B, $N_{rgc} = 26$, $N_{sc} = 22$

Operating the FCCU as in model B should damp out fluctuations in catalyst circulation rate since relative changes in regenerator bed height are small owing to the large cross sectional area of the regenerator section. It must be stressed that the critical modification made in model B is the flooding of the weir and standpipe.

3.4.1 Open Loop Analysis of Model B

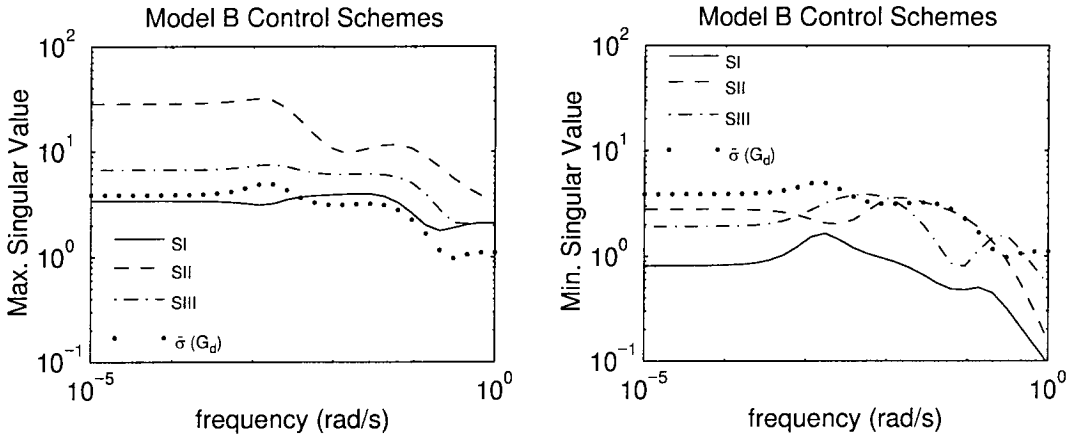

Figure 3.10: Frequency response plots for disturbance model and schemes SI, SII & SIII, Model B

Figure 3.10 is a plot of the maximum and minimum singular values of the control schemes SI, SII and SIII as a function of frequency. The maximum singular value of the disturbance transfer function matrix is also plotted. Note that as in model A the maximum plant gain for scheme SI is smaller than the maximum disturbance gain suggesting possible manipulated variable constraint problems.

Catalyst flow characteristics for model B are different from those in model A. Contrary to Model A, in model B increased reactor pressure results in *decreased* catalyst circulation rate at steady–state *i.e.* negative gain between changes in catalyst flow rate and changes in reactor pressure (Figure 3.11). Figure 3.11 was obtained in the same manner as Figure 3.4.

Bounds similar to those for model A relating the dependence of changes in catalyst circulation rate on changes in reactor pressure are derived for model B. Note that the parameter α described for model A does not apply to model B as all th catalyst transferred to the regenerator ends up in the regenerator dense bed *i.e.* $\Delta W_{reg} = \Delta W_{str}$.

Regenerated catalyst U-bend: To exactly counter balance the increased reactor pressure so that there is no change in catalyst driving force in the regenerated catalyst

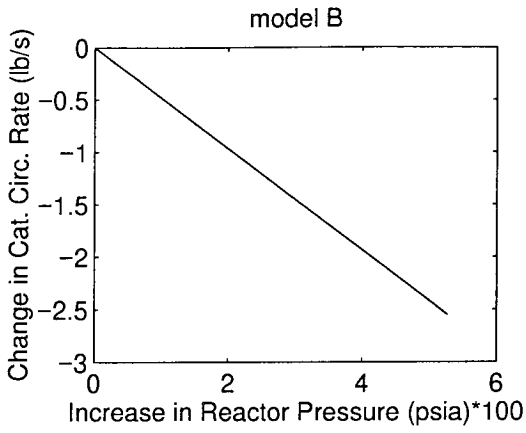

Figure 3.11: Model B dependence of catalyst circulation rate on changes in reactor pressure at steady–state

U-bend, it is required that:

$$144 \times \Delta P_r = \Delta \frac{\Delta W_{reg} \frac{g}{g_c}}{A_{reg}} \tag{3.23}$$

Note that for model B, $\Delta W_{reg} = \Delta W_{str} = \Delta H_{str} A_{str} \rho_c$. Substituting this into the previous equation, we get the condition for a net decrease in regenerated catalyst flow rate at steady–state for step increase in ΔP_r to be:

$$\frac{\Delta H_{str}}{\Delta P_r} < \frac{A_{reg}}{A_{str}} \frac{1}{\rho_c} \frac{144}{g/g_c} \tag{3.24}$$

Spent catalyst U-bend: To exactly counter balance the increased reactor pressure so that there is no change in catalyst driving force in the spent catalyst U-bend, it is required that the increase in the catalyst head in the regenerator and the stripper balance the increased reactor pressure:

$$144 \times \Delta P_r = \frac{\Delta W_{reg} \frac{g}{g_c}}{A_{reg}} + \frac{\Delta W_{str} \frac{g}{g_c}}{A_{str}} \tag{3.25}$$

Therefore, the condition for a net decrease in spent catalyst flow rate at steady–state

Scheme	Condition #	RHPT zero
SI	4.22	2.86×10^{-3}
SII	10.2	$1.858 \pm i11.1$
SIII	3.51	1.762×10^{-3}

Table 3.4: Steady–state plant condition number and location of RHPT zero for Model B control schemes.

for a step increase in ΔP_r is given by:

$$\frac{\Delta H_{str}}{\Delta P_r} > \frac{A_{reg}}{A_{reg} + A_{str}} \frac{1}{\rho_c} \frac{144}{g/g_c} \tag{3.26}$$

Combining the conditions in Equation 3.24 and Equation 3.26 gives bounds on $\Delta H_{str}/\Delta P_r$ for which there will be a *decrease* in catalyst flow rate for an increase in reactor pressure:

$$\frac{A_{reg}}{A_{reg} + A_{str}} \frac{1}{\rho_c} < \frac{\Delta H_{str}}{\Delta P_r} < \frac{A_{reg}}{A_{str}} \frac{1}{\rho_c} \tag{3.27}$$

Clearly an increase in reactor pressure cannot possibly lead to an increase in catalyst circulation rate at steady–state for model B regardless of the cross-sectional areas of any of the units $(A_{sp}, A_{reg}, A_{str})$. The bounds for model A which would result in a decrease in catalyst circulation rate are given by Equation 3.19:

$$\frac{A_{reg}}{A_{reg} + (1-\alpha)A_{str}} \frac{1}{\rho_c} < \frac{\Delta H_{str}}{\Delta P_r} < \frac{1}{\alpha} \frac{A_{sp}}{A_{str}} \frac{1}{\rho_c} \tag{3.28}$$

By suitable interpretation of α (for model B) the bounds for model A and model B can be shown to be similar. Note that A_{sp} in model A must be replaced by A_{reg} in model B.

3.4.2 Closed Loop Analysis for Model B

The steady–state plant condition numbers as well as any RHPT zeros for model B schemes SI, SII and SIII are summarized in Table 3.4.

The steady–state plant condition numbers for model B schemes are much lower than the corresponding values for model A schemes. Control scheme SII has a RHPT

zero outside the frequency range of interest and should not limit the achievable performance. However schemes SI and SIII have RHPT zeros which are within the frequency range of operation and limit the achievable performance. $\mu_{RP} \simeq 4$ for scheme SI and $\mu_{RP} \simeq 7$ for scheme SIII. In rejecting unit step disturbances, large overshoots in controlled variables were observed for schemes SI and SIII compared to scheme SII. The plots are not shown for brevity.

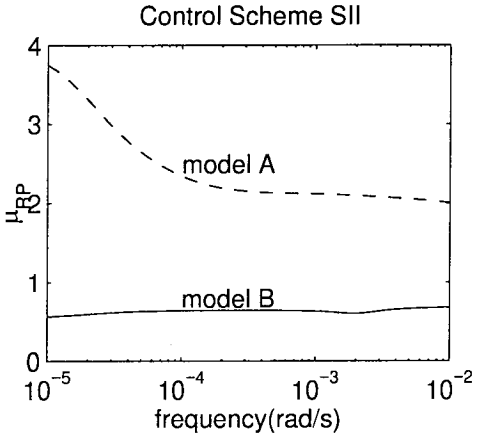

Figure 3.12: Robust performance comparison for Model A & Model B. Identical uncertainty & performance specs. $\omega_p = 0.01$

Figure 3.12 is a μ_{RP} plot for model A scheme SII and model B scheme SII for identical uncertainty and performance specifications. Note that $\omega_p = 0.01$ for both cases although model B can be expected to have faster closed loop response. A μ-optimal controller was designed for model B that guaranteed robust performance while the μ-optimal controller for model A could not guarantee desired performance given the expected uncertainties, disturbances and performance requirements.

Figure 3.13 shows the closed loop response of model B, control scheme SII to a unit step disturbance in fractionator pressure. Compared to the closed loop response for model A, scheme SII (Figure 3.6) the fluctuations in catalyst flow rate as well as controlled variable deviations from their steady–state values during the process transients are significantly reduced. Model B response is also faster than Model A response. A significant improvement in closed loop robust performance of the model IV FCCU is attainable simply by operating the unit as in model B. Physical

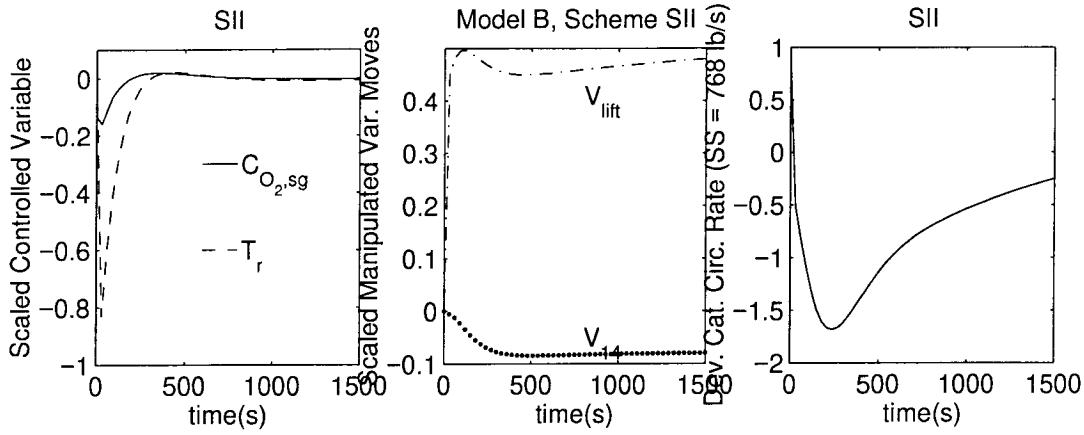

Figure 3.13: Closed loop time response of Model B, scheme SII to a unit step in ΔP_{frac}. $\omega_p = 0.01$

justification for the improved performance of model B compared to model A will be discussed next in the context of the different flow characteristics of models A and B.

3.5 Comparison of Flow Characteristics for Models A and B

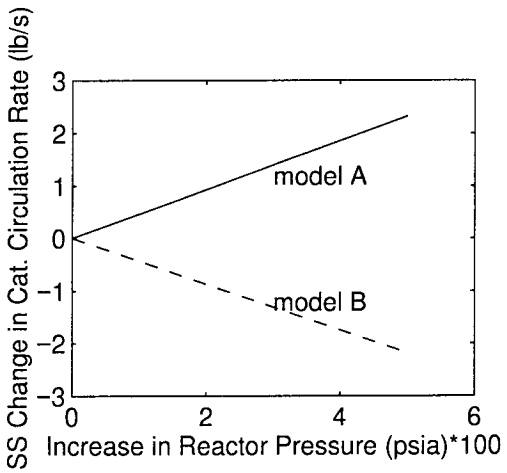

Figure 3.14: Steady–state variation in catalyst flow rate with increase in reactor pressure (nonlinear models)

Figure 3.14 shows steady–state changes in catalyst flow rate as a function of

increase in reactor pressure for models A and B. In addition to reactor pressure fluctuations, temperature variations in the reactor and regenerator also affect catalyst circulation rates as follows:

- Regenerator - variations in regenerator dense bed temperature affect regenerator gas pressure. However regenerator temperature does not change appreciably under normal conditions ($\pm 15°F$) and regenerator gas volume is large. Regenerator gas pressure changes are thus small and are ignored.

- Reactor riser - temperature variations in the reactor riser affect wet gas production rate which in turn affects reactor pressure.

Thus reactor temperature has the most significant effect on catalyst circulation rate. We show that due to the effect of temperature changes on catalyst circulation rate it is desirable to have a decrease in catalyst circulation rate at steady–state for an increase in reactor pressure (negative gain between reactor pressure changes and catalyst circulation rate changes).

Suppose an FCCU such as model A where there is a positive gain between reactor pressure and catalyst circulation rate is subjected to a disturbance which increases reactor pressure. Catalyst flow rate increases, elevating riser temperature. Increased riser temperature results in higher wet gas production rate and yet higher reactor pressure. Steady–state is reached when the net increase in driving force (due to pressure and catalyst head) is balanced by the additional pressure drop due to increased catalyst circulation rate. The effect of the disturbance is therefore amplified for FCCUs with positive gain between changes in reactor pressure and catalyst circulation rate.

The argument can be reversed for a setup like model B with a negative gain between changes in reactor pressure and changes in catalyst circulation rate. In model B the net effect of disturbances is reduced. This phenomenon is shown in Figure 3.15a where the actual reactor pressure change at steady–state is plotted as a function of change in ΔP_{frac}. The solid line is the expected reactor pressure change (ΔP_{frac}) in the absence of any other effects. The actual reactor pressure changes are larger than

expected for model A and lower than expected for model B as predicted. Figure 3.15b shows the corresponding steady–state change in catalyst circulation rate. For each model the change in catalyst circulation rate is plotted as a function of the change in ΔP_{frac} when temperature effects are ignored and when temperature effects are taken into consideration. Note that for model A the increase in catalyst circulation rate for the actual process operation is much larger than if temperature effects were ignored - showing that the effect of the disturbance is amplified in model A. For model B the absolute change in catalyst circulation rate is lower in actual operation than when temperature effects are ignored.

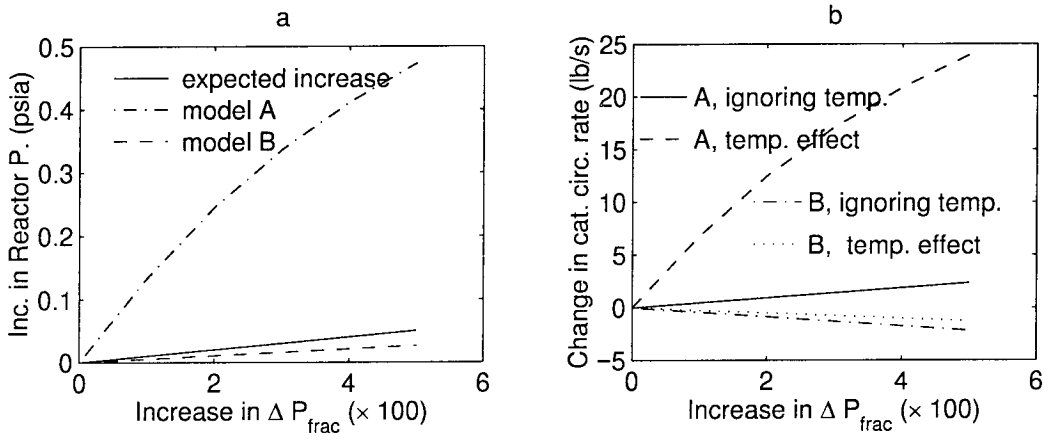

Figure 3.15: Effect of change in ΔP_{frac} on Models A & B (nonlinear models)

Note from Figure 3.14 that for a given increase in reactor pressure, the absolute change in catalyst circulation rate is essentially the same for models A and B. Furthermore, the changes in catalyst circulation rate are proportional to changes in reactor pressure for both models. Figure 3.15a shows that there are larger changes in reactor pressure for model A than model B for identical disturbances (ΔP_{frac}) to the systems. Thus if one could independently control reactor pressure in model A and keep variation in reactor pressure small, then the fluctuations in catalyst circulation rates would be reduced for model A. It is common practice in industry to control reactor pressure by manipulating the wet gas compressor throughput (Hovd and Skogestad 1993, Lee and Groves Jr. 1985). Our quantitative arguments support

this practice.

Important controlled variables like riser temperature and flue gas O_2 concentration are directly related to catalyst circulation rate. Changes in circulation rates lead to proportional changes in controlled variables (Figure 3.16). Increased catalyst flow for model A results in higher coke transport rate to the regenerator which consumes additional O_2 from the air supply and $C_{O_2,fg}$ decreases in the absence of any corrective action. Reactor temperature rises with increased regenerator temperature. Since catalyst circulation rate is lower for model B there is less coke being transported to the regenerator and less O_2 being consumed in combustion and $C_{O_2,fg}$ goes up. Reactor temperature decreases with regenerator temperature.

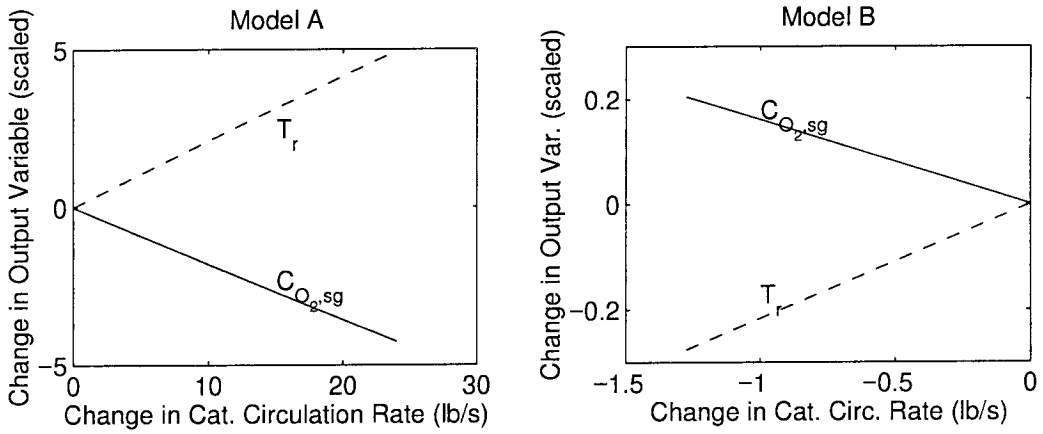

Figure 3.16: Relation between controlled vars. and changes in catalyst circ. rate (nonlinear models)

3.5.1 FCCU Design Guidelines

From the discussions in the last section the following design guidelines can be deduced so that FCCUs have low disturbance sensitivity. Ideally there should be no variations in catalyst circulation rate in the face of disturbances. In practice the objectives should be:

1. Design the FCCU so that the gain between changes in reactor pressure and changes in catalyst circulation rate at steady–state is negative.

2. Design the FCCU flow system so that only small variations in catalyst flow rate occur when subjected to disturbances.

Most FCCUs have slide valves installed in the catalyst circulation lines to actively control catalyst circulation rate. The improvement in achievable performance when slide valves are installed in the catalyst U-bends of model B is now compared to the achievable performance of model B.

3.6 Installing Control Slide Valves in Catalyst Flow Lines

The main objective of using control slide valves in catalyst circulation lines is to control catalyst flow rates but these are not available in model A or model B except for emergency closure in the event of catalyst flow reversal. Model IV FCCUs are sometimes refitted to incorporate slide valves that can be used to control catalyst circulation rate between the reactor and regenerator. This design modification was modeled and studied. The slide valve model used is described in detail in Appendix C. Slide valves were introduced into both the regenerated catalyst line and the spent catalyst line and were nominally 50% open. To regain some of the pressure drop across the slide valves it was necessary to implement the following *design* modifications as well, Figure 3.17.

1. fresh feed inlet point was lowered from 124.5 ft to 118 ft
2. lift air inlet to standpipe was lowered from 134 ft to 98 ft
3. length of lift pipe was increased from 34 ft to 70 ft
4. J-bends were introduced to assist in feed oil and lift air entry
5. overall catalyst inventory was raised so that catalyst level in the regenerator was higher than the weir. Thus the weir was flooded and standpipe was operated so

Notation	Controlled Variables	Manipulated Variables
SIV	$C_{O_2,fg}$, T_r	V_{lift}, $X_{sv,rgc}$

Table 3.5: Additional control scheme for Model C.

that is was always full (dense bed height = $19.7ft$) [this is an identical situation to model B].

The last modification was necessary since variations in pressure drop across the regenerated catalyst line result in large fluctuations in catalyst levels in the standpipe leading to occasional standpipe overflow. Such an overflow would result in significant process disturbances since process dynamics when the standpipe is not flooded and when it is flooded are considerably different. We will refer to the original model IV FCCU modified to incorporate slide valves and including modifications (1) - (5) above as **Model C**. Model C has 2 additional manipulated variables - slide valve opening on regenerated and spent catalyst lines. An additional control scheme is therefore available - Table 3.5.

3.6.1 Open Loop Analysis of Model C

Figure 3.18 is a plot of the maximum and minimum singular values of the control schemes SII and SIV as a function of frequency. The maximum singular value of the disturbance transfer function matrix is also plotted.

The flow characteristics for model C are very similar to those of model B. In model C as in model B, an increase in reactor pressure results in decreased catalyst circulation rate at steady–state (negative gain). The steady–state plant condition numbers as well as any RHPT zeros for model C schemes SII, and SIV are summarized in Table 3.6. Both control schemes have lower condition numbers than model A schemes. Scheme SIV has no RHPT zeros and should not have any inherent performance limitations. Scheme SII has a RHPT zero although it is outside the frequency range of interest.

It might be argued that if slide valves were installed to control catalyst flow rate

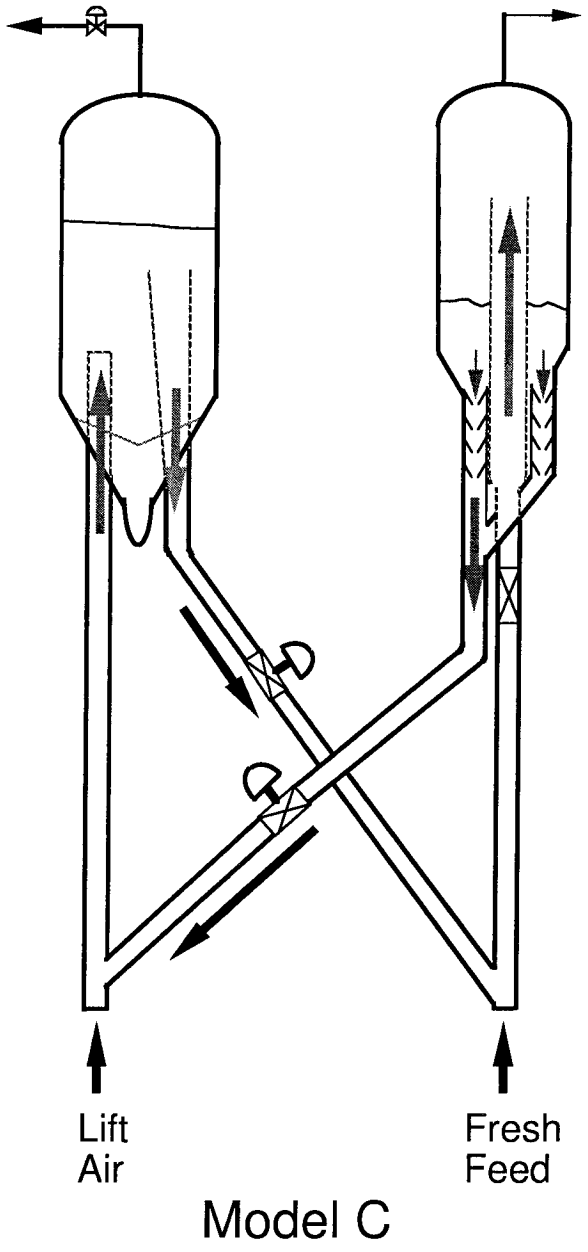

Figure 3.17: Design modification to Model A - slide valves in catalyst flow lines

Scheme	Condition #	RHPT zero
SII	16.1	3.71
SIV	17.3	none

Table 3.6: Steady-state plant condition number and location of RHPT zero for Model C control schemes

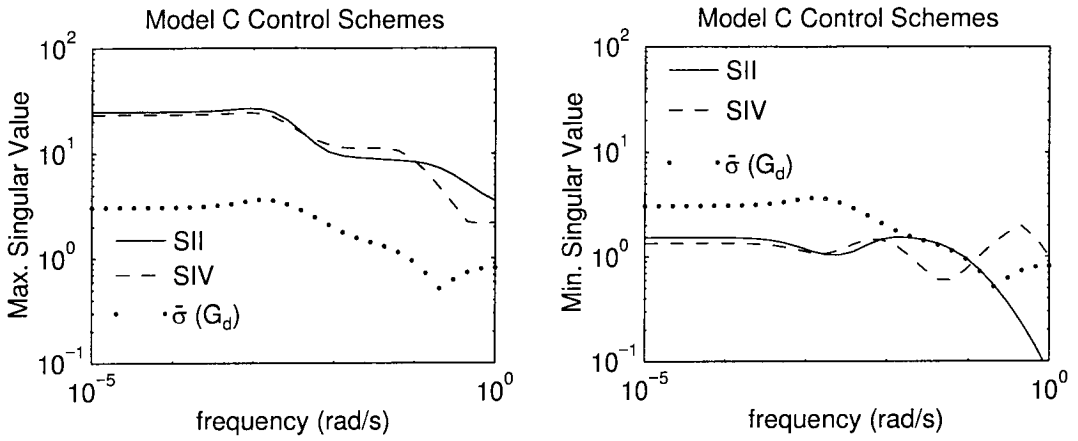

Figure 3.18: Frequency response plots for disturbance model and schemes SII & SIV, Model C

that they would be used as manipulated variables and control schemes like SI, SII and SIII would not be considered. However, the aim is to compare model B modifications with model C modifications. In fact, model C, scheme II (in this case the slide valve openings were held constant) is identical to model B, scheme SII except for the pressure drop across the J-bends which are not considered in model B and different cross-sectional areas for the slide valves.

3.6.2 Closed Loop Analysis of Model C

μ-optimal controllers could be designed for model C scheme SII and model C scheme SIV that guaranteed robust performance. However, better robust performance is achievable for model C scheme SIV (max. $\omega_p = 3.3$ rad/s) than for model C scheme SII (max. $\omega_p = 0.2$ rad/s). Recall that a higher value of ω_p implies faster closed loop response. Model C scheme SIV should be expected to provide better closed loop performance than model B schemes since the slide valves in scheme SIV can be used to directly and rapidly damp out variations in catalyst flow rate which is not possible for model B schemes. To compare the improvement in achievable performance due to the introduction of slide valves the μ-plots for model C scheme SII and SIV are graphed in Figure 3.19 for identical uncertainty and performance conditions ($\omega_p = 0.2$

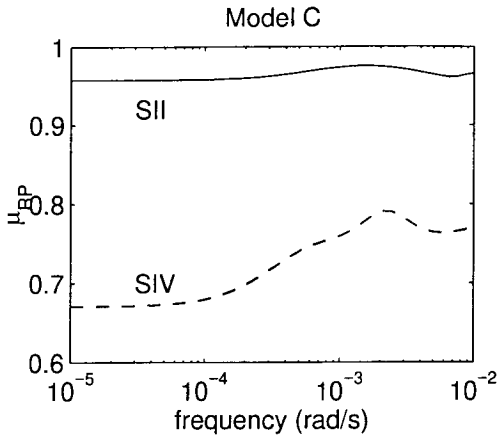

Figure 3.19: Robust performance comparison for scheme SII & scheme SIV. Identical uncertainty & performance specs. $\omega_p = 0.2$ rad/s

rad/s).

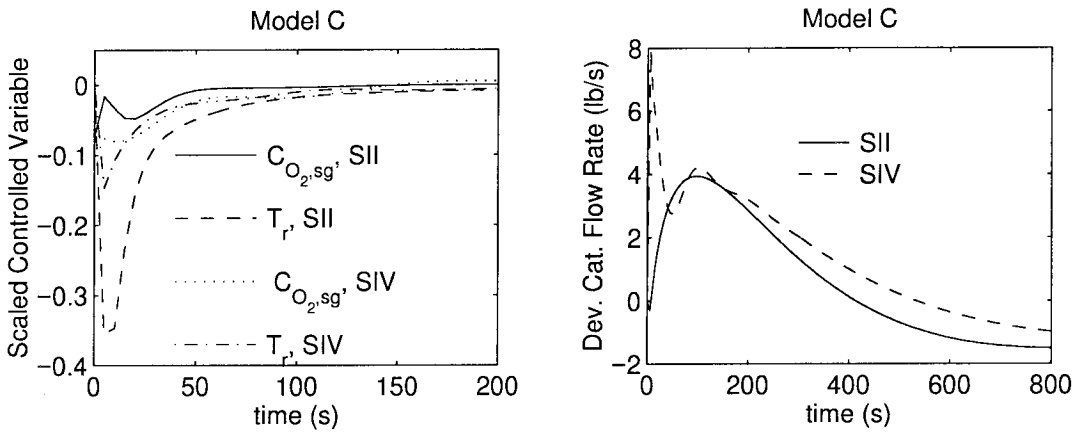

Figure 3.20: Closed loop time response to a unit disturbance in d_3 for Model C, scheme SII & scheme SIV, $\omega_p = 0.2$ rad/s.

Figure 3.20 shows the closed loop (nominal) response to a unit step in ΔP_{frac} for both SII and SIV. The deviations of controlled variables from setpoints are larger for scheme SII than scheme SIV. The fluctuations in catalyst circulation rate are comparable. The manipulated variable moves required to reject the disturbance are well within bounds and have not been plotted.

Figure 3.19 and Figure 3.20 are essentially comparisons of model B and model C since model C scheme SII is identical to model B scheme SII except for the differences

mentioned above. Note however that in model B only a simple operational modification is needed while model C would entail significant revamping of the model IV FCCU.

3.7 Manipulated Variable Saturation at the Regulatory Level

Table 3.7 and Table 3.8 tabulate the largest individual disturbances that can be rejected (at steady–state) by each control scheme for models A and B without saturating the manipulated variables. The corresponding manipulated variable moves required are also indicated. The disturbance condition number (Morari and Zafiriou 1989, Skogestad and Morari 1987) for each disturbance and each scheme is also tabulated.

	SI			SII			SIII		
	d_1	d_2	d_3	d_1	d_2	d_3	d_1	d_2	d_3
Max. Dist. Rejected max 1	1	0.3259	0.2394	1	1	1	1	1	1
Manip. Var.									
V_{14}	0	0	0	-0.0169	-0.0597	-0.0903	0	0	0
V_{lift}	0.8131	0.8685	0.8839	0.3026	0.2326	0.2759	0.4433	0.5431	0.7915
F_3	0.5451	1.0	1.0	0	0	0	0	0	0
T_2	0	0	0	0	0	0	-0.0238	-0.1501	-0.2089
Dist. Condt. #	2.22	5.00	4.79	7.15	3.04	2.56	2.45	1.68	1.71
Plant Condt. #	207	207	207	363	363	363	59.4	59.4	59.4

Table 3.7: Steady–state process variables after disturbance rejection for Model A schemes

Tables 3.7 and 3.8 indicate that constraints are sometimes encountered in rejecting expected disturbances regardless of the configuration (model A or model B). Note however that in all cases the disturbance condition numbers are much smaller than the plant condition number indicating that individual disturbances are closely aligned

	SI			SII			SIII		
	d_1	d_2	d_3	d_1	d_2	d_3	d_1	d_2	d_3
Max. Dist. Rejected max 1	1	0.8603	0.4639	1	1	1	1	1	0.6837
Manip. Var.									
V_{14} ($\times 10^3$)	0	0	0	8.636	49.9	-79.6	0	0	0
V_{lift}	0.3329	-0.7616	0.8033	0.4464	-0.2936	0.4885	0.0712	0.2306	-0.3083
F_3	-0.1654	-1.0	1.0	0	0	0	0	0	0
T_2	0	0	0	0	0	0	0.4884	-0.8170	1.0
Dist. Condt. #	1.00	2.97	2.82	9.15	3.97	4.06	2.39	2.93	3.04
Plant Condt. #	4.22	4.22	4.22	10.2	10.2	10.2	3.51	3.51	3.51

Table 3.8: Steady–state process variables after disturbance rejection for Model B schemes

Scheme	U	Σ	V	Cond. #	RHPT Zero
SI	0.663 0.749 −0.749 0.663	92.8 0 0 0.449	0.871 −0.491 −0.491 −0.871	207	none
SII	−0.635 −0.772 0.772 −0.635	957 0 0 2.64	0.996 −0.084 −0.084 −0.996	363	0.273
SIII	−0.627 −0.779 0.779 −0.627	225 0 0 3.80	0.358 −0.934 −0.934 −0.358	59.4	none

Table 3.9: Steady–state SVD analysis and plant RHPT zeros, Model A control schemes

Scheme	U	Σ	V	Condition #	RHPT Zero
SI	−0.036 1.00 1.00 0.036	3.43 0 0 0.81	0.920 −0.391 −0.391 −0.920	4.22	2.860×10^{-3}
SII	0.866 −0.500 −0.500 −0.866	28.4 0 0 2.79	0.998 −0.067 −0.067 0.998	10.2	$1.86 \pm i11.1$
SIII	0.333 −0.943 0.943 0.333	6.72 0 0 1.92	0.891 −0.454 0.454 0.891	3.51	1.762×10^{-3}

Table 3.10: Steady–state SVD analysis and plant RHPT zeros, Model B control schemes

with the best disturbance direction. The best disturbance direction is the disturbance input direction requiring the *least* action by the manipulated variables. A disturbance input aligned exactly with the best direction has a disturbance condition number of 1.

Table 3.9 gives a singular value decomposition (SVD), (Equation 3.29) of the steady–state gain matrix for the three control schemes in Table 3.6 for model A. Any significant RHPT zeros are also tabulated. Table 3.10 tabulates the corresponding values for model B.

$$G(0) = U\Sigma V^* \tag{3.29}$$

The maximum singular value of the plant gain matrix in schemes SI for both models A and B are significantly lower than the maximum singular value in schemes SII for models A and B. The manipulated variable combination in scheme SI does not have a strong enough effect on the outputs to compensate for the effect of expected disturbances. This is also evident in the open loop frequency response plots for model A (Figure 3.3) and model B (Figure 3.10) where the maximum disturbance gain is often greater than the maximum plant gain. Note that scheme SIII, model B cannot compensate for expected disturbances in d_3 for a similar reason.

It is interesting to note that a plant input in the direction of high plant gain results in one output variable increasing while the other decreases for most control

schemes, *e.g.* for model A scheme SI an input along the direction $[0.871 - 0.491]^T$ results in an increase in $C_{O_2,fg}$ and a decrease in T_r (Table 3.9). Thus relatively small control action is required to move both the controlled variables in opposite directions but a large control action is required to move both in the same direction (increase *both* T_r and $C_{O_2,fg}$) . This behavior can be physically justified. In the absence of any other energy source to heat up the riser, such as direct heating of the feed to the riser (control scheme SIII), an increase in riser temperature must result from an increase in regenerator temperature. An increase in regenerator temperature results from burning coke at a higher rate in the regenerator, requiring additional oxygen supply. In the absence of any control action, $C_{O_2,fg}$ would decrease.

For model A scheme SIII, riser temperature could be raised by heating the feed to the FCCU. Higher riser temperature results in higher wet gas production rate and therefore an increase in reactor pressure. Since there is a *positive* gain between changes in reactor pressure and changes in catalyst circulation rate for model A, catalyst circulation rate would increase. The rate of coke transfer from the reactor to the regenerator would increase requiring additional oxygen for combustion. In the absence of any control action, $C_{O_2,fg}$ would decrease. This is observed in Table 3.9, scheme SIII where an input along the direction $[0.358 - 0.934]^T$ results in a decrease in $C_{O_2,fg}$ and an increase in T_r.

For model B scheme SIII, riser temperature could be raised by heating the feed to the FCCU. Higher riser temperature results in higher wet gas production rate and therefore an increase in reactor pressure. Since there is a *negative* gain between changes in reactor pressure and changes in catalyst circulation rate for model B, catalyst circulation rate would decrease. The rate of coke transfer from the reactor to the regenerator would decrease requiring less oxygen for combustion. In the absence of any control action, $C_{O_2,fg}$ would increase. Thus both T_r and $C_{O_2,fg}$ would increase. This is observed in Table 3.10, scheme SIII where an input along the direction $[0.891 \;\; 0.454]^T$ results in an increase in $C_{O_2,fg}$ and an increase in T_r.

Suppose it is desired to increase both T_r and $C_{O_2,fg}$. Increasing T_r is achieved by increasing coke transport rate to the regenerator resulting in reduced $C_{O_2,fg}$. The air

	SII			SIV		
	d_1	d_2	d_3	d_1	d_2	d_3
Max. Dist. Rejected max 1	1	1	1	1	1	1
Manip. Var.						
V_{14} ($\times 10^3$)	-0.34	85.8	-63.3	0	0	0
V_{lift}	0.1777	-0.6863	0.7274	0.3592	-0.110	-0.0174
$X_{sv,rgc}$ ($\times 10^3$)	0	0	0	-7.69	-99.7	85.4
Dist. Condt. #	16.1	7.16	9.30	16.7	1.43	1.03
Plant Condt. #	16.1	16.1	16.1	17.3	17.3	17.3

Table 3.11: Steady–state process variables after disturbance rejection for Model C schemes

Scheme	U	Σ	V	Condition #	RHPT Zero
SII	0.967 −0.254 −0.254 −0.967	24.8 0 0 1.54	1.00 −0.001 −0.001 −1.00	16.1	3.71
SIV	−0.741 0.672 0.672 0.741	23.3 0 0 1.35	0.04 1.00 1.00 −0.04	17.3	none

Table 3.12: Steady–state SVD analysis and plant RHPT zeros, Model C control schemes

supply has to be increased beyond what is needed to burn off the additional coke to increase $C_{O_2,fg}$. Thus large control action is required to increase both T_r and $C_{O_2,fg}$. The gain in this direction is therefore low. The arguments for scheme SIII can be deduced from the last two paragraphs.

For completeness we tabulate the largest disturbances that can be rejected (at steady–state) by each control scheme for model C and the corresponding manipulated variable moves required in Table 3.11. The SVD analysis of the steady–state gain matrix and RHPT zeros for control schemes SII and SIV, model C is tabulated in Table 3.12. All the individual disturbances can be rejected with available control action.

3.8 Conclusions

1. The conventional setup of a model IV FCCU where a weir and standpipe arrangement is used in the regenerator section is found to be the source of the following undesirable characteristics in the FCCU process:

   - High disturbance sensitivity - disturbances result in large fluctuations of catalyst circulation rate leading to significant deviations in output variables from setpoint.

- Plant directionality - the plant is ill-conditioned.

2. Operating the conventional model IV FCCU with the weir and standpipe flooded at all times leads to a significant reduction in disturbance sensitivity and better control.

3. The installation of control slide valves in catalyst J-bends is found to improve closed loop performance over both the original model IV FCCU and the FCCU modified to operate with the weir flooded.

4. The most significant disturbances to FCCU operation were found to be variations in feed coking characteristics and variations in reactor pressure. One can attempt to minimize fluctuations in reactor pressure and therefore reduce the effect of reactor pressure disturbances. Our analysis corroborates the common industrial practice of maintaining reactor pressure at setpoint by manipulating wet gas compressor throughput. However, since the coking characteristics of the feed to the FCCU are not known accurately, variations in coking characteristics cannot be avoided in practice.

5. The control objective at the regulatory level was to reject expected disturbances and maintain flue gas O_2 concentration ($C_{O_2,fg}$) and riser temperature (T_r) at pre-specified setpoints. Two manipulated variables were selected from a set of available manipulated variables to achieve this objective. The other manipulated variables were maintained at their nominal values. Using fresh feed rate (F_3) and lift air supply (V_{lift}) as manipulated variables resulted in plant gains that were too low to reject the expected disturbances at steady–state. However, manipulating lift air supply (V_{lift}) and flue gas valve position (V_{14}) resulted in significantly higher plant gains and therefore provided effective disturbance rejection for all FCCU designs considered. For the standard model IV FCCU, feed temperature (T_2) and lift air supply (V_{lift}) were also found to be effective manipulated variables in rejecting expected disturbances. Incorporating slide valves to control the catalyst circulation rate through the FCCU provided an

additional effective manipulated variable when used in conjunction with lift air supply at the regulatory level.

6. Based on this study the following design guidelines for low disturbance sensitivity have been established for FCCUs:

   - The FCCU flow system should be designed so that increased reactor pressure results in decreased catalyst circulation rate.
   - The FCCU should be designed so that catalyst circulation rates are minimally affected by changes in process conditions.

This study is based on the FCCU reactor/regenerator model developed by McFarlane et al. (1993). We considered only the regulatory level of the control hierarchy and overall process optimization was not addressed. The emphasis was on understanding those aspects (both design and operational) of model IV FCCUs that render them difficult to control. The aim was not to design controllers for actual model IV FCCUs based on this model. Instead, controllers were designed for similar performance and stability objectives to compare alternate operating modes and different possible design modifications to the model IV FCCU. Based on our observations we identified some desirable characteristics of FCCUs that make control easier.

It must be stressed that the findings reported in this paper for the original model IV FCCU are based on the assumption that the underlying nonlinear model adopted from McFarlane et al. (1993) captures the dynamic characteristics of model IV FCCU operation with a reasonable degree of accuracy.

We have not explicitly considered process constraints in this analysis except to the extent of determining the largest individual disturbances that can be rejected at steady–state. Industrial experience indicates that constraints are effectively handled at higher levels of the control hierarchy (above the regulatory level). The focus of this work was at the regulatory level and process constraints were not considered in the analysis.

Our linear analysis strictly applies to a narrow region around the operating point described. However, the dynamic characteristics of the FCCU are qualitatively the

same as long as the FCCU is operated under total combustion mode (Arbel et al. 1995). Therefore, the results are generally valid for FCCU operation in the total combustion mode.

3.9 Acknowledgments

Financial support from Chevron Research and Technology Company is gratefully acknowledged. We would also like to thank Serban Agachi, John Bomberger and Bruno Donno for their help with this project. Finally, we thank Professor Reuel Shinnar for some enlightening discussions.

3.10 Nomenclature

A_i	-	cross-sectional area of unit i (ft^2)
$C_{O_2,fg}$	-	flue gas O_2 conc. (mol %)
$\hat{d}$	-	non-dimensional input disturbance
d	-	disturbance variable
E_{lift}	-	elevation of regenerator lift air injection (ft)
E_{oil}	-	elevation where oil enters reactor riser (ft)
f_{of}	-	weir overflow factor ($\frac{lb}{ft^2 s}$)
F_3	-	fresh feed rate (lb/s)
F_{rgc}	-	regenerated catalyst flow rate (lb/s)
F_{sp}	-	catalyst flow rate over weir (lb/s)
g_c	-	Newtons law proportionality constant (32 $ftlb_m/lb_f s^2$)
G(jω)	-	plant transfer function matrix evaluated at s = jω
h_{lift}	-	height of lift pipe (ft)
N	-	# of velocity heads
T_{atm}	-	ambient temperature (°F)
T_r	-	riser temperature (°F)
T_{reg}	-	regenerator temperature (°F)

T_2	-	feed temperature to riser base (°F)
$\hat{u}$	-	non-dimensional input variable
u	-	input variable
U	-	left singular vectors of G(0)
v	-	velocity through restriction (ft/s)
V	-	right singular vectors of G(0)
V_{lift}	-	lift air steam governor position
V_6	-	combustion air blower suction valve position (0-1)
V_{11}	-	wet gas compressor suction valve position (0-1)
V_{14}	-	flue gas slide valve position (0-1)
w_i	-	freq. dependent uncertainty wt. for each input variable
w_o	-	freq. dependent uncertainty wt. for each output variable
w_p	-	freq. dependent performance wt. for each output variable
W_I	-	diagonal matrix of input uncertainty wts, diag(w_i)
W_O	-	diagonal matrix of output uncertainty wts, diag(w_o)
W_P	-	diagonal matrix of performance wts, diag(w_p)
$X_{sv,rgc}$	-	regenerated catalyst U-bend slide valve position (0-1)
$X_{sv,sc}$	-	spent catalyst U-bend slide valve position (0-1)
$\hat{y}$	-	non-dimensional output variable
y	-	output variable
z_{bed}	-	regenerator dense bed height (ft)
α	-	fraction catalyst shifted from reactor to standpipe
β	-	constant (lb/s)
ΔP_{frac}	-	pressure drop between reactor and main fractionator (psia)
ΔP_r	-	change in reactor pressure (psia)
ΔW_i	-	catalyst inventory change in unit i (lb)
ΔH_i	-	catalyst level change in unit i (ft)
μ	-	structured singular value
ψ_F	-	effective coke factor for gas-oil feed
ρ_c	-	settled catalyst density (45 lb/ft^3)

Σ - diagonal matrix of plant gains

Subscripts:

dim	-	actual (dimensional) value
reg	-	regenerator
rgc	-	regenerated catalyst line
sc	-	spent catalyst line
$scale$	-	diagonal scaling matrix
sp	-	standpipe
ss	-	steady–state
str	-	reactor stripper
RP	-	robust performance

Chapter 4 Control Structure Selection for Optimal Regulatory Control of the FCC Process

Summary

A quantitative rank ordering of possible control structures for FCC operation in both partial combustion (PC) mode and complete combustion (CC) mode operation is undertaken. 2×2 control structures are considered. Subsequently, a simple 1×1 (SISO) control strategy for CC mode operation is proposed and analyzed.

For PC mode regulation, riser temperature (T_r) and regenerator dense bed temperature (T_{rgn}) - $[T_r, T_{rgn}]$ are the most suitable choice for controlled variables. For CC mode regulation, $[T_r, C_{O_2,fg}]$ are the most suitable choice for controlled variables, where $C_{O_2,fg}$ is the flue gas O_2 molar concentration. This analysis suggests that two sets of manipulated variables can in fact result in comparable steady–state and dynamic characteristics. These are: $[F_{air}, F_{cat}]$ and $[F_{air}, T_{feed}]$, where F_{air} is the combustion air flow rate, F_{cat} is the catalyst circulation rate, T_{feed} is the fresh feed temperature. The possibility of using T_{feed} has been reported in the past, but the benefits do not appear to have been quantitatively analyzed. We find that the achievable performance with these two manipulated variable options is comparable, regardless of the type of uncertainty weight (input, additive) or structure (diagonal, full block). Thus, for older FCCUs where direct manipulation of F_{cat} is not possible (*e.g.* Exxons Model IV FCCU), the feed temperature T_{feed} could also be an effective manipulated variable for regulatory control in both CC and PC mode operation. The most suitable control structures for PC and CC mode are in agreement with that recently given in (Arbel et al. 1996), although the ranking is done quantitatively in this work, and with significantly less effort. Furthermore, this analysis shows that while the most suitable control structure reported in (Hovd and Skogestad 1993) for PC mode operation might be adequate if the FCC is operated over a narrow range,

it is shown to have undesirable characteristics over a wider operating range. Current FCCs are typically required to operate over a wider range, due to economic and operational reasons. A simple control strategy for CC mode operation is proposed and analyzed. The strategy involves: (1) always operating the combustion air compressor at full capacity and (2) using a single loop controller ($K(s) = C(s)\frac{1}{s}$, $C(s)$ stable) with integral action to control T_r using F_{cat}. It is shown that this strategy provides good performance, guarantees that the process will not revert to PC mode operation (ensured using integral action), and can process the same range of feed qualities as the 2×2 control scheme where $[T_r, T_{rgn}]$ are controlled using $[F_{air}, F_{cat}]$.

4.1 Problem Statement

Recall that FCCUs can operate in two possible modes: the complete combustion mode **(CC mode)** and the partial combustion mode **(PC mode)** (Chapter 2). Typically, a given FCCU will operate in one mode or the other, and intentional switching between these two modes is unlikely. Specific problems arising from switching between these two modes might include:

- **CC mode → PC mode-** In CC mode, essentially no CO is produced, and no downstream equipment is generally installed to handle the *ppm* levels of CO. Switching to PC mode operation will generate significant amounts of CO, which cannot be processed, without additional down–stream equipment.

- **PC mode → CC mode-** Heavier feeds can be processed in PC mode (discussed in Chapter 6) than in CC mode. A transition to CC mode operation might result in excessive regenerator temperatures if heavy feeds were being processed in the PC mode. Excessive regenerator temperatures are undesirable (Chapter 2).

- **PC mode → CC mode-** Coke combustion to both CO and CO_2 requires less air than if the coke were combusted to CO_2 only. Thus, while the combustion air compressor might provide sufficient air for PC mode operation, the available capacity might be too low for CC mode operation.

Intentional and frequent switching between these two modes is therefore clearly undesirable. In this work, it is therefore assumed that most FCCUs operate in either PC mode or CC mode, and switching between these modes is *never* done. Given this operating restriction, we would like to examine the following issues:

- Is it possible to find a fixed control scheme and a fixed linear controller that will provide acceptable performance with respect to:

    1. ability to induce significant changes in other important process variables (that are not explicitly controlled) by changing available set–points.

2. effective integration of the selected regulatory control scheme within the overall plant operation.
3. acceptable tracking due to supervisory level commands.
4. effective rejection of process disturbances.
5. satisfactory closed loop speed of response.
6. satisfactory performance over a wide range of possible operating points in the selected operating regime.

- Moreover, if the desired closed loop performance specifications can be achieved by more than one control scheme for a given operating region, is it possible to rank order these control schemes with respect to the criteria described above?

Recent work by Arbel et al. (1996) has examined the first and second issue in detail. Their analysis is however necessarily unit–specific and deriving general conclusions regarding FCC operation is difficult. Moreover, it was concluded that all the control schemes studied for the PC model had a comparable effect on the set of "other important process variables" that were not explicitly controlled. They have also analyzed the overall FCC control strategy including both regulatory and supervisory control in a qualitative manner. Qualitative conclusions are drawn regarding the rank ordering of different control schemes. The five–step procedure for controllability analysis suggested by (Arbel et al. 1996) requires a very detailed understanding of both the steady–state and dynamic characteristics of the process under study - in this case the FCC. The portability of the procedure is also not clear, as application to some other process application will initially require building up an extensive understanding of that new process. Experiences derived from one process cannot be readily transferred to the next. Furthermore, this procedure will at best yield a qualitative ranking of the different control structures under study. A more systematic, quantitative and generic procedure will be used here.

Another recent effort to determine the most suitable regulatory control structure for FCC operation is the work of (Hovd and Skogestad 1993). However, the model

used in their study is adopted from (Lee and Groves Jr. 1985), which does not reflect the operating range currently in practice in present day FCCs (Arbel et al. 1995). In particular, the coke and CO combustion kinetics used to describe regenerator operation are valid for $T_{rgn} < 1240°F$, which is close to the lower limit of typical present day FCC regenerators ($1200°F \leq T_{rgn} \leq 1470°F$) reported by (Avidan and Shinnar 1990). We show in Section 4.4.3 that the control structure rank ordering obtained in (Hovd and Skogestad 1993) is not appropriate for the wider range of operation currently demanded of the FCCU. The procedure for controllability analysis proposed by (Hovd and Skogestad 1993) utilizes generic, easy to calculate measures, is simple to use, does not require detailed process understanding, and experience developed during one application can readily be utilized during the next application. It is also one of the first to attempt a quantitative rank ordering of possible control structures for the FCC, and requires significantly less effort than using the procedure from (Arbel et al. 1996). It is important to point out here that our analysis utilizes some additional measures for controllability analysis, specifically the structured singular value, the relative gain array, and the determinant of the steady–state gain matrix, and can be viewed as an extension of the procedure of Hovd and Skogestad (1993). This procedure also explicitly accounts for process uncertainties, and allows the comparison of the best achievable performance.

The focus of this chapter will be the regulatory level control of a Fluid Catalytic Cracking (FCC) process. In particular, we will focus on issues 3–6 mentioned above. A main objective is to *quantitatively* rank order different possible control structures for the FCC operation in both PC mode and CC mode. It is important to note that the methods proposed in Hovd and Skogestad (1993) and the extensions used here utilize generic measures from control theory that can also be effectively applied to other processes besides the FCC.

4.2 Preliminaries

4.2.1 Mathematical Model of the FCC Dynamics

In this chapter, we will use the first principles mathematical model of the FCC developed by Arbel et al. (1995). This model was referred to as the Mobil/CCNY model in Chapter 2, and some pertinent features are described in some detail in Section 2.8.

4.2.2 Process Constraints

Process variables that are constrained to values within a prespecified lower and upper bound for normal FCC operation are tabulated in Table 4.1 and are compiled from (Arbel et al. 1995, McFarlane et al. 1993, Sorensen 1993, Upson et al. 1993). The numerical values of the lower and upper bounds are also indicated. Note the following:

Variable	Units	Lower Limit	Upper Limit
Manipulated Variables			
F_{cat}/F_{oil}	$\frac{lbcat.}{lbfeed}$	0	10
F_{air}/F_{oil}	$\frac{lbair}{lbfeed}$	0	1
T_{feed}	$^\circ F$	400	700
Output Variables			
T_r	$^\circ F$	950	1050
T_{rgn}	$^\circ F$	1200	1400
C_{rgc}	$wt.\%$	0	0.5
$C_{O_2,fg}$	$mol.\%$	0.5	2

Table 4.1: Manipulated and process variables with constraints.

- For normal FCC operation, the lower limit on F_{cat}/F_{oil} is greater than 0. The FCC unit obviously cannot operate if there is no catalyst circulation between the reactor and the regenerator. Because the minimum required catalyst circulation rate is strongly unit specific, the absolute lower bound of 0 is assumed. The upper limit is adopted from Arbel *et al.* (Arbel et al. 1996).

- For normal FCC operation, the lower limit on F_{air}/F_{oil} is greater than 0. The catalyst in the regenerator must be fluidized for normal FCC operation. The

upper limit depends on the combustion air compressor capacity. The underlying FCC model does not incorporate a compressor model, and the upper limit is assumed to be 1. However, as discussed in Section 4.3, this upper limit is not active for any of the operating conditions considered.

- The feed mixture must be at a temperature above some minimum mixing temperature (which depends on feed composition). This requirement sets the lower limit for T_{feed}. The upper limit on T_{feed} is set by the need to prevent premature coking of feed in the feed tubes, which is undesirable.

- There is no specific bound on the lower limit of riser outlet temperature except for the obvious necessity to operate at a high enough riser temperature to ensure feed cracking. However, most FCCs operate at $T_r > 950°F$ (Arbel et al. 1995). A practical lower limit of $950°F$ is therefore selected. Excessive riser temperatures can lead to unacceptable levels of thermal cracking and undesirable product yields. An upper limit of $1050°F$ is therefore assumed although higher temperatures have been reported in the literature *e.g.* Upson et al. (1993).

- A reasonable rate of coke and CO combustion must be maintained in the regenerator to ensure an acceptable feed cracking rate in the riser. This is ensured by maintaining T_{rgn} above some lower limit. Excessive T_{rgn} will cause permanent deactivation of the zeolite catalyst and/or damage the regenerator internals, which is clearly undesirable. This requirement sets an upper limit on T_{rgn}.

- The regenerator cyclone exit flue gas temperature (T_{fg}) is often considered in the set of constrained variables (Ljungquist 1990). However, we do not include T_{fg} in Table 4.1 for reasons detailed in Appendix B.

- The lower limit on $C_{O_2,fg}$ is set to a conservative minimum to ensure CC mode operation. The upper limit is set by the economically driven requirement not to waste energy in pumping additional air unnecessarily.

4.2.3 Input and Output Scalings

Each manipulated variable is scaled so that the normally allowable maximum deviations from the nominal value represents unit deviation in that manipulated variable. Thus, all physically implementable manipulated variable modes are of magnitude less than one. The three manipulated variables as well as the maximum allowable deviation is indicated in Table 4.2.

Manipulated Variable	Notation	Units	Max. Deviation
Air Flow Rate	$\frac{F_{air}}{F_{oil}}$	$\frac{lb/s}{lb/s}$	$\pm 5\%$ from steady–state
Catalyst Flow Rate	$\frac{F_{cat}}{F_{oil}}$	$\frac{lb/s}{lb/s}$	$\pm 10\%$ from steady–state
Feed Temperature	T_{feed}	$^\circ F$	$\pm 50^\circ F$ from steady–state

Table 4.2: Possible manipulated variables for regulatory level control, and allowed deviations from steady–state.

The elements of the output error vector are scaled to make each error equally significant to the process. The scaling factors used to scale the deviations in relevant process outputs are indicated in Table 4.3 and are adopted from (Sorensen 1993).

Controlled Variable	Units	scale factor
T_r	$^\circ F$	3
T_{rgn}	$^\circ F$	30
T_{cyc}	$^\circ F$	30
$C_{O_2,fg}$	mol.%	0.5
$\Delta T = T_{fg} - T_{rgn}$	$^\circ F$	30

Table 4.3: Scaling factors for deviations of controlled variables from nominal values.

Note that the scaling factors in Table 4.3 are based on the 'equal concern error' (Sorensen 1993), and can be interpreted as follows, using T_r and T_{rgn} as examples: A deviation of $3^\circ F$ in T_r would be as significant (disruptive) to the process as a $30^\circ F$ change in T_{rgn}. An alternative interpretation is that it is more critical (by a factor of $30/3 = 10$) to maintain T_r at set–point that T_{rgn} at set–point. The scaling factors are therefore used to scale the outputs such that any scaled output deviation of magnitude 1 indicates the same degree of significance.

4.2.4 Primary FCC Disturbance

The most significant disturbance for FCC operation is reported to be changes in feed coking characteristics (Grosdidier et al. 1993, Hovd and Skogestad 1993, McFarlane et al. 1993). The feed coking characteristic reflects the rate of coke deposition on cracking that specific feed. This was also identified as a major process disturbance in Chapter 3. In this study, only the effect of changes in feed coking characteristics will therefore be considered.

Quantifying the feed coking characteristics is still an active area of research (Sadeghbeigi 1995). The FCC feed typically consists of a mixture of a number of different hydrocarbon sources each with different feed coking characteristics. For example, it is reported (McFarlane et al. 1993) that many slurries (typically bottoms product from distillation units) produce more coke on cracking that normal gas oil, while diesel oil produces less coke than normal gas oil. A relative coking factor (γ) is therefore often used to rank order the relative coking characteristics of different feed components. For example, if normal gas oil has $\gamma_{gasoil} = 1$, then the slurry has $\gamma_{slurry} > 1$ and diesel oil has $\gamma_{diesel} < 1$.

The incoming feed to the FCC is generally a mixture of many such different hydrocarbons. The actual coking characteristic of the feed will obviously depend on the fractional contributions from each component type. The contribution of each feed component can be accounted for by using a weighted relative coking rate - the weight being the mass fraction (for example) of each feed component. Such a weighted sum of relative feed coking characteristics to quantify the feed coking characteristics of the overall incoming feed is modeled in (Arbel et al. 1995, McFarlane et al. 1993) as in Equation 4.1.

$$\Psi = \sum_i \gamma_i y_i(0) \tag{4.1}$$

where γ_i indicates the relative coking tendency of feed component i and $y_i(0)$ is the weight fraction of feed component i in the incoming fresh feed stream. We will model changes in feed coking characteristics by a factor F_q that multiplies Ψ in Equation 4.1

(Equation 4.2).

$$\Psi = F_q \times \sum_i \gamma_i y_i(0) \tag{4.2}$$

Note the following:

- F_q lumps all the possible variations in the mass fraction of specific feed components into one factor. Thus, the emphasis is on changes in the inlet feed coking characteristic, and not on the component of the feed that contributed to the change in the overall feed coking characteristic.

- the transient behavior of F_q is determined by the mixing dynamics of the fresh feed holdup tank. Because the feed storage tank mixing dynamics are not modeled in Arbel et al. (1995), we adopt a first order dynamic model for changes in F_q with an assumed time constant of τ_{F_q}= 5 min..

$$G_{F_q}(s) = \frac{1}{\tau_{F_q} s + 1} \tag{4.3}$$

4.2.5 Actuator Dynamics

The model by Arbel et al. (1995) does not account for the complex hydrodynamic interactions between the reactor and the regenerator that can affect F_{cat}. The dynamics of the combustion air compressor are also ignored. The primary focus in Arbel et al. (1995) was on steady-state analysis, and ignoring the actuator dynamics had little consequence. However, our focus is on the dynamic characteristics and considering actuator dynamics is important as it indicates the upper limit on the available bandwidth for effective control. Specifically, the combustion air compressor used to vary the combustion air rate (F_{air}), the catalyst slide valves used to vary circulation rate (F_{cat}), and the feed pre-heat furnace used to vary the fresh feed temperature (T_{feed}) are large process components. The dynamics associated with these components cannot be ignored in analyzing the achievable closed loop performance of the FCC (Grosdidier et al. 1993).

The dynamics associated with the final control element are modeled as first order lags with an appropriate time constant as described below. The manipulated variables considered for this study are given in Table 4.2.

- F_{cat}: Slide valves allow the actual catalyst circulation rate ($F_{cat}\ |_{actual}\ (t)$) to be quickly adjusted to the desired value ($F_{cat}\ |_{desired}\ (t) = F_{cat}(t)$) when changes are required to compensate for process upsets *i.e.* the dynamics between $F_{cat}\ |_{desired}\ (t) = F_{cat}(t)$ and $F_{cat}\ |_{actual}\ (t)$ is fast, with a time scale of 1–2 mins. (Shinnar 1997). The dynamic behavior between $F_{cat}\ |_{desired}\ (t) = F_{cat}(t)$ and $F_{cat}\ |_{actual}\ (t)$ is modeled by a first order lag with a time constant of 0.5 min (Sorensen 1993, Shinnar 1997).

$$G_{\text{cat}}(s) = \frac{1}{0.5s + 1} \tag{4.4}$$

- F_{air}: the dynamics between the desired combustion air flow rate ($F_{cat}\ |_{desired}\ (t) = F_{air}(t)$) and the actual combustion air flow rate ($F_{air}\ |_{actual}\ (t)$) is also modeled by first order dynamics with an assumed time constant of 0.5 min (Sorensen 1993).

$$G_{\text{air}}(s) = \frac{1}{0.5s + 1} \tag{4.5}$$

- T_{feed}: In a typical FCC unit, feed can be pre–heated in a furnace and/or by heat exchange with other process streams. Utilizing an integrated heat exchange setup may give rise to complicated and possibly undesirable interactions (Ray 1981). Our goal is to gain insight into FCC operations, and for simplicity, it is assumed that the fresh incoming feed is heated using a stand–alone feed pre–heater. The transient behavior of the incoming feed temperature will therefore be determined by the heat transfer characteristics of the feed pre–heater. It has been assumed that feed temperature changes with a time constant of 3 min. and is adopted from McFarlane et al. (1993).

$$G_{\text{T}_{\text{feed}}}(s) = \frac{1}{3s + 1} \tag{4.6}$$

Note that the simplifications indicated at the beginning of this section, namely ignoring the complex hydrodynamic interactions between the reactor and regenerator sections, is not generally valid for all FCC units. It was shown in Chapter 3 that for the older Model IV FCCUs without slide valves, changes in catalyst inventory and reactor/regenerator pressure result in significant changes in F_{cat}. Because F_{cat} is a dominant variable, fluctuations in F_{cat} have a significant (and undesirable) effect on important process variables such as T_r. The introduction of slide valves in the model IV FCCU allowed for direct control of, and significantly reduced fluctuations in F_{cat}. Several design modifications (also detailed in Chapter 3) must also be made in order to operate the FCCU with slide valves. The effect of changes in the reactor and regenerator catalyst inventory and pressure on overall F_{cat} dynamics for such a modified model IV FCCU was shown to be small and can therefore be ignored. The model of Arbel et al. (1995) effectively describes the operation of such a modified FCCU and therefore ignoring the F_{cat} dynamics is justified.

4.2.6 Procedure for Steady–State Analysis

The steady–state characteristics of the set of locally linearized plants obtained by linearizing the available non–linear model over the entire operating regime of interest is analyzed. In particular, we focused on the following common characteristics of the chemical process industries to guide the control structure selection process:

- integral action is required in all channels to allow offset free tracking of all important process variables.
- the open loop plants are typically stable.

Under the assumptions that

- the plant $G(s)$ is open loop stable,
- the controller has integral action in each channel *i.e.* $K(s) = C(s)\frac{1}{s}$ with $C(s)$ stable,

(Morari and Zafiriou 1989) show that a *necessary* condition for integral stabilizability is that:

$$\det[G(0)C(0)] > 0 \tag{4.7}$$

If a fixed linear controller is used, then a change in the sign of $\det[G(0)C(0)]$ must be due to a change in the sign of $\det[G(0)]$. It is particularly important to check for changes in the sign of $\det[G(0)]$ when operation over a wide operating regime is required. Thus, if the sign of $\det[G(0)]$ changes over the required operating regime, then any fixed controller $K(s) = C(s)\frac{1}{s}, C(s)$ stable, designed for stable operation at one operating point (with a particular sign of $\det[G(0)]$) will result in an unstable closed loop system at those operating points where $\det[G(0)]$ has a different sign. Thus, the controller with integral action can provide stability only over a limited sub–region within the entire operating regime. This is clearly undesirable, and any control schemes that do indicate a change in $\det[G(0)]$ over the required operating regime can be discarded because of this inherent limitation on the operating range.

Other controllability measures such as the steady–state relative gain array (RGA), the performance relative gain array (PRGA), the closed loop disturbance gain (CLDG) have also been proposed (*e.g.* Hovd and Skogestad (1993)). In general a combination of these measures will be required to effectively screen the alternatives.

4.2.7 Procedure for Dynamic Analysis

Recall that our goal is to determine whether some control scheme with an appropriate fixed linear controller can provide the required performance over the entire operating regime. The solution methodology used for the dynamic analysis of the different control structures is as follows:

1. Select an operating regime (partial or complete combustion regime).

2. Postulate a set of possible control schemes to be used in this operating regime. Select one of the control schemes.

3. Select a set of steady–state operating points to cover the *entire* regime of operation.

4. Linearize the available nonlinear model at each of the selected operating points thereby obtaining a set of locally linearized models describing local behavior over the entire operating regime for the selected control scheme. Alternatively, a set of linear models identified from plant data could also be utilized.

5. Decide on a nominal linear model for this set of linear models.

6. Determine an uncertainty description that describes all the plants in the set. (Because an additional goal is to rank order the different control schemes for the selected operating region, this same uncertainty model must be used to analyze all the postulated control schemes for a reasonable comparison.)

7. Select a performance weight that reflects (directly or indirectly) all the closed loop performance requirements. Once again, as with the uncertainty weights, the same performance weight must be used during the design and analysis stages for all postulated control schemes for a reasonable comparison.

8. Design an optimal controller for the nominal plant with the associated uncertainty and performance specifications. μ-optimal controllers have been designed for this study.

9. Analyze the closed loop behavior (nominal stability, nominal performance, robust stability, and robust performance) for the selected control scheme and the designed controller.

10. Select another possible control scheme from the set of postulated schemes. Repeat the procedure (4–9) for this postulated control scheme and the chosen operating regime.

11. Repeat the analysis (2–10) above for other operating regimes that might be under consideration.

Rank ordering the different control schemes postulated for each operating regime involves:

- Comparison of the robust performance structured singular value (μ_{RP}) for each scheme. Higher μ_{RP} means higher sensitivity to uncertainty and/or less acceptable worst case closed loop performance.
- Comparison of closed loop time responses with the optimal controllers designed for each control scheme.

With respect to the above procedure, please note the following specific details:

- *Step 6* - It is essentially never possible to derive an exact model of a physical plant. Some control structures might be inherently more sensitive to uncertainty than others. Understanding and explicitly accounting for this uncertainty is important in obtaining a realistic rank ordering of available control structures.
- *Step 8* - Designing an optimal controller is important as this allows a comparison of the best achievable closed loop performance with the given control structure, and hence allows *quantitative* ranking of the control structure candidates.

In utilizing the procedure outlined above for control structure selection, two parameters need to be quantified:

1. plant uncertainty description (uncertainty weight)
2. performance specification (performance weight)

The derivation of these quantities is described next, for the FCC process. Note that unless explicitly stated, the analysis is carried out on the linearized models.

Uncertainty Description

The dynamic analysis is based on linear models derived by linearizing the nonlinear model around selected operating points as just described. The control objective is

effective disturbance rejection. For each control scheme an optimal controller was synthesized and the closed loop performance achievable with this controller examined. μ-(sub)optimal controllers were therefore designed to minimize the ∞-norm of an appropriately weighted and scaled transfer function. The controllers were synthesized using software available in the μ - Analysis and Synthesis Toolbox (Balas et al. 1991) in MATLAB. Excellent descriptions of the calculation, interpretation and use of μ are given in (Balas et al. 1991) and (Morari and Zafiriou 1989).

As discussed in step 6 above, and pointed out by (Lee, Braatz, Morari and Packard 1995, Braatz, Lee and Morari 1996) quantitative rank ordering of control structures requires information on the process uncertainties. A reasonable representation of model uncertainty is therefore needed before the controllers can be synthesized.

The block diagram used for closed loop analysis is shown in Figure 4.2. The blocks Δ_I and Δ_A are unknown transfer matrices. Δ_I and Δ_A are used to parameterize the difference between the nominal plant $G(s)$ and the real plant *i.e.* the model uncertainty. The structures of Δ_I and Δ_A are pre-specified but the actual transfer functions are unknown except that they are norm bounded (when appropriately weighted):

$$\bar{\sigma}(\Delta_I) \leq 1 \qquad\qquad \bar{\sigma}(\Delta_A) \leq 1 \tag{4.8}$$

Transfer functions W_I and W_A are used to scale Δ_I and Δ_A respectively so that Equation 4.8 holds. At any frequency, the actual uncertainty level is given by $|W_I|$ and $|W_A|$. The specific transfer functions used for W_I and W_A will be presented in the appropriate sections. Δ_I and Δ_A are assumed to be of block diagonal structure:

$$\Delta_I = \begin{bmatrix} \delta_1 & 0 \\ 0 & \delta_2 \end{bmatrix} \qquad \Delta_A = \begin{bmatrix} \delta_3 & 0 \\ 0 & \delta_4 \end{bmatrix} \qquad \delta_1, \delta_2, \delta_3, \delta_4 \in \mathcal{C} \tag{4.9}$$

Since this choice for the structure of Δ_I and Δ_A is arbitrary, the sensitivity of our results to other possible structures will be examined.

Performance Specifications

The control objective for all cases in this paper is effective disturbance rejection. The performance requirements are:

1. no steady–state offset for step changes in feed coking quality. *i.e.* integral action required
2. settling time of 20–30 minutes
3. high frequency disturbance amplification by a factor of at most 10/3.

The transfer function for the performance weights is:

$$w_{\mathrm{p}} = 500\frac{\frac{1}{\omega_p}s+1}{\frac{500}{0.3\omega_p}s+1}$$
$$W_{\mathrm{P}} = w_{\mathrm{p}}I \tag{4.10}$$

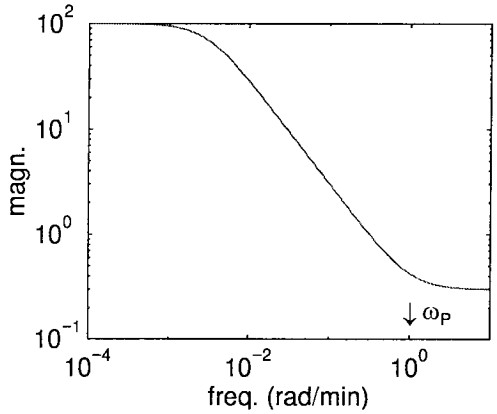

Figure 4.1: Performance weight magnitude plot.

The performance requirement for each output variable is assumed to be the same. This is justified since the output variables are scaled so that each output error is equally significant. A magnitude/frequency plot for the performance weight is plotted in Figure 4.1. The 'corner frequency' ω_p (Equation 4.10) is used as an adjustable

parameter to quantify the best achievable performance for a given control scheme. Higher ω_p (Figure 4.1) implies faster closed loop response (Lundström et al. 1991).

The frequency range of interest (expected closed loop bandwidth) was taken to be 10^{-2}rad/min to 10^{0}rad/min which corresponds to process variations on time scales of minutes to hours. Unless otherwise stated, the dynamic response plots are those obtained with the linear model.

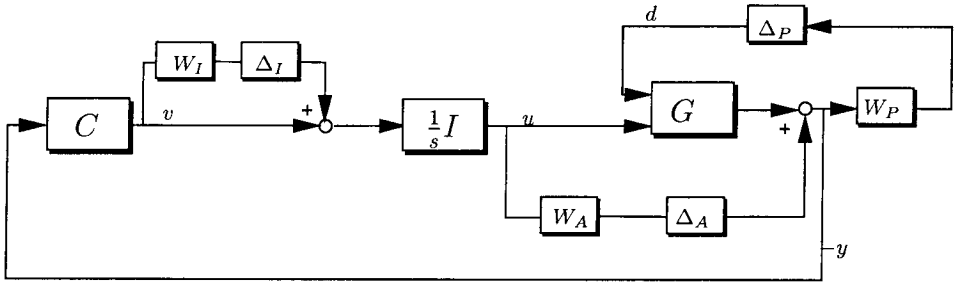

Figure 4.2: Closed loop analysis setup.

4.3 Steady–State Feasible Operating Region

We will refer to the region where the FCC unit operates at steady–state and satisfies all the constraints specified in Table 4.1 as the steady–state feasible operating region.

The reactor riser is the heart of the cracking process. Here feed oil (in vapor state) is cracked into lighter more valuable components. A critical process variable for FCC operating economics is therefore the riser temperature (T_r), as it determines the cracking severity and the relative product distribution. Since T_r is a critical process variable, the steady–state feasible operating region will be determined with respect to contours of constant T_r. The feasible operating region is indicated in Figure 4.3 by the "+" for PC mode and "×" for CC mode for three contour plots of constant riser temperature: $T_r = 950°F$, $T_r = 1000°F$ and $T_r = 1050°F$. The following conditions are used in deriving the feasible operating region:

1. constant fresh feed rate - F_{oil}

2. constant fresh feed temperature - T_{feed}

3. F_{cat} is adjusted to ensure that $T_r = 1000°F$

Under these conditions, there is one degree of freedom, and we specify F_{air} to fix the problem. The operating region was determined by tracking the T_r=constant contour as a function of F_{air} with the software AUTO (Doedel 1986), using the full non–linear model, developed by (Arbel et al. 1995).

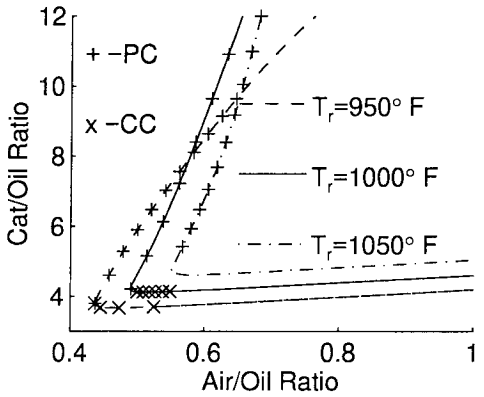

Figure 4.3: Steady–state analysis of $T_r = 950°F, 1000°F, 1050°F$ contours indicating steady–state feasible operating region. $F_q = 1.0$.

The region marked by "×" on the T_r=constant contour plots in Figure 4.3 lie in the feasible operating region for complete combustion, while the region marked by "+" lie in the partial combustion feasible operating regime. Note that the T_r=constant contour also indicates a range of operating points not marked by a "+" or "×". FCC operation would be possible at these operating regimes but one or more of the constraints in Table 4.1 would be violated. For example, complete combustion operation is not possible for $T_r = 1050°F$ because the steady–state regenerator temperature would be unacceptably high.

The steady–state feasible operating region will change when process variables, in particular the feed coking characteristics change. For example, Figure 4.4 displays the feasible operating region when $F_q = 1.3$. Note that feasible steady–state operation is possible only in the partial combustion mode for $F_q = 1.3$. Clearly, there is a maximum value of F_q for which operation in either mode is feasible. Figure 4.4 indi-

cates qualitatively that for operation in the complete combustion mode, the allowable range of F_q variations is less than the allowable range of F_q variations in partial combustion mode. In particular, from Figure 4.4 the largest allowable F_q is less than 1.3 for steady–state operation in complete combustion. This issue is examined in greater detail in Chapter 6.

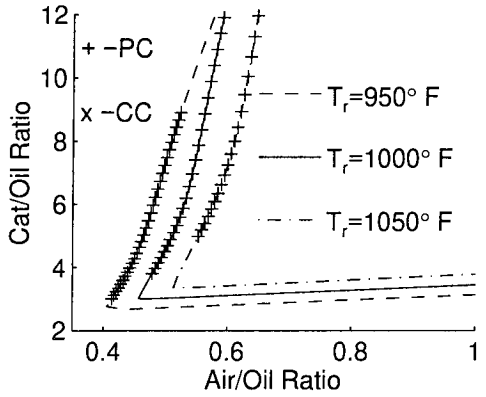

Figure 4.4: Steady–state analysis of $T_r = 950°F, 1000°F, 1050°F$ contours indicating steady–state feasible operating region. $F_q = 1.3$. Note that operation in CC mode is not feasible in CC mode as the steady–state regenerator temperature is too high.

Several operating points spanning the entire operating region are selected and the corresponding set of locally linearized models obtained. Thus, we have a set of linear models that describes the local dynamic behavior of the nonlinear system over the entire operating range in question. It is these sets of linear models that are used for the subsequent dynamic analysis.

To quantify the largest allowable F_q, while ensuring feasible steady–state operation in one of the modes, the following constrained nonlinear optimization problem is solved:

$$\max_{x,u,F_q} F_q \tag{4.11}$$

subject to:

$$\dot{x} = F(x, u, F_q) = 0 \tag{4.12}$$

$$x(i)_{lo} \leq x(i) \leq x(i)_{hi} \tag{4.13}$$

$$u(i)_{lo} \leq u(i) \leq u(i)_{hi} \tag{4.14}$$

$$0 < F_q \tag{4.15}$$

Note that:

- F(x,u,F_q) = 0 imposes the steady–state operation requirement (non–linear model).
- The constraints on the states ($x(i)_{lo}$ and $x(i)_{hi}$) as well as the constraints on the manipulated variables ($u(i)_{lo}$ and $u(i)_{hi}$) are provided in Table 4.1.

The largest possible disturbance that the unit can handle at steady–state is indicated in Table 4.4. Also indicated are the actual operating points in the partial and complete combustion modes where operation with the maximum possible F_q is feasible. Table 4.5 indicates the sensitivity of the solution of the optimization problem (Equation 4.11) to changes in the constraint boundary, if that constraint is active. A 10% change in the constraint boundary based on the maximum possible range of that variable is considered.

	Partial Combustion	Complete Combustion
Worst Case F_q	2.20	1.17
Operating Point		
F_{cat}/F_{oil} $(\frac{lbcat.}{lbfeed})$	2.5545	3.624
F_{air}/F_{oil} $(\frac{lbair}{lbfeed})$	0.3908	0.5521
T_{feed} $(°F)$	700	574.4
T_r $(°F)$	950	950
T_{rgn} $(°F)$	1400	1400
C_{rgc} $(wt.\%)$	0.5	0.01306
$C_{O_2,fg}$ $(mol.\%)$	0	2

Table 4.4: Largest feasible feed coking quality at steady–state.

From Table 4.4, note the following:

- Heavier feed processing (max. $F_q = 2.20$) is possible in PC mode than CC mode (max. $F_q = 1.17$).

- For complete combustion, the solution lies on the upper T_{rgn} constraint. This is because all the coke on catalyst is burned off completely to CO_2 with an associated large enthalpy of combustion and a large steady–state T_{rgn} value. Note that the solution also lies at the upper limit of $C_{O_2,fg}$. However, the solution to Equation 4.11 is relatively insensitive to changes in the upper limit on $C_{O_2,fg}$ compared to changes in the upper limit of T_{rgn} *e.g.* changing the upper limit of $C_{O_2,fg}$ to 2.15 *mol.*% (10% increase) (see Table 4.5) gives a worst case $F_q = 1.1716$ (0.14% increase). For comparison, increasing the upper limit on T_{rgn} from $1400°F$ to $1430°F$ (10% increase) results in a worst case $F_q = 1.256$ (7.35% increase). This is to be expected. The excess oxygen in the flue gas line simply ensures that essentially all the coke on catalyst is burned off. Changing the upper limit on $C_{O_2,fg}$ allows a higher combustion air flow rate. However, there is a negligible increase in T_{rgn} due to additional coke combustion - there is essentially no more coke to combust. In fact, a slight decrease in T_{rgn} might be observed due to the energy required to heat up the additional air. The effect of changing the upper limit on $C_{O_2,fg}$ on FCC operation is thus minimal.

- In partial combustion, most of the coke is burned to CO with a substantially lower enthalpy change of combustion, and a lower increase in T_{rgn} compared to the $C \rightarrow CO_2$ combustion. The limit for partial combustion lies on the constraint boundaries of T_{rgn} and C_{rgc}. The sensitivity of the maximum value of F_q to changes in the upper limit of either T_{rgn} or C_{rgc} is comparable (Table 4.5).

- The solution to the optimization problem (Equation 4.11) lies at the lower limit of riser temperature ($T_r = 950°$F) for operation in either mode. As already noted, T_{rgn} lies at the upper limit ($T_{rgn} = 1400°F$). The endothermic enthalpy of cracking is highest under these conditions and the associated rate of energy transfer through cracking is the highest in this case. Thus, the largest amount of coke can be combusted under these conditions. However, reducing the lower

limit on T_r is not justified as the rate of feed cracking will decrease further, leading to reduced overall feed conversions, which is undesirable.

- The sensitivity of the maximum F_q in either mode to the actual fresh feed temperature is negligible.

Variable	Units	Limits		10% max. range	Actual change	% change in max F_q	
		Low	High			PC (2.20)	CC (1.17)
T_{rgn}	$(^\circ F)$	1100	1400	30.0	1400→1430	3.18	7.35
C_{rgc}	$(wt.\%)$	0.0	0.5	0.05	0.5→0.55	3.64	N/A
$C_{O_2,fg}$	$(mol.\%)$	0.5	2	0.15	2.0→2.15	N/A	0.14
T_r	$(^\circ F)$	950	1050	10.0	950→940	1.82	2.34
T_{feed}	$(^\circ F)$	400	700	30.0	700→730	0.52	N/A

Table 4.5: Sensitivity of maximum possible steady–state F_q to changes in the active constraint limit for both PC mode and CC mode operation. N/A = not active constraints (Table 4.4).

4.4 Operation in Partial Combustion Mode

In this section different 2×2 control schemes are analyzed for their ability to provide satisfactory regulatory control over the entire range of partial combustion operation. The postulated control schemes are given in Table 4.7 together with the notation used to describe each scheme. The controlled variables considered for partial combustion are given in Table 4.6. The set of possible manipulated variables is given in Table 4.2. In this study, we define ΔT as in Equation 4.16. An identical definition is used in (Arbel et al. 1995), (Hovd and Skogestad 1993) and (Ljungquist 1990) for ΔT. A comparison with these works can therefore be made.

$$\Delta T = T_{fg} - T_{rgn} \tag{4.16}$$

4.4.1 Steady–State Analysis

Figure 4.5 shows the steady–state determinant and steady–state RGAs (for the 1,1 element of the RGA matrix) for controls schemes PC1, PC2 and PC3 where T_r and T_{rgn} are controlled variables.

Controlled Variable	Notation
Riser Temperature	T_r
Regenerator Temperature	T_{rgn}
Flue Gas Exit Temperature	T_{fg}
Temp. rise between regenerator and cyclone	$\Delta T = T_{fg} - T_{rgn}$

Table 4.6: Possible controlled variables for partial combustion mode operation.

	Manipulated Variable Combinations		
	$[F_{air}, F_{cat}]$	$[F_{air}, T_{feed}]$	$[F_{cat}, T_{feed}]$
$[T_r, T_{rgn}]$	PC1	PC2	PC3
$[T_r, T_{fg}]$	PC4	PC5	PC6
$[T_r, \Delta T]$	PC7	PC8	PC9

Table 4.7: Postulated control schemes for partial combustion mode. Notation for each scheme is indicated.

Figure 4.6 shows the steady–state determinant and steady–state RGAs (for the 1,1 element of the RGA matrix) for controls schemes PC4, PC5 and PC6 where T_r and T_{fg} are controlled variables.

Figure 4.7 shows the steady–state determinant and steady–state RGAs (for the 1,1 element of the RGA matrix) for controls schemes PC7, PC8 and PC9 where T_r and ΔT are controlled variables.

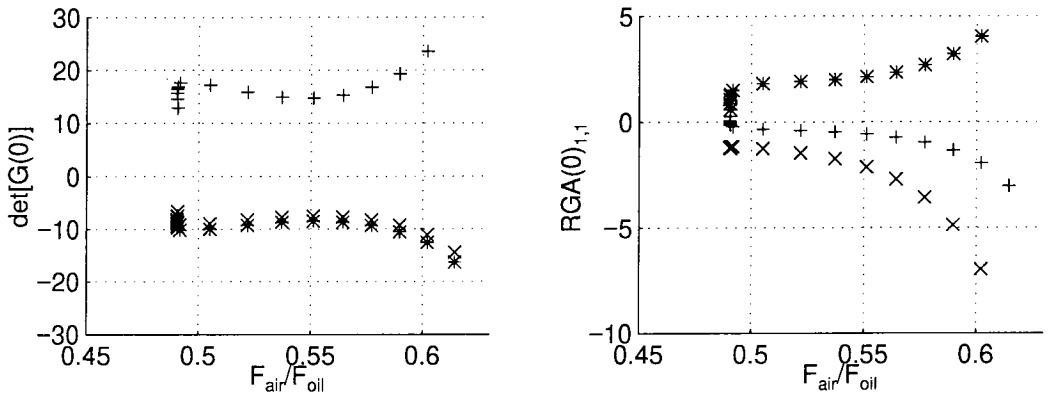

Figure 4.5: Determinant ($\det[G(0)]$) and RGA ($[G(0) \times G(0)^{-T}]_{1,1}$) of partial combustion control schemes with T_r and T_{rgn} as controlled variables at steady–state. $*-$ PC1, $\times-$ PC2, $+-$ PC3, Table 4.7.

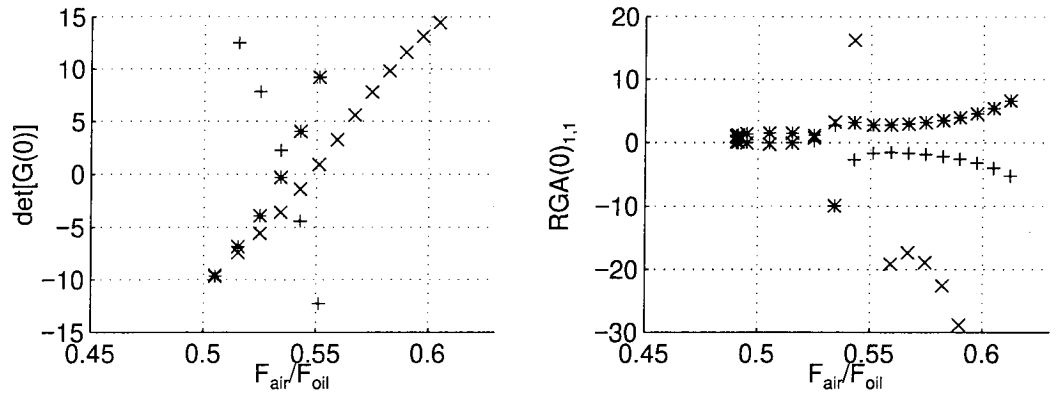

Figure 4.6: Determinant ($\det[G(0)]$) and RGA ($[G(0) \times G(0)^{-T}]_{1,1}$) of partial combustion control schemes with T_r and T_{fg} as controlled variables at steady–state. $*-$ PC4, $\times-$ PC5, $+-$ PC6, Table 4.7.

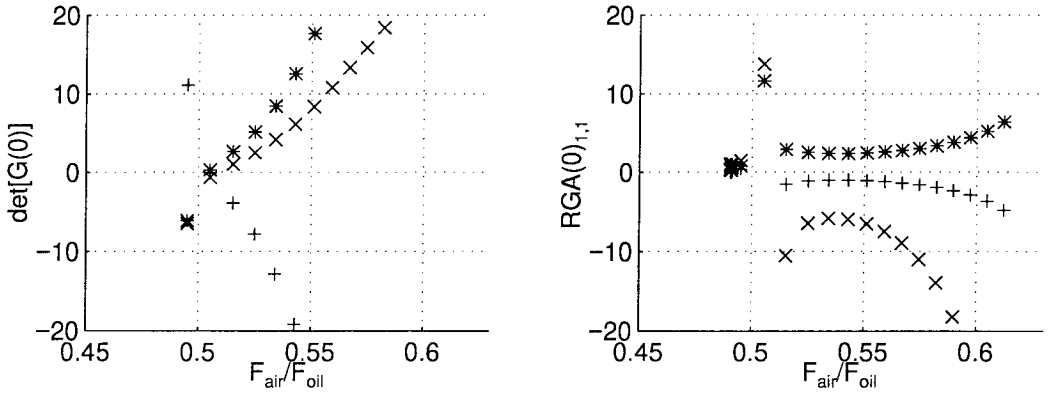

Figure 4.7: Determinant ($\det[G(0)]$) and RGA ($[G(0) \times G(0)^{-T}]_{1,1}$) of partial combustion control schemes with T_r and $\Delta T = T_{fg} - T_{rgn}$ as controlled variables at steady–state. $*-$ PC7, $\times-$ PC8, $+-$ PC9, Table 4.7.

Recall that one of our performance requirements is that of zero steady–state offset *i.e.* integral action is required. Note the following:

- Figure 4.5 shows that the sign of $\det[G(0)]$ is the same (always positive or always negative) for all the control schemes where T_r and T_{rgn} are controlled variables (PC1, PC2, PC3) regardless of the actual operating point. The linearized plants have acceptable steady–state RGA values over the entire operating range.

- Figure 4.6 and Figure 4.7 show that the sign of $\det[G(0)]$ depends on the actual

operating point in partial combustion mode for all the control schemes where T_r and T_{fg} or T_r and ΔT are controlled variables (PC4, PC5, PC6, PC7, PC8, PC9). This is undesirable, as discussed in Section 4.2.6. The steady–state RGA values are reasonable over most of the range except where $\det[G(0)] = 0$ as expected.

The steady–state analysis of the nine control schemes PC1–PC9, and a comparison with previously published work indicates that:

- Using any control scheme where T_{fg} and T_r or T_r and ΔT are both controlled variables is undesirable. There is no controller $K(s) = C(s)\frac{1}{s}$, $C(s)$ stable, that can stabilize the process over the entire operating range, because the sign of $\det[G(0)]$ depends on the actual operating point, and changes over the desired operating regime.

- (Arbel et al. 1996) have considered schemes PC1, PC4 and PC7 in their rank ordering, and identified PC1 to be the best control structure for regulatory control. This conclusion can also be reached simply by analyzing $\det[G(0)]$ for a number of locally linearized plants over the operating range as done here, and in fact shows that PC1 is the best (and only) option out of PC1, PC4 and PC7.

- (Hovd and Skogestad 1993) also compared PC1, PC4 and PC7. However, they reported that PC4 was the best control structure, with PC1 a close second option. This is contrary to our findings. This discrepancy will be analyzed in greater detail in Section 4.4.3.

- Control schemes PC1, PC2, and PC3 where T_r and T_{rgn} are controlled variables appear acceptable, but there is no clear indicator as to which set of manipulated variables is most suitable for rejecting disturbances in feed coking factor. The steady–state RGA values are reasonable. This steady–state analysis does not provide sufficient information to rank order these control schemes. The PRGA and CLDG analysis proposed by (Hovd and Skogestad 1993) suggests PC2 to be the most favorable control structure, followed by PC1. However, as we will

see next, this ordering may not be suitable for operation over a wider regime. PC3 shows high values of the CLDG, and would be eliminated. It is unclear whether the procedure proposed in (Arbel et al. 1996) could rank order PC1, PC2 and PC3 - the qualitative nature of their criteria does not permit a more definite answer.

Since a clear advantage for control schemes PC1, PC2, and PC3 has been demonstrated, we will focus on rank ordering these three control structure candidates only. However, for comparison to the work of (Hovd and Skogestad 1993), we will also consider PC4, but using their model to predict T_{fg}.

4.4.2 Closed Loop Dynamic Analysis

The uncertainty weights used for the analysis (refer to Figure 4.2) are

$$\begin{aligned} w_{\mathrm{i}} &= 0.1 \\ W_{\mathrm{I}} &= w_{\mathrm{i}} I \end{aligned} \tag{4.17}$$

and

$$\begin{aligned} w_{\mathrm{a}} &= \frac{0.3s + 0.0572}{s + 0.0816} \\ W_{\mathrm{A}} &= w_{\mathrm{a}} I \end{aligned} \tag{4.18}$$

Note that the magnitude of the additive uncertainty at low frequency is 0.7 and the magnitude at high frequency is 0.3. This additive uncertainty weight W_{A} (Equation 4.18) has been selected specifically to ensure that $\mu_{\mathrm{RP}} \simeq 1$ over the frequency range of interest for control scheme PC1. The performance weight is exactly as in Equation 4.10 with $\omega_P = 1.0$.

Robust analysis results for partial combustion with control schemes PC1, PC2 and PC3 are indicated in the Figure 4.8. Also shown in Figure 4.8 are typical closed loop step response plots for a unit step in feed coking characteristic. Note the following:

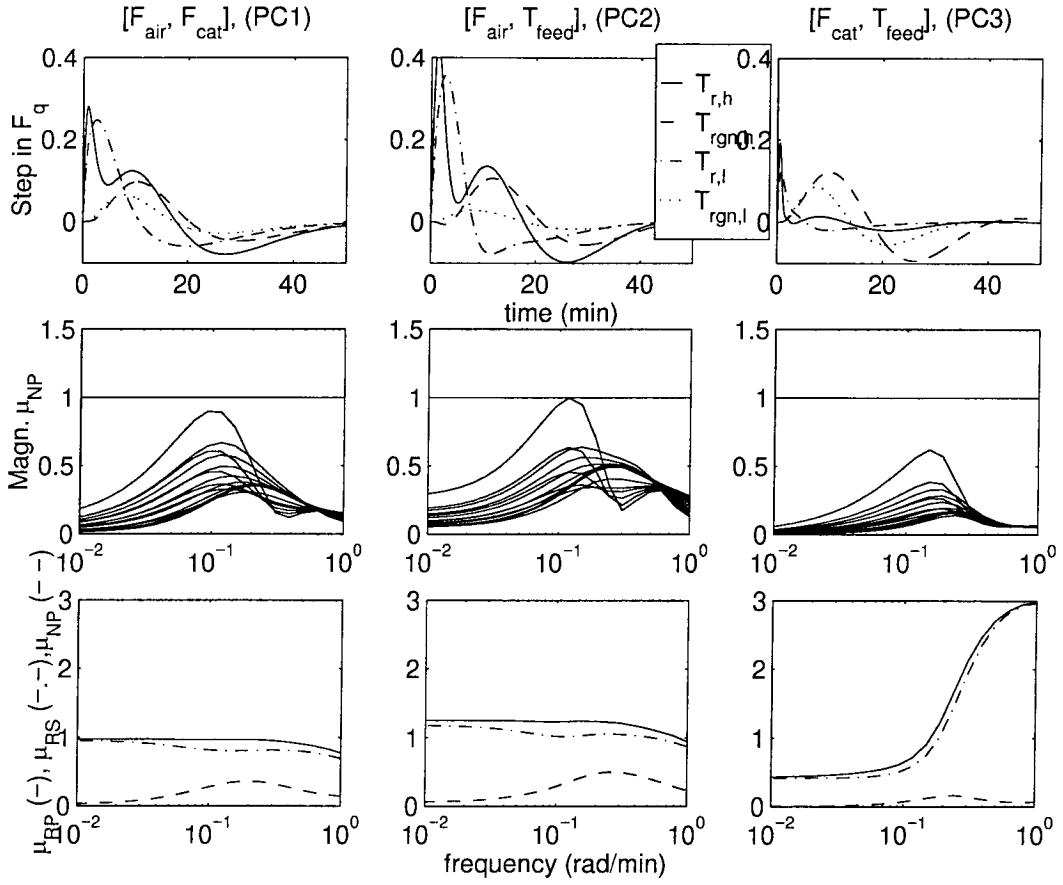

Figure 4.8: Robust analysis, step response to unit step in feed coking quality, nominal performance comparison over the entire partial combustion operating range: ($T_r = 1000°F, 1200°F \leq T_{rgn} \leq 1400°F$, $F_q = 1.0$). Control schemes PC1, PC2 and PC3 of Table 4.7. $\omega_p = 1.0$.

- It was found that the plants corresponding to all three control structures are stable over the entire PC mode operating regime (not shown).

- None of the three control schemes have right half plane transmission zeros (RHPT zeros) over the entire range of operating points. RHPT zeros are known to limit the achievable performance (Holt and Morari 1985a).

- Each element of the set of linearized plants is closed loop stable with the designed μ-optimal controller.

- The observed closed loop response with the designed controller obviously de-

pends on the actual operating point. We show in Figure 4.8 the closed loop time response at extreme ends of the partial combustion operating regime considered. The additional subscript h is used to denote the operating point closest to the upper limit of F_{cat}. The additional subscript l is used to denote the operating point closest to the lower limit of F_{cat}. For example, $T_{r,h}$ in Figure 4.8 refers to the closed loop response of T_r to a unit step in F_q for the operating point at the upper limit of F_{cat}. The closed loop response is comparable over the entire operating regime.

- It is evident from Figure 4.8 that control scheme PC1 provides the best closed loop performance over the entire partial combustion operating range. PC1 sensitivity to uncertainty is lowest i.e. μ_{RP} lowest, and nominal performance is acceptable over entire operating regime i.e. $\mu_{NP} < 1$. The performance achievable with PC2 is only slightly less satisfactory, and a more detailed model might affect the relative ranking. This analysis suggests that T_{feed} might also be suitable as a manipulated variable for regulatory control for PC mode operation.

4.4.3 Comparison of PC1 and PC4 using the Cyclone Combustion Model of Hovd *et al.*

We compare here the performance of PC1 and PC4, when the empirical model of Hovd *et al.* is used for predicting T_{fg}. We note in particular that the steady–state behavior of T_{fg} and T_{rgn} are similar within the operating region they considered ($T_{rgn} \simeq 1280°F$) *i.e.* an increase in T_{rgn} leads to an increase in T_{fg} for both PC1 and PC4. This is discussed in detail in Appendix B, with reference to Figure B.2. Therefore, the steady–state and dynamic characteristics of schemes PC1 and PC4 should be similar in that range. The results of the dynamic analysis for PC1 and PC4 are presented in Figure 4.9. Here we consider a wider operating range for T_{rgn} than considered in Hovd and Skogestad (1993): $1250°F \leq T_{rgn} \leq 1400°F$. The PC1 scheme obtained from the model of Arbel et al. (1995), and the PC4 scheme using the T_{fg} prediction from Hovd and Skogestad (1993) are used in this section. We note

that:

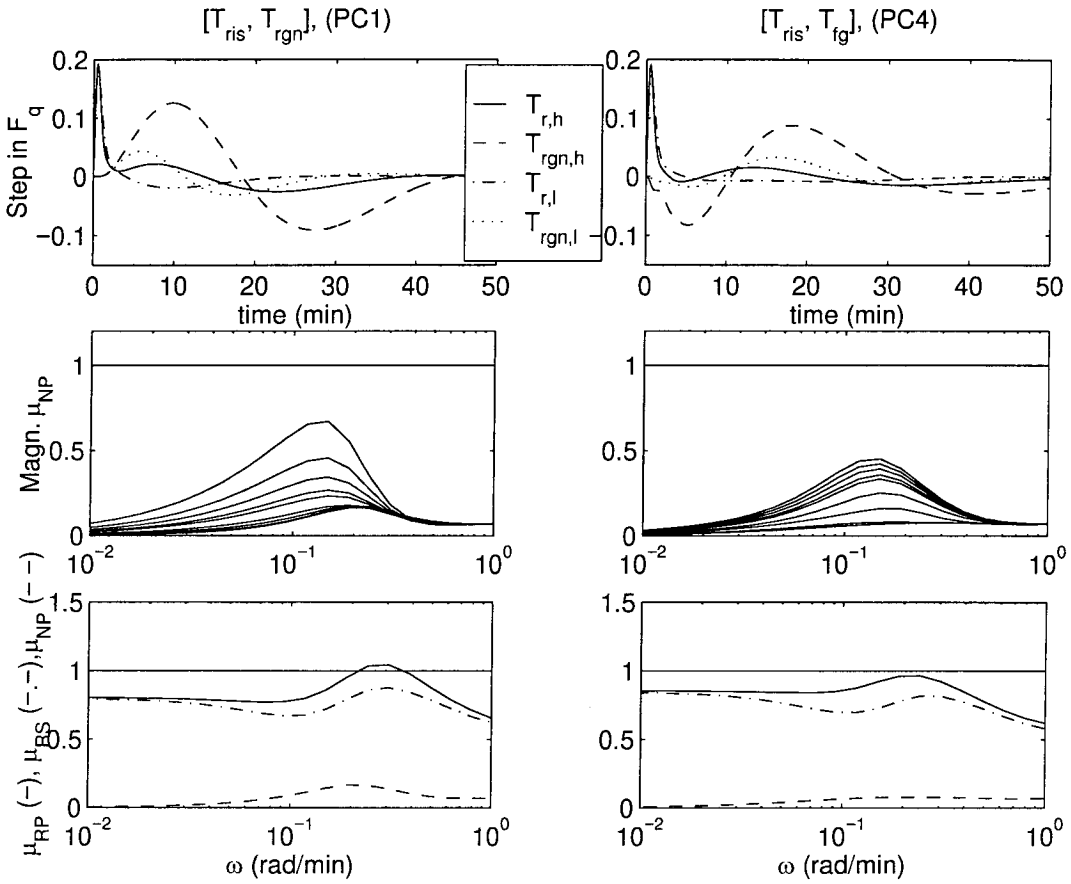

Figure 4.9: Closed loop performance comparison for schemes PC1 and PC4 of Table 4.7 with the T_{fg} prediction model of Hovd *et al.*. $\omega_p = 1.0$.

- det$[G(0)]$ calculated for PC4 using the (Hovd and Skogestad 1993) model does not change sign over the rather limited operating range they considered (not shown). The two operating points they examined are rather close to each other - T_{rgn} differs by 1.2K and T_r by 6.3K. Details on the implementation of their model, which is based on the Kurihara model are given in Appendix B.

- Figure 4.9 shows that the dynamic characteristics of PC1 and PC4 are similar for the operating range considered. The achievable performance with PC4 might actually be considered slightly superior. As Hovd and Skogestad (1993) were more concerned with controlling the cyclone exit temperature, to prevent dam-

aging the cyclones, they selected PC4 as the most appropriate control structure for regulatory control. However, as shown in Appendix B, excessive flue gas temperatures are not of significant concern for high regeneration temperatures, which is the norm for modern FCCUs.

There is however an important reason for not selecting control scheme PC4. As shown in Appendix B, the steady–state plot of T_{fg} over the PC mode operating points suggests that T_{fg} goes through a minimum, regardless of the models used to predict T_{fg} - including the model used by Hovd and Skogestad (1993) (based on the Kurihara model). This results in a sign change of det$[G(0)]$ over the operating regime. The actual minimum T_{fg}, and the T_{rgn} at which it will occur is unit specific, and probably cannot be accurately predicted. Therefore, selecting PC4 might inadvertently limit operation to a limited sub–region of the desired operating range, which is obviously undesirable from a plant operations viewpoint.

4.5 Operation in Complete Combustion Mode

The list of controlled variables considered for complete combustion is given in Table 4.8. The set of manipulated variables considered is given in Table 4.2.

Controlled Variable	Notation
Riser Temperature	T_r
Regenerator Temperature	T_{rgn}
Flue gas O_2 concentration	$C_{O_2,fg}$

Table 4.8: Possible controlled variables for complete combustion mode.

In this study different 2×2 control schemes are examined. Subsequently, one 1×1 control scheme will be proposed and analyzed for the complete combustion mode. The postulated control schemes are given in Table 4.9 together with the notation used to describe each scheme.

	Manipulated Variable Combinations		
	$[F_{air}, F_{cat}]$	$[F_{air}, T_{feed}]$	$[F_{cat}, T_{feed}]$
$[T_r, C_{O_2,fg}]$	CC1	CC2	CC3
$[T_r, T_{rgn}]$	CC4	CC5	CC6

Table 4.9: Postulated control schemes for complete combustion mode. Notation for each scheme is indicated.

4.5.1 Steady–State Analysis

Figure 4.10 shows the steady–state determinant and steady–state RGAs (1,1 element of the RGA matrix) for control schemes CC1, CC2 and CC3 where T_r and $C_{O_2,fg}$ are controlled variables.

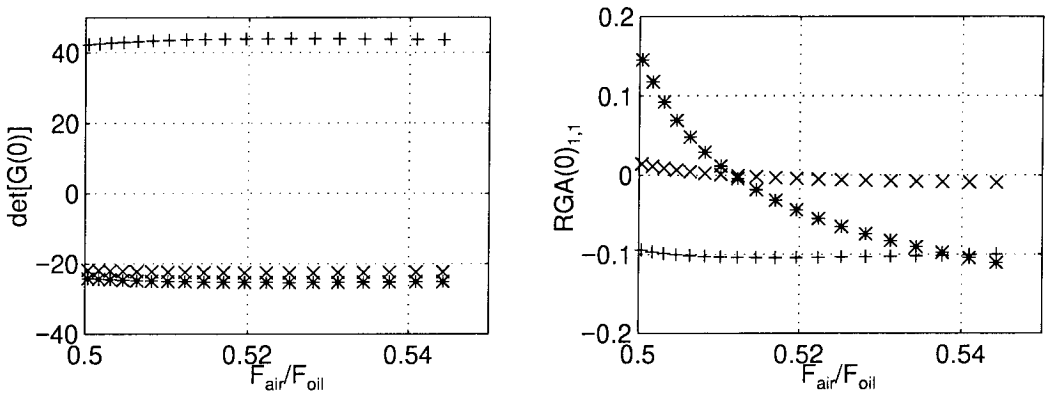

Figure 4.10: Determinant ($\det[G(0)]$) and RGA ($[G(0) \times G(0)^{-T}]_{1,1}$) for complete combustion control schemes with T_r and $C_{O_2,fg}$ as controlled variables at steady–state. $*-$ CC1, $\times-$ CC2, $+-$ CC3 (Table 4.9).

Figure 4.11 shows the steady–state determinant and steady–state RGAs (1,1 element of the RGA matrix) for controls schemes CC4, CC5 and CC6 where T_r and T_{rgn} are controlled variables.

Recall that one of our performance requirements is that of zero steady–state offset for step changes in feed coking quality *i.e.* integral action is required. In view of this requirement, note the following:

- Figure 4.10 shows that the sign of $\det[G(0)]$ is the same (always positive or always negative) regardless of the actual operating point in complete combustion

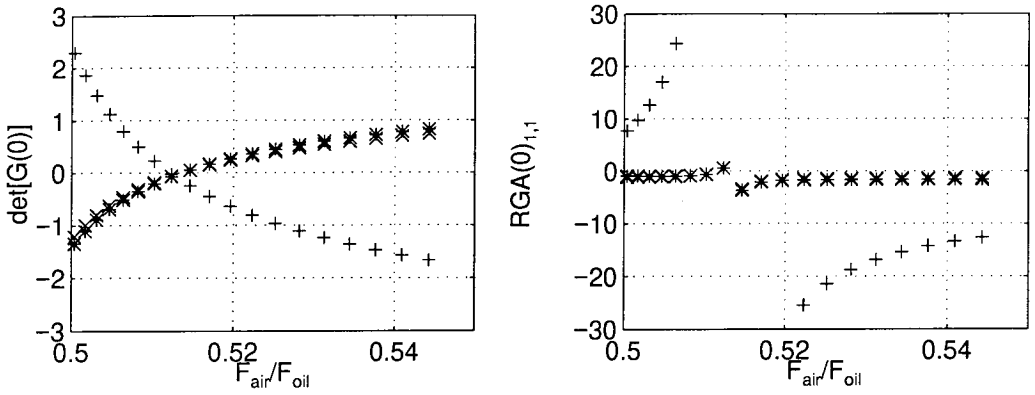

Figure 4.11: Determinant ($\det[G(0)]$) and RGA ($[G(0) \times G(0)^{-T}]_{1,1}$) for complete combustion control schemes with T_r and T_{rgn} as controlled variables at steady–state. $*-$CC4, $\times-$CC5, $+-$CC6 (Table 4.9).

mode for all the control schemes where T_r and $C_{O_2,fg}$ are controlled variables (CC1, CC2, CC3). The linearized plants have acceptable steady–state RGA values over the entire operating range.

- Figure 4.11 shows that the sign of $\det[G(0)]$ depends on the actual operating point in complete combustion mode for all the control schemes where T_r and T_{rgn} are controlled variables (CC4, CC5, CC6). At the operating point where $\det[G(0)] = 0$, $\text{rank}[G(0)] = 1$. The normal rank of all these control schemes is two. These control schemes are therefore not suitable for CC mode regulation.

The steady–state analysis of the six control schemes CC1–CC6 indicates that:

- Using any control scheme where T_{rgn} and T_r are both controlled variables is undesirable. There is no stable controller with integral action that can stabilize the process over the entire operating range, because the sign of $\det[G(0)]$ depends on the actual operating point, and changes over the operating regime. It is interesting to note that Arbel et al. (1996) report that they are not aware of any industrial cases where T_r and T_{rgn} are used as controlled variables for CC mode operation.

- Control schemes CC1, CC2 and CC3 appear reasonable, but there is no clear indicator of the most suitable set of manipulated variables for rejecting disturbances in feed coking factor. This steady–state analysis does not provide sufficient information to rank order the control schemes CC1, CC2 and CC3.

Since a clear advantage for control schemes CC1, CC2, and CC3 has been demonstrated, we will focus on rank ordering these three control structure candidates through the dynamic analysis.

4.5.2 Closed Loop Dynamic Analysis

The goal of the dynamic analysis is to design an optimal controller and compare the best possible performance of the three control schemes CC1, CC2 and CC3. In this study, μ-optimal controllers will be designed for each of the three control schemes, and the closed loop properties will be compared.

The uncertainty weights used for the analysis (refer to Figure 4.2) are

$$\begin{aligned} w_{\mathrm{i}} &= 0.1 \\ W_{\mathrm{I}} &= w_{\mathrm{i}} I \end{aligned} \tag{4.19}$$

and

$$\begin{aligned} w_{\mathrm{a}} &= \frac{0.7s + 0.2055}{s + 0.0734} \\ W_{\mathrm{A}} &= w_{\mathrm{a}} I \end{aligned} \tag{4.20}$$

Note that the magnitude of the additive uncertainty at low frequency is 2.8 and the magnitude at high frequency is 0.7. The performance weight is exactly as in Equation 4.10 with $\omega_P = 1$.

Robust analysis results for complete combustion using T_r and $C_{O_2,fg}$ as controlled variables with control schemes CC1, CC2 and CC3 are indicated in Figure 4.12. Note that the additive uncertainty weight W_{A} (Equation 4.20) has been selected specifically to ensure that $\mu_{\mathrm{RP}} \simeq 1$ over the frequency range of interest for control scheme CC1.

Also shown in Figure 4.12 is a typical closed loop response plot to an unit step in feed coking characteristic. Note the following:

- the plants corresponding to all three control structures are stable over the entire CC mode operating regime.
- None of the three control schemes have right half plane transmission zeros (RHPT zeros) over the entire range of operating points. RHPT zeros are known to limit the achievable performance (Holt and Morari 1985a).
- Each element of the set of linearized plants is closed loop stable with the designed μ-optimal controller.
- For each of the control schemes CC1, CC2 and CC3 the closed loop step response plots for each element of the set of linearized plants is similar to the representative step response plots shown in Figure 4.12. The nominal performance with the designed controllers is close over the entire operating range.
- CC1 sensitivity to uncertainty is lowest i.e. μ_{RP} lowest, and nominal performance is acceptable over entire operating regime i.e. $\mu_{NP} < 1$. The performance achievable with CC2 is only slightly less satisfactory, and a more detailed model might affect the relative ranking. This indicates that T_{feed} might also be suitable as a manipulated variable for regulatory control in CC mode as well.
- It is unlikely that F_{air} would not be used as a manipulated variable. The ability to burn off coke would be limited if F_{air} was maintained constant at any value below the maximum possible. Moreover, the dynamic characteristics (step response, μ_{RP}, μ_{RS}) are more favorable for those control schemes where F_{air} is manipulated. Control scheme CC1 appears to be the most attractive, but the difference between CC1 and CC2 is not significant, and the relative ranking might change if a more detailed FCC model is used (see discussion in section 4.2.5).
- The settling time for CC2 is smaller than CC1 but with larger initial deviations.

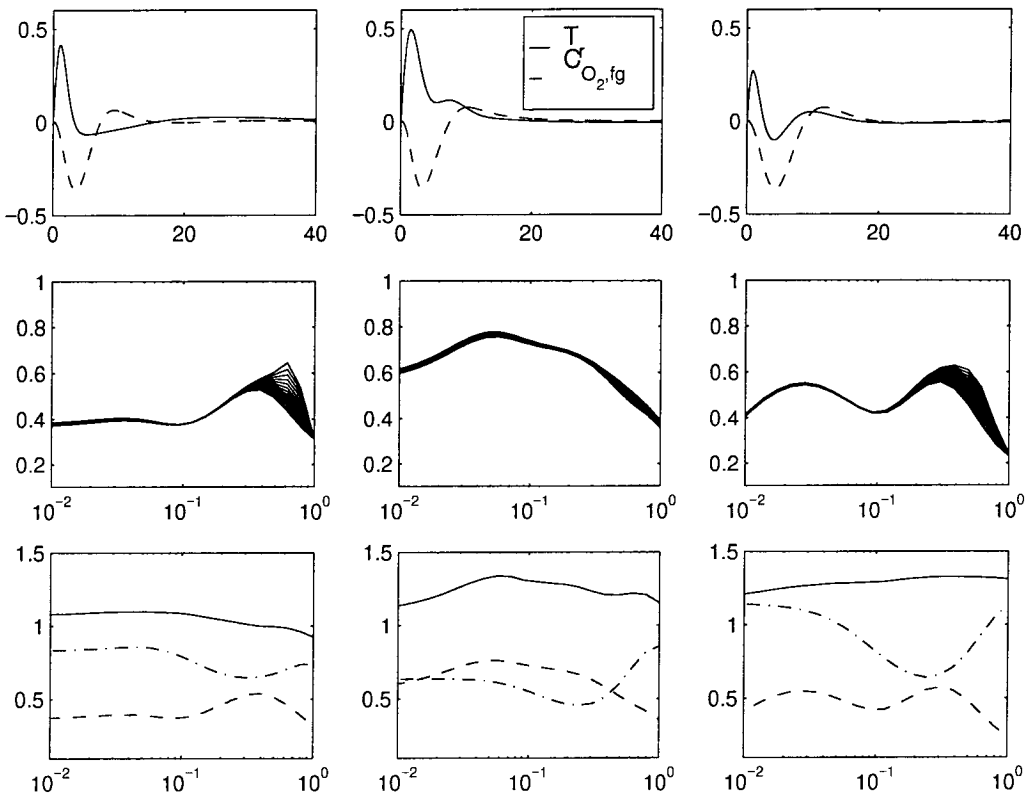

Figure 4.12: Robust analysis for complete combustion. Step response to unit step in feed coking quality. Control schemes CC1, CC2 and CC3, Table 4.9. $\omega_p = 1.0$.

- For CC3, both actuators have a fast and direct effect on T_r but only an indirect effect on $C_{O_2,fg}$. Thus, the T_r response is fastest in CC3, but the response of $C_{O_2,fg}$ is slow and has large deviations as expected.
- Both (Arbel et al. 1996) and (Hovd and Skogestad 1993) indicated that CC1 was the best regulatory control structure for CC mode operation.

SISO Control Schemes for Complete Combustion

As we have just seen, the performance of all the control schemes where T_r and T_{rgn} are *both* controlled variables (schemes CC4, CC5 and CC6) is unacceptable. We would like to examine why controlling both T_r and T_{rgn} leads to unacceptable closed

loop performance in complete combustion, and examine whether there might be any other simpler control structures for CC mode regulation. To begin, note the following observations for the control schemes CC4, CC5, and CC6:

- The plot of T_{rgn} *vs.* F_{air} when $T_r = 1000°F$ goes through a peak over the complete combustion operating regime (Figure 4.13). The physics of the FCC process indicates why this is the case. Owing to the excess air supplied to the regenerator, essentially all the coke on the spent catalyst is burned off. Increasing the combustion air supply initially results in more coke being burned off, increasing T_{rgn}. Additional increase in air supply results in a *decrease* in T_{rgn} because energy is required to heat up the additional air, hence the peak in Figure 4.13.

- The peak in T_{rgn} results in zero steady–state gain for the linearized transfer function between F_{air} and T_{rgn}. This zero gain by itself only indicates that at steady–state the 2×2 plants becomes one–way coupled at this operating point (with multi–variable controller). However, we note from (Figure 4.14) that the gain for the transfer function between F_{air} and T_r also becomes zero at exactly the same operating point. This is because F_{air} affects T_r indirectly through T_{rgn}, and at this operating point, F_{air} has no effect on T_{rgn} and hence T_r. An operating point therefore exists in complete combustion mode where these control schemes have a transmission zero at $s = 0$ *i.e.* the rank of the 2×2 control scheme drops to one at $s = 0$.

- From Figure 4.13 we observe that the change in the steady–state value of T_{rgn} over the entire complete combustion mode is about $1.1°F$ when $T_r = 1000°F$. T_{rgn} remains essentially constant at a value determined by the selected steady–state riser temperature, and the feed quality to the riser.

We can make the following physically justifiable conclusions:

- there is little need to control T_{rgn} when the FCC is operated in CC mode, and as we have just shown, the variation of T_{rgn} over the entire operating range, for

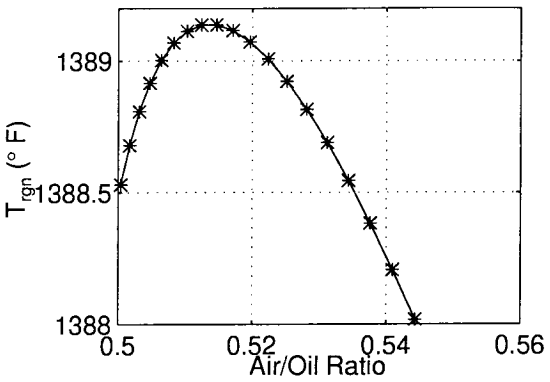

Figure 4.13: Steady–state variation in T_{rgn} as function of F_{air} in complete combustion mode with $T_r = 1000°F$.

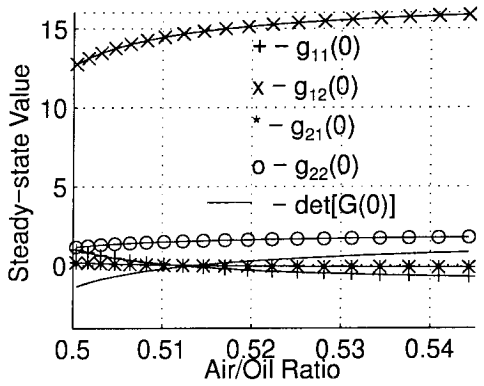

Figure 4.14: $g_{ij}(0)$ and $\det[G(0)]$ for complete combustion control scheme: T_r and T_{rgn} are controlled variables and F_{air} and F_{cat} are manipulated variables.

a given feed quality is very small anyway. The actual value of T_{rgn} is primarily determined by the rate of $C \rightarrow CO_2$ combustion.

- it is well known (*e.g.* (McFarlane et al. 1993, Sadeghbeigi 1995), etc.) that the primary motivation for including $C_{O_2,fg}$ as a controlled variable is to ensure excess O_2 supply, and therefore maintain CC mode operation. We note from Table 4.4 that the steady–state value of F_{air}/F_{oil}, that allows processing the heaviest feed is $F_{air}/F_{oil} = 0.5521$. From Figure 4.10 (or Figure 4.11) this air flow rate is at the upper limit of F_{air}/F_{oil} for feasible CC mode operation. This is

physically justified as the heaviest feed will lead to the highest coke deposition rate in the riser, and will require the maximum air supply rate for complete $C \rightarrow CO_2$ combustion. There is no specific justification for maintaining $C_{O_2,fg}$ at a specific value.

- as always, the importance of tight control on T_r is undiminished.

These observations suggest that a simpler 1×1 control scheme might suffice for regulatory level control of an FCCU in CC mode operation. The following operating strategy is proposed:

1. operate combustion air compressor at full capacity.
2. control T_r
3. manipulate either F_{cat} or T_{feed}

F_{cat} and T_{feed} both appeared to be reasonable manipulated variables when 2×2 control schemes were considered, and so will be considered here. Of course, F_{air} is no longer available as a manipulated variable since the air compressor is operated at full capacity. We examine the following two control structure candidates:

	Manipulated Variable	
	F_{cat}	T_{feed}
T_r	CCA1	CCA2

Table 4.10: Postulated 1×1 control schemes for complete combustion mode. Notation for each scheme is indicated.

The block diagram used for SISO design and analysis is exactly as in Figure 4.2 with the appropriate changes in dimensions. The uncertainty weights used for the analysis are exactly as in Equation 4.20 for the 2×2 CC mode control schemes. The performance weight is exactly as in Equation 4.10 with $\omega_P = 10$. The steady-state $\det[G(0)]$ is shown in Figure 4.15, and the results of the dynamic analysis are shown in Figure 4.16. For these SISO schemes, $\det[G(0)] = g(0)$, a scalar transfer function. However, for consistency, we will continue with the $\det[G(0)]$ notation. We

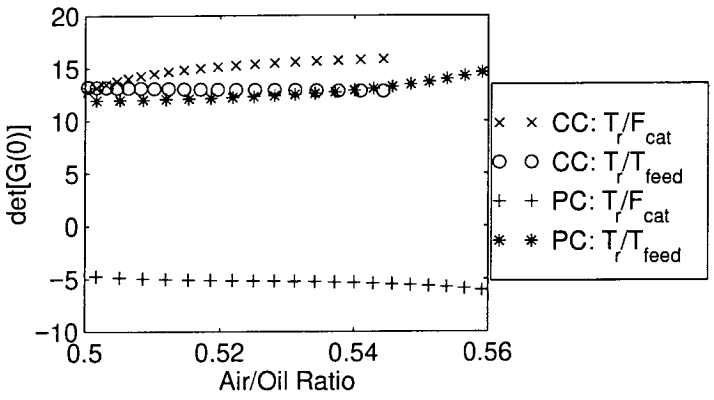

Figure 4.15: Determinant (det[$G(0)$]) for complete combustion control schemes with T_r as controlled variable at steady–state. Solid -T_r/F_{cat}. Dash -T_r/T_{feed}.

note that det[$G(0)$] does not change sign for either CCA1 or CCA2 over the entire CC mode operating range. Furthermore, the performance of both control schemes is satisfactory, but CCA1 is clearly favored. Neither CCA1 or CCA2 have RHPT zeros over the entire operating range. Thus, CCA1 appears to be a viable option for CC mode regulatory control. We are not aware of any published work in the open literature that discusses this control strategy. We address some possible criticism of this control scheme below:

1. An obvious criticism of this 1×1 strategy might be that not controlling $C_{O_2,fg}$ would not guarantee CC mode operation and lead to possible transition to PC mode operation. We submit that this is not the case:

   - for operation at maximum combustion air flow rate , the control scheme CCA1 has det[$G(0)$] > 0 for all plants in the CC mode operating regime, and det[$G(0)$] < 0 for PC mode operation, as seen from Figure 4.15. Thus the process with a controller $K(s) = C(s)\frac{1}{s}$, $C(s)$ stable, tuned for CC mode operation will NOT be closed loop stable in PC mode, and therefore a transition to PC mode operation is *never possible.*

   - CCA1 has a clear advantage over CCA2 on this account. The sign of

$\det[G(0)] > 0$ in both PC mode and CC mode for CCA2. While this does not imply that a transition from CC mode to PC mode operation is imminent, there is no guarantee that such a transition will not occur. CCA2 would therefore not be recommended.

2. Another criticism might be that heavier feeds can be processed if one utilizes the 2×2 control scheme CC1. This is also not justified:

   - by operating at maximum air flow rate, the maximum F_q that can be processed using CCA1 is *exactly identical* to the maximum F_q that can be processed using the 2×2 control scheme CC1. To process the heaviest feed, the set–point for $C_{O_2,fg}$ in CC1 would have to be at the upper allowable limit (2 mol% in this study), and the process would be at exactly the same operating point in the operating space, regardless of whether CCA1 or CC1 was the regulatory level control scheme.

3. It could also be argued that this operating strategy might be expensive because of the potential for large excesses of O_2 in the flue gas - which implies that energy is being wasted in providing unnecessary air flow rates. However, if this is indeed the case, then one of both of the following conditions would prevail:

   (a) higher feed throughputs could be sustained *i.e.* the FCC unit is in sub–optimal operation,

   (b) the combustion air compressor has been significantly over designed for the overall FCC unit.

   Neither of these options is desirable, and would not occur for an appropriately designed unit operating in a reasonable operating regime.

Of course we have assumed that the incoming feed can be processed in the FCC operating in CC mode. Should even heavier feed be introduced, this would require supervisory level intervention, regardless of whether CCA1 or CC1 was used. This is beyond the scope of this work.

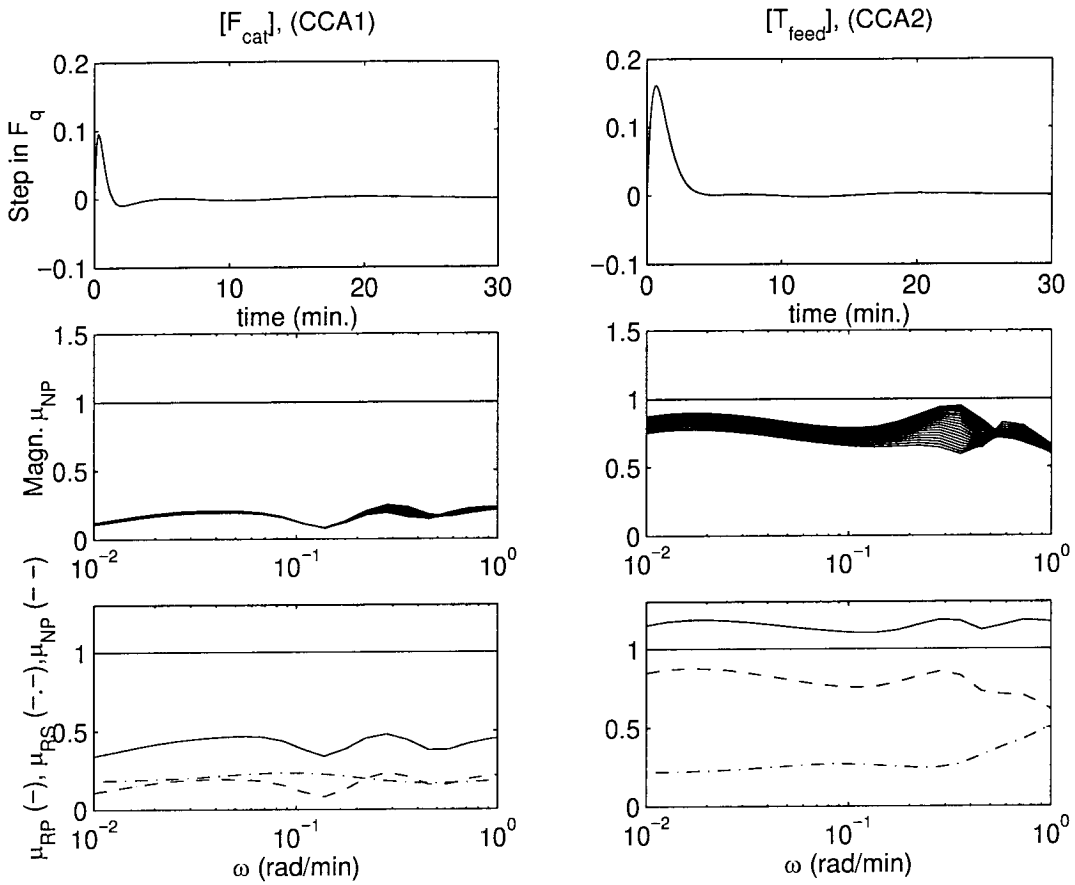

Figure 4.16: Robust analysis for SISO schemes for complete combustion mode. Step response to unit step in feed coking quality. T_r is controlled. $\omega_p = 10.0$.

4.6 Summary and Conclusions

- For PC mode regulation, $[T_r, T_{rgn}]$ are the most suitable choice for controlled variables.
- For CC mode regulation, $[T_r, C_{O_2,fg}]$ are the most suitable choice for controlled variables.
- This analysis suggests that two sets of manipulated variables can in fact result in comparable steady–state and dynamic characteristics. These are:
  1. $[F_{air}, F_{cat}]$
  2. $[F_{air}, T_{feed}]$.

The achievable performance with these two options is comparable, regardless of the type of uncertainty weight (input, additive) or structure (diagonal, full block). Thus, for older FCCUs where direct manipulation of F_{cat} is not possible (*e.g.* Exxons Model IV FCCU), the feed temperature T_{feed} could also be an effective manipulated variable for regulatory control in both CC and PC mode operation.

- The rank ordering of 2×2 control schemes reported in (Arbel et al. 1996) could have been obtained with significantly less effort simply by examining the variation of $\det[G(0)]$ over the entire operating range.

- (Hovd and Skogestad 1993) indicated that the 2×2 control scheme with $[T_r, T_{fg}]$ as controlled variables, and $[F_{air}, F_{cat}]$ as manipulated variables was the most appropriate choice for regulatory control. However, our analysis shows this choice to be undesirable if operation over a wider regime is considered.

- A simple control strategy for CC mode operation is proposed and analyzed. The strategy involves:

  1. operating the combustion air compressor at full capacity at all times
  2. using a single loop controller with integral action ($K(s) = C(s)\frac{1}{s}$, $C(s)$ stable), with T_r controlled be manipulating F_{cat}.

  It is shown that this strategy:

  - provides good performance
  - guarantees that the process will not revert to PC mode operation (guaranteed by integral action)
  - can process the same range of feed qualities as the 2×2 control scheme where $[T_r, T_{rgn}]$ are controlled using $[F_{air}, F_{cat}]$.

- This study reiterates the intuitively plausible notion that it is important to obtain process information over the entire expected operating range of interest.

Often, the analysis of the characteristics of a set of linear models describing the local dynamics over the entire operating range is sufficient to eliminate a large number of control structure candidates.

- In general, a combination of steady–state analysis and dynamic analysis is required to correctly rank order the available control structures. As shown with this FCC example, simply looking at either steady–state or dynamic characteristics might yield insufficient information, and lead to incorrect rank ordering. For example, the steady–state analysis of partial combustion control structures PC1 and PC2 would not be sufficient to rank order these two options. The rank ordering was achieved through the dynamic analysis.

Chapter 5 Decentralized Regulatory Control of the FCC Process in Partial Combustion Mode

Summary

In this chapter, several aspects of decentralized regulatory control of the FCC process operating in the partial combustion mode are analyzed. The control of the FCC where riser temperature (T_r) and regenerator temperature (T_{rgn}) are controlled by manipulating catalyst circulation rate (F_{cat}) and combustion air supply rate (F_{air}) or F_{cat} and fresh feed temperature (T_{feed}) is examined. The pairings where T_r is controlled using F_{cat} and T_{rgn} controlled using F_{air} or T_{feed} - the [T_r/F_{cat}, T_{rgn}/F_{air}] pairing, and the [T_r/F_{cat}, T_{rgn}/T_{feed}] pairings respectively are shown to be the preferred choices:

- the achievable performance is superior to the alternate pairings with decentralized PI controllers, regardless of the source of uncertainty (additive, input multiplicative).
- the effort required to tune the decentralized PI controller for acceptable performance is shown to be minimal.

Moreover, it is shown that for these two pairings: (1) The performance degradation when using decentralized PI controllers instead of full μ-optimal controllers is not significant. (2) Decentralized PI controllers can be designed for acceptable performance over a wide operating regime. (3) If it is established that process interactions are significant, performance improvements can be achieved by "tightening" the decentralized PI controller, as the operating bandwidth is then pushed into a region of lower process interactions. (4) Reasonable transitions to unstable operating points can be effectively handled with an appropriately tuned decentralized PI controller.

Finally, a theoretical development that provides insight into possible changes in the sign of the steady–state and infinite frequency RGA elements is also presented. It is found to be related to the non–minimal phase behavior of one or more of the following: (1) the overall plant, (2) the individual loop transfer functions, (3) the remaining system if a set of controlled variables and the associated manipulated variables is removed. Stable plants for which pairing for performance can correspond to negative steady–state RGA pairings are identified

5.1 Introduction

Decentralized control remains popular in industry despite developments in advanced control synthesis procedures that lead to full multivariable controllers. Decentralized control involves using a diagonal or block–diagonal controller. Some benefits of decentralized control include:

- tuning and retuning the loops to account for changing process conditions is simpler
- they are simpler to understand and implement
- sensors or manipulated variables may fail. Tolerance to such failures is more easily incorporated into the design of decentralized controllers than full controllers.
- the control system can be brought gradually into service during startup, and gradually taken out of service during process shutdown.

The design of decentralized controllers consists of three steps:

1. Control structure selection: the selection of sets of controlled variables and sets of manipulated variables for effective process control.
2. Pairing selection: pairing of the selected inputs and outputs.
3. Controller design: design of the individual controllers for each loop.

For the FCC process, the control structure selection (Step 1) was carried out in detail in Chapter 4. In this chapter, we will focus on Step 2 and Step 3.

5.2 Problem Statement

We have seen in Chapter 4 that in partial combustion mode operation, two different 2×2 control structures can provide comparable regulatory level performance for the FCC. In particular, the following conclusions were made:

- The most suitable set of controlled variables are the riser temperature (T_r), and the regenerator dense bed temperature (T_{rgn}).

- The analysis suggested that two sets of manipulated variables can in fact lead to comparable steady–state and dynamic characteristics. These are:

  1. the combustion air rate (F_{air}) and the catalyst circulation rate (F_{cat}).
  2. the combustion air rate (F_{air}) and the fresh feed pre-heat temperature (T_{feed}).

  The achievable performance with these two options was shown to be comparable, regardless of the type of uncertainty weight (input, additive) or structure (diagonal, full block).

These conclusions were based on analyzing closed loop robust performance with a full order μ-optimal controller designed for each control structure studied. Because of the many advantages of using decentralized controllers described in the introduction, the current practice in industry is to use single–loop controllers for FCC regulatory control. A main objective in this chapter is therefore to investigate the significant characteristics of the above 2×2 control schemes when decentralized controllers are used. The major emphasis will be on some more specific problems:

- What is the most suitable pairing for decentralized regulatory control with single–loop PI controllers? Single–loop, fixed structure controllers are most relevant from an applications viewpoint. The goal here will be to compare the best performance achievable with single loop fixed order controllers for the two possible pairings.

- What degree of performance degradation can be expected by using decentralized PI controllers instead of the full μ-optimal controllers ?

- Which control structure and associated pairing is most suitable from an "ease of operation" viewpoint? This is discussed in Section 5.7.1.

5.3 Preliminaries

5.3.1 Notation

We will follow the same notation as used in Chapter 4, which will be summarized here for continuity of presentation:

- **PC mode** - refers to FCC operation in the partial combustion mode. In this mode, coke on spent catalyst is burned partially to CO (ΔH_{comb}= 47.5 KJ/mol) and partially to CO_2 (ΔH_{comb} = 169.3 KJ/mol) in the regenerator. Significant quantities of both CO and CO_2 are present in the regenerator flue gas. The focus of this chapter is on the PC mode operating regime.

- The controlled variables and manipulated variables we will consider are indicated in Table 5.1.

Variable Description	Notation
Manipulated Variables	
Combustion air flow rate	F_{air}
Catalyst circulation rate	F_{cat}
Fresh feed pre–heat temperature	T_{feed}
Controlled Variables	
Riser top temperature	T_r
Regenerator dense bed temperature	T_{rgn}

Table 5.1: Nomenclature for manipulated and controlled variables for partial combustion mode operation.

- **Control structure (control scheme)** - refers to the set of manipulated variables and controlled variables selected to provide 'acceptable' regulatory level control of the overall process. Specifically, we will consider 2×2 control structures *i.e.* a combination of two manipulated variables and two controlled variables.

- As in Chapter 4, 2×2 control structures will be analyzed, as they were found to provide acceptable (and comparable) performance with the full order μ-optimal

controllers. The combination of the two manipulated variables and the two controlled variables are given in Table 5.2, together with the notation used to define them (exactly as in Chapter 4).

	Manipulated Variable Combinations	
	$[F_{air}, F_{cat}]$	$[F_{air}, T_{feed}]$
$[T_r, T_{rgn}]$	PC1	PC2

Table 5.2: Regulatory level control structures for PC mode operation.

- Since one objective is to analyze and compare the performance of the possible pairings for the two control structures PC1 and PC2, we will also adopt the additional notation indicated in Table 5.3 to denote the two possible pairings for each control structure. We note the following points about Table 5.3:

SISO Loop combination	Notation
Control Scheme PC1	
T_r/F_{cat} & T_{rgn}/F_{air}	$PC1^C$
T_r/F_{air} & T_{rgn}/F_{cat}	$PC1^N$
Control Scheme PC2	
T_r/T_{feed} & T_{rgn}/F_{air}	$PC2^C$
T_r/F_{air} & T_{rgn}/T_{feed}	$PC2^N$

Table 5.3: Nomenclature for pairing possibilities for PC1 and PC2 control structures.

  - the superscript 'C' signifies 'conventional' as the indicated pairings $PC1^C$ and $PC2^C$ are the most commonly reported in the FCC literature, and are the intuitively appealing choice.
  - the superscript 'N' signifies 'non–conventional' as the indicated pairings $PC1^N$ and $PC2^N$ are either not reported, or are deemed non–intuitive, and usually not used in industrial practice.
  - The choice of pairings corresponding to $PC1^C$ is essentially obvious due to a large number of publications indicating the use of this pairing. However, the choice of $PC2^C$ is not as clear, since the PC2 control scheme has not

been rigorously discussed and analyzed in the FCC literature. We have termed the pairing T_r/T_{feed} and T_{rgn}/F_{air} the "conventional pairing" for PC2 based on heuristic arguments similar to those used in (Arbel et al. 1996) for the PC1 control scheme. Of course we will quantitatively analyze both pairings $PC2^C$ and $PC2^N$, and show in Section 5.7.2 that the preferred pairing for PC2 is indeed $PC2^C$.

5.3.2 Range of PC Mode Operation

The feasible steady–state operating region is indicated as the solid line in Figure 5.1, where the feasible operating points are shown as the locus of the steady–state values of F_{air}/F_{oil} and F_{cat}/F_{oil}. The following conditions are used in deriving the feasible operating region:

1. constant fresh feed rate - F_{oil}
2. constant fresh feed temperature - T_{feed}
3. F_{cat} is adjusted to ensure that $T_r = 1000°F$

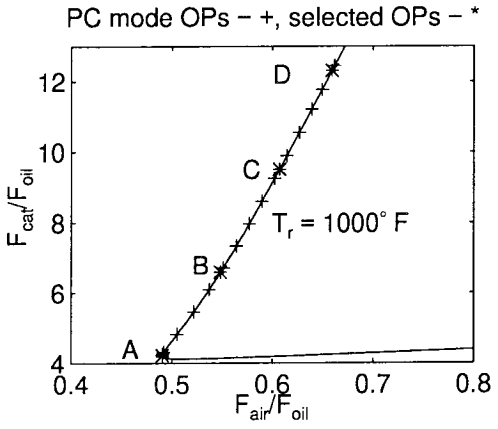

Figure 5.1: FCC operating region indicating the four points selected for nominal stability analysis in PC mode. The solid line indicates the entire range of feasible FCC operation for $T_r = 1000°F$, including complete combustion mode (compare Figure 4.3 and Figure 4.4).

Under these conditions, there is one degree of freedom, and we specify F_{air}. Steady–states are determined for a range of F_{air} values, and the results are plotted in Figure 5.1. Note that the solid line indicates both partial combustion and complete combustion operation (not discussed in this chapter). The PC mode operating regime is taken to be:

1. $T_r = 1000°F$

2. $1100°F \leq T_{rgn} \leq 1400°F$

and this PC mode operating regime is marked by the "+" in Figure 5.1. Note however, that most FCCs typically operate at $T_{rgn} \geq 1200°F$, and the lower limit actually allows for possible regenerator temperatures considerably below this normal range. The lower limit on T_{rgn} is taken to be $1100°F$ to allow investigation of possible operation at unstable operating points. Moreover, for ease of discussion, four representative points are selected spanning the entire operating range considered. These points are marked A, B, C, D, and the steady–state values of some selected process variables at each of these points are tabulated in Table 5.4.

		Operating Point			
Process var.	Units	A	B	C	D
Coke on spent cat.	$wt.\%$	0.9159	0.9247	0.9512	0.9898
Stripper Cat. temp.	$°F$	975.0	975.0	975.0	975.0
Coke on regen. cat.	$wt.\%$	0.03164	0.1821	0.3671	0.5133
Regenerator temp. (T_{rgn})	$°F$	1380.3	1248.8	1173.8	1134.2
Riser temp. (T_{rgn})	$°F$	1000.0	1000.0	1000.0	1000.0
F_{air}/F_{oil}	$\frac{lbair}{lbfeed}$	0.490	0.548	0.607	0.659
F_{cat}/F_{oil}	$\frac{lbcat.}{lbfeed}$	4.22	6.59	9.50	12.31
Stability	–	Stable	Stable	Stable	Unstable

Table 5.4: Process conditions at selected PC mode operating points - A, B, C, D in Figure 5.1.

5.4 Some Characteristics of Open Loop FCC Operation

5.4.1 Steady–State Operating Characteristics

An interesting property of the CCNY/Mobil model is that at constant T_r in partial combustion mode operation, the steady–state combustion air requirement decreases as the regenerator temperature increases. This steady–state characteristic in the T_{rgn} *vs* $/F_{air}/F_{oil}$ plot when T_r is constant is shown graphically in Figure 5.2. For this setup, there is only one degree of freedom and as in Figure 5.1 the combustion air rate (scaled by the fresh feed rate (F_{oil})) is specified. This operational characteristic can be rationalized by the following arguments:

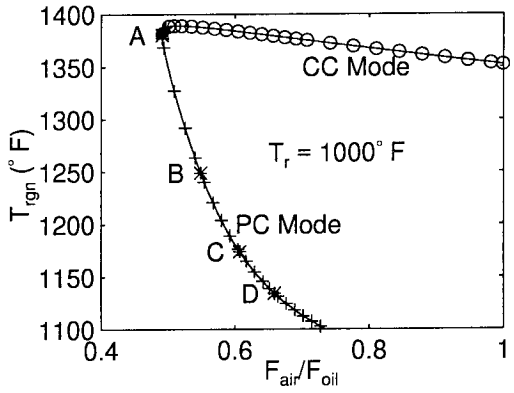

Figure 5.2: Steady–state operating characteristic for partial combustion mode (+) and complete combustion mode (o). The points A, B, C, D are the same as in Figure 5.1.

- at constant T_r, the required F_{cat} (equivalently F_{cat}/F_{oil}, F_{oil} = constant) is lower at a higher T_{rgn} value.
- because the F_{cat}/F_{oil} ratio in the riser is then lower (F_{oil} constant), the rate of coke production (Ck_p) is lower because the relative number of available active sites is lower.
- since Ck_p is lower, the required air rate to combust the produced coke is lower.

Therefore, at constant T_r, operating at a higher steady–state T_{rgn} will require lower amounts of F_{air}. Note however that the cracking severity, which can be defined as Ck_p/F_{cat} is in fact higher at higher T_{rgn}. The cracking severity is a measure of how much cracking product can be obtained from a given amount of hot catalyst.

5.4.2 F_{cat} as an Independent Variable

F_{cat} has been assumed for modeling purposes to be an independent variable. However, it is clear from the physical setup of the FCC that F_{cat} is not an independent variable, but rather depends on the relative pressure and inventory differences between the reactor and regenerator sections.

However, the slide valves (if available) allow the actual catalyst circulation rate ($F_{cat}\ |_{actual}\ (t)$) to be quickly adjusted to the desired value ($F_{cat}\ |_{desired}\ (t)$) when changes are required to compensate for process upsets *i.e.* the dynamics between $F_{cat}\ |_{desired}\ (t)$ and $F_{cat}\ |_{actual}\ (t)$ is fast, with a time scale of 1–2 mins. (Shinnar 1997). Because these time constants are much faster than the overall FCC time constant (20 – 50 mins., and dominated by the regenerator dynamics), it is assumed for modeling purposes that $F_{cat}\ |_{desired}\ (t) = F_{cat}(t) \forall t$, and $F_{cat}(t)$ is therefore taken to be an independent variable. The obvious dependence of F_{cat} on time is not always explicitly indicated for brevity. Moreover, as discussed in Chapter 4, Section 4.2.5 the dynamic behavior between $F_{cat}\ |_{desired}\ (t) = F_{cat}(t)$ and $F_{cat}\ |_{actual}\ (t)$ is modeled by a first order lag with a time constant of 0.5 min (Sorensen 1993, Shinnar 1997).

$$G_{\text{cat}}(s) = \frac{1}{0.5s + 1} \tag{5.1}$$

5.5 Decentralized Control

In this Chapter, $G(s)$ refers to the square 2×2 plant and $C(s)$ refers to the decentralized controller, as shown in Figure 5.3.

Furthermore, without loss of generality, we will assume that $C(s)$ is diagonal, after possibly rearranging the order of the columns or rows of the plant $G(s)$. It will

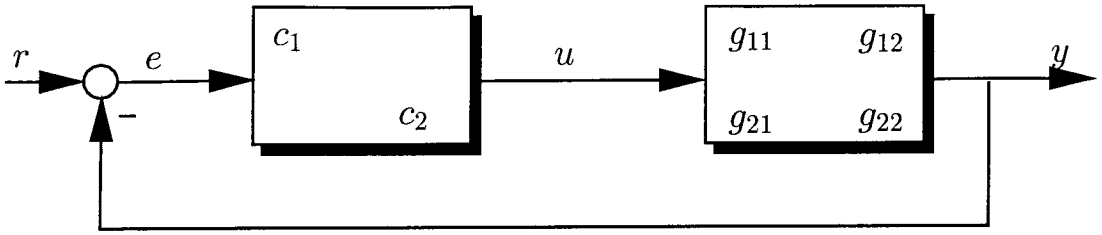

Figure 5.3: Decentralized control structure. $C(s) = \text{diag}\{K_1[1 + \frac{1}{\tau_1 s}], K_2[1 + \frac{1}{\tau_2 s}]\}$

be assumed throughout that the controller $C(s)$ contains integrators in all channels. Several methods for tuning decentralized controllers have been proposed in the literature. In this section, an overview of the current methods for decentralized controller design will be described.

- *Sequential loop closing:* This design approach involves designing each element (or block) in $C(s)$ sequentially. Typically, the controller corresponding to the fastest loop is designed first. This loop is then closed before the design proceeds to the next control loop. This means that the information about the "lower–level" controllers is directly incorporated into the design of subsequent loops. The final test is to examine the closed loop characteristics of the overall system. The main disadvantages of this sequential procedure include (Skogestad and Morari 1989):

  - failure tolerance is not guaranteed when "lower–level" loops fail.
  - overall closed loop properties (*e.g.* robust performance) depend strongly on the order in which loops are closed.
  - the design typically proceeds by trial–and–error.

  At least two methods for sequential loop design have been proposed in the recent past. These are:

  1. Procedure of Hovd and Skogestad (1994).
  2. Procedure of Chiu and Arkun (1992) for robust performance.

- *Independent design of each loop:* In this design method (e.g. Skogestad and Morari (1989)), each controller is designed independently of the others. This method has the following advantages:
  - robust performance of the overall closed loop is guaranteed if certain conditions on each loop are satisfied, and the closed loop is internally stable. These conditions are detailed in Skogestad and Morari (1989).
  - built in failure tolerance. Nominal stability of the remaining system is guaranteed if any combination of loops fail.
  - each loop is designed directly with no need for a trial–and–error procedure.
- *Parameter optimization for fixed controller structure:* This design approach involves optimizing the tuning parameters of a fixed order controller directly to realize some performance objective. The controller structure is typically fixed (*e.g.* decentralized controller, PI/PID controllers etc.). The main advantage of this method is that the tunings are determined to be optimal with respect to some closed loop property. The main drawback is that typically, there is no guarantee that the resulting tunings yield the globally optimal value of the objective function. For example, the minimization of the infinity norm of the closed loop transfer function using a fixed order controller is a non–convex optimization problem with many local minima (Zhou, Doyle and Glover 1996).

In this Chapter, we are interested in comparing the best achievable performance of the two possible pairings for each control structure. While the independent and sequential procedures can be used to design robust decentralized controllers, nothing can be said about the optimality of the resulting closed loop. As indicated in Section 5.2, the common industrial practice at the regulatory level is to use PI controllers. We will therefore fix the overall controller to be diagonal PI controllers and tune the four parameters (two gains, two reset times) to minimize an objective function, to be described next.

5.5.1 Performance Analysis Setup

One of our objectives is to compare the best achievable performance of the possible pairing options for each selected control structure (*i.e.* $PC1^C$ *vs* $PC1^N$ and $PC2^C$ *vs* $PC2^N$). In this Chapter, the achievable performance is quantified using the structured singular value (μ) introduced by (Doyle 1982). The main advantage of the structured singular value that is relevant for this work is that it allows for a rigorous and explicit consideration of process uncertainty which is always present in practice. In particular, we will consider:

1. Input uncertainty - the combustion air compressor used to vary the combustion air rate (F_{air}), the catalyst slide valves used to vary circulation rate (F_{cat}), and the feed pre–heat furnace used to vary the fresh feed temperature (T_{feed}) are large process components. The dynamics associated with these components cannot be ignored in analyzing the achievable closed loop performance of the FCC (Grosdidier et al. 1993). However, as is the case for the overall process model, the actuator dynamics are not precisely known. Therefore, we will be have to be concerned with the following issues:

   - possible (uncertain) time delays in the actuator dynamics,
   - uncertain structure of the actuator dynamics model.

   The input uncertainty weight used is exactly as in Chapter 4, and repeated in Equation 5.2. Note that this input uncertainty weight accounts for neglected time delays of up to one minute, which is the largest time delay in the actuator dynamics reported in Grosdidier et al. (1993).

$$w_{\mathrm{i}} = \frac{2s + 0.1629}{s + 1.6285}$$
$$W_{\mathrm{I}} = w_{\mathrm{i}} I \tag{5.2}$$

2. Additive uncertainty - the model of the FCC used is only an approximate de-

scription of the actual process. Possible uncertainties in the model structure, as well as the dynamic behavior of the model are accounted for by incorporating an additive uncertainty block. The actual values of the uncertainty weights are exactly as in Chapter 4, and repeated in Equation 5.3.

$$w_{\mathrm{a}} = \frac{0.3s + 0.0572}{s + 0.0816}$$
$$W_{\mathrm{A}} = w_{\mathrm{a}} I \tag{5.3}$$

Note that it is important to evaluate the sensitivity of our conclusions to possibly different sources of uncertainty. In particular, we have examined the effect of multiplicative input uncertainty and additive uncertainty, as was also done in Chapter 4.

The objective function we will utilize to quantify the achievable performance is the robust performance μ (μ_{RP}). The optimization problem will involve selecting the controller tuning parameters to minimize $\max_\omega \mu_{RP}(\omega)$ over some frequency range. This will result in a μ-(sub)optimal PI controller. By μ-(sub)optimal PI controller we mean a 2×2 decentralized controller consisting of two PI controllers along the main diagonal, with the tuning parameters selected to minimize $\max_\omega \mu_{RP}(\omega)$ for the interconnection shown in Figure 5.4 over the selected frequency range. The frequency range of interest is taken to be $10^{-2} - 1$rad/min., which represents process changes on time scales of minutes to hours. This controller is designed to give the best possible performance for the worst combination of uncertainties and disturbances. Furthermore, every effort will be made to determine whether the conclusions remain (at least qualitatively) unchanged despite different assumptions on the sources and/or magnitudes of the assumed uncertainty description.

The "optimal tuning" for the decentralized PI controller is obtained by a general purpose constrained optimization routine provided in the Optimization Toolbox in MATLAB. In general, there is no guarantee that these values reflect the true optimum, hence the terminology "(sub)optimal" is used. In particular, it is known that for fixed structure controllers, the minimization of the infinity norm of the closed loop transfer

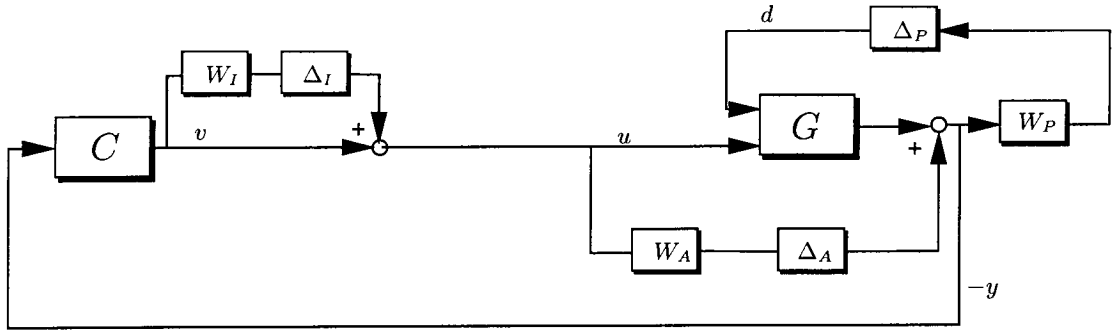

Figure 5.4: Closed loop analysis setup. $C(s)$ is a decentralized PI controller.

function is a non–convex optimization problem with possibly many local minima. However, a large number of optimization runs were carried out for each case reported, starting from a wide range of different initial guesses, and it is unlikely that tunings can be found for which the resulting μ_{RP} values would be significantly lower than the values reported here. It was also found that many significantly different sets of tuning parameters resulted in comparable robust performance.

5.6 Relative Gain Array Analysis for PC Mode Schemes

The steady–state RGA matrix $[\lambda_{ij}(0)]$, any RHPT zeros, and any RHP zeros in the individual elements of the transfer matrix are tabulated in Table 5.5. Referring to Table 5.5, we note the following:

	Control Scheme					
	PC1			PC2		
Steady–state RGA	T_r T_{rgn}	−1.1 2.1 2.1 −1.1	F_{cat} F_{air}	T_r T_{rgn}	3.02 −2.02 −2.02 3.02	F_{cat} T_{feed}
RHPT Zeros	–			–		
RHP zeros in elements		0.0566 −− −− −−			−− −− −− −−	

Table 5.5: Steady–state RGA values, RHPT zeros and check of any RHP zeros in individual elements.

- The PC1^C scheme corresponds to pairing on *negative* steady–state RGAs ($\lambda_{11}(0) = \lambda_{22}(0) = -1.1$). Recall the definition of decentralized integral controllability

(DIC) (Morari and Zafiriou 1989): (1) the overall closed loop is stable, and (2) the controllers of any subset of loops can be arbitrarily detuned without affecting the closed loop stability. A necessary condition for DIC is that $\lambda_{ii}(0) > 0$ for each loop i. From a DIC viewpoint, the alternate PC1^N pairing would be favored, as it corresponds to positive steady–state RGA pairings. In particular, for PC1^C with negative feedback, if the decentralized PI controller is designed with positive gains for both PI controllers, then the T_r/F_{cat} loop would be unstable if the other loop (T_{rgn}/F_{air}) failed or were put on manual, which is clearly undesirable. It is however reported in (Arbel et al. 1996) that "such failures are rare, and fortunately the system is quite slow to respond, giving the operator ample time to intervene". We will show in Section 5.7.1 that despite this possible disadvantage, the achievable performance with the PC1^C pairing is superior to the performance achievable with the PC1^N pairing with positive gains for both c_1 and c_2 in the decentralized PI controller for PC1^C. Furthermore, internal stability is guaranteed for the conventional pairing over a wide range of controller tuning parameters if both controllers are tuned with positive gain as shown in Section 5.7.1.

- For PC2^C, the diagonal steady–state RGA value corresponds to pairing on *positive* RGAs. Stability for this pairing is therefore unaffected by failure, detuning or opening of either of the two loops *i.e.* PC2^C is DIC.

- Control schemes PC1 and PC2 are both minimum phase, and thus there are no inherent limitations to the achievable performance (Morari and Zafiriou 1989, Skogestad and Postlethwaite 1996) imposed by non–minimal phase behavior.

- The transfer function from catalyst circulation rate (F_{cat}) to riser temperature (T_r) has a RHP zero at $s = 0.0566$, and the steady–state gain of this transfer function is *negative* which is counterintuitive. One would expect that for a constant catalyst temperature, an increase in F_{cat} should raise T_r. Several complex interactions are involved here.

It is interesting to note that (Edwards and Kim 1988) have defined the "open loop" operation of the FCC by the following set of conditions for the $PC1^C$ pairing:

1. fixed feed rate
2. fixed feed temperature
3. fixed combustion air rate i.e. T_{rgn}/F_{air} loop open
4. fixed T_r i.e. T_r/F_{cat} loop *closed*

As we will argue now, such an operating strategy in fact results in an unstable process, even if the 'true open loop' is stable. By 'true open loop', we mean that conditions (1–3) above remain identical, but the T_r/F_{cat} is also open, unlike condition (4). Edwards and Kim (1988) reported that under these conditions (1–4), the unit drifted to the complete combustion mode. These observations made on an actual operational FCC are easily explained by our analysis. The details are described in Chapter 4 Section 4.5.2, and summarized here:

- we can assume that PI controllers (specifically integral action) were used in the FCC described by (Edwards and Kim 1988). Essentially all the FCC literature indicates that the use of PI controllers *e.g.* (Sadeghbeigi 1995) at the regulatory level is standard.
- the preferred sequence for loop closing for the $PC1^C$ pairing has been qualitatively argued to be: (1) T_{rgn}/F_{air} loop, and then (2) T_r/F_{cat} loop in (Arbel et al. 1996). For this sequence of loop closing, both PI controllers will be designed with positive gains.
- the steady–state gain of the T_r/F_{cat} loop is negative, but since the PI controller on the T_r/F_{cat} loop is tuned with positive gain, opening the T_{rgn}/F_{air} loop will lead to instability in the T_r/F_{cat} loop. However, as shown in Chapter 4, Section 4.5.2, a positive controller gain for the T_r/F_{cat} loop is necessary for stable operation in complete combustion mode. Therefore, the FCC should

drift to the complete combustion mode, and this was indeed what was observed in the actual FCC unit by Edwards and Kim (1988).

The process will therefore be unstable when operated in open loop as per the above definition (1–4) if the sign of the gain on the T_r/F_{cat} loop is not reversed when the T_{rgn}/F_{air} air loop is opened. However, (Edwards and Kim 1988) did not indicate if this sign change was also part of the standard procedure when switching the FCC operation to open loop mode.

5.7 Pairing Selection for PC1 and PC2

5.7.1 Control Structure - PC1

Achievable performance comparison

As already detailed one objective is to compare the performance achievable with the PC1^C and PC1^N pairing using μ_{RP} as the measure of performance. The constrained optimization routine in the Optimization Toolbox in MATLAB was used to determine the controller tunings which minimize $\max_\omega \mu_{RP}(\omega)$ over the desired frequency range, with the constraint of closed loop stability. It was found that several, significantly different sets of tunings yielded a comparable minimum $\max_\omega \mu_{RP}(\omega)$. One set of results for the PI controller parameters are tabulated in Table 5.6. Also tabulated are the values of the achieved μ^*_{RP}, where:

$$\mu^*_{RP} := \min_{c_1,c_2} \max_\omega \mu_{RP}(\omega) \tag{5.4}$$

In Table 5.6, note that there are two columns titled 'W_I active' and two titled 'W_A active'. As mentioned in Section 5.5.1, it is important to analyze the sensitivity of any conclusions to different possible sources of uncertainty. In this case, we investigate whether the presence/absence of additive or multiplicative uncertainty would affect the basic conclusion that the achievable performance is superior for PC1^C than PC1^N. 'W_I active' indicates that the input uncertainty in Figure 5.4 is exactly as in

Control Structure - PC1				
	PC1^C - Conventional Pairing		PC1^N - Non-conventional Pairing	
	W_I active	W_A active	W_I active	W_A active
K_1	3.23	32.93	3.40	4.51
τ_1	4.47	5.76	6.68	9.67
K_2	8.26	14.62	-4.54	-3.34
τ_2	5.59	5.69	12.40	3.19
μ^*_{RP}	0.533	0.775	0.782	1.323

Table 5.6: Optimal PI controller tunings for control structure PC1, for both PC1^C and PC1^N pairings.

Equation 5.2, while $W_A = 0.001I_2, \forall\omega$. Thus, W_I is the primary (active) source of uncertainty. Similarly, 'W_A active' indicates that the additive uncertainty in Figure 5.4 is exactly as in Equation 5.3, while $W_I = 0.1I_2, \forall\omega$. W_A is therefore the primary (active) source of uncertainty for this case. Note that $W_I = 0.1I_2, \forall\omega$ since any lower weight resulted in unacceptably large control moves (beyond constraint limits). It is evident from Table 5.6 that the performance of the PC1^C is superior to that of PC1^N, regardless of the source of uncertainty, since μ^*_{RP} for PC1^C is lower than μ^*_{RP} for PC1^N regardless of whether W_I is active or W_A is active. The plot of $\mu_{RP}(\omega)$ as a function of frequency obtained with the tunings in Table 5.6 are shown in Figure 5.5.

We also point out that the closed loop with μ-(sub)optimal decentralized PI controller for the PC1^C pairing was stable over the entire range of operating points considered (Figure 5.6) - regardless of whether W_I or W_A is active. The operating range considered is discussed in Section 5.3.2. Moreover the nominal performance with the locally linearized dynamics over the entire range was acceptable ($\mu_{NP} < 1$ at each operating point considered). This was not the case for the PC1^N pairing. The μ-optimal PI controller for this case guaranteed internal stability only over a limited range of operating points (Figure 5.6). Even for those operating points where internal stability was achieved, the nominal performance was often highly oscillatory with $\mu_{NP} > 1$.

Thus, an appropriately tuned decentralized PI controller for the PC1^C pairing provides internal stability and acceptable performance over the entire operating range.

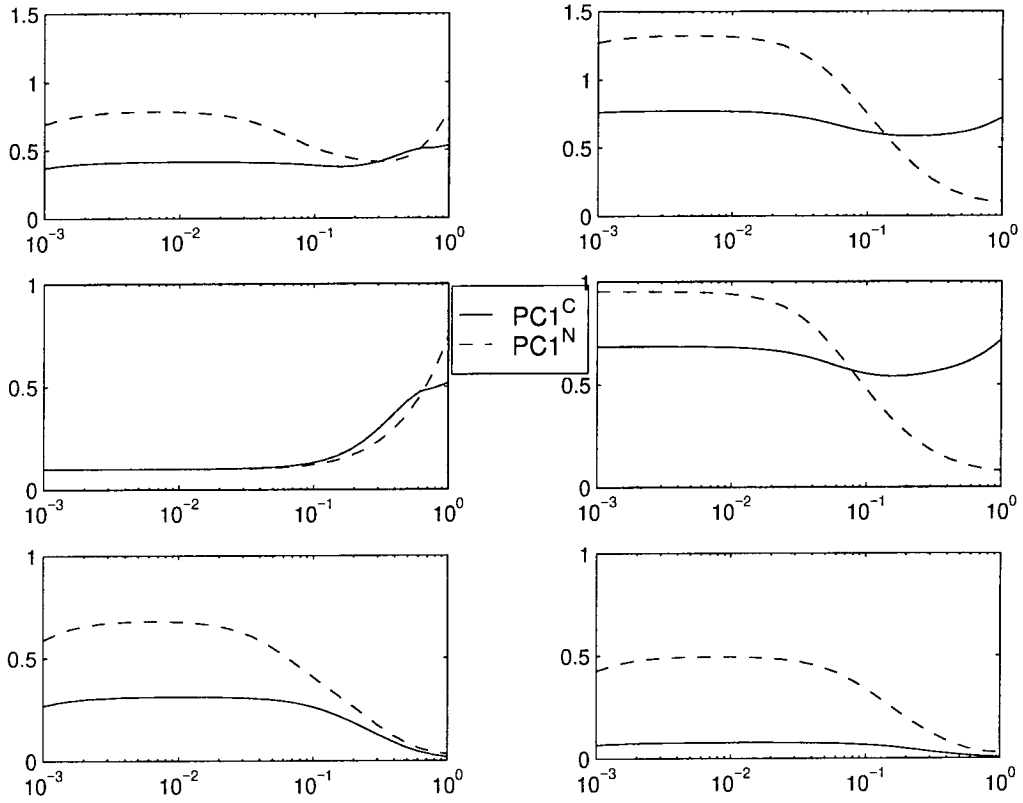

Figure 5.5: Comparison of achievable performance for the conventional and non–conventional pairing with the designed μ-(sub)optimal controllers for PC1.

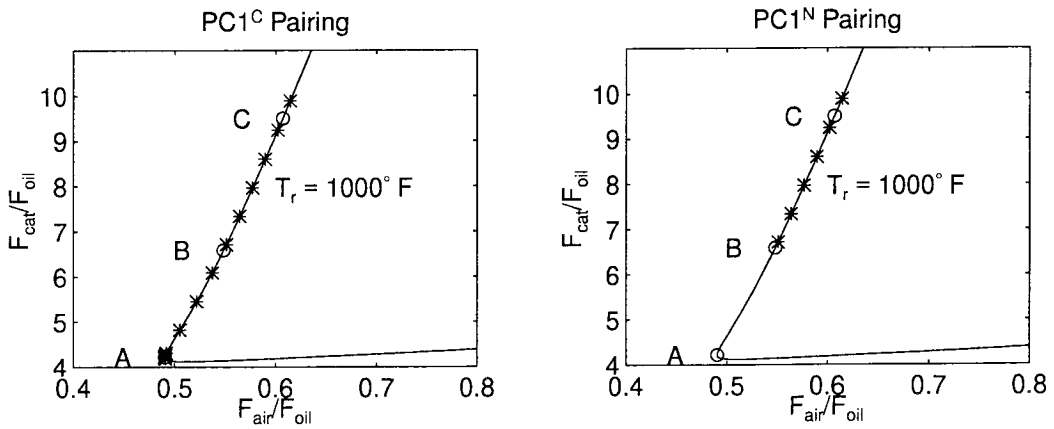

Figure 5.6: Range of operating points in PC mode where closed loop is nominally stable with designed μ-(sub)optimal PI controllers for PC1.

$PC1^N$ is stable only over a limited operating regime, and even then the closed loop response is often unsatisfactory.

Range of PI tuning parameters for stability

From an operational viewpoint, it is desirable that the closed loop characteristics are not excessively sensitive to the controller tuning as significant effort will be required for both initial tuning, as well as subsequent retuning to account for operating changes. Such high sensitivity is clearly undesirable, and can be used as a screening criterion to eliminate pairings that are excessively sensitive to the controller tuning. As we will now show, $PC1^C$ has a decisive advantage over $PC1^N$ with respect to this operational requirement. The following procedure is one way to quantify this screening criterion:

1. Select reasonable values of τ_1 and τ_2, the reset times for the two PI controllers. These reset times are held constant at the values indicated in Figure 5.7 ($\tau_1 = \tau_2 = 3$min. and $\tau_1 = \tau_2 = 10$min.).

2. Select a range of K_1 and K_2 values, and grid the region in the $K_1 - K_2$ space to give a set of $[K_1, K_2]$ values (PI controller gains) - call this set Γ.

3. Select a few operating points spanning the entire operating range under study. Here, three points are selected, and indicated in Figure 5.1 as A, B, and C. The process conditions at these three operating points are listed in Table 5.4.

4. Select one operating point, and derive a linear model representing the local dynamics at this operating point.

5. Select one value of $[K_1, K_2]$ in the set Γ and determine the specific decentralized PI controller $C(s) = \text{diag}\{K_1[1+\frac{1}{\tau_1 s}], K_2[1+\frac{1}{\tau_2 s}]\}$, using the reset times selected in Step 1.

6. Determine internal stability with this controller and the linear model at this operating point obtained in Step 4. If the closed loop is internally stable, mark the point in the $K_1 - K_2$ space.

7. Repeat Steps 5–6 for all the $[K_1, K_2]$ combinations in Γ.

8. Repeat Steps 4–7 for another selected operating point.

Figure 5.7 shows the region in the $[K_1, K_2]$ space where internal stability can be achieved for the PC1^C pairing as well as the PC1^N pairing for all three operating points A, B, C. Note that:

- each $[K_1, K_2]$ combination results in a specific decentralized PI controller.
- the values of $[K_1, K_2]$ that result in a stable closed loop for the linear plants at points A, B, and C are overlapped in Figure 5.7 for easy comparison.
- for PC1^C the intersection of the $[K_1, K_2]$ region where internal stability is achieved at all three operating points A, B, and C simultaneously is large. This indicates that if the decentralized PI controller is tuned with almost any reasonable tuning parameters, internal stability at least, would be achieved over a wide operating regime. Furthermore, at a given point a large range of $[K_1, K_2]$ values results in closed loop stability. In this sense, tuning the two PI controllers for the PC1^C pairing can be considered to be "easy".
- for PC1^N a much smaller range of $[K_1, K_2]$ values guarantees internal stability (note also the different scales in Figure 5.7) for each operating point. Therefore, care would be required in tuning the decentralized PI controller to ensure stability at even one operating point. Ensuring stability over the entire operating range would require significantly more effort. This is clearly undesirable from an operational viewpoint.
- we also note that for a given set of tuning parameters, the observed performance is insensitive to the actual operating point for PC1^C, but strongly dependent on the operating point for PC1^N (not shown).

It is reported (Arbel et al. 1996, Upson et al. 1993, Arbel et al. 1995) that in the past, the main concern at the regulatory level was maintaining stable operation. It is

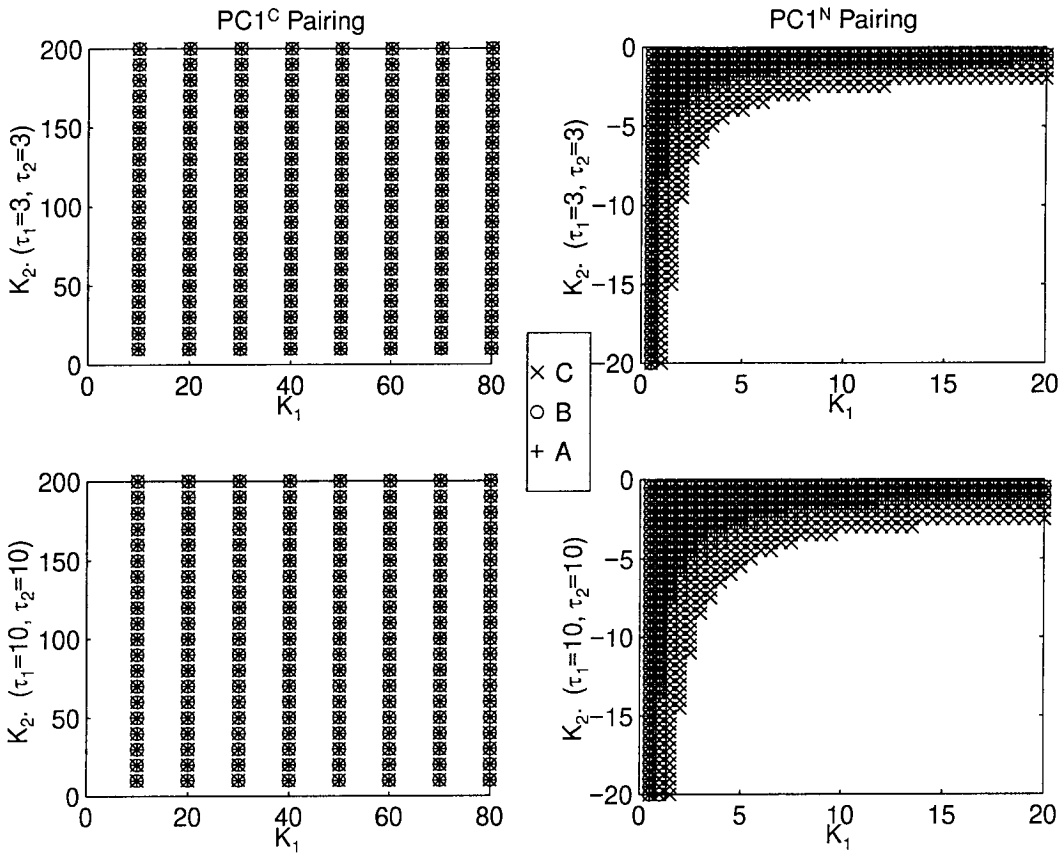

Figure 5.7: Range of PI controller gains K_1 and K_2 showing region where closed loop stability is achieved with the decentralized controller $C(s) = \text{diag}\{K_1[1+\frac{1}{\tau_1 s}], K_2[1+\frac{1}{\tau_2 s}]\}$ for all three operating points A, B, C in Figure 5.1 for PC1.

therefore this feature of the PC1^C pairing that the single loop PI controllers can be easily tuned to guarantee closed loop stability over a wide range of operating points (in this case it is in fact the entire range considered) that probably had a more significant bearing on the historical decision to select what is now called the conventional pairing (PC1^C) than the fact that achievable closed loop performance with the conventional pairing is better than the performance achievable with the non–conventional scheme (PC1^N).

We can conclude that for the PC1 control structure, the PC1^C pairing is the preferred choice over PC1^N based on:

- for PC1^C, the achievable performance is better (lower μ^*_{RP}) than the achievable

performance with the PC1^N scheme, regardless of the source of uncertainty (additive, input multiplicative) (Section 5.7.1).

- for PC1^C, the effort required to tune the decentralized PI controller is minimal:
  1. at a given operating point, internal stability and acceptable performance can be realized with a wide range of PI controller tunings.
  2. with a specific decentralized PI controller, acceptable performance is possible over a wide range of operating points.

  Thus tuning the decentralized PI controller for PC1^C stability is "easy".

Because of the clear benefits derived from the PC1^C pairing over the PC1^N pairing, the latter will not be further considered. We will investigate some additional properties of the PC1^C pairing scheme in Section 5.8.

5.7.2 Control Structure - PC2

Following the same heuristic arguments as indicated in (Arbel et al. 1996) for the PC1 control scheme, the intuitive choice of pairings for PC2 was argued to be the T_r/T_{feed} loop and T_{rgn}/F_{air} loop. This was referred to as the conventional pairing for PC2 (PC2^C) in Section 5.3.1. The alternate pairing is the non–conventional pairing (PC2^N). An analysis identical to that carried out for PC1 is undertaken to determine the more suitable pairing for PC2. Since the conclusions are very similar to the PC1 control structure, the details are left out. We summarize now the pertinent points:

- PC2 does not have any RHPT zeros or RHP zeros in the individual elements. (Table 5.5).
- For PC2^C, the steady–state RGA for the conventional pairing is positive at steady–state (+3.02 for the nominal plant) , and goes to 1.0 at high frequencies. Thus the PC2^C pairing is the obvious choice from DIC viewpoint.
- The achievable performance with the PC2^C pairing is better than the performance achievable with the PC2^N pairing (lower μ^*_{RP}).

- For PC2^C, the optimal PI controller for the conventional pairing provides internal stability over the entire operating range considered.

- At a given operating point, internal stability can be attained with a wide range of controller tunings. This range of tunings is larger than the allowable range for the PC2^N pairing. The relative area in the $[K_1, K_2]$ region for PC2^C and PC2^N is comparable to that shown for the PC1 control structure in Figure 5.7.

- Because the PC2^C pairing is essentially decoupled at high frequencies, tightening the controller tunings improves the overall regulatory performance. A trend similar to that indicated in Figure 5.12 for PC1^C is observed when the individual loops are "tightened".

We can conclude that for the PC2 control structure, the PC2^C pairing is the preferred choice over PC2^N because:

- for PC2^C, the achievable performance is better (lower μ^*_{RP}) than the achievable performance with the PC2^N scheme.

- for PC2^C, the effort required to tune the decentralized PI controller is minimal:

  1. at a given operating point, internal stability and acceptable performance can be realized with a wide range of PI controller tunings.
  2. with a specific decentralized PI controller, acceptable performance is possible over a wide range of operating points.

  Thus tuning the decentralized PI controller for PC2^C stability is "easy".

5.7.3 Achievable Performance Comparison: PC1^C and PC2^C

In Chapter 4 it was shown that the achievable performance of PC1 and PC2 was comparable, regardless of the type of uncertainty weight (input, additive) or structure (diagonal, full block). However, that analysis was performed with full μ-optimal controllers. In this section we investigate whether the indicated ranking might be

affected by the use of decentralized PI controllers. The comparison will obviously be between $PC1^C$ and $PC2^C$. The μ_{RP} plots for these two pairings are shown in Figure 5.8. Even with decentralized control, it is evident that the $PC1^C$ pairing results in better performance (lower μ^*_{RP}) than the $PC2^C$ pairing, regardless of the uncertainty source (input, additive).

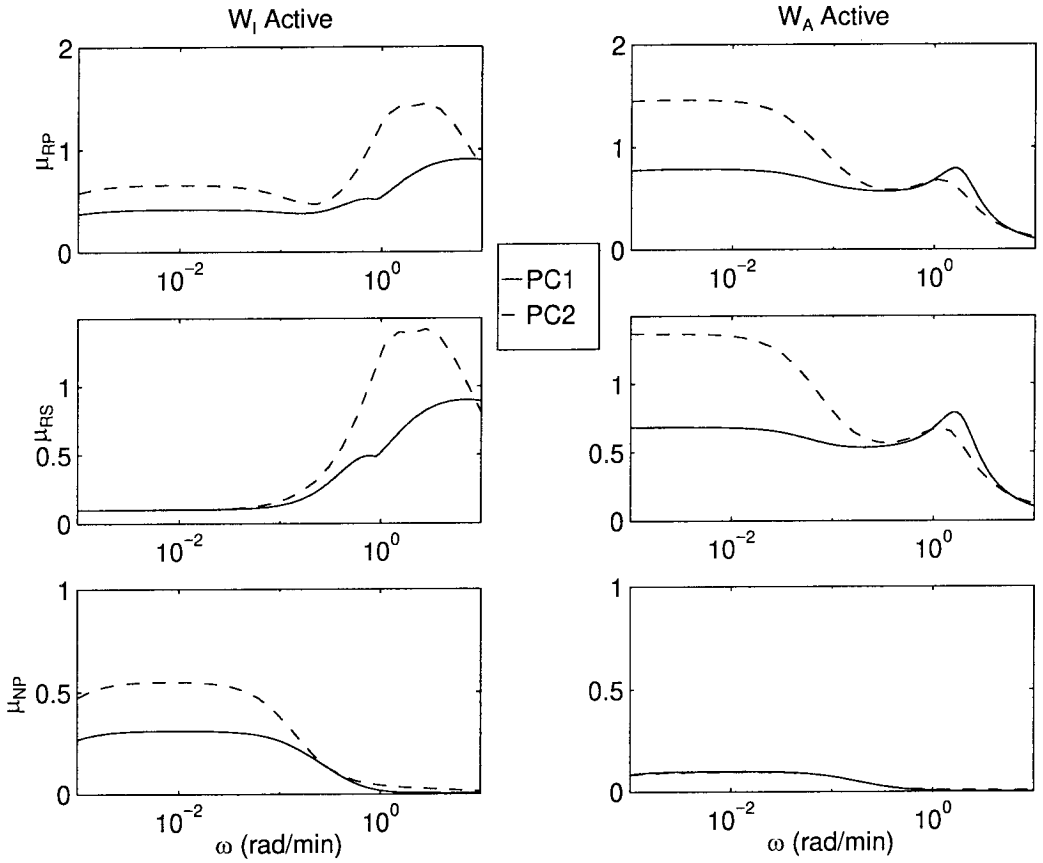

Figure 5.8: Closed loop performance comparison between PC1 and PC2 with conventional pairing for each case. μ-optimal PI controllers were used.

5.8 Some Properties of the $PC1^C$ Pairing

In this section, we provide some additional insights into the $PC1^C$ pairing, which is by far the most common regulatory level control strategy in the FCC industry.

5.8.1 Decentralized PI *vs.* Full Order μ-Optimal Controller

Because of the constraints imposed by the requirements of fixed order decentralized controllers, a degradation in the achievable performance must be expected (Morari and Zafiriou 1989), but the actual degree of performance degradation is case specific. Figure 5.9 shows that for the FCC regulatory problem, the observed performance degradation is not significant when decentralized PI controllers are used instead of full μ-optimal controllers. Note that the achievable robust performance for $PC1^C$ with the decentralized PI controllers is comparable to that possible with a full order μ-optimal controller - in the sense that μ^*_{RP} achieved with the decentralized scheme (solid lines) is comparable to μ^*_{RP} achieved with a full μ-optimal controller. Therefore, the simpler decentralized PI controllers can provide some benefits of the simpler control strategy with only a slight degradation in performance compared to that attained with a full μ-optimal controller.

5.8.2 Infeasibility of Independent Loop Design Procedure

Because the pairing in $PC1^C$ corresponds to negative steady–state RGA pairing, the closed loop system will have one or more of the following two undesirable properties (Morari and Zafiriou 1989):

1. the overall closed loop is unstable

2. one of the two single loops by itself is unstable.

As mentioned in Section 5.5, the independent design procedure involves designing each loop separately, and each loop is designed to be stable. If we also assume that all loops are operational, then we see from the two cases above that the only remaining possibility is that the overall system is unstable. Thus, the independent design procedure cannot be used to design a decentralized controller that stabilizes the overall closed loop. This might initially seem counterintuitive since the $PC1^C$ pairing is essentially decoupled at high frequencies, and it might be assumed that a reasonable procedure for tuning the two loops would be to tune each loop independently.

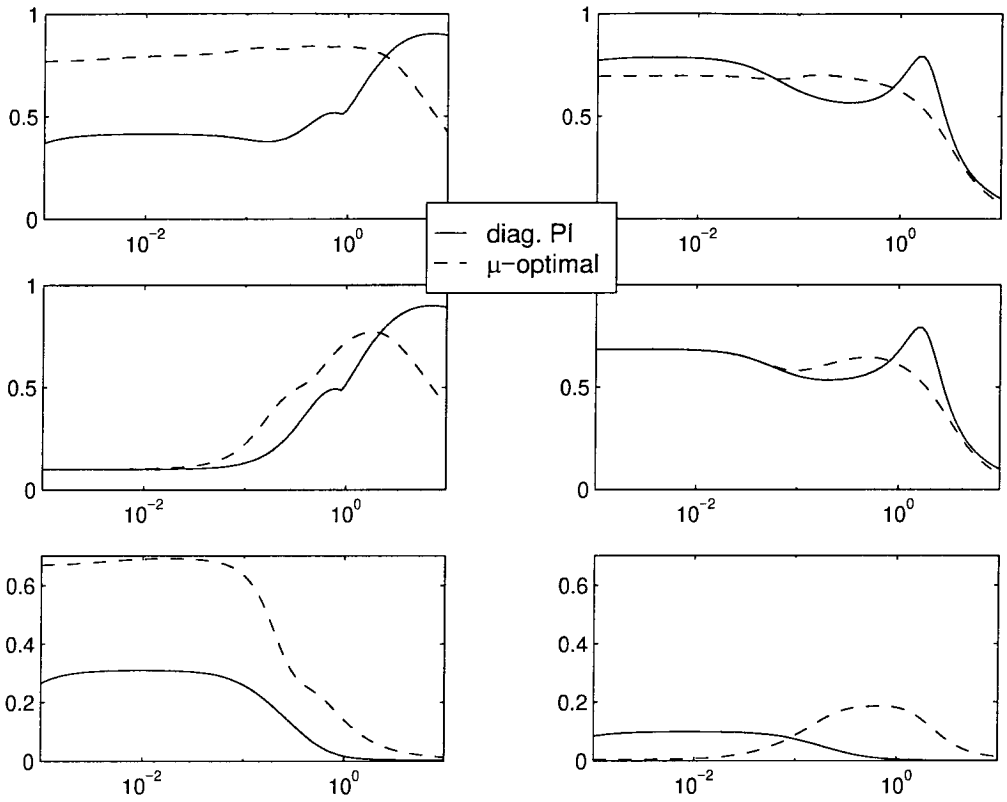

Figure 5.9: Comparison of achievable performance of $PC1^C$ with decentralized PI controllers (tunings in Table 5.6 and with full μ-optimal controllers.

5.8.3 Tuning to Reduce Process Interactions

The diagonal RGA elements ($\lambda_{ii}(s), i = 1, 2$) for the $PC1^C$ pairing are negative at steady–state and approach one at higher frequencies (Figure 5.10). On the other hand, the diagonal RGA elements for the $PC1^N$ pairing are positive at steady–state and approach zero at higher frequencies. Some properties and a quantification of such possible changes in the sign of the RGA elements is discussed in more detail in Section 5.9. It is evident from Figure 5.10 that below the desired closed loop bandwidth ($\omega \simeq 0.1 - 1$ rad/min) a significant degree of interaction exists between the two loops ($|\lambda_{ii}| > 1, i = 1, 2$). However at higher bandwidths ($\omega \geq 0.1$ rad/min), the interactions are significantly reduced for the $PC1^C$ pairing. This has an important implication for tuning to reduce interactions for the $PC1^C$ pairing: if it is suspected

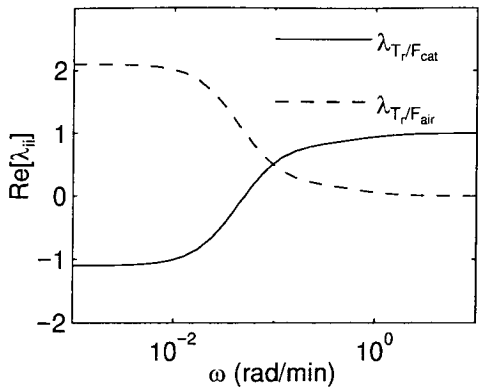

Figure 5.10: RGA plot for PC1^C pairing and PC1^N pairing.

that process interactions are limiting performance, the appropriate corrective action is to tune both the regulatory loops more tightly *i.e.* increase K_1 and K_2 - the individual gains of the decentralized PI controller. This pushes the closed loop bandwidth into the region where interactions are *reduced* for this pairing, and the performance can be expected to improve. To verify this hypothesis, we compare the performance attained by a "base case" PI controller, to the performance achieved with two other controllers where the gains of both PI controllers are changed by the same factor. The nominal tunings are tabulated in Table 5.7.

K_1	τ_1	K_2	τ_2
6	5	6	5

Table 5.7: "Base case" tuning parameters for decentralized PI controllers for PC1^C.

The controller tunings are "tightened" by multiplying the gains for both PI controllers by a factor of 2.0 from the base case values. The tunings are "relaxed" by dividing the nominal gains by a factor of 2.0. The performance characteristics with the three sets of tunings are plotted in Figure 5.11. The time response plots to a step change in feed quality is also shown in Figure 5.12, and corroborates the results obtained using μ_{RP}. As expected, "tightening" the controller tunings *improves* both the nominal and robust performance of the system, regardless of whether the additive uncertainty or the multiplicative input uncertainty is dominant. This observation is

counterintuitive - typically, operators will detune the regulatory controllers if it is suspected that interactions are the cause of the observed poor performance (Skogestad and Lundström 1990). Detuning at least the T_r loop has also been recommended recently in (Arbel et al. 1996). As will be shown shortly, this strategy can in fact increase the process sensitivity to uncertainty. Note that while only one case is shown, several different base tunings were compared, and the qualitative ranking is the same in all these cases. We note that these remarks apply for cases where the closed loop bandwidth is in the region where interactions are significant. In such cases, tightening both control loops can be expected to result in improved performance. Obviously, if the closed loop bandwidth is already near the maximum achievable limit, further tightening the controller could in fact degrade robust performance, due to increased sensitivity to high frequency process uncertainties. It is also interesting to note that tightening the loops for the PC1^N pairing will typically lead to instability, as evident from Figure 5.7. Relaxing the tuning will lead to a sluggish response.

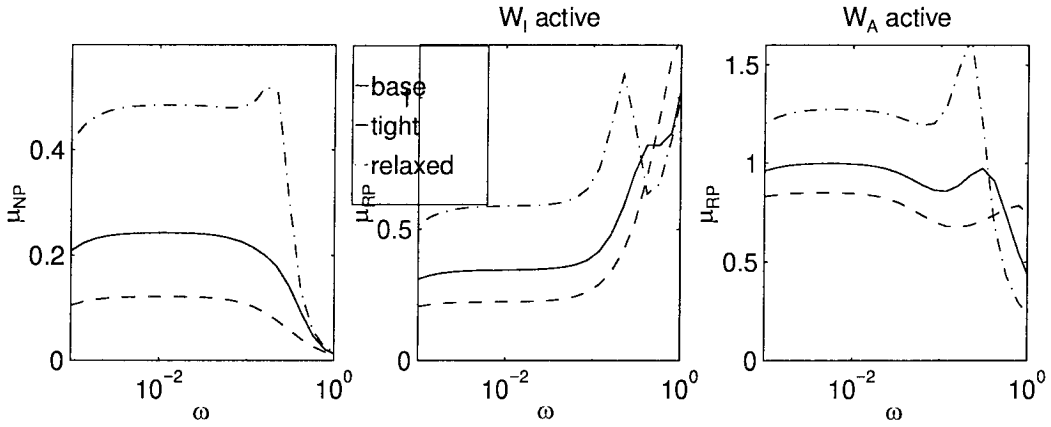

Figure 5.11: Effect of tightening and relaxing the PI controller tunings for the PC1^C pairing.

It is reported in (Arbel et al. 1996) (Section 4.3.4) that with a decentralized controller, *reducing* the gain on the T_r/F_{cat} PI controller results in less oscillatory response in T_{rgn} for a step change in T_r for PC1^C. Moreover, the settling time for T_{rgn} is reduced slightly. Note that in that work, the inputs and output deviations were not scaled, thereby ignoring the relative importance of the deviations in T_{rgn}

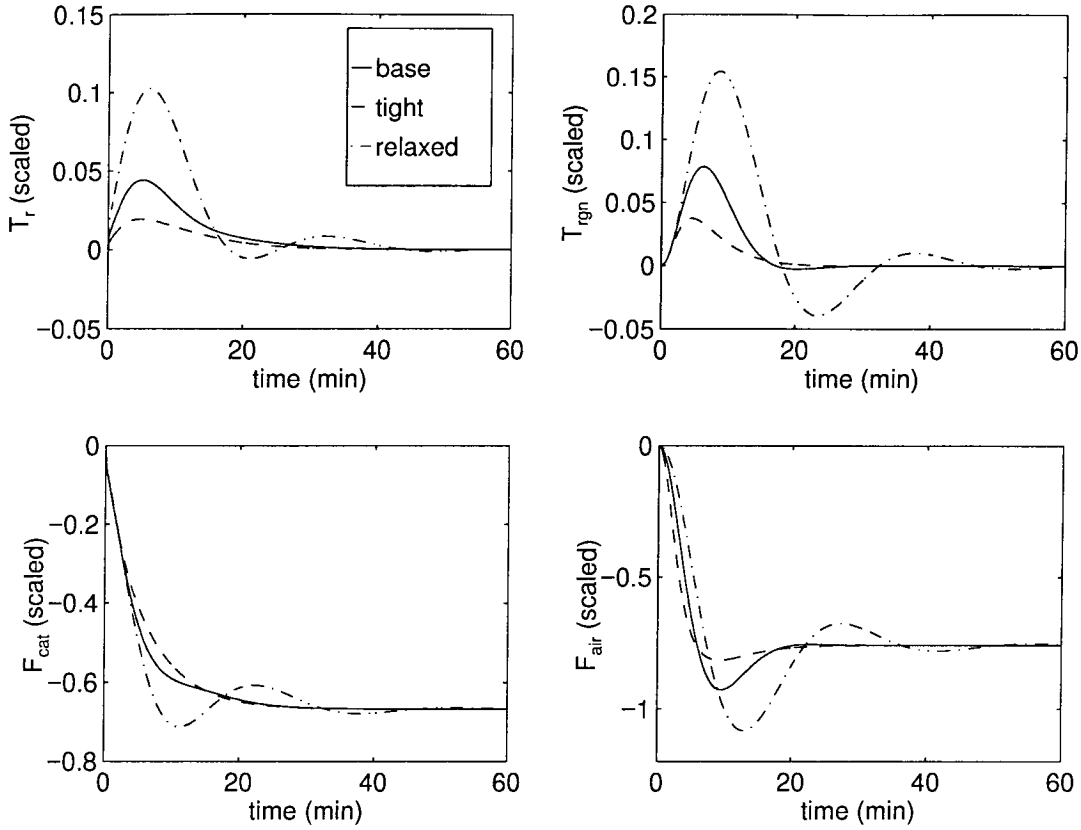

Figure 5.12: Time response plots for the PC1^C pairing with base, tightened, and relaxed controller tunings.

and deviations in T_r, which is in fact significant in practice. Reducing the gain in the T_r/F_{cat} PI controller pushes the operating bandwidth lower, and therefore into the region of higher interactions. Moreover, μ_{RP} increases, indicating a greater sensitivity to uncertainty. These two conclusions are demonstrated graphically in Figure 5.13. Thus detuning the T_r/F_{cat} would not be a recommended procedure for reducing sensitivity to uncertainties for the PC1^C pairing.

5.8.4 Operation at Unstable Operating Points

At the unstable operating points considered, there is one real unstable pole. Moreover, it is found that this unstable pole is always the slowest pole of the process. It is also found that the real, unstable pole crosses into the left half plane through the

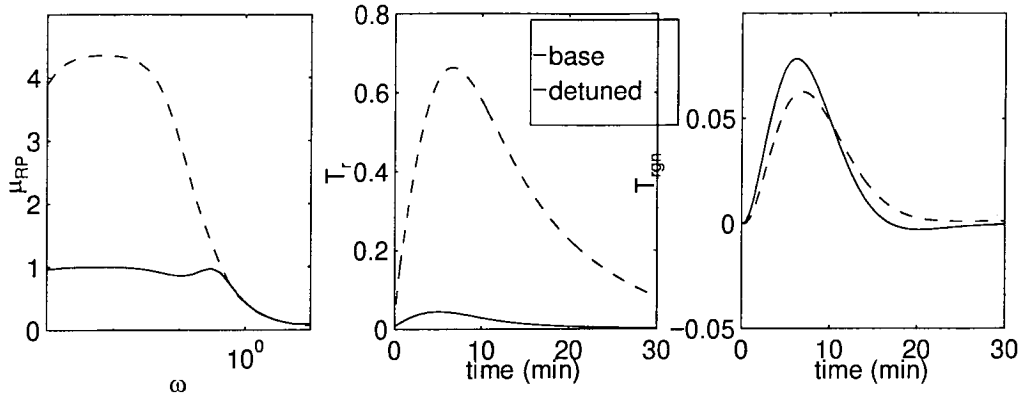

Figure 5.13: Effect of detuning the T_r/F_{cat} loop controller gain by a factor of 20 from the base case in Table 5.7.

origin should the operating point change to one where the open loop is stable. A much wider range of operating points were checked: $950°F \leq T_r \leq 1050°F$ and $1100°F \leq T_{rgn} \leq 1400°F$, and the characterization above was invariant for all these cases. An example of these observations is shown in Table 5.8 where the poles of the locally linearized plant at both a stable and an unstable operating point are indicated.

Stable Operating Point (B)	Unstable Operating Point (D)
-11.9944	-11.9755
-0.6614	-1.2755
-0.5751	-1.1703
-0.2800	-0.2661
-0.0444	0.0058

Table 5.8: Linear system poles for PC1 control scheme. Linearization around points B (stable) and D(unstable), Figure 5.1.

Hovd and Skogestad (1994) proposed pairing rules at $s = 0$ for integrity of the closed loop system for unstable plants. They defined integrity as follows:

> Consider a plant $G(s)$ and a controller $C(s)$. Then the closed loop system possesses integrity if the controller $C'(s) = \Delta C(s)$ stabilizes the system for all $\Delta = \text{diag}(\delta_i) \mid \delta_i \in \{0, 1\}, i = 1, 2, \ldots, n$

Hovd and Skogestad (1994) show that for plants with one single unstable pole that appears in every element of the transfer matrix, the pairing for integrity should be on *negative* $s = 0$ values of the RGA. Note that while the RGA is calculated at $s = 0$, it is not called the steady–state RGA since steady–state has little relevance for unstable systems.

The $s = 0$ RGA matrix calculated for $PC1^C$ at the unstable operating point D in Figure 5.1 is:

$$RGA(s=0) = \begin{bmatrix} 13.6122 & -12.6122 \\ -12.6122 & 13.6122 \end{bmatrix} \tag{5.5}$$

and therefore, the $PC1^C$ pairing does not possess integrity at the unstable operating points, and once again the alternate $PC1^N$ pairing would be favored even for operation at an unstable operating point.

However, since we are more interested in performance, we will analyze the effect of operating the FCC at an unstable operating point on performance. It is reassuring to note that the μ-(sub)optimal decentralized PI controller indicated in Table 5.6, column 1 (with W_I active) yields $\mu_{RP} \simeq 0.97$ with the linear plant describing the local dynamics at the unstable operating point D in Figure 5.1. However, this does not indicate how much more positive the unstable pole could be before robust performance is compromised *i.e.* $\mu_{RP} > 1$. Some additional investigation is required to ascertain this upper limit, and we will proceed to determine this upper limit by addressing the following two questions:

1. how positive can the single, real, unstable pole be before the closed loop performance $\mu_{RP} > 1$?

2. are there unstable operating points at which the performance (μ_{RP}) with the decentralized PI controllers is unacceptable?

As the nominal operating point, we take point B in Figure 5.1, and use the decentralized PI controller tuning indicated in Table 5.6. To address the first question above, we proceed as follows:

1. obtain a local linearization of the non–linear model around a selected operating point, and determine the state–space matrices (A_0, B_0, C_0, D_0). For this study, operating point B in Figure 5.1 was selected because it reflects typical operating conditions for most modern FCCs (McFarlane et al. 1993). Thus controller design would be performed at such operating points rather than at an unstable operating point such as D where T_{rgn} is significantly lower.

2. diagonalize A_0 through a similarity transformation. Since all the eigenvalues of A_0 (see Table 5.8) are distinct, the similarity transform is the inverse of the matrix of eigenvectors of A_0. Call the transformed state–space matrices $\tilde{A}, \tilde{B}, \tilde{C}, \tilde{D}$.

3. reorder the states of the diagonalized system $(\tilde{A}, \tilde{B}, \tilde{C}, \tilde{D})$ so that the eigenvalue closest to the origin is in the lower most right corner of $\tilde{A}$. Call this eigenvalue λ_u. At the operating point B, $\lambda_u = -0.0444$.

4. as our focus is on examining how positive the real unstable pole λ_u of the process can be, we can express the possible range for λ_u as real parametric uncertainty. To this end, we assume that the parametric variations in the diagonal $\tilde{A}$ matrix can be represented as:

$$\tilde{A} + B_2(\delta k_u)C_2 \tag{5.6}$$

where $B_2 = [0, 0, \ldots, 1]'$, $\delta \in [-1, 1]$, $k_u \in \Re$ is the real weight on δ, $C_2 = [0, 0, \ldots, 1]$. Note that this uncertainty description assumes that the slowest eigenvalue λ_u is the only one that varies. All the other poles of the process remain unchanged. Moreover, it is assumed that $\tilde{B}$, $\tilde{C}$, $\tilde{D}$ remain constant for all the operating points. The focus is then on changes in the location of the slowest pole. The actual plant is therefore given by:

$$G_{actual}(s) = \left[\begin{array}{c|c} \tilde{A} + B_2(\delta k_u)C_2 & \tilde{B} \\ \hline \tilde{C} & \tilde{D} \end{array}\right] \tag{5.7}$$

With these assumptions, we can express the entire set of possible plants $G_{actual}(s)$

as an LFT of δ:

$$G_{actual}(s) = \mathcal{F}_l[G_{nom}(s), \delta] \tag{5.8}$$

where:

$$G_{nom}(s) = \left[\begin{array}{c|cc} \tilde{A} & \tilde{B} & B_2 \\ \hline \tilde{C} & \tilde{D} & 0 \\ k_u C_2 & 0 & 0 \end{array}\right] \tag{5.9}$$

with B_2, C_2 and k_u have been defined above.

5. recall that the goal is to determine the largest possible real, unstable pole for which the closed loop system in Figure 5.14 has $\max_\omega \mu_{RP}(\omega) = 1$. Thus the objective is to find the maximum $k_u \in \Re$ such that $\max_\omega \mu_{RP}(\omega) = 1$ for the given controller $C(s)$. Call this maximum k_u - k_u^*. For this analysis, $C(s)$ is taken to be the optimal decentralized PI controller with tunings given in Table 5.6, column 2.

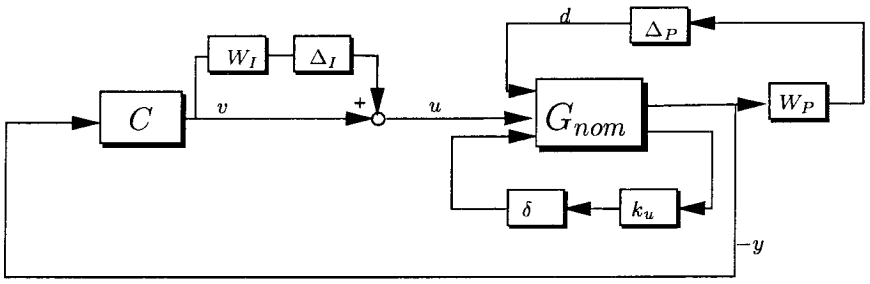

Figure 5.14: Analysis setup for determining maximum k_u. $C(s) = \text{diag}\{3.23[1 + \frac{1}{4.47s}], 8.26[1 + \frac{1}{5.59s}]\}$

It was found numerically that $k_u^* = 0.0733$. Note that the uncertainty description in Equation 5.6 is formulated as additive uncertainty. Thus, the largest allowable unstable pole is $0.0733 - 0.0444 = 0.0289$.

Figure 5.15 shows the slowest pole of the linearized system at each operating point in PC mode operation (Figure 5.1, including A, B, C, D) as a function of the PC mode operating point. Also indicated for reference are the four operating points already discussed in Figure 5.1. We note the following:

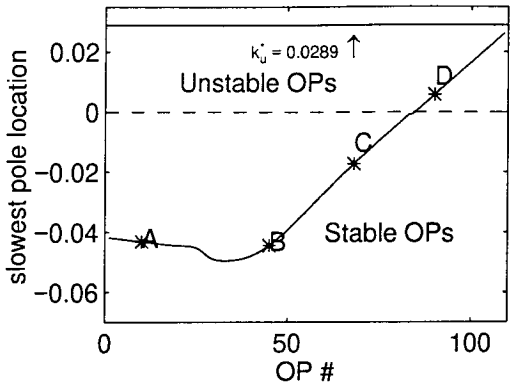

Figure 5.15: Plot of the smallest eigenvalue of the A matrix of the linearized plant at the operating points indicated in Figure 5.1 as a function of the operating point. Shown for reference are the operating points A, B, C, D.

- the operating point D corresponds to $T_{rgn} = 1134.2°F$ and $T_r = 1000°F$, and $\mu_{RP} \simeq 0.97$ at this point. Most modern FCCs operate at significantly higher regenerator temperatures ($T_{rgn} > 1200°F$) in PC mode, and all such operating points were found to be stable in this analysis. In the unlikely event of a transition to an unstable operating point, the results above show that there is a reasonable margin before robust performance is compromised. The operating points we considered were all well within this margin, as seen in Figure 5.15.

We can therefore conclude that reasonable transitions to an unstable operating point will not result in a significant deterioration of performance of the closed loop system with an appropriately tuned decentralized PI controller.

5.9 The Sign Difference of the Diagonal Elements of the PC1^C RGA Matrix at $s = 0$ and $s = \infty$

As we saw in Section 5.6, the pairing for tight performance for PC1^C with a decentralized controller corresponds to a negative steady–state RGA pairing ($\lambda_{ii}(0) = -1.10, i = 1, 2$), while the high frequency value of the diagonal RGA elements is unity ($\lambda_{ii}(\infty) = 1, i = 1, 2$). Thus, for PC1^C, the pairing for DIC and performance

is *different.* Such a pairing might have been eliminated if the pairing criterion was based primarily on the steady–state RGA matrix. On the other hand, for $PC2^C$, $\lambda_{ii}(0) = 3.02 > 0, i = 1, 2$ and $\lambda_{ii}(0) = 1 > 0, i = 1, 2$. For $PC2^C$, the pairing for DIC and performance is *the same.*

Similar differences in the sign of $\lambda_{ii}(0)$ and $\lambda_{ii}(\infty)$ have been pointed out in Skogestad and Hovd (1990), but the plant characteristics leading to such differences were not investigated. We analyze here, in a more general framework some properties of plants such as $PC1^C$ and $PC2^C$ that lead to these differences in the sign of $\lambda_{ii}(0)$ and $\lambda_{ii}(\infty)$. At the end of this section, some guidelines will be provided to aid in identifying such plants.

To begin, note that the elements of the RGA matrix of a square plant ($G(s)$) can be written as the ratio of two transfer functions, as follows (Morari and Zafiriou 1989, Skogestad and Postlethwaite 1996):

$$\lambda_{ij} = (-1)^{i+j} \frac{g_{ij} \cdot \det(G^{ij})}{\det(G)} \tag{5.10}$$

where G^{ij} is $G(s)$ with the i^{th} row and j^{th} column deleted. If we define the new matrix:

$$G_{ij} = \text{diag}\{g_{ij}, G^{ij}\} \tag{5.11}$$

then, $\det(G_{ij}) = g_{ij} \cdot \det(G^{ij})$ and the RGA elements can be equivalently written as:

$$\lambda_{ij} = (-1)^{i+j} \frac{\det(G_{ij})}{\det(G)} \tag{5.12}$$

and in particular, the diagonal SISO elements of the RGA matrix are given by:

$$\lambda_{ii} = \frac{\det(G_{ii})}{\det(G)} \tag{5.13}$$

We will focus on the diagonal elements of the RGA matrix without loss of generality - the inputs and outputs can always be interchanged accordingly.

In this section, we limit ourselves to stable plants, and require that the decentral-

ized controllers have integral action in each channel (*e.g.* decentralized PI controllers). The following are the assumptions made on the plant and controller:

- the plant ($G(s)$)is stable
- the controller ($C(s)$) is diagonal, and each channel incorporates integral action, but is otherwise stable.

Suppose that $\hat{G}(s)$ is some other transfer matrix with the same number of inputs/outputs as $G(s)$, and that $\hat{G}(s)$ is stable. $\hat{G}(s)$ can be considered an "alternate representation" of the plant $G(s)$. Also, for notational purposes, assume that:

- $G(s)$ has z open right half plane zeros,
- $\hat{G}(s)$ has $\hat{z}$ open right half plane zeros,
- $G(s)C(s)$ and $\hat{G}(s)C(s)$ are both strictly proper.

Furthermore, define $\mathcal{N}[0, b(s)]$ to be the net number of clockwise encirclements of the origin by the image of the Nyquist D contour under $b(s)$, indenting to the right around $j\omega$ axis poles. Then, the following extension of Theorem 14.4-2 from (Morari and Zafiriou 1989) is obtained:

Lemma 1 *Assume that $G(s)$ and $\hat{G}(s)$ have z and $\hat{z}$ open RHP zeros respectively, and that $\hat{S} = (I+\hat{G}C)^{-1}$ is stable. Then the overall closed loop system $S = (I+GC)^{-1}$ is stable if and only if*

$$\mathcal{N}[0, \det(I - \hat{S}L_E)] = \hat{z} - z \tag{5.14}$$

Proof:

The following relation can be verified:

$$G^{-1}(I + GC) = \hat{G}^{-1}(I + \hat{G}C)(I - \hat{S}L_E) \tag{5.15}$$

where:

$$\hat{S} = (I + \hat{G}C)^{-1} \tag{5.16}$$

$$L_E = (G - \hat{G})G^{-1} \tag{5.17}$$

Note that $G^{-1}(I + GC)$ has z open RHP poles since $G(s)C(s)$ is stable except for the integrators in $C(s)$. Similarly, $\hat{G}^{-1}(I + \hat{G}C)$ has $\hat{z}$ open RHP poles. Thus by the Nyquist stability criterion, S is stable if and only if:

$$\mathcal{N}[0, \det(G^{-1}(I + GC))] = \mathcal{N}[0, \det(\hat{G}^{-1}(I + \hat{G}C))] + \mathcal{N}[0, \det((I - \hat{S}L_E))] = -z \tag{5.18}$$

By assumption, $\mathcal{N}[0, det(\hat{G}^{-1}(I+\hat{G}C))] = -\hat{z}$ since the closed loop $\hat{S} = (I+\hat{G}C)^{-1}$ is stable. The result follows immediately by substitution. □

Lemma 1 can be used to derive necessary conditions for overall closed loop stability based on the infinite frequency ratio of the determinants of $G(s)$ and $\hat{G}(s)$:

Lemma 2 *Assume that $G(s)$, $\hat{G}(s)$ and the controller $C(s)$ have the following properties:*

1. *$G(s)$ and $\hat{G}(s)$ are both strictly stable*
2. *$G(s)$ and $\hat{G}(s)$ have z and $\hat{z}$ open RHP zeros respectively*
3. *the decentralized controller $C(s)$ has integral action in every channel, but is otherwise stable*
4. *$G(s)C(s)$ and $\hat{G}(s)C(s)$ are both strictly proper.*

Then if

$$Re\left[\left.\frac{\det[\hat{G}(j\omega)]}{\det[G(j\omega)]}\right|_{s\to\infty}\right] \quad \text{is} \quad \begin{cases} < 0 & \text{for} \quad \hat{z} - z \quad \text{even} \\ > 0 & \text{for} \quad \hat{z} - z \quad \text{odd} \end{cases} \tag{5.19}$$

then at least one of the following instabilities will occur:

1. *the closed loop with $G(s)C(s)$ is unstable*

2. *the closed loop with $\hat{G}(s)C(s)$ is unstable*

Proof:

Since it is assumed that (i) integral action is present in each channel and (ii) GC as well as $\hat{G}C$ are strictly proper, the following limiting conditions follow:

$$\hat{S}(0) = 0 \qquad \hat{S}(j\infty) = I \tag{5.20}$$

Thus, we note that:

$$\det(I - \hat{S}L_E)\Big|_{s\to 0} = 1 \tag{5.21}$$

and

$$\det(I - \hat{S}L_E)\Big|_{s\to\infty} = \det(\hat{G}G^{-1})\Big|_{s\to\infty} \tag{5.22}$$

Thus the Nyquist plot of $\det(I - \hat{S}L_E)$ starts at 1 when $\omega = 0$ and ends up at $\det(\hat{G}G^{-1})\Big|_{s\to\infty}$ as $\omega \to \infty$. A careful analysis of the Nyquist plot indicates that $\mathcal{N}[0, \det(I - \hat{S}L_E)]$ is *even* if $Re\left[\det(\hat{G}G^{-1})\Big|_{s\to\infty}\right] \geq 0$ and $\mathcal{N}[0, det(I - \hat{S}L_E)]$ is *odd* if $Re\left[\det(\hat{G}G^{-1})\Big|_{s\to\infty}\right] < 0$. In particular, if $\hat{z} - z$ is even, a necessary condition for DIC is $Re\left[\det(\hat{G}G^{-1})\Big|_{s\to\infty}\right] > 0$. Similarly, if $\hat{z} - z$ is odd, a necessary condition for DIC is $Re\left[\det(\hat{G}G^{-1})\Big|_{s\to\infty}\right] < 0$. Thus, the parity of odd/even for $\hat{z} - z$ and the sign of $Re\left[\det(\hat{G}G^{-1})\Big|_{s\to\infty}\right]$ can be used to formulate the above two necessary conditions for stability of the above class of plants, and the result follows. □

Note:

- Nothing can be said if $Re\left[\det(\hat{G}G^{-1})\Big|_{s\to\infty}\right] = 0$, as the number of encirclements can be odd or even.

- The results hold even if the limit is unbounded.

- $C(s)$ is not required to be decentralized for the results above to hold. However, the application of Lemma 2 to the RGA, and the subsequent interpretation will require that $C(s)$ is decentralized.

5.9.1 Application to the RGA Pairing Criterion

As noted in Equation 5.13, the diagonal RGA elements can be expressed as a ratio of two determinants. We can thus utilize Lemma 2 to obtain necessary conditions for closed loop stability for stable plants with decentralized control with integral action in each channel. For the application of Lemma 2 to the diagonal RGA elements (λ_{ii}), we note that $G_{ii}(s) = \hat{G}(s)$.

Lemma 3 *Assume that* $G(s)$, $G_{ii}(s) = \text{diag}\{g_{ii}, G^{ii}\}$ *and the controller* $C(s)$ *have the following properties:*

1. $G(s)$ *and* $G_{ii}(s)$ *are both strictly stable*
2. $G(s)$ *and* $G_{ii}(s)$ *have* z *and* $\hat{z}$ *open RHP zeros respectively*
3. *the decentralized controller* $C(s)$ *has integral action in every channel, but is otherwise stable*
4. $G(s)C(s)$ *and* $G_{ii}(s)C(s)$ *are both strictly proper.*

Define $\lambda_{ii}(s)$ *as the RGA element of* $G(s)$ *for loop* i. *Then if*

$$Re[\lambda_{ii}(\infty)] \quad \text{is} \quad \begin{cases} < \ 0 \quad \text{for} \quad \hat{z} - z \quad \text{even} \\ > \ 0 \quad \text{for} \quad \hat{z} - z \quad \text{odd} \end{cases} \tag{5.23}$$

then at least one of the following instabilities will occur:

1. *the closed loop with* $G(s)C(s)$ *is unstable*
2. *the* i *loop itself is unstable*
3. *the system with loop* i *removed is unstable.*

Proof:

Substitute $G_{ii}(s) = \text{diag}\{g_{ii}, G^{ii}\} = \hat{G}(s)$ into Lemma 2. Note that instability (1) above is exactly the same as instability (1) in Lemma 2. Another possible instability

indicated in Lemma 2 is that the closed loop with $G_{ii}(s)C(s)$ can be unstable. Since $G_{ii}(s) = \text{diag}\{g_{ii}, G^{ii}\}$, this means that either the loop i $(g_{ii}(s)c_i(s))$ is unstable (instability 2 above), or the system without the loop i $(G^{ii}(s)C^{ii}(s))$ is unstable (instability 3 above), or both the previous two cases are unstable. $C^{ii}(s)$ is $C(s)$ with row i and column i removed. □

Note:

- the case $\hat{z} - z = 0$ is included in the $\hat{z} - z$ even case,
- nothing can be said if $Re[\lambda_{ii}(\infty)] = 0$, as the number of encirclements can be even or odd.
- while separate conditions exist for $\lambda_{ii}(\infty)$, depending on whether $\hat{z} - z$ is even or odd, only one condition exists for stable plants at steady–state *i.e.* $\lambda_{ii}(0) < 0$ leading to one or more of the three instabilities indicated. This steady–state condition is stated for example, in Corollary 14.3-4 in Morari and Zafiriou (1989):

Lemma 4 *Assume that:*

1. *$G(s)$ is strictly stable*
2. *the decentralized controller $C(s)$ has integral action in every channel, but is otherwise stable*
3. *$G(s)C(s)$ is strictly proper.*

Then if

$$\lambda_{ii}(0) < 0 \tag{5.24}$$

where $\lambda_{ii}(0)$ is the steady–state RGA element for loop i of $G(s)$, then at least one of the following instabilities will occur:

1. *the closed loop with $G(s)C(s)$ is unstable*
2. *the i loop itself is unstable*

3. the system with loop i removed is unstable.

Proof: See Morari and Zafiriou (1989).

To show that the two conditions in Lemma 3 converge to the single condition at steady–state as stated in Lemma 4, we use the following result from Skogestad and Hovd (1990):

Lemma 5 *Based on the element by element definition of the diagonal RGA as:*

$$\lambda_{ii}(s) = \frac{g_{ii}(s) \cdot \det(G^{ii}(s))}{\det(G(s))} \tag{5.25}$$

and defining the following integers:

z_{Rg} $= \#$ *of open RHP zeros of* $g_{ii}(s)$

p_{Rg} $= \#$ *of open RHP poles of* $g_{ii}(s)$

z_{0g} $= \#$ *of zeros of* $g_{ii}(s)$ *at origin*

p_{0g} $= \#$ *of poles of* $g_{ii}(s)$ *at origin*

$z_{RG_{ii}}$ $= \#$ *of open RHP zeros of* $G_{ii}(s)$

$p_{RG_{ii}}$ $= \#$ *of open RHP poles of* $G_{ii}(s)$

$z_{0G_{ii}}$ $= \#$ *of zeros of* $G_{ii}(s)$ *at origin*

$p_{0G_{ii}}$ $= \#$ *of poles of* $G_{ii}(s)$ *at origin*

z_{RG} $= \#$ *of open RHP zeros of* $G(s)$

p_{RG} $= \#$ *of open RHP poles of* $G(s)$

z_{0G} $= \#$ *of zeros of* $G(s)$ *at origin*

p_{0G} $= \#$ *of poles of* $G(s)$ *at origin*

α $=$ *relative degree of* $\lambda_{ii}(s)$

the change in the phase of $\lambda_{ii}(j\omega)$ *as* ω *goes from* 0 *to* ∞ *is given by:*

$$\Phi_i = \pi[(p_{Rg}+p_{RG_{ii}}-p_{RG})-(z_{Rg}+z_{RG_{ii}}-z_{RG})]-\frac{\pi}{2}[(z_{0g}-p_{0g})+(z_{0G_{ii}}-p_{0G_{ii}})-(z_{0G}-p_{0G})]-\frac{\pi}{2}\alpha \tag{5.26}$$

Proof: Write each component of $\lambda_{ii}(j\omega)$ as a ratio of a numerator polynomial and a denominator polynomial. □

The following lemma shows that if (1) the plant is strictly stable, (2) $\lambda_{ii}(\infty) \neq 0$ and bounded, and (3) the plant has no zeros on the $j\omega$ axis, then the two conditions at $j\infty$ in Equation 5.23 are exactly equivalent to the single steady–state condition in Equation 5.24.

Lemma 6 *Under the conditions on* $G(s)$, $\hat{G}(s)$ *and* $C(s)$ *in Lemma 3, the two conditions at* ∞ *in Lemma 3 are exactly equivalent to the steady–state condition* $\lambda_{ii}(0) < 0$ *in Lemma 4:*

$$Re[\lambda_{ii}(\infty)] \quad \text{is} \quad \begin{cases} < \ 0 \quad \text{for} \quad \hat{z}-z \quad \text{even} \\ > \ 0 \quad \text{for} \quad \hat{z}-z \quad \text{odd} \end{cases} \iff \lambda_{ii}(0) < 0 \tag{5.27}$$

and for either case, one or more of the following instabilities will occur:

1. *the closed loop with* $G(s)C(s)$ *is unstable*
2. *the i loop itself is unstable*
3. *the system with loop i removed is unstable.*

Proof: For the class of plants we are considering, the following simplifications can be made:

1. $\hat{z} = z_{Rg} + z_{RG_{ii}}$
2. $z = z_{RG}$

3. $p_{Rg} = p_{RG_{ii}} = p_{RG} = p_{0g} = p_{0G_{ii}} = p_{0G} = 0$ (stable plant assumption)

4. $z_{0g} = z_{0G_{ii}} = z_{0G} = 0$ (by assumption)

5. $\alpha = 0$ since $\lambda_{ii}(\infty) \neq 0$ and bounded

and the following expression for Φ_i, the phase change for $\lambda_{ii}(j\omega)$ as ω goes from 0 to ∞ is obtained:

$$\Phi_i = -\pi[\hat{z} - z] \tag{5.28}$$

Using this simplified formula for the phase change, we observe that:

1. **LHS condt. I:** $\lambda_{ii}(j\infty) < 0$, $\alpha = 0$, and $\hat{z} - z$ even $\Rightarrow \Phi_i = 2\pi n, n \in [0, \pm 1, \pm 2, \ldots]$ from Equation 5.28. Thus, $\lambda_{ii}(0)$ and $\lambda_{ii}(j\infty)$ have the same sign, and $\lambda_{ii}(0) < 0$, and vice versa.

2. **LHS condt. II:** $\lambda_{ii}(j\infty) > 0$ and $\hat{z} - z$ odd $\Rightarrow \Phi_i = (2n+1)\pi, n \in [0, \pm 1, \pm 2, \ldots]$ from Equation 5.28. Thus, $\lambda_{ii}(0)$ and $\lambda_{ii}(j\infty)$ have opposite signs, and since $\lambda_{ii}(j\infty) > 0$, $\lambda_{ii}(0) < 0$, and vice versa. □

Thus, the two conditions in $\lambda_{ii}(\infty)$ are exactly equivalent to the condition at $\lambda_{ii}(0)$. For either case, the same three possibilities for instability can arise.

Lemma 3 therefore identifies plants where the sign of the RGA element corresponding to a specific pairing can be different at steady–state and at ∞ frequency. Often, the RGA value at ∞ frequency closely reflects the RGA value within the operating bandwidth, and thus examining the ∞ frequency RGA can therefore indicate the more suitable pairing for performance. Lemma 3 identifies those plants where the corresponding steady–state RGA will be positive or negative.

One example demonstrating this class of plants is the PC1^C pairing for the 2×2 PC1 control structure. For this case:

- the plant $G(s)$ is MP $\Rightarrow z = 0$
- g_{11} the T_r/F_{cat} transfer function is NMP, and $G^{11} = g_{22}$ is MP $\Rightarrow \hat{z} = 1$

- $\lambda_{11}(j\infty) = 1 \Rightarrow \alpha = 0$

and therefore, Equation 5.28 gives $\Phi_1 = \Phi_2 = -\pi$ and thus $\lambda_{11}(0) < 0$, which corresponds to *negative* steady–state pairing. However, as has been shown, the performance with this pairing is satisfactory, and better than that achievable with the alternate pairing on positive steady–state RGAs.

Another example demonstrating this class of plants is the PC2^C pairing for the 2×2 PC2 control structure. For this case:

- the plant $G(s)$ is MP $\Rightarrow z = 0$
- g_{11} and $G^{11} = g_{22}$ are both MP $\Rightarrow \hat{z} = 0$
- $\lambda_{11}(j\infty) = 1 \Rightarrow \alpha = 0$

and therefore, Equation 5.28 gives $\Phi_1 = \Phi_2 = 0$ and thus $\lambda_{11}(0) > 0$, which corresponds to *positive* steady–state pairing. For this case, the pairing selection would be the same whether the criterion at ∞ frequency or at steady–state were used.

Design Implications: For stable plants it is important to determine whether:

1. the overall plant is non–minimal phase (NMP),
2. the individual plants elements are NMP,
3. or the system with any loop removed is NMP.

If one or more of these three conditions is true, then pairing for performance can correspond to pairing on negative steady–state RGAs. Such pairings might therefore have been eliminated if the pairing criterion were based primarily on the steady–state RGA. The precise conditions are given in Lemma 3.

5.10 Summary and Conclusions

In this chapter, several aspects of decentralized regulatory control of the FCC process operating in the partial combustion mode have been analyzed.

The control of the FCC where riser temperature (T_r) and regenerator temperature (T_{rgn}) are controlled by manipulating catalyst circulation rate (F_{cat}) and combustion air supply rate (F_{air}) was analyzed. The conventional pairing where T_r is controlled using F_{cat} and T_{rgn} controlled using F_{air} - the $[T_r/F_{cat}, T_{rgn}/F_{air}]$ pairing was found to be the favored pairing over the alternate $[T_r/F_{air}, T_{rgn}/F_{cat}]$ pairing:

- the achievable performance is better with decentralized PI controllers, regardless of the source of uncertainty (additive, input multiplicative).
- the effort required to tune the decentralized PI controller is minimal:
    1. at a given operating point, internal stability and acceptable performance can be realized with a wide range of PI controller tunings.
    2. with a specific decentralized PI controller, acceptable performance is achieved over a wide range of operating points.

Thus tuning the decentralized PI controller for the $[T_r/F_{cat}, T_{rgn}/F_{air}]$ pairing can be considered to be "easy", and was probably a main factor in the historical decision to choose this pairing for FCC regulatory control. Moreover, it is shown that for this $[T_r/F_{cat}, T_{rgn}/F_{air}]$ pairing:

- the performance degradation when using decentralized PI controllers instead of full μ-optimal controllers is not significant.
- decentralized PI controllers can be designed for acceptable performance over a wide operating regime.
- if it is established that process interactions are significant, performance improvements can be achieved by "tightening" the decentralized PI controller, as the operating bandwidth is then pushed into a region of lower process interactions.
- reasonable transitions to unstable operating points can be effectively handled with an appropriately tuned decentralized PI controller.

- the property of decentralized integral controllability (DIC) does not hold, and thus steps must be taken to ensure that the control loops do not fail. In this context, it was pointed out that what some industrial practitioners (e.g. Edwards and Kim (1988)) refer to as 'open loop' could in fact result in an unstable system, even if the actual operating point is stable!

The control of the FCC where riser temperature (T_r) and regenerator temperature (T_{rgn}) are controlled by manipulating catalyst circulation rate (F_{cat}) and fresh feed temperature (T_{feed}) was also analyzed. It was postulated that the pairing where T_r is controlled using F_{cat} and T_{rgn} controlled using T_{feed} - the $[T_r/F_{cat}, T_{rgn}/T_{feed}]$ pairing would be the intuitively favored choice. However, both pairings were then quantitatively analyzed, and the indicated pairing was indeed found to be the preferred option:

- the achievable performance is superior with decentralized PI controllers, regardless of the source of uncertainty (additive, input multiplicative).
- the effort required to tune the decentralized PI controller is minimal:
    1. at a given operating point, internal stability and acceptable performance can be realized with a wide range of PI controller tunings.
    2. with a specific decentralized PI controller, acceptable performance is achieved over a wide range of operating points.

Thus tuning the decentralized PI controller for the $[T_r/F_{cat}, T_{rgn}/T_{feed}]$ pairing can be considered to be "easy". Moreover, it is shown that for this $[T_r/F_{cat}, T_{rgn}/T_{feed}]$ pairing:

- the performance degradation when using decentralized PI controllers instead of full μ-optimal controllers is not significant.
- decentralized PI controllers can be designed for acceptable performance over a wide operating regime.

- if it is established that process interactions are significant, performance improvements can be achieved by "tightening" the decentralized PI controller, as the operating bandwidth is then pushed into a region of lower process interactions.

- reasonable transitions to unstable operating points can be effectively handled with an appropriately tuned decentralized PI controller.

- the property of decentralized integral controllability (DIC) does hold. Thus any subset of loops can be arbitrarily detuned without affecting stability.

It was also found that the achievable performance with the $[T_r/F_{cat},\ T_{rgn}/F_{air}]$ pairing was superior to that of the $[T_r/F_{cat},\ T_{rgn}/T_{feed}]$ pairing with decentralized PI controllers, regardless of the source of uncertainty (additive, input multiplicative). A similar relative ranking was also obtained with μ-optimal controllers.

It was also pointed out that the diagonal RGA elements corresponding to the $[T_r/F_{cat},\ T_{rgn}/F_{air}]$ pairing is positive at high frequency, and *negative* at steady–state. On the other hand, for the $[T_r/F_{cat},\ T_{rgn}/T_{feed}]$ pairing, the diagonal RGA elements are positive at high frequency, and *positive* at steady–state. A theoretical development that provides insight into such differences is presented. It is related to the non–minimal phase behavior of one or more of (1) the overall plant, (2) the individual loop transfer functions, (3) the remaining system if some loop is removed.

Chapter 6 Options for Heavier Feed Processing in Fluid Catalytic Cracking Units

Summary

There is a growing need in the oil refining industry to process higher coking feeds in the available Fluid Catalytic Cracking (FCC) units. However, FCC units operated in the complete combustion mode (CC mode) might not be able to process sufficiently high coking feeds, and design modifications would be necessary to accommodate this greater feed processing flexibility. Two refitting options studied are: (1) catalyst cooler installation to extend CC mode operation (CCE mode) and (2) *CO* boiler installation to allow partial combustion (PC) mode operation. Both of these refitting options alleviate the constraint on regenerator temperature. A two parameter model describing the catalyst cooler dynamics is developed for the analysis of CCE mode operation. Because the proper installation of a *CO* boiler downstream from the regenerator flue gas line can be expected to minimally affect the FCC operation, no additional modeling of the *CO* boiler was undertaken. The main objective is to compare the steady–state and dynamic characteristics of these two refitting options. From a steady–state viewpoint, the catalyst cooler option is preferred if high coking feeds are to be processed. In particular, the product yields and feed conversions are higher. Moreover, the regenerated catalyst is clean burned regardless of the operating conditions or the incoming feed quality. A 3×3 control structure for the FCC refitted with a catalyst cooler is examined. The controlled variables are: riser temperature (T_r), regenerator temperature (T_{rgn}) and flue gas oxygen concentration ($C_{O_2,fg}$) - $[T_r, T_{rgn}, C_{O_2,fg}]$. The manipulated variables are catalyst circulation rate between the reactor and regenerator (F_{cat}), catalyst circulation rate to/from the catalyst cooler (F_{cc}), and combustion air supply (F_{air}) - $[F_{cat}, F_{cc}, F_{air}]$. It is argued on physical grounds, and verified through the μ-interaction analysis that the pairing T_r/F_{cat},

$C_{O_2,fg}/F_{air}$, and T_{rgn}/F_{cc} is essentially decoupled. A 2×2 control structure for PC mode operation is analyzed: the controlled variables are: $[T_r, T_{rgn}]$, and the manipulated variables are: $[F_{cat}, F_{air}]$. It is found that while a simple decentralized control strategy suffices for satisfactory performance over a wide operating regime in PC mode, a more sophisticated control strategy might be required to achieve tight control over a comparable operating range in CCE mode with the catalyst cooler. At a specific operating point, the performance of the PC mode and CCE mode operation can be made comparable by appropriately tuning for example decentralized PI controllers.

6.1 Introduction

Because of economic pressure, the demand on refineries to process heavier and dirtier feeds in their Fluid Catalytic Cracking Units (FCCUs) is increasing (Upson et al. 1993). By heavier and dirtier feeds, we mean feeds that during cracking have a relatively high coke generation rate. The coke, which is an undesirable by–product of the catalytic cracking reactions that occur in the reactor riser, is deposited on the active sites of the catalyst particles rendering the catalyst inactive. Inactive catalyst in this state is called *spent catalyst*. The coke is transported to the regenerator section where it is burned off.

At the same time, the regenerator operation has tended towards more severe conditions with the goal of essentially clean burning the regenerated catalyst. Clean burning refers to the process where the coke on the spent catalyst is essentially completely burned off in the regenerator, resulting in very low regenerated catalyst coke levels ($\leq$ 0.1 wt%). Clean burned catalyst has the desirable property that it has higher activity as well as selectivity than catalyst that still has a significant amount of coke bonded to the catalyst active sites.

Recall from the discussion in Chapter 4, Section 4.2.4 that when processing high coking feeds, a significant amount of coke is deposited on the catalyst particles. Clean burning catalyst used for high coking feeds means that essentially all of the significant coke deposits must be burned off when the catalyst is regenerated. Because of the associated large enthalpy change, the resulting regenerator temperature increase can be significant. High regenerator temperatures are undesirable, leading to:

- excessive thermal (permanent) deactivation of the cracking catalyst,
- damage to regenerator internals.

The range of feed qualities that can be processed in an FCCU might therefore be limited by the safe upper limit on regenerator temperature. The objective of this Chapter is to determine the heaviest possible feed that can be processed by a FCCU and analyze different design alternatives that would allow processing of even heavier

feeds. The comparison between the possible design alternatives is based on both steady–state and dynamic considerations.

6.2 FCC Unit Operating Modes

Catalyst regeneration in the regenerator proceeds through two combustion reactions:

$$C + O_2 \rightarrow CO_2 \qquad \Delta H_{comb} = 169.3 KJ/mol \tag{6.1}$$

$$C + \frac{1}{2}O_2 \rightarrow CO \qquad \Delta H_{comb} = 47.5 KJ/mol \tag{6.2}$$

The coke on catalyst is combusted to both CO and CO_2 but the relative ratio depends on the actual regeneration conditions. If significant quantities of both CO and CO_2 are produced, the regenerator is characterized as operating in *partial combustion mode* **(PC mode)**. However, if very little CO (ppm levels) is present, then the regenerator is characterized as operating in *complete combustion mode* **(CC mode)** respectively. The operational characteristics of each of these two modes that will be of primary concern in this Chapter include:

- One advantage of PC mode operation is that a wide range of feed qualities can typically be processed. This is because the coke is burned partially to CO (ΔH_{comb}= 47.5 KJ/mol) and partially to CO_2 (ΔH_{comb} = 169.3 KJ/mol). The net enthalpy change is therefore low enough to maintain acceptable regenerator temperatures at steady–state. The disadvantage of PC operation is that the catalyst is not typically clean burned as the regeneration conditions are not severe enough to ensure essentially complete coke combustion. The benefits of high regenerated catalyst activity and the associated high product yields are thus generally not realized in PC mode.

- Because of the more severe regeneration conditions associated with CC operation, the regenerated catalyst is typically clean burned. However because of the

large combustion enthalpy change during complete $C \rightarrow CO_2$ combustion only high quality feeds (low coking tendency) can be processed, and the physical restrictions on regenerator temperature limits the amount of coke that can be combusted, and therefore the range of feed qualities that can be processed.

The need to process higher coking feeds is therefore a more pressing issue for FCCs operating in the CC mode than those operating in PC mode. The operators of an FCCU operating in CC mode can therefore be faced with requirements that are impossible to simultaneously satisfy: There is the critical need to process heavier feeds. However, it is also necessary to clean burn the spent catalyst while ensuring that the regenerator temperature is below some operationally safe upper limit. As shown in Section 6.3.2, the maximum feed coking qualities that can be processed in the conventional CC model operation is rather limited, compared to the maximum possible feed qualities that can be processed in the PC mode. If typical feed quality variations in the refinery exceed the capacity of the available FCCU operating in CC mode, it might be necessary to modify the design of the FCCU operating in CC mode by installing additional equipment.

6.3 Preliminaries

6.3.1 Feasible Operating Regime

We are concerned with the effect of processing high coking feeds on the FCCU operation. These higher coking feeds deposit relatively large quantities of coke on the catalyst particles during cracking. The relative coke production rates that different feeds have is quantified using the "feed quality factor" (F_q). The feed coking factor has been discussed in detail in Chapter 4, Section 4.2.4. The mathematical model that we have used for describing the FCC dynamics is often used in the literature (Arbel et al. 1995, McFarlane et al. 1993). The different components of the incoming fresh feed have different feed coking characteristics (feed qualities) and are modeled as in Equation 6.3.

$$\Psi = \sum_i \gamma_i y_i(0) \tag{6.3}$$

where γ_i indicates the relative coking tendency of feed component i and $y_i(0)$ is the weight fraction of feed component i in the incoming fresh feed stream. We will lump the effect of changes in the weight fraction of different components and thus the incoming feed quality into the factor F_q that multiplies Ψ in Equation 6.3 (Equation 6.4).

$$\Psi = F_q \times \sum_i \gamma_i y_i(0) \tag{6.4}$$

The feasible operating regime will taken to be the set of $[T_{rgn}, T_{ris} F_q]$ combinations where operation is possible without violating any of the constraints indicated in Table 6.1, which we have adopted from (Arbel et al. 1995, McFarlane et al. 1993).

Variable	Units	Lower Limit	Upper Limit
Manipulated Variables			
F_{cat}/F_{oil}	$\frac{lbcat.}{lbfeed}$	0	10
F_{air}/F_{oil}	$\frac{lbair}{lbfeed}$	0	1
T_f	$^\circ F$	400	700
Output Variables			
T_r	$^\circ F$	950	1050
T_{rgn}	$^\circ F$	1100	1400
C_{rgc}	$wt.\%$	0	0.5
$C_{O_2,sg}$	$mol.\%$	0.5	2
Design Specification			
F_q		1.0	1.5

Table 6.1: Manipulated and process variables with constraints.

Since the range in feed quality is a design specification, we will assume for this analysis that the normal range for F_q is $1.0 \leq F_q \leq 1.5$.

6.3.2 Largest Feasible F_q

To quantify the largest allowable F_q, while ensuring feasible steady–state operation in either the PC or CC modes, the following constrained nonlinear optimization problem is solved:

$$\max_{x,u,F_q} F_q \tag{6.5}$$

subject to:

$$\dot{x} = F(x, u, F_q) = 0 \tag{6.6}$$

$$x(i)_{lo} \leq x(i) \leq x(i)_{hi} \tag{6.7}$$

$$u(i)_{lo} \leq u(i) \leq u(i)_{hi} \tag{6.8}$$

$$0 < F_q \tag{6.9}$$

Note that:

- F(x,u,F_q) = 0 imposes the steady–state operation requirement (non–linear model).
- The constraints on the states ($x(i)_{lo}$ and $x(i)_{hi}$) as well as the constraints on the manipulated variables ($u(i)_{lo}$ and $u(i)_{hi}$) are provided in Table 6.1.

The largest possible F_q that the unit can handle at steady–state while operating within the limits specified in Table 6.1 is indicated in Table 6.2. Also indicated are the operating points in the partial and complete combustion modes where operation with the maximum possible F_q is feasible.

The specific limits and their physical justification are discussed in detail in Section 4.3. Moreover, it was shown in Section 4.3 that the constraint that most severely limits the heaviest processable feed in CC mode operation is the upper limit on regenerator temperature. Design modifications that can alleviate this constraint can be expected to allow heavier feed processing. Two possible revamp options have been suggested and briefly discussed recently in Arbel, Rinard and Shinnar (1997) and will be further analyzed in this Chapter:

	Partial Combustion	Complete Combustion
Worst Case F_q	2.20	1.17
Operating Point		
F_{cat}/F_{oil} $(\frac{lbcat.}{lbfeed})$	2.5545	3.624
F_{air}/F_{oil} $(\frac{lbair}{lbfeed})$	0.3908	0.5521
T_f $(°F)$	700	574.4
T_r $(°F)$	950	950
T_{rgn} $(°F)$	1400	1400
C_{rgc} $(wt.\%)$	0.5	0.01306
$C_{O_2,sg}$ $(mol.\%)$	0	2

Table 6.2: Largest feasible feed coking quality at steady–state.

1. The installation of a catalyst cooler in the regenerator section to provide an additional independent variable for regenerator temperature control.

2. Conversion to PC mode operation which would allow operation over a wider F_q range (Table 6.2). This would require the installation of a downstream CO boiler to combust the significant amounts of CO produced during partial coke combustion. The enthalpy change of combustion can be recovered.

Note that catalyst coolers and especially CO boilers have been utilized in industry (Sadeghbeigi 1995) for some time but a detailed analysis examining the operational implications of these options does not appear to have been quantitatively addressed in the open literature, in particular from a dynamic viewpoint. The recent work by Arbel et al. (1997) addresses a semi–quantitative comparison based on steady–state arguments.

The goal in this Chapter is to compare both the steady–state and dynamic characteristics of the FCCU refitted with each of these two options to determine which option might be more desirable for processing a wider range of feed qualities. We will start with a physical description of the two options.

6.4 Equipment Description

6.4.1 *CO* Boiler

For FCC operation in the PC mode, significant amounts of both CO and CO_2 are produced during the combustion of coke. Owing to current environmental regulations (Evans and Quinn 1993) and for safety reasons, it is necessary to treat (convert) the CO produced further before the regenerator exhaust gases can be discharged. The common industrial practice is to combust the CO to CO_2 in the CO boiler which is installed down stream from the regenerator exhaust gas line (Figure 6.1). The enthalpy change of combustion is recovered in the CO boiler. However, we will not be concerned with heat integration in this Chapter. Since the CO boiler is installed downstream of the regenerator flue gas line, and heat integration is not considered, it is unlikely that the proper installation of a CO boiler would significantly affect either the steady–state or the dynamic performance of the FCCU. From an FCCU operational view–point , the only consequence of installing a CO boiler is therefore the ability to operate the FCC in PC mode.

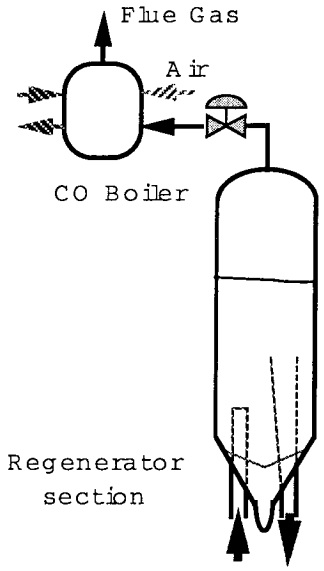

Figure 6.1: Schematic of downstream CO boiler.

6.4.2 Catalyst Cooler

Heat transfer systems have been long used in commercial FCCUs. In the past however, most designs were plagued by either poor mechanical reliability or lack of range in heat transfer capacity. Recently, new improved designs using an external dense phase flow–through or back–mixed tube bundles have shown excellent mechanical reliability. These designs have also demonstrated a wide range of easily controlled heat removal duties (Upson et al. 1993). Catalyst coolers based on such designs take advantage of two properties of fluidized dense phase catalyst beds:

- fluidized bubbling beds mix well in the vertical direction
- fluidized FCC catalyst acts as an excellent heat transfer medium.

Upson et al. (1993) also report that using such catalyst coolers:

- the heat transfer coefficient between fluidized catalyst on the shell side and water/steam on the tube side can be closely controlled over the range of 10 – 100 Btu/(hr ft^2 °F),
- the catalyst flow rate through the catalyst cooler can be independently controlled, and
- a single catalyst cooler can be operated and controlled anywhere within a heat removal duty of 20 – 150 $\times 10^6$ Btu/hr.

The mechanical design of the catalyst cooler is also a very important factor in determining the overall effectiveness of the catalyst cooler, for example determining the effectiveness of the cooled catalyst and hot regenerator catalyst mixing. However, we will not be concerned with the detailed mechanical design of the catalyst cooler. A mathematical model that accounts for the primary heat exchange functions of the catalyst cooler is developed in Section 6.4.2. Note also that at least two possible configurations exist for regenerator temperature control:

1. Heat is transfered away from the hot regenerated catalyst just prior to transportation to the bottom of the reactor riser. This allows one to reduce the

temperature of regenerated catalyst entering the bottom of the reactor riser. However, this configuration does not permit any control over the regenerator dense bed temperature. The higher catalyst/oil ratio required to achieve the same riser top temperature with cooler regenerated catalyst results in higher conversions and yields (Upson et al. 1993). Assuming that the heat removal rate is Q, pseudo steady–state operation, and perfect mixing, the temperature of the regenerated catalyst at the bottom of the reactor riser is given by Equation 6.10.

$$T_{exit} = \frac{F_{cat}C_{pc}T_{rgn} - Q}{F_{cat}C_{pc}} \tag{6.10}$$

Such a catalyst cooling scheme is more suited for the following situation:

- FCCs processing conventional, lower coking feeds (*e.g.* vacuum gas oil (VGO)). Regenerator temperatures would be within acceptable limits under normal operation because the associated low coke combustion rates would not generate enough heat. In such a case it is therefore beneficial to reduce the temperature of the regenerated catalyst at the bottom of the reactor riser to achieve higher conversions. It is reported that higher catalyst/oil ratios in the reactor riser result in higher yields and conversions (Upson et al. 1993, Arbel et al. 1997).

2. Heat is transfered directly from the bulk of the dense bed regenerator catalyst (Figure 6.2). The overall regenerator dense bed temperature is therefore lower. Such a catalyst cooling scheme might be useful in the following situation:

   - FCCs processing high coking feeds. Here, the enthalpy release due to the combustion of significant amounts of coke would result in excessive regenerator temperatures in the absence of the dense bed catalyst cooler.

Recall that our objective is to analyze possible modifications to the FCC design to allow processing of high coke generating feeds. In the first setup above, there is no control on the regenerator dense bed temperature. As we have just argued in

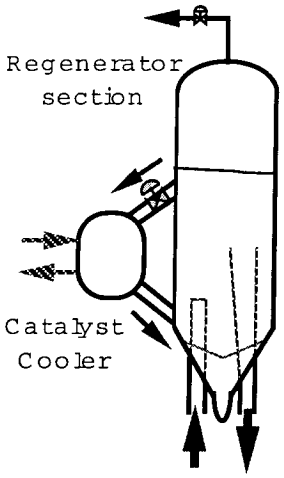

Figure 6.2: Schematic of regenerator catalyst cooler.

the second point above, this is a severe restriction if we want to clean burn catalyst when processing high coking feeds. We will therefore not consider the first option further. Our focus will be on the ability to control the bulk regenerator temperature (Figure 6.2).

It will be assumed for simplicity that the catalyst cooler is a shell and tube heat exchanger attached to the regenerator as in Figure 6.2. The physical design of the catalyst cooler can depend on many factors including:

- catalyst cooler shell diameter
- internal tube diameter
- distance between tubes inside the cooler
- tube bundle layout (square/triangular setup)
- tube length

The range of specific heat transfer coefficients reported by (Upson et al. 1993) is given in Equation 6.11.

$$10\frac{Btu}{ft^2hr^\circ F} \leq U \leq 100\frac{Btu}{ft^2hr^\circ F} \tag{6.11}$$

Moreover, the mass of catalyst contained in the catalyst cooler is directly related to the size of the catalyst cooler (and thus the heat transfer area). Therefore while it might appear from the list above that a large number of parameters need to be determined, we can in fact capture the effect of changes in all these parameters by the following two parameters:

1. catalyst mass in the catalyst cooler
2. heat transfer coefficient UA which is the product of the specific heat transfer coefficient (U) (Equation 6.11) and the heat transfer area A, which is dependent on the factors listed above.

This two parameter catalyst cooler model will be developed next and utilized in the subsequent steady–state and dynamic analysis.

One of the underlying justifications for installing a catalyst cooler to allow for independent regenerator temperature control is the ability to extend the range of possible operation (*i.e.* allow processing feeds with a wider range of coking characteristics), while maintaining operation in the CC mode. For notational convenience, we will define the **CCE mode**: *complete combustion operating mode extended by the installation of a catalyst cooler.*

Two parameter catalyst cooler model

The energy conservation equation around the regenerator yields:

$$\frac{dT_{rgn}}{dt} = \frac{1}{W_{rgn}C_{pc}}\{Q_{comb} - [Q_{fg} + Q_{air} + Q_{sc} + Q_{lost} + Q_{cc}]\} \qquad (6.12)$$

where:

Q_{comb}	=	heat of combustion for burning coke to CO, CO_2, H_2O
Q_{fg}	=	enthalpy change due to flue gas outflow
Q_{air}	=	enthalpy change due to combustion air inflow
Q_{sc}	=	enthalpy change due to spent catalyst inflow

Q_{lost}	=	enthalpy transfer from regenerator wall to environment
Q_{cc}	=	enthalpy transfer to catalyst cooler

The model published by Arbel et al. (1995) is used to model all the terms in Equation 6.12 except for Q_{cc} - the enthalpy transfer due to the catalyst cooler. Q_{cc} is given by Equation 6.13.

$$Q_{cc} = F_{cc}C_{pc}\left[T_{rgn} - T_{ce}\right] \tag{6.13}$$

In Equation 6.13, T_{ce} is the catalyst temperature at the exit of the catalyst cooler, or equivalently the temperature of cooled catalyst re–entering the regenerator dense bed from the catalyst cooler. The dynamic behavior of T_{ce} clearly depends on the model used to describe the catalyst cooler, and will be developed below. The assumptions made in modeling the catalyst cooler are:

- saturated water/steam flows in the tube side of the catalyst cooler while fluidized catalyst flows in the shell side.
- the tube side pressure is maintained constant (3–4 bar). At this pressure, the boiling point of water is T_{bw}.
- the water flow in the tube side is adjusted so as to ensure that there is saturated vapor (at temperature T_{bw}) at the exit of the tube side at all times.
- the heat transfer coefficient between the shell–side and the tube–side is constant. Moreover, we will lump the heat–exchange area with the specific heat transfer coefficient (UA).
- the manipulated variable used to control T_{rgn} is the rate of catalyst flow to the catalyst cooler - F_{cc}. Arbel et al. (1997) indicate that a typical range for F_{cc} as a ratio of the fresh oil feed rate (F_{oil}) is given in Equation 6.14. F_{cc} is scaled by F_{oil} simply for consistency with the common practice of scaling F_{cat}/F_{oil} and F_{air}/F_{oil}, used for example in Chapter 4 and Chapter 5.

$$0 \leq \frac{F_{cc}}{F_{oil}} \leq 10 \tag{6.14}$$

- there is no accumulation of catalyst in the catalyst cooler *i.e.* the catalyst flow rate into the catalyst cooler is exactly equal to the catalyst flow rate out. The shell side fluidized catalyst hold–up is $W_{cc} = 50000$ lb, and remains constant at all times.

- the shell side fluidized catalyst is assumed to be well mixed. If T_{ce} is the shell side bulk (and exit) catalyst temperature, then

$$\frac{dT_{ce}}{dt} = \frac{1}{W_{cc}C_{pc}} \{F_{cc}C_{pc}[T_{rgn} - T_{ce}] - Q_{hx}\} \tag{6.15}$$

- the heat transfer from the shell side to the tube side is given by Equation 6.16.

$$Q_{hx} = UA[T_{ce} - T_{bw}] \tag{6.16}$$

We will analyze the sensitivity of our results to changes in both the catalyst cooler parameters as well as the model structure itself in Section 6.7.2. Note that from a steady–state viewpoint, the only significant quantity in Equation 6.15 is Q_{hx}.

6.5 Steady–State Comparison

6.5.1 Maximum Achievable F_q Comparison

We begin by investigating whether the FCC refitted with the catalyst cooler is indeed capable of processing higher coking feeds without violating any process constraints. The same steady–state optimization problem (Equation 6.5) is posed for the "modified design" with the catalyst cooler. The result of this optimization is tabulated in Table 6.3, where the maximum F_q value for the CCE mode is compared to that achieved during the original CC mode operation, as well as in PC mode operation.

It is evident that the design modification is capable of processing the required range of feed qualities, and in fact for the selected catalyst cooler parameters, exceeds the limit achievable if PC mode operation were used.

	FCC Operating Mode		
	CC	PC	CCE
Maximum steady–state F_q	1.17	2.20	**2.27**

Table 6.3: Maximum possible steady–state value of F_q. Comparison between CC (original design), PC (CO boiler), and CCE (catalyst cooler) modes of operation.

6.5.2 Product Yield Comparisons

The main objective of the FCC process is to crack high boiling hydro–carbons of low economic value to lighter more valuable hydro–carbon products including:

- wet gas (C_4 and lighter gases)
- gasoline

Furthermore, during process operation, the operators are concerned with:

- coke production rate
- overall feed conversion

For the steady–state analysis we will compare the relative benefits of CCE mode operation to the PC mode operation from a product yield and overall conversion viewpoint. In particular, we will be concerned with comparing the wet gas yield, gasoline yield and overall feed conversion that can be expected from each of the two modified designs at steady–state for feasible combinations of $[T_r, T_{rgn}, F_q]$.

The rate of coke and CO combustion depends strongly on the regenerator temperature and the O_2 partial pressure. The dependence on the coke concentration is less pronounced. One consequence of this phenomenon is that the amount of coke left unburned is higher if the spent catalyst has a significant coke fraction (due to

cracking high coking feeds). Equivalently, when processing low coking feeds, the coke fraction remaining on the regenerated catalyst will be lower than when processing high coking feeds. This is particularly true for PC mode operation where the lack of excess O_2 in the regenerator and lower regeneration temperatures can result in significant levels of unburned coke on the regenerated catalyst as shown in Figure 6.3 for two different values of F_q.

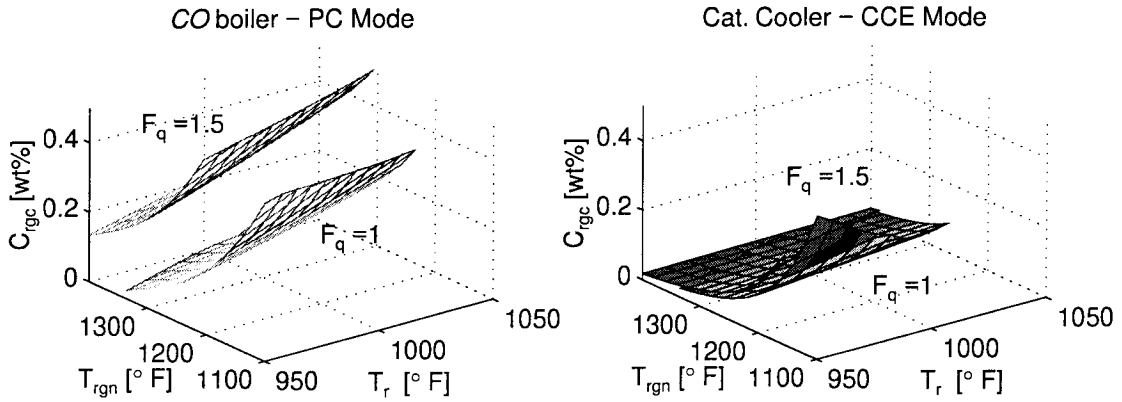

Figure 6.3: Comparison of coke on regenerated catalyst for CO boiler. F_q=1.0 and F_q=1.5.

Recall that one of the benefits of operating in conventional CC mode is that the catalyst is clean burned and thus the catalytic activity is essentially completely restored. Recall also that the most significant constraint for CC mode operation is the limit on regenerator temperature. The installation of a catalyst cooler alleviates the constraint on T_{rgn} by providing additional heat transfer capacity away from the regenerator and can be viewed as a means of extending the feasible CC mode operating regime. We can therefore expect that the regenerated catalyst coke level will remain low over the entire feasible operating regime, and regenerated catalyst activity, and consequently the conversion and yields will be high. This should be the case regardless of the feed quality, as long as constraints are not violated. With the catalyst cooler installed, the significant constraints can include:

- limits on catalyst cooling capacity
- limits on available combustion air

The coke remaining on the regenerated catalyst is determined over the entire $[T_r, T_{rgn}, F_q]$ operating range for the CCE mode operation and plotted in Figure 6.3. From Figure 6.3 it is evident that:

- the coke level on the regenerated catalyst is low for CCE mode over the entire operating regime,
- the level of coke on regenerated catalyst in CCE mode operation is comparable regardless of the feed coking quality (F_q=1 or F_q=1.5). Thus for CCE mode operation, the regenerated catalyst is therefore clean burned over the entire operating regime, and the catalyst activity is therefore essentially fully restored, regardless of the incoming feed coking quality and the actual operating point.

It is instructive to replot the information presented in Figure 6.3 in a slightly different format, as presented in Figure 6.4. In Figure 6.4, the coke level on regenerated catalyst is compared for low coking feeds ($F_q = 1$) and high coking feeds ($F_q = 1.5$) for both the CCE and PC modes. Referring to Figure 6.4, we note the following:

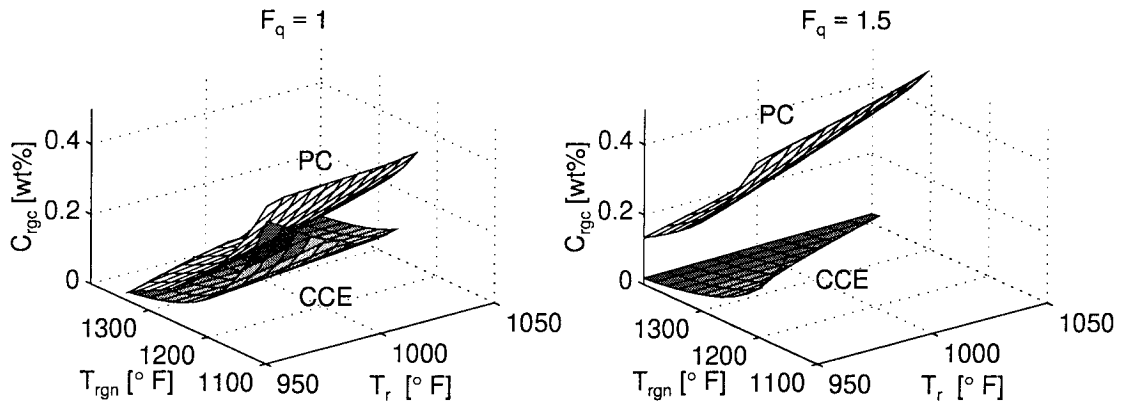

Figure 6.4: Comparison of coke on regenerated catalyst for PC mode (CO boiler) and the CCE mode (catalyst cooler) for F_q=1.0 and F_q=1.5.

- When processing low coking feeds (F_q=1), the regenerated catalyst coke levels are comparable when operating in either the PC or the CCE modes. Thus for low coking feeds, no specific advantage from a steady–state viewpoint is apparent for the PC or CCE operating modes.

- When processing high coking feeds (F_q=1.5), there is a significant amount of unburned coke on regenerated catalyst during PC mode operation, compared to the CCE mode. As argued in Section 6.2, this is mainly because of the limited O_2 supply in PC mode operation.

Because the regenerator catalyst is clean burned over the entire operating range in CCE mode operation, one therefore expects that the extended CC mode operation with the catalyst cooler will result in higher steady–state product yields (higher than the PC mode) and higher overall conversions. This is indeed the case as seen from Figure 6.5, where selected product yields as well as overall feed conversions are compared. Note from Figure 6.5 that:

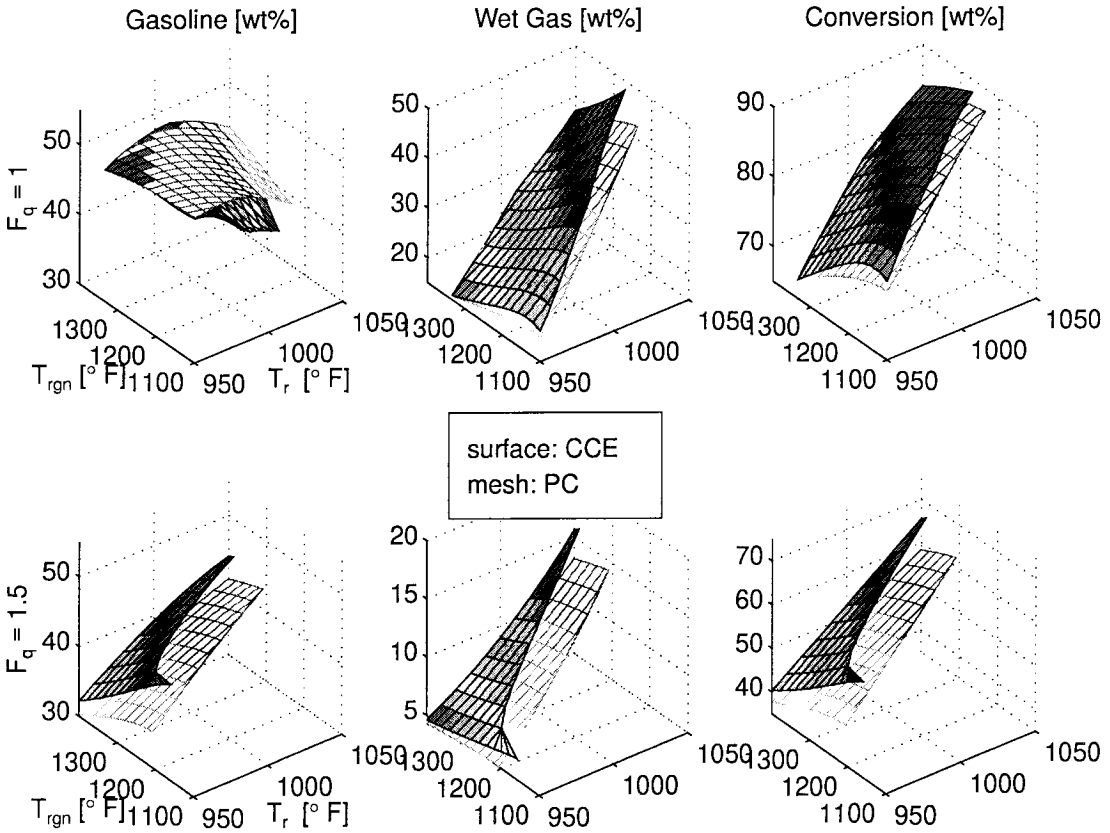

Figure 6.5: Comparison of gasoline yield, wet–gas yield and overall conversion for the CO boiler and the catalyst cooler. F_q=1.0 and F_q=1.5.

- the wet gas yield and the overall conversion is higher for CCE mode operation

regardless of the incoming feed quality.

- the difference in the wet gas yield and feed conversion for CCE mode operation and PC mode operation are more significant at the higher $F_q = 1.5$. As demonstrated in the discussion related to Figure 6.4, this can be attributed to the fact that the catalyst is essentially clean burned in CCE mode operation, and activity is therefore essentially fully restored, regardless of the operating point. This allows for higher conversions and yields.

- at high T_r and low T_{rgn}, the gasoline yield in PC mode operation is higher than in CCE mode operation (top left plot Figure 6.5). We note that under these conditions,

  - T_r is high and the rate of feed cracking is therefore high, but
  - coke on regenerated catalyst is significantly higher for PC mode operation than CCE mode operation (Figure 6.4), and thus catalyst activity is lower.

  These two conditions have opposed impacts on gasoline cracking. The subsequent cracking of gasoline to coke and wet gas is therefore limited in PC mode operation due to the coke on regenerated catalyst, but not in CCE mode operation. Thus, in CCE mode operation, there should be higher levels of wet gas and lower gasoline levels and this is indeed what is observed in the top middle plot in Figure 6.5.

6.5.3 Conclusions: Steady–State Comparison

From the steady–state analysis, we can conclude that:

- For CCE mode operation, the regenerated catalyst is clean burned regardless of:

  - the incoming feed quality,
  - riser temperature,

- regenerator temperature.

- It is found that installing the catalyst cooler allows complete combustion operation over a wide $[T_r, T_{rgn}, F_q]$ operating range. The particular benefit of clean burned regenerated catalyst is thus achieved over this wider operating range, regardless of the incoming feed quality. Installing the catalyst cooler therefore extends the feasible operating regime in complete combustion mode.

- No particular ranking between PC and CCE mode operation is apparent if only low coking feeds are to be processed. However, a wide range of feed qualities are processed during normal FCC operation, and there is no guarantee that the feed coking quality will remain low. Therefore, if the feed is 'typically' low coking, then PC mode operation might be preferred, as there would be no incentive to install the additional fluidized bed required for CCE mode operation. It would be operationally simpler to burn off the excess CO in a CO boiler. Moreover, for low coking feeds the coke on regenerated catalyst is comparable in PC mode and CCE mode operation.

- Installing the catalyst cooler (CCE mode operation) has a distinct advantage over installing the CO boiler (PC mode operation) when processing high coking feeds - because the regenerated catalyst is always clean burned. In particular, the product yields as well as overall conversions are higher.

6.6 Control Structure Selection

In this section, we will investigate which control structures will allow for effective FCC regulatory control. By control structure, we mean the choice of a set of controlled variables and manipulated variables. Control structure selection for PC mode and conventional CC mode operation was discussed in detail in Chapter 4. In this section, we will very briefly discuss the PC mode control structure, and analyze a postulated CCE mode control structure in detail. The nominal operating conditions for CCE

mode operation are listed in Table 6.4. The non–linear model was linearized at these operation points, and the linear models obtained.

	Operating Regime	
	PC	CCE
$T_{rgn}(°F)$	1240	1340
$T_r(°F)$	1000	1000
$F_q(--)$	1.25	1.25

Table 6.4: Process conditions at selected PC mode and CCE mode operating points.

6.6.1 *CO* Boiler

Since the *CO* boiler is installed downstream of the regenerator flue gas line, and heat integration is not considered in this study, it is unlikely that the proper installation of a *CO* boiler would significantly affect the dynamic performance of the FCC unit. From an operational viewpoint, the only consequence of installing a *CO* boiler is therefore the ability to operate the FCC in PC mode. It will be assumed that the installation of the catalyst cooler does not contribute any additional dynamic effects to the FCCU operation. The dynamic analysis for this options is therefore exactly as in Chapter 4, control scheme PC1.

It was shown in Chapter 4 that the most appropriate control structure for regulatory FCC control in PC mode is the following 2×2 control structure:

- Manipulated variables:
  1. catalyst circulation rate between reactor and regenerator (F_{cat})
  2. combustion air flow rate to regenerator (F_{air})
- Controlled variables:
  1. riser top temperature (T_r)
  2. regenerator temperature (T_{rgn})

This 2×2 control scheme will be used for the dynamic performance comparison between the CO boiler option and the catalyst cooler option.

6.6.2 Catalyst Cooler

Conventional FCC operation in complete combustion mode typically uses the following 2×2 control scheme for regulatory control (Chapter 4):

- Manipulated variables:
  1. catalyst circulation rate between reactor and regenerator (F_{cat})
  2. combustion air flow rate to regenerator (F_{air})
- Controlled variables:
  1. riser top temperature (T_r)
  2. flue gas O_2 concentration ($C_{O_2,fg}$)

However, it has been shown in Section 6.3.2 that processing a wide range of feed qualities is not possible when the FCCU is operated in the conventional complete combustion mode, with the upper limit on regenerator temperature being the most serious constraint. As discussed in Section 6.3, the installation of the catalyst cooler provides an additional manipulated variable (regenerated catalyst flow rate to/from catalyst cooler) that allows for independent regenerator temperature control. Therefore, in addition to the manipulated and controlled variables used for regulatory control for the conventional complete combustion operation, one has the catalyst flow rate to/from the catalyst cooler and the regenerator temperature as additional manipulated and controlled variables respectively. For the FCC operation in CCE mode the following 3×3 control scheme for regulatory control is therefore the most intuitive, and will be analyzed in this study:

- Manipulated variables:
  1. catalyst circulation rate between reactor and regenerator (F_{cat})

2. combustion air flow rate to regenerator (F_{air})
3. catalyst flow rate to/from catalyst cooler (F_{cc})

- Controlled variables:

1. riser top temperature (T_r)
2. flue gas O_2 concentration ($C_{O_2,fg}$)
3. regenerator temperature (T_{rgn})

Based on physical insight, it can be argued that under the assumption that the regenerator conditions are such that all the coke on spent catalyst is burned off in the regenerator section (ideal catalyst regeneration), the 3×3 regulatory control scheme for CCE operation is essentially decoupled:

- *Effect of change in F_{air}. (F_{cat}, F_{cc}=constant)*: Additional combustion air will provide additional O_2 for coke combustion. But by assumption, the regenerator conditions are such that all the coke is already completely combusted, and adding additional O_2 will not affect regenerator operation. The lack of additional combustion means that there will be no additional increase in regenerator temperature. In fact, one could expect a slight drop in regenerator temperature because of the enthalpy change associated with heating the incoming combustion air to the regenerator temperature. This was discussed in Chapter 4, Section 4.5.2. Furthermore, for F_{cat}=constant and complete catalyst regeneration, no change in regenerator temperature implies no change in reactor temperature. The main effect of increasing combustion air flow rate will therefore be an increase in $C_{O_2,fg}$.

- *Effect of change in F_{cc}. (F_{cat}, F_{air}=constant)*: The physical setup of the catalyst cooler as a heat exchange unit cooling the regenerated catalyst and directly connected to the regenerator suggests that changing the catalyst flow rate to the catalyst cooler should affect the regenerator temperature most significantly.

- *Effect of change in F_{cat}. (F_{air}, F_{cc}=constant)*:

- at constant T_{rgn}, increasing F_{cat} will increase the energy transfer rate to the reactor riser, and therefore riser temperature.
- increasing F_{cat} increases the coke transfer rate to the regenerator, and therefore increases regenerator temperature due to an increased coke combustion rate (ideal catalyst regeneration assumption). Because of the higher coke combustion rate, regenerator temperature will increase.
- additional O_2 will be consumed during combustion but since F_{air}= constant, the flue gas O_2 concentration will decrease.

Therefore changing F_{cat} affects all the three outputs in general. However, the three controlled variables have different degrees of significance, reflected by the different output weights – Table 6.5. Note that the scaling factors in Table 6.5 are based on the 'equal concern error' (Sorensen 1993), and can be interpreted as follows, using T_r and T_{rgn} as examples: A deviation of $3°F$ in T_r would be as significant (disruptive) to the process as a $30°F$ change in T_{rgn}. An alternative interpretation is that it is more critical (by a factor of $30/3 = 10$) to maintain T_r at set–point that T_{rgn} at set–point. The scaling factors are therefore used to scale the outputs such that any scaled output deviation of magnitude 1 indicates the same degree of significance. Because of this weighting, one can argue that the while increasing F_{cat} affects all three outputs, the most significant effect of increasing F_{cat} is on the riser temperature.

Controlled Variable	Physical Units	Weight
T_r	$°F$	3.0
$C_{O_2,fg}$	mol %	0.5
T_{rgn}	$°F$	30.0

Table 6.5: Weights for deviation of controlled variables from nominal values.

Based on these physical arguments, the following pairings for the 3×3 regulatory level plant can be postulated:

- T_r / F_{cat} pair

- $C_{O_2,fg}$ / F_{air} pair
- T_{rgn} / F_{cc} pair

Note that the assumption of ideal catalyst regeneration was used in the arguments above. However, extensive analysis over the entire $[T_r, T_{rgn}]$ operating range indicates that the arguments also hold for the relatively low coke levels on regenerated catalyst typical of CCE mode operation. Low regenerated catalyst coke levels are common for the entire operating range considered in this work, as was evident from Figure 6.3. Of course, excess O_2 in the regenerator is also required to ensure ideal catalyst regeneration, but this is always the case for CCE mode operation. We will investigate the characteristics of this proposed 3×3 control scheme further.

Steady–state RGA analysis

The steady–state RGA matrix $[\lambda_{ij}(0)]$ and any RHPT zeros for the PC mode and CCE mode control structures are tabulated in Table 6.6. Referring to Table 6.6, we note the following:

	Operating Regime	
	PC	CCE
Steady–state RGA	T_r / T_{rgn} $\begin{bmatrix} -1.1 & 2.1 \\ 2.1 & -1.1 \end{bmatrix}$ F_{cat} / F_{air}	T_r / $C_{O_2,fg}$ / T_{rgn} $\begin{bmatrix} 3.08 & 0.59 & -2.68 \\ -0.01 & 0.96 & 0.05 \\ -2.07 & -0.55 & 3.62 \end{bmatrix}$ F_{cat} / F_{air} / F_{cc}
RHPT Zeros	–	–

Table 6.6: Steady–state RGA values and RHPT zeros

- The PC control scheme corresponds to pairing on *negative* steady–state RGAs ($\lambda_{11}(0) = \lambda_{22}(0) = -1.1$). Recall the definition of decentralized integral controllability (DIC) (Morari and Zafiriou 1989): (1) the overall closed loop is stable, and (2) the controllers of any subset of loops can be arbitrarily detuned without affecting the closed loop stability. A necessary condition for DIC is that $\lambda_{ii}(0) > 0$ for each loop i (Morari and Zafiriou 1989). From a DIC viewpoint, this pairing is not desirable, but as shown in Chapter 5, this is the most suitable choice from an operational viewpoint.

- The postulated pairing for CCE mode operation corresponds to pairing on positive steady–state RGAs, which is necessary for decentralized integral controllability.

- Both control structures are minimum phase.

μ-interaction measure analysis

In this section, we will examine the constraints that are imposed on the closed loop transfer function of the three individual loops which guarantee that the overall closed loop system is stable. Intuitively, if stringent constraints on the individual loops are required to ensure overall stability, the plant is strongly interacting. On the other hand, mild constraints on the individual loops can imply an essentially decoupled plant. For notational convenience, we define the following:

- the plant transfer matrix (3×3)

$$G(s) = [g_{ij}(s)], i = 1, 2, 3 \quad j = 1, 2, 3 \tag{6.17}$$

- matrix of diagonal elements of $G(s)$

$$\tilde{G}(s) = \text{diag}\{g_{11}, g_{22}, g_{33}\} \tag{6.18}$$

- the decentralized controller

$$\tilde{C}(s) = \text{diag}\{c_1, c_2, c_3\} \tag{6.19}$$

Note that for this study, we will use decentralized PI controllers for c_1, c_2 and c_3 as in Chapter 5. Also define the following sensitivity ($E(s)$) and complementary sensitivity ($H(s)$) matrices for the overall system (with $G(s)$ and $C(s)$):

$$E(s) = (I + G(s)C(s))^{-1} \qquad H(s) = G(s)C(s)(I + G(s)C(s))^{-1} \tag{6.20}$$

and the sensitivity ($\tilde{E}(s)$) and complementary sensitivity ($\tilde{H}(s)$) matrices for the system with $\tilde{G}(s)$ and $C(s)$:

$$\tilde{E}(s) = (I + \tilde{G}(s)C(s))^{-1} \qquad \tilde{H}(s) = \tilde{G}(s)C(s)(I + \tilde{G}(s)C(s))^{-1} \tag{6.21}$$

We also define the following matrices that capture the difference between the actual plant $G(s)$ and the diagonal elements of the plant $\tilde{G}(s)$.

$$L_H = (G - \tilde{G})\tilde{G}^{-1} \tag{6.22}$$

and

$$L_E = (G - \tilde{G})G^{-1} \tag{6.23}$$

Note that:

$$G(s) = (I + L_H(s))\tilde{G}(s) \tag{6.24}$$

and L_H can be considered to represent the plant interactions as multiplicative output "uncertainty". Furthermore,

$$G(s) = (I - L_E(s))^{-1}\tilde{G}(s) \tag{6.25}$$

and L_E can be considered to represent the plant interactions as output inverse multiplicative "uncertainty". Note that L_E and L_H are integral parts of the plant and considering them as uncertainty allows us to use the tools from robust theory to quantify the degree of interaction. The following two theorems from Morari and Zafiriou (1989) specify bounds on the individual loop sensitivity and complementary functions so that the overall closed loop (with $G(s)$ and $C(s)$) is stable:

1. *Bounds on* $\bar{\sigma}[\tilde{H}(j\omega)]$:

   Theorem 1 *Assume that* $G(s)$ *and* $\tilde{G}(s)$ *are both stable and that* $\tilde{H}(s)$ *is stable.*

Then, the closed loop system $H(s)$ is stable if:

$$\bar{\sigma}[\tilde{H}(j\omega)] < \mu_{\tilde{H}}^{-1}[L_H(j\omega)] \tag{6.26}$$

2. *Bounds on $\bar{\sigma}[\tilde{E}(j\omega)]$:*

Theorem 2 *Assume that $G(s)$ and $\tilde{G}(s)$ are both stable and that $\tilde{H}(s)$ is stable. Then, the closed loop system $H(s)$ is stable if:*

$$\bar{\sigma}[\tilde{E}(j\omega)] < \mu_{\tilde{E}}^{-1}[L_E(j\omega)] \tag{6.27}$$

Note that:

- Theorem 1 gives a bound on the individual loop complementary sensitivity functions for overall closed loop stability. Note that $\mu_{\tilde{H}}^{-1}[L_H(j\omega)] = \infty$ if the plant is decoupled *i.e.* $G(s) = \tilde{G}(s)$. In this case, $L_H(s) = 0$ in Equation 6.22. This is to be expected since there are no restrictions due to interactions for a decoupled plant.

- Theorem 2 gives a bound on the individual loop sensitivity functions for overall closed loop stability. Note that $\mu_{\tilde{E}}^{-1}[L_E(j\omega)] = \infty$ if the plant is truly decoupled *i.e.* $G(s) = \tilde{G}(s)$. In this case, $L_H(s) = 0$. This is to be expected since there are no restrictions due to interactions for a decoupled plant.

- The two bounds indicated in Theorem 1 and Theorem 2 cannot be combined over different frequency ranges. This is because L_E and L_H do not describe the same "uncertainty set".

The bounds on the individual sensitivity and complementary sensitivity functions based on Theorem 1 and Theorem 2 are plotted in Figure 6.6.

From Figure 6.6, note that:

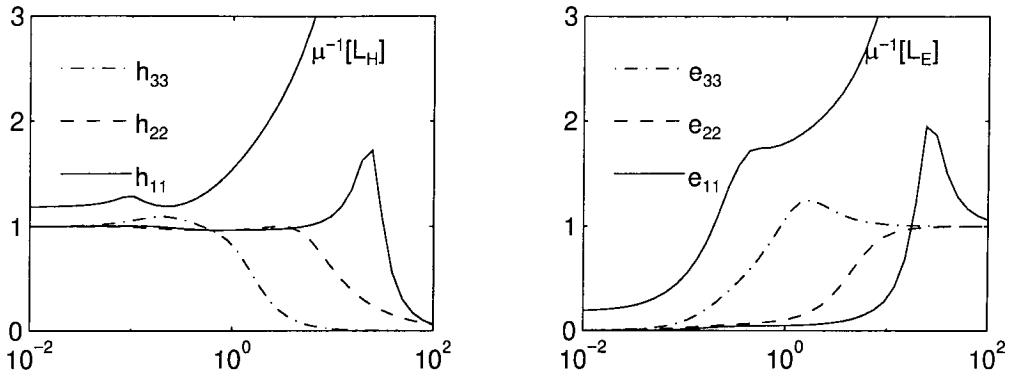

Figure 6.6: Bounds on individual single loop sensitivity ($\tilde{E}_{ii}$) and complementary sensitivity ($\tilde{H}_{ii}$) functions for $C(s) = \text{diag}\{4.06\left[1+\frac{1}{4.68s}\right], 8.73\left[1+\frac{1}{4.73s}\right], -13.97\left[1+\frac{1}{3.35s}\right]\}$. The CCE mode operating point is indicated in Table 6.4.

- $\tilde{H}(s)$ is stable (not shown).
- the bounds on $\bar{\sigma}[\tilde{H}(j\omega)] = \max\{|h_{11}(j\omega)|, |h_{22}(j\omega)|, |h_{33}(j\omega)|\}\forall\omega$ are easily satisfied with the decentralized PI controller.
- the bounds on $\bar{\sigma}[\tilde{E}(j\omega)] = \max\{|e_{11}(j\omega)|, |e_{22}(j\omega)|, |e_{33}(j\omega)|\}\forall\omega$ are easily satisfied with the decentralized PI controller.

The μ-interaction analysis suggests that the interactions in the 3×3 control structure are not significant from a stability viewpoint.

6.6.3 Conclusions: Control Structure Selection

Based on the RGA and μ-interaction analysis in Section 6.6, we can make the following conclusions about the proposed control structures for PC and CCE mode operation:

- For PC mode operation, the most suitable control structure is the 2×2 structure. The manipulated variables are: $[F_{cat}, F_{air}]$ and the controlled variables are: $[T_r, T_{rgn}]$. It was shown in Chapter 5 that the most suitable pairing for performance is the T_r/F_{cat} pairing and the T_{rgn}/F_{air} pairing.
- For CCE mode operation, a 3×3 control structure is proposed. The manipulated variables are: $[F_{cat}, F_{air}, F_{cc}]$ and the controlled variables are: $[T_r, C_{O_2,fg}, T_{rgn}]$.

It was argued on physical grounds that the pairing T_r/F_{cat}, $C_{O_2,fg}/F_{air}$ and T_{rgn}/F_{cc} was the most suitable. Subsequent analysis using the steady–state RGA matrix as well as the μ-interaction measure indicated that:

1. the T_r/F_{cat}, $C_{O_2,fg}/F_{air}$ and T_{rgn}/F_{cc} pairing corresponds to pairing on positive steady–state RGAs (necessary for DIC), and
2. the μ-interaction measure indicates that the plant is essentially decoupled, and the restrictions imposed on the individual loops to guarantee a stable overall system are mild, and easily satisfied by using an appropriately tuned decentralized PI controller.

Decentralized PI controllers will therefore be used for the dynamic analysis of both the catalyst cooler and CO boiler options.

6.7 Sensitivity to Catalyst Cooler Model Parameters

A two parameter dynamic model for the catalyst cooler was developed in Section 6.4.2. The two parameters are:

1. W_{cc} - the catalyst mass in the catalyst cooler
2. UA - the catalyst cooler heat transfer coefficient

While it is clear that W_{cc} and UA cannot be arbitrarily, and independently selected, the actual choices of W_{cc} and UA will affect the closed loop performance of the FCC process as these parameters determine the achievable rate of heat transfer as well as the range of possible heat duties. The relative values of W_{cc} and UA can vary, depending on the catalyst cooler geometry and the degree of catalyst fluidization in the catalyst cooler. It is therefore important to determine how sensitive the closed loop performance is to the actual choices of W_{cc} and UA. One can make general conclusions with a fair degree of certainty if the closed loop response is insensitive

to the actual choice of UA and W_{cc}. As a reference, the physical design of the heat exchanger will be based on the design guidelines provided in Perry and Green (1984). The closed loop performance will be analyzed for a range of W_{cc} and UA values. The reference catalyst cooler geometry will be described next.

6.7.1 Catalyst Cooler Geometry

The following assumptions are made about the physical geometry of the catalyst cooler:

- fluidized catalyst flows in the shell side
- saturated cooling water at 3.0 bar (B.P. $= 272.3°F$) flows in the tube side
- settled catalyst density, $\rho_c = 68lb/ft^3$
- catalyst cooler shell is a cylinder of diameter, $d_s = 15ft$
- internal tubes have diameter, $d_t = 1/3ft$
- distance between center of one tube to center of next tube (as factor of d_t), $2 \leq \alpha \leq 3$
- fluidized catalyst void fraction, $\epsilon_f = 0.55$
- all internal tubes are in a square layout
- from the pipe layout pattern indicated above, the total number of tubes is n^2, where:

$$n = \text{floor}\left\{\frac{\frac{d_s}{\sqrt{2}d_t} - 1}{\alpha} + 1\right\} \tag{6.28}$$

  and floor{x} refers to rounding to the nearest integer towards minus infinity.

- for a given value of W_{cc}, the required length of the catalyst cooler L:

$$L = \frac{\frac{W_{cc}}{\rho_c[1-\epsilon_f]}}{\frac{\pi}{4}\left[{d_s}^2 - n^2 d_t^2\right]} \tag{6.29}$$

- the effective heat transfer area is calculated as A:

$$A = \pi n^2 d_t L \tag{6.30}$$

6.7.2 Closed Loop Sensitivity to Choice of UA

To analyze the closed loop sensitivity of the 3×3 CCE control scheme to the choice of UA, we will proceed as follows:

1. Choose an operating point defined by the set of process parameters $[T_r, T_{rgn}, F_q]$.
2. Choose a value of W_{cc}.
3. Based on the catalyst cooler geometry detailed above, the effective heat transfer area (A) corresponding to the selected W_{cc} is calculated.
4. The allowable range for UA is calculated for the selected value of W_{cc}, using the range of specific heat transfer coefficients given in Equation 6.11.
5. A controller structure is selected, and the controller tuned.
6. A specific value of UA within the range calculated in Step 4 is selected.
7. The closed loop response for the selected value of UA and the designed controller is determined.
8. Other values of UA within the range selected in step 4 are selected, and step 7 is repeated.
9. A different operating point is selected, and the procedure from 6–8 is repeated to investigate sensitivity to choice of operating point.
10. A different controller structure and/or tuning is selected. Steps 5–9 are repeated to analyze sensitivity of results to controller tuning, or controller structure.

A summary of the of such an analysis is plotted in Figure 6.7. With respect to Figure 6.7, note the following:

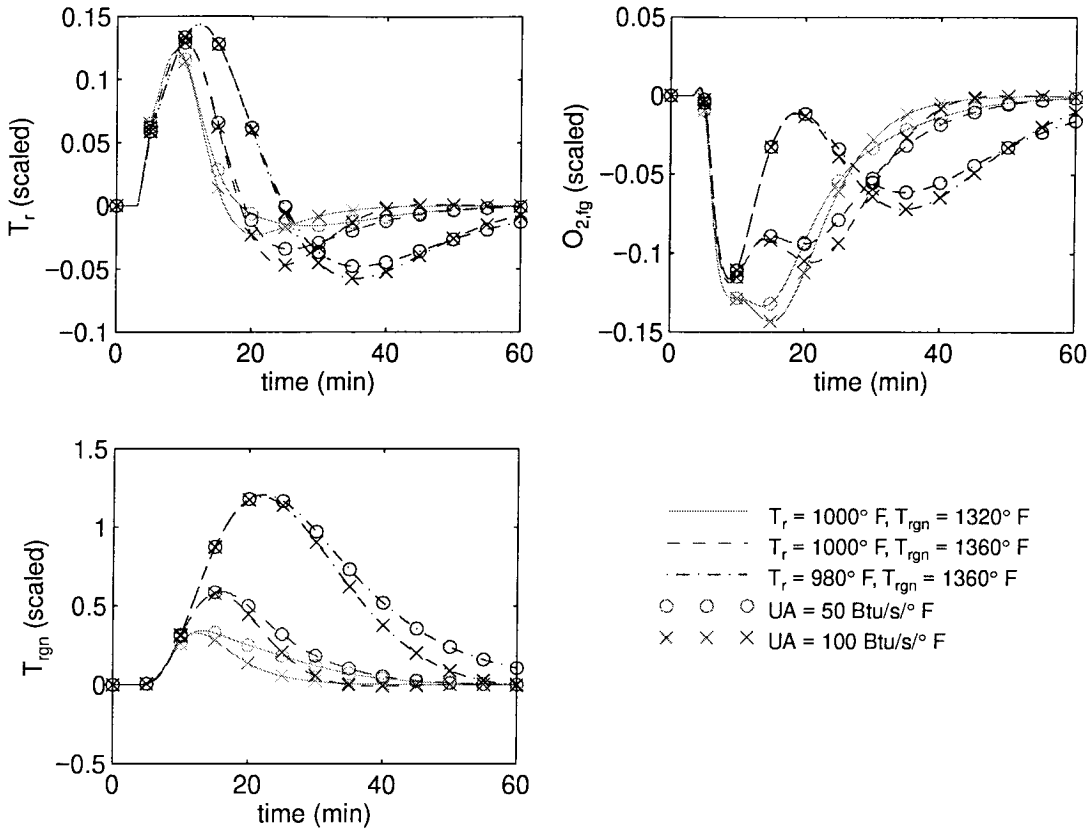

Figure 6.7: Comparison of closed loop response to a rate–limited step in feed quality: $F_q = 1$ for $t \leq 3$; $F_q = 1.25$ for $t \geq 5$. UA takes on two different values. $W_{cc} = 50,000lb$. Diagonal PI controller tuning: T_r/F_{Cat} loop: $2\left[1 + \frac{1}{3s}\right]$, $O_{2,fg}/F_{air}$ loop: $2\left[1 + \frac{1}{3s}\right]$, T_{rgn}/F_{cc} loop: $-10\left[1 + \frac{1}{2s}\right]$.

- W_{cc}=50000lb = constant for all runs.
- three different operating points are considered, denoted by the different line types. These operating points are listed in Figure 6.7.
- the circles on the closed loop response plots indicate the closed loop response for $UA = 50\frac{Btu}{s°F}$. The crosses on the closed loop response plots indicate the closed loop response for $UA = 100\frac{Btu}{s°F}$. If there were absolutely no sensitivity to the choice of UA, then the circles and the crosses would overlap exactly for each operating point. However, there is a slight difference in the responses for $UA = 50\frac{Btu}{s°F}$ and $UA = 100\frac{Btu}{s°F}$.

A different set of tuning parameters for the diagonal PI controllers could be used to determine whether the apparent insensitivity of the closed loop response is dependent on the controller tuning parameters. The closed loop response at the same operating points as in Figure 6.7 for a different set of controller tunings are plotted in Figure 6.8. The interpretation is exactly as for Figure 6.7.

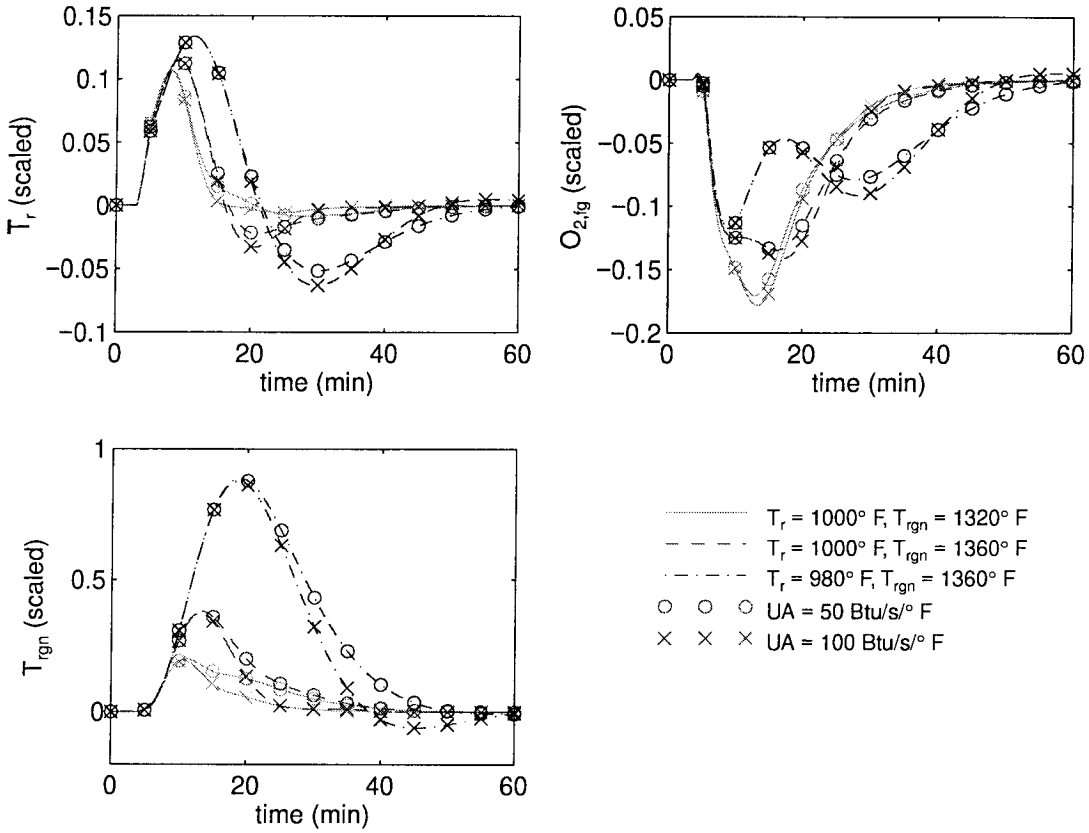

Figure 6.8: Comparison of closed loop response to rate–limited step in feed quality: $3 \leq t$, $F_q = 1$; $t \geq 5$, $F_q = 1.25$. $W_{cc} = 50,000lb$. Diagonal PI controller tuning: T_r/F_{Cat} loop: $2\left[1 + \frac{1}{3s}\right]$, $O_{2,fg}/F_{air}$ loop: $2\left[1 + \frac{1}{3s}\right]$, T_{rgn}/F_{cc} loop: $-15\left[1 + \frac{1}{1.5s}\right]$.

From Figure 6.7 and Figure 6.8 it is evident that the closed loop response of the FCCU with the catalyst cooler installed is *insensitive* to the actual choice of UA. This conclusion is independent of:

- the operating point
- the controller tuning

6.7.3 Closed Loop Sensitivity to Choice of W_{cc}

A similar analysis to that in Section 6.7.2 was carried out to assess the closed loop sensitivity to the choice of W_{cc}. It was found that the closed loop response of the FCCU with the catalyst cooler installed is also *insensitive* to the actual choice of W_{cc}. This conclusion is independent of:

- the operating point
- the controller tuning

An analysis of the poles of the locally linearized model obtained at several different operating points suggests why one should expect low operational sensitivity to the actual choice of reasonable catalyst cooler parameters. A plot of the real parts of the poles at several operating points with a catalyst cooler and with the CO boiler is presented in Figure 6.9. We note that the pole associated with the catalyst cooler is about 10^2 times faster than the slowest process pole - associated with the regenerator dynamics. To obtain Figure 6.9, the following procedure was followed:

1. one operating regime is selected (say PC mode)
2. several operating points defined by $[T_r, T_{rgn}, F_q]$ combinations are selected within the limits indicated in Table 6.1.
3. one operating point is selected from the $[T_r, T_{rgn}, F_q]$ combinations chosen in step 2.
4. at each operating point, the non–linear model is linearized. The eigenvalues of of the Jacobian matrix are determined, and sorted by magnitude. One example is shown in Table 6.7 for the PC (and CCE) operating points indicated in Table 6.4. Note that in most cases analyzed, all the process poles are real. Similar tables are obtained at each of the other operating points considered.
5. step 4 is repeated at each all the other operating points selected in step 2.

PC mode operation	CCE mode operation
-11.9945	-11.9977
-0.6525	-0.9340
-0.5734	-0.4854
-0.2014	-0.3721
–	-0.3538
-0.0519	-0.0394

Table 6.7: Linear system poles for PC mode and CCE mode control schemes. Linearization around operating points indicated in Table 6.4.

6. the largest eigenvalue at each operating point is selected, and the resulting list of largest eigenvalues is sorted. The real part of these largest eigenvalues as a function of the ranking on this sorted list is plotted in Figure 6.9, for comparison.

7. step 6 is repeated for the second largest eigenvalue and so on.

8. the next operating regime is selected (CCE mode) and steps 2–7 repeated. Figure 6.9 shows graphically the final result of this analysis.

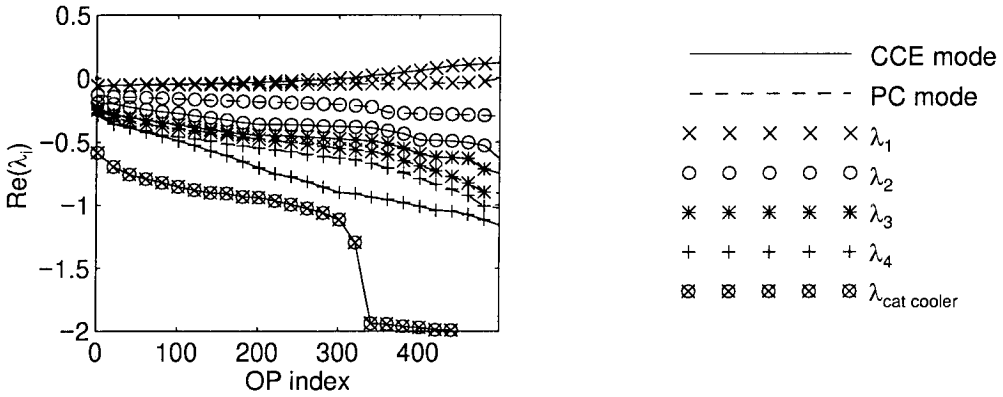

Figure 6.9: Plot of the real part of eigenvalues associated with CCE mode operation and PC mode operation indicating pole associated with the catalyst cooler.

With respect to Figure 6.9, note the following:

- one pole (the fastest in Table 6.7) is not shown. This location of this pole does not change significantly over the entire operating regime considered.

- the introduction of the catalyst cooler does not significantly affect the eigenvalues, and therefore the dynamic characteristics of the FCCU. The sorted eigenvalues for the PC and CCE modes are comparable in magnitude. Take λ_2 for example (symbol "o"): We note that the eigenvalue for the PC mode ("o", dash–line) is close to the corresponding eigenvalue for the CCE mode ("o", solid–line). The same observations hold for λ_1, λ_3, and λ_4.

- there is one eigenvalue for the CCE mode operation that does not have a corresponding counterpart for PC mode operation. This is taken to be the eigenvalue associated with the catalyst cooler.

- the eigenvalue associated with the catalyst cooler is significantly faster ($\simeq 10^2$ times) than the slowest eigenvalue (λ_1) at a given operating point. λ_1 is related to regenerator temperature and coke on catalyst changes. This difference is because:

    1. the catalyst cooler has a significantly smaller catalyst hold–up (50,000 lb) than the regenerator (274,000 lb). Moreover,

    2. the catalyst flow rate to/from the catalyst cooler is typically significantly higher than the catalyst cooler to/from the regenerator (not shown) in CCE mode operation.

  Therefore, the catalyst residence time in the catalyst cooler is significantly lower than the catalyst residence time in the regenerator.

It is found that this large relative difference in the magnitude of eigenvalues associated with regenerator dynamics and the catalyst cooler dynamics is not significantly changed by the choice of reasonable values of the catalyst cooler parameters UA and W_{cc}. Thus, the closed loop response of the overall FCC is relatively insensitive to the actual choice of UA and W_{cc}.

The implication of the closed loop insensitivity to the actual choice of UA or W_{cc}, regardless of the controller tuning or operating point is significant: the conclusions regarding the relative comparison of the catalyst cooler option to the CO boiler option can be expected to be independent of the actual catalyst cooler size (reflected by W_{cc}) or geometry (reflected by UA).

6.7.4 Conclusions: Sensitivity to Model Parameters UA and W_{cc}

The close loop dynamic response of the CCE mode control scheme is insensitive to the choice of reasonable values of W_{cc} and UA. This conclusion is independent of:

- the operating point
- the controller tuning

An analysis of the linearized process poles indicates that the catalyst cooler dynamics are significantly faster than the regenerator dynamics for reasonable choices of UA and W_{cc}, and this relative difference is not significantly affected by physically realistic choices of UA and W_{cc}.

6.8 Dynamic Comparison

For processing higher coking feeds, the catalyst cooler option (CCE mode operation) was shown to have significant advantages at steady–state over the CO boiler (PC mode operation) option:

- the feed conversions are higher,
- the product yield is higher,
- the regenerated catalyst is clean burned regardless of the feed coking quality or the operating point.

Therefore the catalyst cooler option would be the preferred FCC refitting option unless the dynamic analysis of the CCE control scheme suggests that there is some significant inherent characteristic of the 3×3 control scheme that limits performance. The goal of this dynamic analysis therefore includes:

- establishing whether the dynamic performance with the CCE mode control scheme is comparable to the dynamic performance of the PC mode control scheme, and
- investigating whether FCC operational performance with the 3×3 CCE control scheme is excessively sensitive to possible changes in the process operating point.

The control objective is effective disturbance rejection, the primary disturbance being variations in the feed quality (F_q). We will investigate whether for the CCE operating mode:

1. The performance with the designed decentralized PI controllers is excessively sensitive to different sources of process uncertainties. Such high sensitivities are obviously undesirable from an operational viewpoint.
2. Controllers can be designed to satisfy the performance specifications and guarantee stability over the entire operating range indicated in Table 6.10.

For each control scheme a controller is designed and the closed loop characteristics with this controller examined. As discussed in Section 6.6.3, decentralized PI controllers are used. The objective function utilized to quantify the achievable performance is the robust performance μ (μ_{RP}). The optimization problem involves selecting the controller parameters (gains, reset times) to minimize $\max_\omega \mu_{RP}(\omega)$ over some frequency range. This will result in a μ-(sub)optimal PI controller. By μ-(sub)optimal PI controller we mean a 3×3 (2×2 for PC mode operation) decentralized controller consisting of three PI controllers (two for PC mode operation) along the main diagonal, with the tuning parameters selected to minimize $\max_\omega \mu_{RP}(\omega)$ for the interconnection shown in Figure 6.10 over the selected frequency range. The frequency range

of interest is taken to be $10^{-2} - 1$rad/min., which represents process changes on time scales of minutes to hours. The decentralized PI controller is designed to give the best possible performance for the worst combination of uncertainties and disturbances.

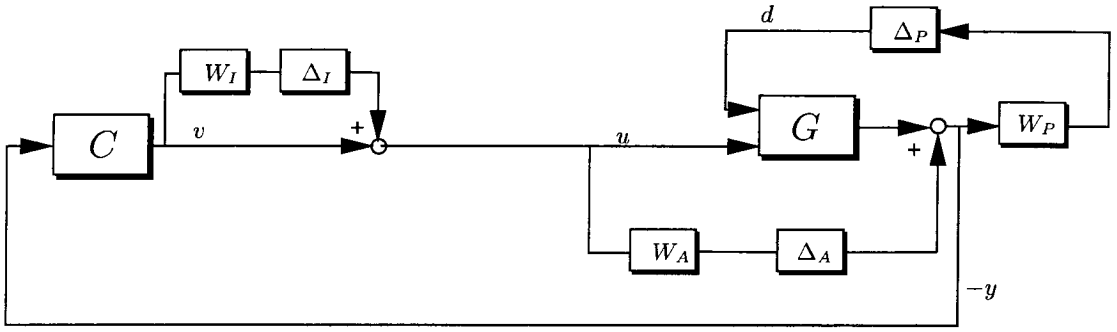

Figure 6.10: Closed loop analysis setup.

6.8.1 Performance Sensitivity to Uncertainties

The objective in this section is to determine whether any comparisons between the CCE and PC mode operation remain (at least qualitatively) unchanged despite different assumptions on the sources and/or magnitudes of the assumed uncertainty description. The *nominal* operating point considered for the dynamic comparison is tabulated in Table 6.4. The analysis is carried out using the linear model obtained by linearizing the full non–linear model around the operating points tabulated in Table 6.4.

Uncertainty specifications

The block diagram used to analyze the sensitivity to uncertainty is shown in Figure 6.10. In Figure 6.10, the blocks Δ_I and Δ_A are used to parameterize the uncertainty. The actual transfer functions they represent are unknown. What is known about Δ_I and Δ_A are:

- the block structures (block–diagonal and full–block respectively)

- they are norm bounded (when appropriately weighted) as in Equation 6.31.

$$\bar{\sigma}(\Delta_{\mathrm{I}}) \leq 1 \qquad\qquad \bar{\sigma}(\Delta_{\mathrm{A}}) \leq 1 \tag{6.31}$$

Transfer functions W_{I} and W_{A} are used to scale Δ_{I} and Δ_{A} respectively so that Equation 6.31 holds. At any frequency, the actual uncertainty level is given by $|W_{\mathrm{I}}|$ and $|W_{\mathrm{A}}|$. The specific transfer functions used for W_{I} and W_{A} are given in Equation 6.32 and Equation 6.33, respectively.

$$\begin{aligned} w_{\mathrm{i}} &= \frac{2s + 0.1629}{s + 1.6285} \\ W_{\mathrm{I}} &= w_{\mathrm{i}} I \end{aligned} \tag{6.32}$$

$$\begin{aligned} w_{\mathrm{a}} &= \frac{1 \times 10^{-4} s + 0.0404}{s + 0.0577} \\ W_{\mathrm{A}} &= w_{\mathrm{a}} I \end{aligned} \tag{6.33}$$

Performance specifications

The control objective for all cases in this Chapter is effective disturbance rejection. The performance requirements are:

1. no steady–state offset for step changes in feed coking quality. *i.e.* integral action required
2. settling time of 20–30 minutes
3. high frequency disturbance amplification by a factor of at most 10/3.

The transfer function for the performance weights is:

$$\begin{aligned} w_{\mathrm{p}} &= 500 \frac{\frac{1}{\omega_p} s + 1}{\frac{500}{0.3\omega_p} s + 1} \\ W_{\mathrm{P}} &= w_{\mathrm{p}} I \end{aligned} \tag{6.34}$$

The performance requirement for each output variable is assumed to be the same. This is justified since the output variables are scaled so that each output error is equally significant. A magnitude/frequency plot for the performance weight is plotted in Figure 6.11. The 'corner frequency' ω_p (Equation 6.34) is used as an adjustable parameter to quantify the performance requirement. Higher ω_p (Figure 6.11) implies faster closed loop response (Lundström et al. 1991).

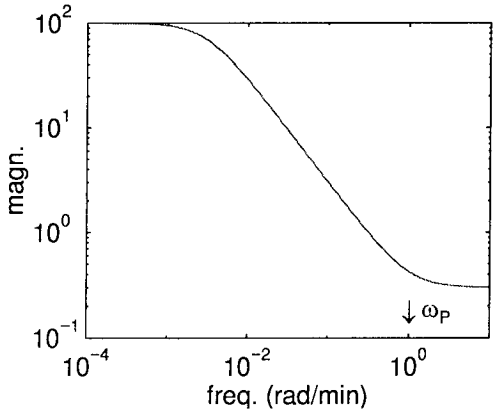

Figure 6.11: Performance weight magnitude plot.

Results

As discussed in Section 6.8, the controllers are designed to minimize $\max_\omega \mu_{RP}(\omega)$ for $10^{-2} \leq \omega \leq 1$rad/min.. The "optimal tuning" for the decentralized PI controller is obtained by a general purpose constrained optimization routine provided in the Optimization Toolbox in MATLAB. In general, there is no guarantee that these values reflect the true optimum, hence the terminology "(sub)optimal" is used. In particular, it is known that for fixed structure controllers, the minimization of the infinity norm of the closed loop transfer function is a non–convex optimization problem with possibly many local minima. However, a large number of optimization runs were carried out for each case reported, starting from a wide range of different initial guesses, and it is unlikely that tunings can be found for which the resulting μ_{RP} values would be significantly lower than the values reported here. It was also found that many

significantly different sets of tuning parameters resulted in comparable robust performance. One set of decentralized PI controller tunings for CCE mode 3×3 control scheme is tabulated in Table 6.8. Also tabulated are the values of the achieved μ^*_{RP}, where:

$$\mu^*_{RP} := \min_{c_1,c_2,c_3} \max_{\omega} \mu_{RP}(\omega) \tag{6.35}$$

CCE Mode Control Structure		
	W_I active	W_A active
K_1	4.06	20.0
τ_1	4.68	1.95
K_2	8.73	20.0
τ_2	4.73	1.00
K_3	-13.97	-20.0
τ_3	3.35	1.0
μ^*_{RP}	1.12	4.36

Table 6.8: Optimal PI controller tunings for CCE mode control structure. Loop 1: T_r/F_{cat}. Loop 2: $C_{O_2,fg}/F_{air}$. Loop 3: T_{rgn}/F_{cc}.

In Table 6.8, note that there are two columns titled 'W_I active' and two titled 'W_A active'. As mentioned in Section 6.8, it is important to analyze the sensitivity of any conclusions to different possible sources of uncertainty. In this case, we investigate whether the presence/absence of additive or multiplicative uncertainty would affect the basic conclusion regarding CCE mode and PC mode sensitivity to different sources of uncertainty. 'W_I active' indicates that the input uncertainty in Figure 6.10 is exactly as in Equation 6.32, while $W_A = 0.001I_3, \forall\omega$. Thus, W_I is the primary (active) source of uncertainty. Similarly, 'W_A active' indicates that the additive uncertainty in Figure 6.10 is exactly as in Equation 6.33, while $W_I = 0.1I_3, \forall\omega$. W_A is therefore the primary (active) source of uncertainty for this case. Note that $W_I = 0.1I_3, \forall\omega$ since any lower weight resulted in unacceptably large control moves (beyond constraint limits). Similarly, one set of decentralized PI controller tunings for PC mode 2×2 schemes to minimize $\max_\omega \mu_{RP}(\omega)$ for $10^{-2} \leq \omega \leq$ 1rad/min. is tabulated in Table 6.9. Also tabulated are the values of the achieved μ^*_{RP}, obviously with the minimization over c_1 and c_2 only (Equation 6.35).

PC Mode Control Structure		
	W_I active	W_A active
K_1	10.14	15.01
τ_1	3.76	3.35
K_2	2.70	19.18
τ_2	3.19	5.02
μ^*_{RP}	1.04	1.00

Table 6.9: Optimal PI controller tunings for PC mode control structure. Loop 1: T_r/F_{cat}. Loop 2: T_{rgn}/F_{cat}.

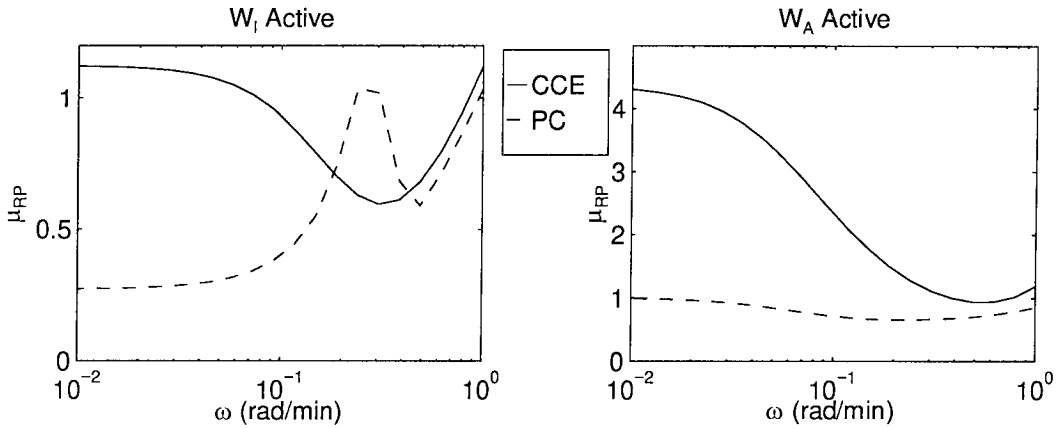

Figure 6.12: μ_{RP} comparison for different types of process uncertainty.

The plot of $\mu_{RP}(\omega)$ is shown in Figure 6.12 for both the 2×2 PC mode schemes as well as the 3×3 CCE mode control scheme. The nominal step response to a step in F_q of $0 \rightarrow 1$ (scaled) is shown in Figure 6.13. From Figure 6.12 and Figure 6.13, note:

- The nominal response of T_r and T_{rgn} to a step change in feed coking quality is acceptable for both PC and CCE modes (scaled deviations less than unity). Moreover, $\mu_{NP}(\omega) < 1$ for both PC and CCE modes (not shown).

- $\mu_{RP} \simeq 1$ for both the PC and CCE mode operation with decentralized PI controllers when W_I is active.

- the step response of F_q from $0 \rightarrow 1$ (scaled) is acceptable for both CCE mode and PC mode. The deviations in controlled variables is less than unity at

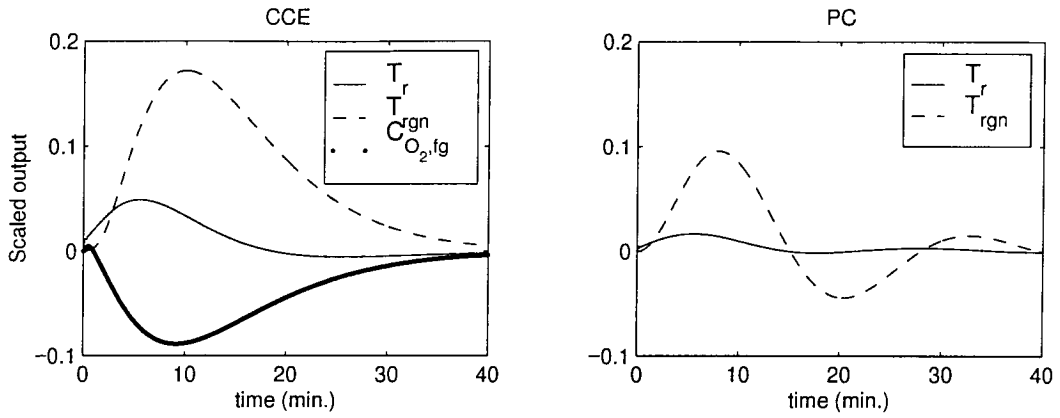

Figure 6.13: Nominal closed loop disturbance step response comparison at the operating points indicated in Table 6.4. Unit step in F_q. W_I active.

all times (Figure 6.13), and the constraints on manipulated variables are not violated (not shown).

- The CCE mode operation appears to be significantly more sensitive to additive uncertainty than the PC mode operation.

Therefore, the performance at a given operating point in either PC or CCE mode operation is acceptable. However, it is still to be investigated whether the same controller can provide acceptable performance over the entire operating regime indicated in Table 6.10. This is determined next.

6.8.2 Performance Sensitivity to Operating Point Changes

The goal in this section is to investigate whether the operational performance changes significantly if the controllers are tuned once and then maintained fixed, but the process operating point changes in the $[T_r, T_{rgn}, F_q]$ space. Such changes are typically initiated by the supervisory and/or overall plant optimization levels of the control hierarchy to maintain optimal operation despite environmental changes. A narrower (and more typical) range of operating points than indicated in Table 6.1 is considered. The range of operating points is defined in terms of the range of desired $[T_r, T_{rgn}, F_q]$

combinations. Table 6.10 defines the range of operating points for both the PC and CCE modes that will be considered for this comparison.

Operating Mode	Limit on					
	T_r (°F)		T_{rgn} (°F)		F_q	
	Low	High	Low	High	Low	High
PC	980	1020	1240	1320	1.0	1.5
CCE	980	1020	1300	1380	1.0	1.5

Table 6.10: Operating point range for dynamic analysis of CCE and PC modes.

With reference to Table 6.10 we note the following:

- The T_r range is identical for both CCE and PC modes. This is reasonable as the rate of feed cracking must proceed at some predetermined level, regardless of the catalyst regeneration mode. This cracking rate is obviously strongly temperature dependent *i.e.* depends on T_r.

- The range for T_{rgn} depends on the actual operating mode, and is typically higher in CCE mode (more severe regeneration conditions) than in PC mode.

- The range of F_q is a design specification, and is therefore the same for both PC and CCE modes.

The analysis of the nominal performance sensitivity to the operating point is based on a set of linear time–invariant (LTI) models derived by linearizing the nonlinear model around selected operating points as follows:

- the desired operating points are given by $[T_r, T_{rgn}, F_q]$ combinations and lie in the 3–dimensional $[T_r, T_{rgn}, F_q]$ space within the bounds indicated in Table 6.10. A sample of operating points in this space of $[T_r, T_{rgn}, F_q]$ values is taken:

  1. T_r values in increments of $10°F$ *i.e.*

     – For CCE, PC modes: $T_r \in \{980, 990, 1000, 1010, 1020\}°F$.

  2. T_{rgn} values in increments of $20°F$ *i.e.*

  - For CCE mode: $T_{rgn} \in \{1300, 1320, 1340, 1360, 1380\}°F$.
  - For PC mode: $T_{rgn} \in \{1240, 1260, 1280, 1300, 1320\}°F$.

3. F_q values in increments of 0.25 *i.e.*
  - For CCE, PC modes: $F_q \in \{1.0, 1.25, 1.5\}$.

- At each $[T_r, T_{rgn}, F_q]$ combination above, the non–linear model corresponding to each operating mode (PC or CCE) is numerically linearized, resulting in an LTI model $G_i(s)$. We define the sets:
  - $\Pi_{CCE} = \{G_i(s), i = 1, 2, \ldots, n_{CCE}\}$, the set of LTI models obtained by linearizing the non–linear FCCU model describing CCE mode operation at all $[T_r, T_{rgn}, F_q]$ combinations indicated above.
  - $\Pi_{PC} = \{G_i(s), i = 1, 2, \ldots, n_{PC}\}$, the set of LTI models obtained by linearizing the non–linear FCCU model describing PC mode operation at all $[T_r, T_{rgn}, F_q]$ combinations indicated above.

The controller tuning parameters indicated in Table 6.8 and Table 6.9 are used for this analysis. Recall that identical performance specifications are used for both modes of operation which is reasonable since the FCC operational requirements are the same whether operating in the PC or the CCE modes. The closed loop response of the linearized plants at selected $[T_r, T_{rgn}, F_q]$ combinations using the controller tunings in Table 6.8 (W_I active) and Table 6.9 (W_I active) is illustrated in Figure 6.14. The values of $\mu_{NP_i} = \bar{\sigma}[(I + G_i(s)C(s))^{-1}W_p]$ for the same $[T_r, T_{rgn}, F_q]$ combinations in the CCE uncertainty set (Π_{CCE}), and in the PC uncertainty set (Π_{PC}) are also illustrated in Figure 6.15. The actual values of $[T_r, T_{rgn}, F_q]$ are not critical for this analysis, and this detail is left out for continuity of presentation. From Figure 6.14 and Figure 6.15 note that:

- each line represents the time response (or μ_{NP}) at a specific operating point.
- there can be a significant degree of variability in the nominal performance of the CCE mode control scheme, depending on the actual operating point. In particular, note that $\mu_{NP}(\omega) > 1$ over some frequency range for several operating

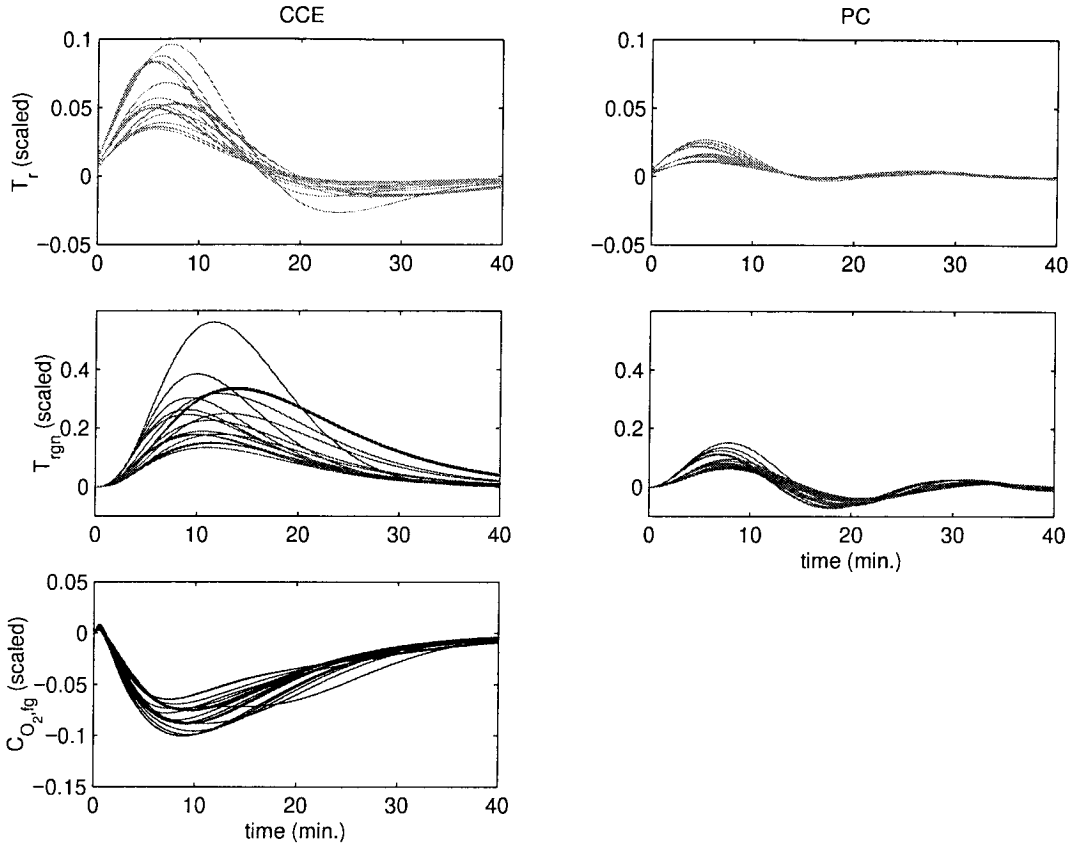

Figure 6.14: Closed loop time response comparison over the operating points indicated in Table 6.10. Step in F_q.

points. However, the closed loop was stable for all $[T_r, T_{rgn}, F_q]$ combinations considered, and also all plants in the sets Π_{CCE} and Π_{PC}.

- the nominal performance in the PC mode is significantly less sensitive to the actual choice of operating point than the CCE mode scheme.

An analysis of the singular value (SV) plots as a function of frequency for the linearized PC and CCE mode control structures at the same operating points selected for the plots in Figure 6.14 and Figure 6.15 suggests the reason for this large variation in the closed loop operational characteristics of the CCE mode operation with the operating point. Figure 6.16 shows this cumulative SVD plot for linearized models for CCE operation and PC operation. $G_{nom}(s)$ is the nominal linear plant obtained by linearizing the non–linear model around the operating points in Table 6.4. With

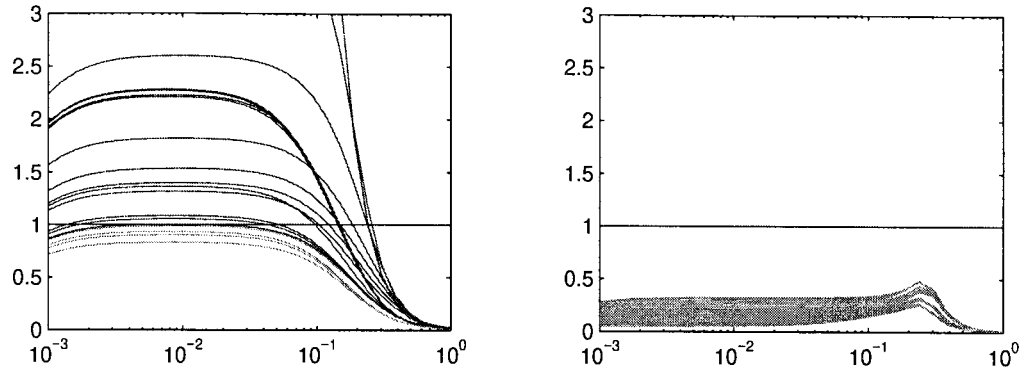

Figure 6.15: Nominal performance analysis over the operating points indicated in Table 6.10. Step in F_q: $1 \rightarrow 1.25$. W_I active.

reference to Figure 6.16, we note the following:

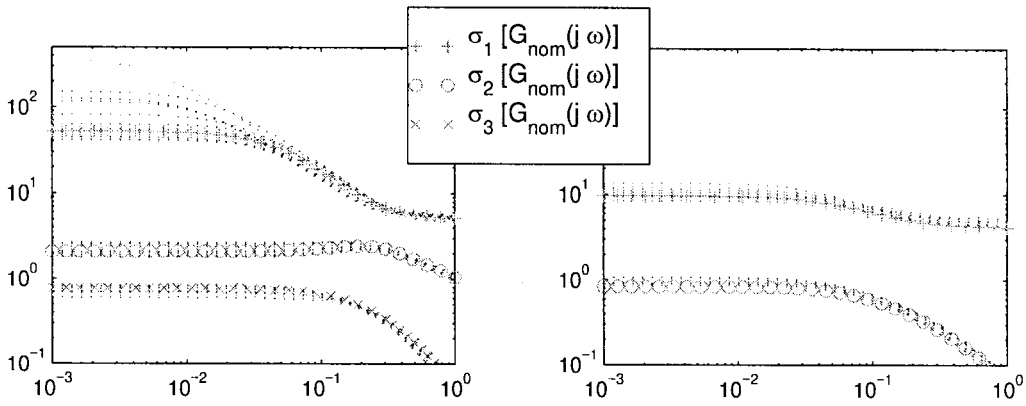

Figure 6.16: Plot of singular values of the linearized 3×3 CCE control scheme and the 2×2 PC control scheme as a function of frequency, over the operating range indicated in Table 6.10.

- for the CCE mode, the largest singular value depend strongly to the actual operating point.
- for the PC mode, the singular values also depend on the operating point, but are significantly less sensitive to the actual operating point.

The plant gains in CCE mode operation change significantly over the operating range considered. On the contrary, the plant gains remain essentially constant for PC mode

operation over a comparable operating range. Therefore, a controller designed to provide acceptable performance at one operating point in PC mode can be expected to provide comparable performance over the entire operating range since the plant gains are similar over the entire operating range. This is not the case for the CCE mode operation where the plant gains depend on the actual operating point, and can vary appreciably from one operating point to the other.

6.8.3 Conclusions: Dynamic Comparison

An analysis of the singular values of the 3×3 CCE mode control structure and the PC mode control structure indicates that:

- for the CCE mode 3×3 control structure, the singular values depend strongly to the actual operating point. For example, the maximum singular value changes by a factor of 5–6 over the operating range.
- for the PC mode 2×2 control structure, the singular values also depend on the operating point, but are significantly less sensitive to the actual operating point. For example, the maximum singular value changes by a factor of 1–1.4 over a comparable operating range.

It is shown in Section 6.8.2 that:

- For PC mode operation, a decentralized controller can be tuned for acceptable performance over the entire operating regime considered in Table 6.10.
- For CCE mode operation, a decentralized PI controller tuned for acceptable performance at one operating point can lead to unacceptable performance if the operating point is changed.

Thus, while the relatively simple decentralized PI controller can be tuned for acceptable performance over the entire operating range in Table 6.10 for PC mode operation, a more sophisticated control strategy can be required for CCE mode operation over a comparable operating range if tight control is required. This sensitivity

of the closed loop performance in CCE mode to changes in the operating point is understandable given the large differences in the magnitudes of the singular values of the CCE mode control structure between possible operating points. However, it is shown in Section 6.8.1 that at a specific operating point, the operational performance sensitivity to input uncertainty is comparable for PC mode operation and CCE mode operation. Moreover, the response to step changes in F_q are also acceptable for both PC and CCE mode operations. The CCE mode control structure appears to be significantly more sensitive to additive uncertainty (higher μ^*_{RP}) than the PC mode control scheme.

6.9 Summary and Conclusions

This Chapter addresses the issue of how to achieve greater operational flexibility in the Fluid Catalytic Cracking (FCC) unit, in particular the need to process higher coking feeds. By higher coking feeds, we mean feeds which upon cracking yield and deposit significant amounts of coke on the cracking catalyst particles.

It is quantitatively shown that FCC units operating in the complete combustion (CC) mode cannot process high coking feeds. This is undesirable (poor flexibility) since the current refinery economics often requires the processing of higher coking feeds, and the FCC might have to be refitted to satisfy this requirement. A particularly important operational feature of CC mode operation is that the regenerated catalyst is clean burned (essentially all the deposited coke burned off). It is also shown that the most significant constraint limiting this operational flexibility is the upper limit on the regenerator temperature. Two refitting options studied are: (1) the installation of a catalyst cooler in complete combustion mode to extend the operation regime (CCE mode), and (2) the installation of a CO boiler to allow partial combustion operation (PC mode). It is known, and our simulations show that both of these options alleviate the constraint on the regenerator temperature (Upson et al. 1993).

A major objective of this work is to compare both the steady–state and the dynamic characteristics of different possible refitting options that can allow the process-

ing of higher coking feeds.

6.9.1 Comparison of Steady–State Characteristics

The steady–state analysis involved:

- Determining the overall feed conversion over the entire $[T_r, T_{rgn}, F_q]$ operating regime defined in Table 6.10. Higher feed conversions are favored from an economic viewpoint.

- Determining the yield of two key cracking products from an economic viewpoint: gasoline and wet gas (C_4 and lighter hydrocarbons).

The comparison of the steady–state characteristics of the two refitting options suggests that:

- Installing the catalyst cooler allows the processing of significantly higher coking feeds (max. $F_q = 2.27$) compared to the conventional CC mode operation (without catalyst cooler) (max. $F_q = 1.17$), as expected. More importantly, the maximum F_q processable with the catalyst cooler option (CCE mode) is comparable to the maximum F_q processable with the CO boiler option (PC mode)(max. $F_q = 2.20$).

- For CCE mode operation, the regenerated catalyst is clean burned regardless of:

  - the incoming feed coking quality,
  - riser temperature,
  - regenerator temperature.

  For the PC mode operation, significant amounts of coke can remain on the regenerated catalyst, particularly when high coking feeds are processed. For a given mass of catalyst, there are obviously more active sites available when the catalyst is clean burned, allowing for a greater extent of cracking reaction.

Installing the catalyst cooler (CCE mode operation) therefore has a distinct advantage over installing the CO boiler (PC mode operation) when processing high coking feeds: the overall feed conversion and wet gas yield is higher with the catalyst cooler option than the CO boiler option. The gasoline yield is also found to be higher in most cases with the catalyst cooler option. The exception occurs at high T_r and low T_{rgn}:

1. In CCE mode operation, three factors contribute to the significant additional cracking of gasoline to wet gas under these conditions: (a) high T_r $\Rightarrow$ high reaction rate, (b) high T_r and low T_{rgn} $\Rightarrow$ high catalyst/oil ratio at steady–state $\Rightarrow$ relatively large number of active sites, (c) catalyst clean burned $\Rightarrow$ large fraction of active sites actually available for cracking. Thus, the yield of gasoline is lower, but the wet-gas yield is consequently proportionately higher.
2. In the PC mode operation, conditions (a) and (b) above also hold, but because of the significant amount of coke on catalyst a larger fraction of the active sites are unavailable for cracking reactions. Therefore, the additional cracking of gasoline can only proceed to a much smaller extent.

- It is also found that no particular ranking between PC and CCE mode operation is apparent if only low coking feeds (low F_q) are processed. This is due to the fact that for low coking feeds the regenerated catalyst is clean burned in both CCE mode and PC operating modes. However, a wide range of feed qualities are generally processed during normal FCC operation, and there is no guarantee that only low coking feeds will be processed.

Note that similar conclusions were made by Arbel et al. (1997) through more physically based arguments. Therefore the catalyst cooler option would be the preferred FCC refitting option from a steady–state viewpoint for processing higher coking feeds.

The comparison of the dynamic characteristics of the catalyst cooler and CO boiler options will therefore focus on determining the relative 'quality' of operation in each

mode, with particular emphasis on investigating any limitations to the achievable performance.

6.9.2 Comparison of Dynamic Characteristics

The dynamic analysis involved:

- Postulating and analyzing suitable control structures for both PC and CCE mode operation
- Establishing whether the CCE mode control scheme can perform comparably to the PC mode control schemes, and
- Investigating whether FCC operational performance is excessively sensitive to possible changes in the process operating point in either the PC or the CCE operating modes.

A 3×3 control structure originally proposed by Arbel et al. (1997) for regulatory control in the CCE mode operation and a 2×2 control structure which was shown to provide satisfactory performance for PC mode operation (Huq and Morari 1997a, Arbel et al. 1996) are analyzed. Some pertinent dynamic characteristics of the catalyst cooler and the CO boiler options are summarized below:

1. For CCE mode operation the manipulated variables are: $[F_{cat}, F_{air}, F_{cc}]$ and the controlled variables are: $[T_r, C_{O_2,fg}, T_{rgn}]$. It is argued on physical grounds that the pairing T_r/F_{cat}, $C_{O_2,fg}/F_{air}$ and T_{rgn}/F_{cc} is the most appropriate. Subsequent analysis using the steady–state relative gain array (RGA) matrix as well as the μ-interaction measure indicated that:
   (a) The T_r/F_{cat}, $C_{O_2,fg}/F_{air}$ and T_{rgn}/F_{cc} pairing corresponds to pairing on positive steady–state RGAs (necessary for *decentralized integral controllability* (Morari and Zafiriou 1989)), and
   (b) The μ-interaction measure indicates that this 3×3 control structure is essentially decoupled, and the restrictions imposed on the individual loops

to guarantee a stable overall system are mild, and can be easily satisfied for example with an appropriately tuned decentralized PI controller.

(c) The singular values of the 3×3 control structure depend strongly on the actual operating point. For example, the maximum singular value changes by a factor of 5–6 over the operating range.

2. For PC mode operation, the manipulated variables are: $[F_{cat}, F_{air}]$ and the controlled variables are: $[T_r, T_{rgn}]$. This control structure was found to be the most suitable for PC mode operation (Huq and Morari 1997a).

   (a) The T_r/F_{cat}, T_{rgn}/F_{air} pairing corresponds to pairing on negative steady–state RGAs, which is undesirable. In particular, if the T_{rgn}/F_{air} loops fails or is put on manual, the T_r/F_{cat} will be unstable, unless the sign of the PI controller gain is also changed. Such failures are reported to be uncommon (Arbel et al. 1996), and barring such failures, it was shown in Huq and Morari (1997b) that this pairing is the most suitable from a performance viewpoint.

   (b) It is also shown in (Huq and Morari 1997b) that acceptable operation over the operating range defined in Table 6.10 can be achieved with an appropriately tuned decentralized PI controller for this pairing. Moreover, a wide range of tuning parameters provided satisfactory performance over this operating range.

   (c) The singular values of the 2×2 control structure also depend on the operating point, but are significantly less sensitive to the actual operating point. For example, the maximum singular value changes by a factor of 1–1.4 over the comparable operating range.

It is shown that at a specific operating point, the operational performance sensitivity to input uncertainty (always present in practice) is comparable for PC mode operation and CCE mode operation. Moreover, the response to step changes in F_q are also acceptable for both CCE and PC mode operations. However, if operation over a

wider range of regenerator and riser temperatures is required, it is found that:

1. For CCE mode operation with a catalyst cooler, a decentralized PI controller tuned for acceptable performance at one operating point can lead to unacceptable performance if the operating point is changed. This sensitivity of the closed loop performance in CCE mode to changes in the operating point is understandable given the large differences in the plant singular values between possible operating points. A more sophisticated control strategy might therefore be required for tight control in CCE mode operation over a comparable operating range in Table 6.10.

2. However, for the PC mode operation with a *CO* boiler, decentralized controllers (e.g. decentralized PI controllers) can be tuned for acceptable performance over the entire operating regime considered in Table 6.10.

6.9.3 Design/Operational Implications

In conclusion, from a steady–state viewpoint, it is found that installing the catalyst cooler (CCE mode operation) has a distinct advantage over installing the *CO* boiler (PC mode operation) when processing high coking feeds - because the regenerated catalyst is always clean burned. In particular, the product yields as well as overall conversions are typically higher.

A comparison of dynamic characteristics suggests that:

1. For CCE mode operation, a decentralized PI controller tuned for acceptable performance at one operating point can lead to unacceptable performance if the operating point is changed, and a more sophisticated control strategy might therefore be required if the FCC is to be operated over a wider operating regime.

2. However, for PC mode operation, decentralized PI controllers can be tuned for satisfactory performance over a comparable operation regime.

Thus while the catalyst cooler would be the favored refitting option for processing higher coking feeds, this analysis suggests that a more sophisticated control strategy

than the simple decentralized PI controller can be required for tight control of the process over the normal operating regime.

Chapter 7 Conclusions

Fluid Catalytic Cracking (FCC) units are widely used in the oil refining industry to crack low value hydrocarbons into a range of higher value hydrocarbons including gasoline. Because of its feed processing flexibility, the FCC process is considered a primary conversion unit in an integrated refinery and optimal FCC operation can have a significant impact on the refinery profitability. Because of its important role in the refinery, the FCC process has recently attracted renewed interest both from academia and industry, with the main emphasis on better understanding and operating the process.

In general, several possible alternatives can usually be postulated or envisioned to realize operational improvements, and the critical task is then to rank order these alternatives. Rank ordering the available alternatives requires the utilization of suitable:

1. process models describing each alternative,

2. tools to quantitatively assess the operational performance achievable with each alternative. "Operational performance" here refers to the quality of closed loop process response.

With respect to the requirements (1) and (2) above for ranking the possible alternatives, we note that:

1. *FCC models:* The renewed interest in improved FCC operation is partially reflected by the recent publication in the open literature of two first principles models claiming to describe the essential features of the FCC process (Arbel et al. 1995, McFarlane et al. 1993) .

2. *Tools for operational performance assessment:* The structured singular value (SSV) framework introduced by Doyle (1982) provides a quantitative measure

of the achievable operational performance, explicitly accounts for plant/model mismatch, and also permits the approximate incorporation of many of the practical requirements indicated above into the analysis.

Utilizing the two first principles FCC models and the structured singular value framework, several aspects of the design and control of FCC processes have been addressed in this thesis, with special emphasis on quantitatively ranking possible design/control options from an operational performance improvement viewpoint. The main contributions and findings of this analysis are listed below, and follows the same order as the thesis chapters.

- **The Significance of Control Studies during Process Design**

  Model IV Fluid Catalytic Cracking Units (FCCUs) differ from other cracking units in that model IV FCCUs do not have slide valves in the catalyst circulation lines to enable direct control of catalyst circulation rate through the unit. Reducing fluctuations in catalyst circulation rate is found to significantly improve closed loop performance of the FCCU. Some design and operational modifications that can be made to model IV FCCUs to improve closed loop performance at the regulatory level based on this insight are mathematically modeled and compared. Closed loop performance of a model IV FCCU operated with the weir and standpipe always flooded is examined. The achievable performance is significantly better than that of the standard model IV FCCU. The closed loop performance of the model IV FCCU modified to incorporate slide valves in the catalyst circulation lines is also examined. The performance of the FCCU with slide valves is better than the performance achievable by the FCCU with the weir flooded. It is found that model IV FCCUs are ill-conditioned owing to the use of the weir and standpipe arrangement in the regenerator section. Both the operational and design modifications studied reduce plant ill-conditioning appreciably.

- **Control Structure Selection for Optimal Regulatory Control of the FCC Process**

A quantitative rank ordering of possible control structures for FCC operation in both partial combustion (PC) mode and complete combustion (CC) mode operation is undertaken. 2×2 control structures are considered. Subsequently, a simple 1×1 (SISO) control strategy for CC mode operation is proposed and analyzed.

For PC mode regulation, riser temperature (T_r) and regenerator dense bed temperature (T_{rgn}) - $[T_r, T_{rgn}]$ are the most suitable choice for controlled variables. For CC mode regulation, $[T_r, C_{O_2,fg}]$ are the most suitable choice for controlled variables, where $C_{O_2,fg}$ is the flue gas O_2 molar concentration.

This analysis suggests that two sets of manipulated variables can in fact result in comparable steady–state and dynamic characteristics. These are: $[F_{air}, F_{cat}]$ and $[F_{air}, T_{feed}]$, where F_{air} is the combustion air flow rate, F_{cat} is the catalyst circulation rate, T_{feed} is the fresh feed temperature. The possibility of using T_{feed} has been reported in the past, but the benefits do not appear to have been quantitatively analyzed. We find that the achievable performance with these two manipulated variable options is comparable, regardless of the type of uncertainty weight (input, additive) or structure (diagonal, full block). Thus, for older FCCUs where direct manipulation of F_{cat} is not possible (*e.g.* Exxons Model IV FCCU), the feed temperature T_{feed} could also be an effective manipulated variable for regulatory control in both CC and PC mode operation.

The most suitable control structures for PC and CC mode are in agreement with that recently given in (Arbel et al. 1996), although the ranking is done quantitatively in this work, and with significantly less effort. Furthermore, this analysis shows that while the most suitable control structure reported in (Hovd and Skogestad 1993) for PC mode operation might be adequate if the FCC is operated over a narrow range, it is shown to have undesirable characteristics over a wider operating range. Current FCCs are typically required to operate over a wider range, due to economic and operational reasons.

A simple control strategy for CC mode operation is proposed and analyzed.

The strategy involves: (1) always operating the combustion air compressor at full capacity and (2) using a single loop controller ($K(s) = C(s)\frac{1}{s}$, $C(s)$ stable) with integral action to control T_r using F_{cat}. It is shown that this strategy provides good performance, guarantees that the process will not revert to PC mode operation (ensured using integral action), and can process the same range of feed qualities as the 2×2 control scheme where $[T_r, T_{rgn}]$ are controlled using $[F_{air}, F_{cat}]$.

- **Decentralized Regulatory Control of the FCC Process in Partial Combustion Mode**

  The control of the FCC where riser temperature (T_r) and regenerator temperature (T_{rgn}) are controlled by manipulating catalyst circulation rate (F_{cat}) and combustion air supply rate (F_{air}) or F_{cat} and fresh feed temperature (T_{feed}) is examined. The pairings where T_r is controlled using F_{cat} and T_{rgn} controlled using F_{air} or T_{feed} - the $[T_r/F_{cat}, T_{rgn}/F_{air}]$ pairing, and the $[T_r/F_{cat}, T_{rgn}/T_{feed}]$ pairings respectively are shown to be the preferred choices:

  - the achievable performance is superior to the alternate pairings with decentralized PI controllers, regardless of the source of uncertainty (additive, input multiplicative).
  - the effort required to tune the decentralized PI controller for acceptable performance is shown to be minimal.

  Moreover, it is shown that for these two pairings: (1) The performance degradation when using decentralized PI controllers instead of full μ-optimal controllers is not significant. (2) Decentralized PI controllers can be designed for acceptable performance over a wide operating regime. (3) If it is established that process interactions are significant, performance improvements can be achieved by "tightening" the decentralized PI controller, as the operating bandwidth is then pushed into a region of lower process interactions. (4) Reasonable transitions

to unstable operating points can be effectively handled with an appropriately tuned decentralized PI controller.

A theoretical development that provides insight into possible changes in the sign of the steady–state and infinite frequency RGA elements is also presented. It is found to be related to the non–minimal phase behavior of one or more of (1) the overall plant, (2) the individual loop transfer functions, (3) the remaining system if some loop is removed. Stable plants for which pairing for performance can correspond to negative steady–state RGA pairings are identified

- **Options for Heavier Feed Processing in Fluid Catalytic Cracking Units**

  There is a growing need in the oil refining industry to process higher coking feeds in the available Fluid Catalytic Cracking (FCC) units. However, FCC units operated in the complete combustion mode (CC mode) might not be able to process sufficiently high coking feeds, and design modifications would be necessary to accommodate this greater feed processing flexibility. Two refitting options studied are: (1) catalyst cooler installation to extend CC mode operation (CCE mode) and (2) *CO* boiler installation to allow partial combustion (PC) mode operation. Both of these refitting options alleviate the constraint on regenerator temperature.

  A two parameter model describing the catalyst cooler dynamics is developed for the analysis of CCE mode operation. Because the proper installation of a *CO* boiler downstream from the regenerator flue gas line can be expected to minimally affect the FCC operation, no additional modeling of the *CO* boiler was undertaken. The main objective is to compare the steady–state and dynamic characteristics of these two refitting options.

  From a steady–state viewpoint, the catalyst cooler option is preferred if high coking feeds are to be processed. In particular, the product yields and feed conversions are higher. Moreover, the regenerated catalyst is clean burned regardless of the operating conditions or the incoming feed quality.

A 3×3 control structure for the FCC refitted with a catalyst cooler is examined. The controlled variables are: riser temperature (T_r), regenerator temperature (T_{rgn}) and flue gas oxygen concentration ($C_{O_2,fg}$) - $[T_r, T_{rgn}, C_{O_2,fg}]$. The manipulated variables are catalyst circulation rate between the reactor and regenerator (F_{cat}), catalyst circulation rate to/from the catalyst cooler (F_{cc}), and combustion air supply (F_{air}) - $[F_{cat}, F_{cc}, F_{air}]$. It is argued on physical grounds, and verified through the μ-interaction analysis that the pairing T_r/F_{cat}, $C_{O_2,fg}/F_{air}$, and T_{rgn}/F_{cc} is essentially decoupled. A 2×2 control structure for PC mode operation is analyzed: the controlled variables are: $[T_r, T_{rgn}]$, and the manipulated variables are: $[F_{cat}, F_{air}]$.

It is found that while a simple decentralized control strategy suffices for satisfactory performance over a wide operating regime in PC mode, a more sophisticated control strategy might be required to achieve tight control over a comparable operating range in CCE mode with the catalyst cooler. However, at a specific operating point, the performance of the PC mode and CCE mode operation can be made comparable by appropriately tuning for example decentralized PI controllers.

Appendix A Addendum to Chapter 3

A.1 Comparison of MATLAB and ACSL Steady–State Data

Independent Variables

State	MATLAB	ACSL	% difference
	$\times 10^{-2}$	$\times 10^{-2}$	
V_{11}	0.00939364940828	0.00970254004002	0.03288292103629
V_{14}	0.00612259309432	0.00617031991482	0.00779519719143
V_{lift}	0.00486081589472	0.00482459008694	0.00745261877210
V_6	0.01000000000000	0.01000000000000	0
F_4	0.05250000000000	0.05250000000000	0
F_5	0.34000000000000	0.34000000000000	0
T_{atm}	0.75000000000000	0.75000000000000	0
ψ_F	0.01000000000000	0.01000000000000	0
T_1	4.60900000000000	4.60900000000000	0

States

	Operating Point		
State	MATLAB	ACSL	% difference
	$\times 10^{-5}$	$\times 10^{-5}$	
T_2	0.00667261066346	0.00667261071841	0.00000000000824
T_3	0.01607550125579	0.01607550120672	0.00000000000305
T_r	0.00995291978294	0.00996499875069	0.00000121361048
C_{sc}	0.00000007824608	0.00000007836361	0.00000150202855
W_r	1.01306273891282	1.02103990275065	0.00000787430386
P_5	0.00023602079389	0.00023517401725	0.00000358772049
P_7	0.00022685743920	0.00022783820709	0.00000432327851
T_{reg}	0.01272060331147	0.01273536874135	0.00000116074918
C_{rgc}	0.00000000853735	0.00000000863013	0.00001086708846
W_{reg}	2.73753960398639	2.72909273274740	0.00000308557042
W_{sp}	0.03577273263140	0.03656797875722	0.00002223051099
P_6	0.00029728295960	0.00029642538299	0.00000288471499
n	0.00245444003316	0.00245693488439	0.00000101646453
ρ_l	0.00003139497567	0.00003150265632	0.00000342986887
P_2	0.00035250215774	0.00035182127873	0.00000193155982
P_3	0.00041185801980	0.00041136288027	0.00000120220928

Variable	Units	Model A	Model B	Model C	Scale Factor
V_{11}	%	93.94	93.94	89.6	10
V_{14}	%	61.23	65.0	61.23	14
V_{lift}	%	48.61	56.0	60.0	60
V_6	%	100.0	95.0	100.0	–
E_{lift}	ft	134.0	134.0	98.0	–
h_{lift}	ft	34.0	34.0	70.0	–
E_{oil}	ft	124.5	124.5	118.0	–
F_3	lb/s	130.0	130.0	126.0	1.8
T_2	$°F$	661.0	661.0	661.0	50
$X_{sv,rgc}$	%	N/A	N/A	50.0	25
$X_{sv,rgc}$	%	N/A	N/A	50.0	25

Table A.1: Steady–state operating points (independent variables)

Outputs

State	MATLAB	ACSL	% difference
	$\times 10^{-2}$	$\times 10^{-2}$	
T_r	9.95291978293919	9.96499875068664	0.00121361047922
P_4	0.33102079388956	0.33017401695251	0.00255807777843
ΔP_{rr}	-0.03373783428858	-0.03374863396088	-0.00032010567759
F_t	0.75714829725553	0.76087023178736	0.00491572726944
$C_{O_2,sg}$	0.01531182334267	0.01460200550035	0.04635749945893
$C_{CO,sg}$	0.56019052029859	0.75215137163798	0.34267065290050

A.2 Steady–State Operating Points

A.2.1 Independent Variables

The nominal values of the independent variables for Models A, B and C are tabulated in Table A.1.

Variable	Units	Model A	Model B	Model C	Scale Factor
T_{atm}	° F	75	75	75	25
ψ_F	–	1	1	1	0.025
ΔP_{frac}	psia	9.5	9.5	9.5	0.5

Table A.2: Steady–state operating points (disturbances)

Variable	Units	Model A	Model B	Model C	Scale Factor
T_r	° F	991.5	993.4	990.8	1
T_{reg}	° F	1275.2	1274.6	1265.9	10
$C_{O_2,sg}$	mol%	1.395	2.11	1.99	0.15
F_{rgc}	lb/s	750.4	768.2	739.2	–

Table A.3: Steady–state operating points (output variables)

A.2.2 Disturbances

The nominal values of the process disturbances for Models A, B and C are tabulated in Table A.2.

A.2.3 Output Variables

The nominal values of the output variables for Models A, B and C are tabulated in Table A.3.

A.2.4 Comparison of Linear & Non-linear Models, Model A

The agreement between the linear and nonlinear models is good within the time scales of interest (minutes to hours) as Figure A.1 shows.

For model A there are significant differences between the linear and nonlinear models at steady–state as Figure A.2 shows.

A.2.5 Comparison of Linear & Non-linear Models, Model B

There is no discernible difference between the linear and nonlinear models for model B within the resolution of the plot (Figure A.3).

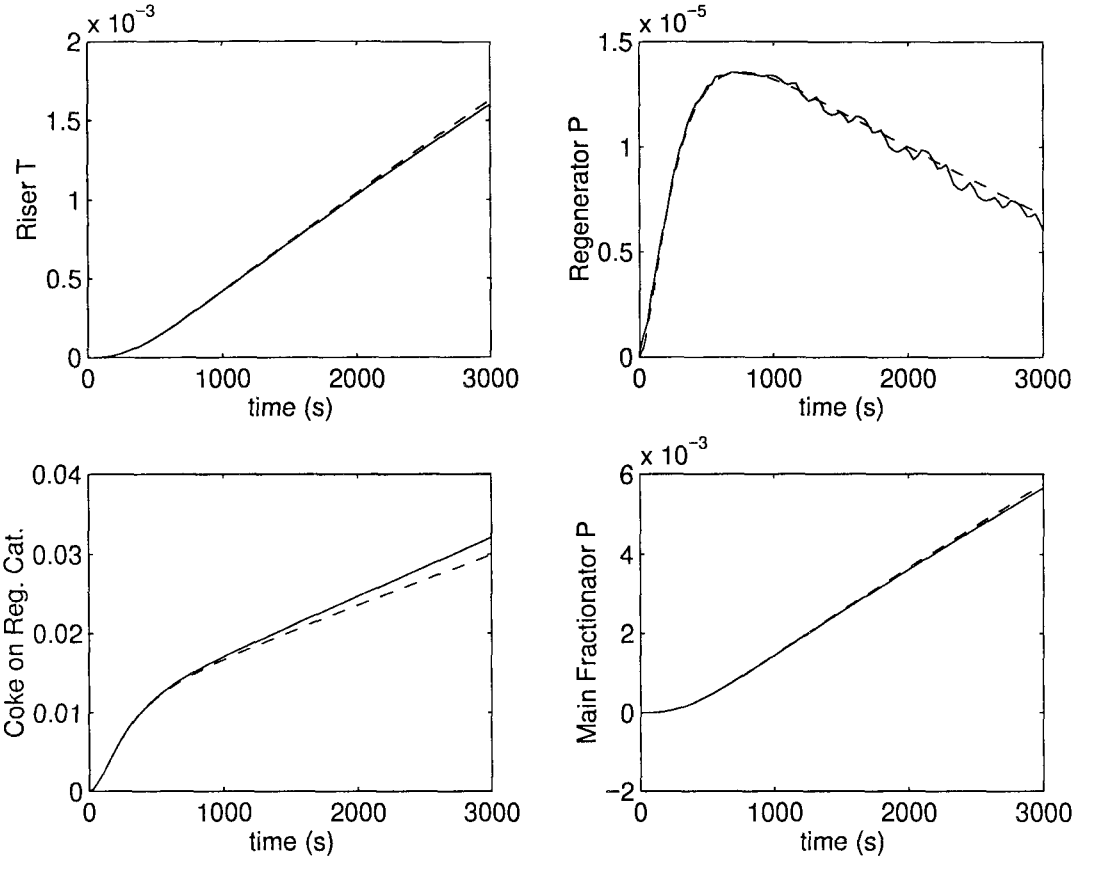

Figure A.1: Open loop step response of linear & non-linear models to 0.2 (scaled) step in ψ_f, Model A. Non-linear model (solid), linear model (dashed)

A.3 Linear State Space Models for Selected Control Schemes

State space realizations for selected control schemes are given below. Note that the matrices are written as follows:

$$A = A_p = A_d; \quad B = [B_p \;\; B_d]; \quad C = C_p = C_d; \quad D = [D_p \;\; D_d] \tag{A.1}$$

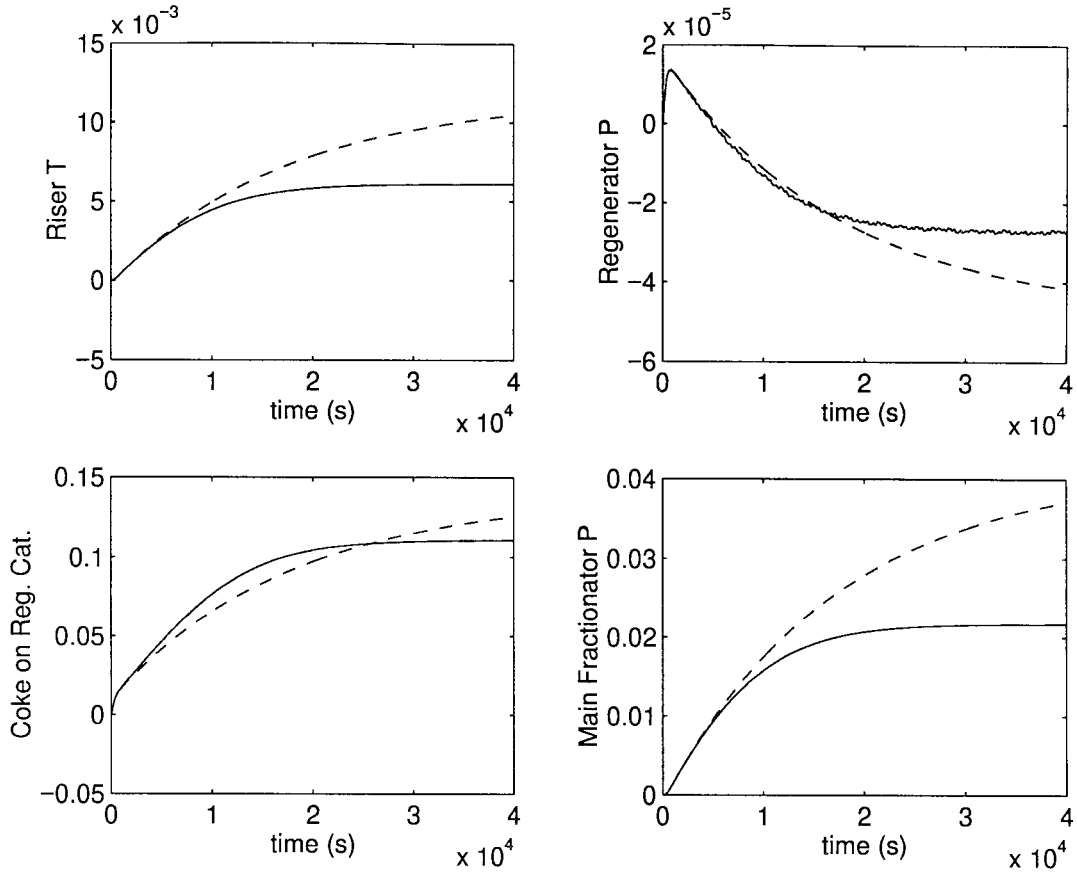

Figure A.2: Open loop step response of linear & non-linear models to 0.2 (scaled) step in ψ_F, Model A. Non-linear model (solid), linear model (dashed)

where subscript p refers to the plant matrices and subscript d refers to the disturbance matrices. The linear time invariant model of the system is given by:

$$\dot{x} = Ax + [B_p \;\; B_d] \begin{bmatrix} u \\ d \end{bmatrix} \tag{A.2}$$

$$y = Cx + [D_p \;\; D_d] \begin{bmatrix} u \\ d \end{bmatrix} \tag{A.3}$$

where:

u = vector of manipulated variables

y = vector of output variables

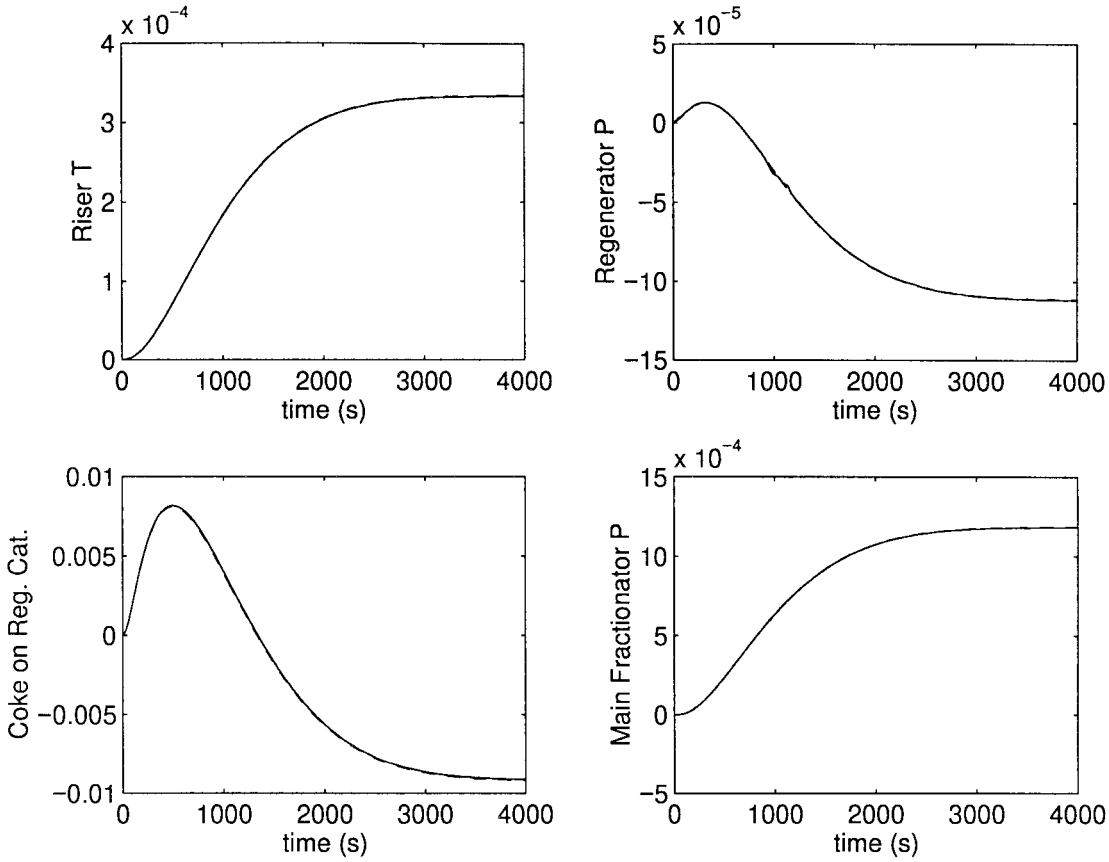

Figure A.3: Open loop step response of linear & non-linear models to 0.2 (scaled) step in ψ_f, Model B. Non-linear model (solid), linear model (dashed)

d = vector of disturbances

x = vector of system states

The plant transfer function matrix is given by:

$$G(s) = C(sI - A)^{-1}B_p + D_p \tag{A.4}$$

and the disturbance transfer function matrix is given by:

$$G_d(s) = C(sI - A)^{-1}B_d + D_d \tag{A.5}$$

The input and output vectors are specified individually for each model. The disturbances are always the same, namely $d^T = [d_1 \;\; d_2 \;\; d_3]$.

The states do not have an obvious physical interpretation as the model dimension was reduced after linearization. The original linear system was balanced and the Hankel singular values examined to determine truncation order. The balanced system was then truncated, yielding the reduced order linear model. This procedure is described by (Balas et al. 1991).

A.3.1 Model A, SII

$$u^T = [V_{14} \;\; V_{lift}], \qquad y^T = [C_{O_2,sg} \;\; T_r] \tag{A.6}$$

$$\mathrm{A} = \begin{bmatrix}
-0.0001 & -0.0004 & -0.0003 & 0.0007 & -0.0002 & 0.0002 & -0.0005 & 0.0009 \\
-0.0007 & -0.0269 & -0.0236 & 0.0872 & -0.0080 & -0.0140 & -0.0167 & -0.0134 \\
0.0003 & 0.0376 & -0.0076 & -0.0136 & -0.0079 & 0.0210 & -0.0244 & 0.0612 \\
-0.0009 & -0.0877 & 0.0457 & -0.0930 & 0.0334 & 0.0294 & 0.0913 & -0.0465 \\
0.0001 & 0.0081 & -0.0037 & 0.0017 & -0.0202 & 0.0214 & -0.0949 & 0.1519 \\
-0.0004 & -0.0327 & 0.0207 & -0.0938 & 0.0685 & -0.2335 & 0.3998 & -0.9782 \\
-0.0002 & -0.0050 & 0.0050 & -0.0547 & -0.0380 & -0.1174 & -0.3890 & 0.6133 \\
-0.0001 & -0.0237 & 0.0140 & -0.0059 & 0.1768 & -0.2759 & 1.2183 & -2.8816
\end{bmatrix}$$

$$B_p = \begin{bmatrix}
0.2499 & -0.0210 \\
1.3762 & 0.1207 \\
-0.5825 & -0.0554 \\
1.4988 & -0.2019 \\
-0.1563 & -0.2848 \\
0.8178 & 0.4819 \\
0.2352 & -0.9369 \\
0.4094 & 2.2000
\end{bmatrix} \qquad B_d = \begin{bmatrix}
0.0106 & 0.0188 & 0.0281 \\
-0.0346 & 0.0004 & -0.0436 \\
0.0193 & 0.0089 & 0.0167 \\
0.0643 & 0.0027 & 0.1882 \\
0.1052 & -0.0192 & 0.1613 \\
-0.1461 & 0.0015 & -0.0248 \\
0.3442 & 0.0245 & -0.0197 \\
-0.8543 & 0.0162 & 0.0284
\end{bmatrix}$$

$$\mathrm{C} = \begin{bmatrix}
-0.1618 & 0.2508 & -0.5771 & 0.1987 & -0.2902 & 0.9296 & -0.8348 & 2.3944 \\
0.1948 & 1.3596 & 0.1001 & -1.5123 & 0.2424 & 0.2427 & 0.5964 & -0.0740
\end{bmatrix}$$

$$D_p = \begin{bmatrix} 1.8199 & 0 \\ 0 & 0 \end{bmatrix} \qquad D_d = \begin{bmatrix} 0 & 0 & -0.1216 \\ 0 & 0 & 0 \end{bmatrix}$$

A.3.2 Model B, SII

$$u^T = [V_{14} \;\; V_{lift}], \qquad y^T = [C_{O_2,sg} \;\; T_r] \tag{A.7}$$

$$\mathrm{A} = \begin{bmatrix} -0.0035 & 0.0092 & -0.0032 & 0.0123 & -0.0465 & 0.0292 & -0.0055 & 0.0002 \\ 0.0129 & -0.0492 & -0.0040 & 0.0318 & 0.1659 & -0.1372 & 0.0170 & -0.0062 \\ -0.0032 & 0.0275 & -0.0038 & 0.0146 & -0.0796 & 0.0504 & -0.0099 & 0.0001 \\ 0.0192 & -0.1224 & 0.0308 & -0.2208 & 0.6949 & -0.3665 & 0.1113 & 0.0195 \\ -0.0114 & 0.0138 & -0.0154 & 0.3274 & -2.2601 & 1.4896 & -0.4788 & -0.0259 \\ -0.0030 & 0.0485 & -0.0069 & -0.0675 & 1.1214 & -0.8382 & 0.2524 & -0.0106 \\ 0.0017 & -0.0124 & 0.0029 & -0.0099 & -0.2406 & 0.2245 & -0.1109 & -0.0155 \\ -0.0009 & 0.0038 & -0.0018 & 0.0251 & -0.1379 & 0.0792 & -0.0249 & -0.0202 \end{bmatrix}$$

$$B_p = \begin{bmatrix} -0.3246 & -0.0047 \\ 0.7858 & -0.0867 \\ -0.2083 & -0.0187 \\ 1.0241 & 0.4649 \\ -0.6821 & -2.0687 \\ -0.0708 & 1.1937 \\ 0.0913 & -0.1700 \\ -0.0426 & -0.0538 \end{bmatrix} \qquad B_d = \begin{bmatrix} 0.0050 & 0.0286 & -0.0303 \\ 0.0375 & 0.0039 & 0.1917 \\ 0.0122 & 0.0026 & -0.0034 \\ -0.2096 & 0.0113 & -0.1478 \\ 1.0602 & 0.0085 & 0.0453 \\ -0.6677 & 0.0153 & 0.0571 \\ 0.2095 & 0.0161 & -0.0943 \\ 0.0399 & 0.0102 & 0.0121 \end{bmatrix}$$

$$\mathrm{C} = \begin{bmatrix} -0.3028 & 0.4836 & -0.2019 & 1.0281 & -2.4224 & 1.3256 & -0.2960 & -0.0213 \\ 0.1241 & -0.6553 & 0.0563 & 0.5233 & -0.0554 & -0.3493 & -0.0516 & -0.0781 \end{bmatrix}$$

$$D_p = \begin{bmatrix} 1.5331 & 0 \\ 0 & 0 \end{bmatrix} \qquad D_d = \begin{bmatrix} 0 & 0 & -0.1337 \\ 0 & 0 & 0 \end{bmatrix}$$

A.3.3 Model C, SII

$$u^T = [V_{14} \;\; V_{lift}], \qquad y^T = [C_{O_2,sg} \;\; T_r] \tag{A.8}$$

$$\mathrm{A} = \begin{bmatrix} -0.0080 & 0.0430 & -0.0016 & 0.0285 & -0.0994 & 0.0109 & -0.0025 \\ 0.0401 & -0.2928 & 0.0211 & -0.2419 & 0.9900 & -0.1192 & 0.0256 \\ -0.0009 & -0.0015 & -0.0004 & 0.0108 & -0.0362 & 0.0041 & -0.0009 \\ 0.0191 & -0.2015 & 0.0055 & -0.3034 & 0.8857 & -0.0878 & 0.0189 \\ -0.0087 & 0.1342 & -0.0111 & 0.7297 & -2.9679 & 0.4821 & -0.1727 \\ -0.0076 & 0.0696 & -0.0013 & 0.0011 & 0.1511 & -0.0624 & 0.0428 \\ 0.0008 & -0.0131 & 0.0006 & -0.0324 & 0.1602 & -0.0247 & -0.0133 \end{bmatrix}$$

$$B_p = \begin{bmatrix} 0.4087 & 0.0379 \\ -1.3925 & -0.4805 \\ 0.0355 & 0.0268 \\ -0.5353 & -0.7414 \\ 0.2471 & 2.4259 \\ 0.2013 & -0.1932 \\ -0.0107 & -0.0630 \end{bmatrix} \qquad B_d = \begin{bmatrix} -0.0147 & -0.0353 & 0.0065 \\ 0.1365 & -0.0126 & -0.0224 \\ -0.0033 & 0.0087 & 0.0215 \\ 0.2538 & -0.0060 & 0.2186 \\ -0.9284 & -0.0054 & 0.0437 \\ 0.1317 & -0.0043 & -0.0161 \\ -0.0217 & 0.0528 & -0.0059 \end{bmatrix}$$

$$\mathrm{C} = \begin{bmatrix} 0.4094 & -1.4734 & 0.0503 & -0.8679 & 2.6079 & -0.2498 & 0.0566 \\ -0.0484 & 0.1346 & 0.0010 & -0.4417 & -0.0944 & 0.1819 & -0.0647 \end{bmatrix}$$

$$D_p = \begin{bmatrix} 1.1564 & 0 \\ 0 & 0 \end{bmatrix} \qquad D_d = \begin{bmatrix} 0 & 0 & -0.0748 \\ 0 & 0 & 0 \end{bmatrix}$$

A.3.4 Model C, SIV

$$u^T = [V_{lift} \;\; X_{sv,rgc}], \qquad y^T = [C_{O_2,sg} \;\; T_r] \tag{A.9}$$

$$\mathrm{A} = \begin{bmatrix} -0.0037 & -0.0052 & -0.0005 & 0.0486 & 0.0032 & -0.0028 & 0.0004 \\ -0.0214 & -0.0851 & 0.0065 & -0.0513 & 0.0165 & -0.0179 & 0.0321 \\ -0.0006 & -0.0101 & -0.0002 & 0.0251 & 0.0011 & -0.0006 & -0.0007 \\ -0.0028 & -0.0437 & -0.0053 & -3.5030 & -0.7640 & 0.5424 & 0.5007 \\ -0.0021 & -0.0162 & -0.0011 & 0.6300 & -0.0073 & 0.0543 & 0.0050 \\ 0.0001 & 0.0014 & -0.0002 & -0.5614 & -0.0483 & -0.0085 & 0.0287 \\ -0.0046 & -0.0360 & -0.0013 & -0.2978 & -0.0119 & -0.0257 & -0.0355 \end{bmatrix}$$

$$B_p = \begin{bmatrix} 0.0061 & -0.3041 \\ -0.1058 & -0.9887 \\ 0.0013 & -0.0337 \\ -2.6860 & -0.0022 \\ -0.0003 & -0.0839 \\ -0.0846 & -0.0082 \\ -0.0410 & -0.1885 \end{bmatrix} \qquad B_d = \begin{bmatrix} -0.0057 & -0.0328 & 0.0122 \\ 0.0303 & 0.0054 & 0.1082 \\ -0.0034 & -0.0041 & -0.0129 \\ 0.9951 & -0.0019 & 0.0072 \\ 0.0600 & 0.0166 & -0.0650 \\ -0.0453 & 0.0041 & -0.0745 \\ -0.0647 & -0.0091 & 0.0365 \end{bmatrix}$$

$$C = \begin{bmatrix} 0.2108 & -0.1366 & 0.0352 & -2.8641 & -0.0814 & 0.0484 & 0.1439 \\ -0.2221 & -0.9913 & -0.0097 & 0.0385 & 0.0923 & -0.1118 & 0.1487 \end{bmatrix}$$

$$D_p = \begin{bmatrix} 0 & 0 \\ 0 & 0 \end{bmatrix} \qquad D_d = \begin{bmatrix} 0 & 0 & -0.0748 \\ 0 & 0 & 0 \end{bmatrix}$$

A.4 Implementation of Design & Operational Changes

A.4.1 Incorporating Modifications to Operate with Weir Flooded

Regenerated catalyst flow rate is given by:

$$F_{rgc} = \Delta P_{rgc} \left[\frac{{A_{rgc}}^2 \rho_c}{L_{rgc} \cdot f_{rgc}} \right] \tag{A.10}$$

The pressure drop across the regenerated catalyst line is given by:

$$\Delta P_{rgc} = 144(P_6 - P_{rb}) + \rho_c(z_{bed} + h_{sp} - z_{sp}) + (E_{tap} - E_{oil})\rho_c - \Delta P_{cons} \tag{A.11}$$

The pressure drop across the constriction is given by:

$$\Delta P_{cons} = \frac{31.1 \times 10^{-3}}{2} \frac{N_{rgc}}{{A_{rgc}}^2 \rho_c} {F_{rgc}}^2 \tag{A.12}$$

Furthermore, the pressure at the reactor bottom (P_{rb}) is given by:

$$P_{rb} = P_4 + \frac{\rho_{ris} \cdot h_{ris}}{144} \tag{A.13}$$

$$\rho_{ris} = \frac{F_3 + F_4 + F_{rgc}}{\frac{F_3+F_4}{\rho_v} + \frac{F_{rgc}}{\rho_{part}}} \tag{A.14}$$

where ρ_{ris} is the density of material in the riser. Combining the above four equations, yields a cubic in F_{rgc}:

$$a{F_{rgc}}^3 + b{F_{rgc}}^2 + cF_{rgc} + d = 0 \tag{A.15}$$

where:

$$a = \frac{31.1 \times 10^{-3}}{2} \frac{N_{rgc}}{{A_{rgc}}^2 \rho_c \cdot \rho_{part}} \tag{A.16}$$

$$b = a \cdot \rho_{part} \frac{F_3 + F_4}{\rho_v} + \frac{L_{rgc} \cdot f_{rgc}}{{A_{rgc}}^2 \rho_c \cdot \rho_{part}} \tag{A.17}$$

$$c = \frac{L_{rgc} \cdot f_{rgc}}{{A_{rgc}}^2 \rho_c} \frac{F_3 + F_4}{\rho_v} - \frac{144(P_6 - P_4)}{\rho_{part}} + h_{ris} - \rho_c \frac{(z_{bed} + h_{sp} - z_{sp}) + (E_{tap} - E_{oil})}{\rho_{part}} \tag{A.18}$$

$$d = h_{ris}(F_3+F_4) - 144(P_6-P_4)\frac{F_3 + F_4}{\rho_v} - \rho_c \left[(z_{bed} + h_{sp} - z_{sp}) + (E_{tap} - E_{oil})\right] \frac{F_3 + F_4}{\rho_v} \tag{A.19}$$

The cubic equation has to be solved for F_{rgc}. Similar equations are derived for the spent catalyst U-bend. However, in this case the equation is a quadratic and the solution for F_{sc} can be derived explicitly.

$$F_{sc} = \Delta P_{sc} \left[\frac{{A_{sc}}^2 \rho_c}{L_{sc} \cdot f_{sc}}\right] \tag{A.20}$$

The pressure drop across the spent catalyst U-bend is given by:

$$\Delta P_{sc} = 144(P_4 - P_6) - (z_{bed} - z_{lp})\rho_{c,dense} - \rho_{lift} \cdot h_{lift} + \frac{W_{str}}{A_{str}} + (E_{str} - E_{lift})\rho_c - \frac{31.1 \times 10^{-3}}{2} \frac{N_{sc}}{{A_{sc}}^2 \rho_c} {F_{sc}}^2 \tag{A.21}$$

These two equations are combined to obtain an expression for F_{sc}:

$$a{F_{sc}}^2 + bF_{sc} + c = 0 \tag{A.22}$$

where:

$$a = \frac{31.1 \times 10^{-3}}{2} \frac{N_{sc}}{{A_{sc}}^2 \rho_c} \tag{A.23}$$

$$b = \frac{L_{sc} \cdot f_{sc}}{{A_{sc}}^2 \rho_c} \tag{A.24}$$

$$c = (z_{bed} - z_{lp})\rho_{c,dense} + h_{lift} \cdot \rho_{lift} - 144(P_4 - P_6) - \frac{W_{str}}{A_{str}} - (E_{str} - E_{lift})\rho_c \tag{A.25}$$

A.4.2 Incorporating the Slide Valve Model

Model C has both slide valves and J-bends in the catalyst circulation lines. The pressure drop across each slide valve is given by :

$$\Delta P_{sv} = \left[\frac{50 F_{cat}}{K A_{sv} \cdot X_{sv}}\right]^2 \frac{1}{\rho_c} \tag{A.26}$$

where:

F_{cat}	- catalyst flow rate (ton/min)
K	- dimensional constant (0.7)
A_{sv}	- open area of slide valve (213 in^2)
X_{sv}	- fractional opening of slide valve
ρ_c	- settled catalyst density (45 lb/ft^3)

The pressure drop across each J-bend is given by:

$$\Delta P_{elb} = \frac{1}{2} N \rho_c v^2 \tag{A.27}$$

where:

N	- # of velocity heads (20)
ρ_c	- settled catalyst density (45 lb/ft^3)
v	- velocity through J-bend (ft/s)

The pressure drop across the regenerated catalyst line is therefore given by:

$$\Delta P_{rgc} = 144(P_6 - P_{rb}) + \rho_c(z_{bed} + h_{sp} - z_{sp}) + (E_{tap} - E_{oil})\rho_c - \Delta P_{sv,rgc} - \Delta P_{elb,rgc} \quad \text{(A.28)}$$

The rest of the development is exactly the same as for Model B above. Once again, a cubic equation will have to be solved to determine F_{rgc} for model C:

$$\hat{a}{F_{rgc}}^3 + b{F_{rgc}}^2 + cF_{rgc} + d = 0 \quad \text{(A.29)}$$

where:

$$\hat{a} = \left(\frac{31.1 \times 10^{-3}}{2} \frac{N_{rgc}}{{A_{rgc}}^2} + 144 \cdot \left[\frac{50 \times \frac{60}{2000}}{KA_{sv,rgc} \cdot X_{sv,rgc}} \right]^2 \right) \frac{1}{\rho_c \cdot \rho_{part}} \quad \text{(A.30)}$$

b,c and d are the same as for model B. The pressure drop across the spent catalyst line is given by:

$$\Delta P_{sc} = 144(P_4 - P_6) - (z_{bed} - z_{lp})\rho_{c,dense} - \rho_{lift} \cdot h_{lift} + \frac{W_{str}}{A_{str}} + (E_{str} - E_{lift})\rho_c - \Delta P_{sv,sc} - \Delta P_{elb,sc} \quad \text{(A.31)}$$

As in model B, a quadratic equation has to be solved for F_{sc}:

$$\hat{a}{F_{sc}}^2 + bF_{sc} + c = 0 \quad \text{(A.32)}$$

where:

$$\hat{a} = \left(\frac{31.1 \times 10^{-3}}{2} \frac{N_{sc}}{{A_{sc}}^2} + 144 \cdot \left[\frac{50 \times \frac{60}{2000}}{KA_{sv,sc} \cdot X_{sv,sc}} \right]^2 \right) \frac{1}{\rho_c} \quad \text{(A.33)}$$

b and c are the same as for model B.

Appendix B Flue Gas Temperature Behavior over PC Operating Range

Afterburning in the regenerator cyclones has been reported by various authors (Avidan and Shinnar 1990, Upson et al. 1993, Arbel et al. 1995) amongst others. Afterburning refers to the spontaneous, free–radical, combustion of CO to CO_2 in the homogeneous phase. It is reported in (Avidan and Shinnar 1990), and quantified in (Upson et al. 1993) that the presence of catalyst particles inhibits the rate of this free radical reaction. Therefore, when the catalyst particles are removed in the regenerator cyclone, the flue gas stream can spontaneously ignite, as long as both CO and O_2 are present. It is important to note that this spontaneous combustion in itself is not detrimental. However, if there is an *appreciable quantity* of both CO and O_2, the enthalpy release due to combustion will be large, and since the flue gas has a low heat capacity, the temperature can rise significantly. This will lead to possibly large increases in the cyclone temperature, leading to possible damage. Thus excessive cyclone temperatures are of concern only when there is significant quantities of *both* CO and O_2 in the regenerator dilute phase. It is therefore important to investigate under which conditions such a situation can occur.

B.0.1 Rate Expression for $CO \rightarrow CO_2$ reaction

Both (Arbel et al. 1995) and (McFarlane et al. 1993) provide Arrhenius dependence rate parameters for the homogeneous phase reaction:

$$CO + \frac{1}{2}O_2 \xrightarrow{k_h} CO_2 \tag{B.1}$$

However, in both cases, the rate expressions describe the rate of reaction *in the presence of catalyst.* As noted above, the presence of catalyst inhibits the combustion reaction. We develop the rate expressions and equations describing the homogeneous

phase combustion without catalyst based on (Arbel et al. 1995). Since no catalyst is present in the cyclones, and assuming perfect mixing, the following equations describing the O_2 flow rate and CO flow rate out of the cyclones, based on the inlet conditions are obtained from (Arbel et al. 1995)

$$\begin{aligned} f_{O_2} &= f_{O_2,in} - V_{cyc}\left[\frac{1}{2}k_h\frac{f_{O_2}}{f_{tot}}\frac{f_{CO}}{f_{tot}}P_{rgn}^2\right] \\ f_{CO} &= f_{CO,in} + V_{cyc}\left[k_h\frac{f_{O_2}}{f_{tot}}\frac{f_{CO}}{f_{tot}}P_{rgn}^2\right] \end{aligned} \tag{B.2}$$

Note that these two expressions are obtained as a special case of the more general derivations for f_{O_2} and f_{CO} discussed in detail in Chapter 2, Section 2.8.1, taking into account that no catalyst particles are present in the cyclone. These two equations can be solved numerically to determine f_{O_2} and f_{CO} at the exit of the cyclones. A numerical solution is required as f_{tot} contains f_{CO} and f_{O_2}. The temperature dependence of k_h is affected by whether catalyst is present or not:

1. In presence of catalyst (dense bed reaction), (Arbel et al. 1995) give:

$$k_h = \exp\left[25.71 - \frac{6.4\times10^4}{T_{cyc}}\right] \tag{B.3}$$

   We note here that the equivalent rate expression used in the McFarlane et al. (1993) model yields very similar rates as well as conversions for the temperature ranges studied. This is shown in Figure B.2 where the flue gas exit temperature predicted using the model by McFarlane et al. (1993) matches closely the exit temperature predicted by the Arbel et al. (1995) model.

2. In absence of catalyst (reaction the cyclones) neither the McFarlane et al. (1993) model nor the Arbel et al. (1995) model provide a rate expression for the homogeneous $CO \rightarrow CO_2$ combustion in the gas phase. Thus, the Arrhenius parameters for the Arbel et al. (1995) model were fitted to data provided by (Upson et al. 1993). The entire list of conditions under which these data were

obtained is not reported in that publication, and a number of assumptions have been made in order to obtain the required parameters. In particular,

- reaction occurs in a CSTR of volume $V_{cyc} = 500ft^3$
- total gas input flow rate is 2 lbmol/s

From Equation B.2 if X=conversion of CO, we get for k_h:

$$k_h = \exp\left[p_0 - \frac{p_1}{T_{cyc}}\right] = \frac{\frac{f_{CO,in}X}{V_{cyc}}}{P_{rgn}^2\left[\frac{f_{O_2,in}}{f_{tot}}\frac{f_{CO,in}}{F_{tot}}\right]} \tag{B.4}$$

Figure B.1 indicates the data points obtained from (Upson et al. 1993) and the predicted values of CO conversion using the estimated parameters.

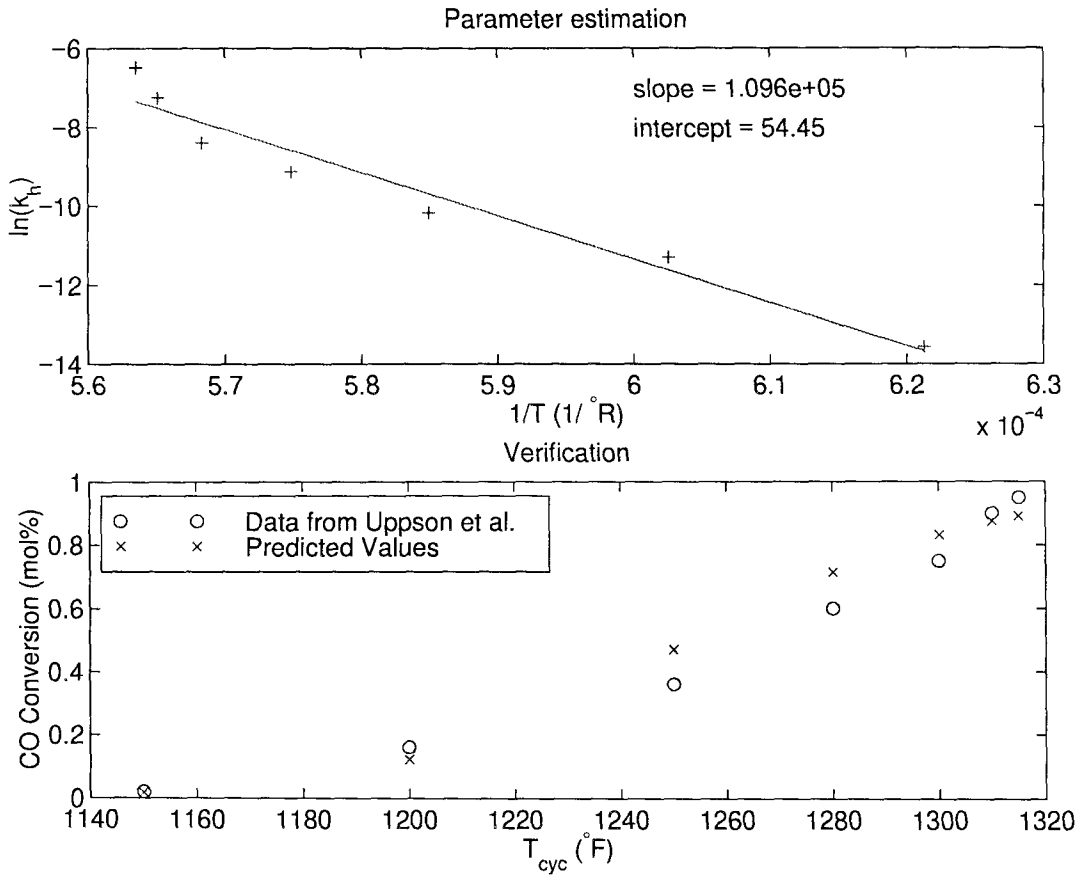

Figure B.1: Estimation of rate expression parameters from data provided by Upson *et al.*,

The following rate expression for the homogeneous phase $CO \rightarrow CO_2$ in the absence of catalyst particles is therefore obtained:

$$k_h = \exp\left[54.45 - \frac{10.96 \times 10^4}{T_{cyc}}\right] \tag{B.5}$$

Using this rate expression, the flue gas temperature at the cyclone outlet is predicted for various conditions, and plotted in Figure B.2.

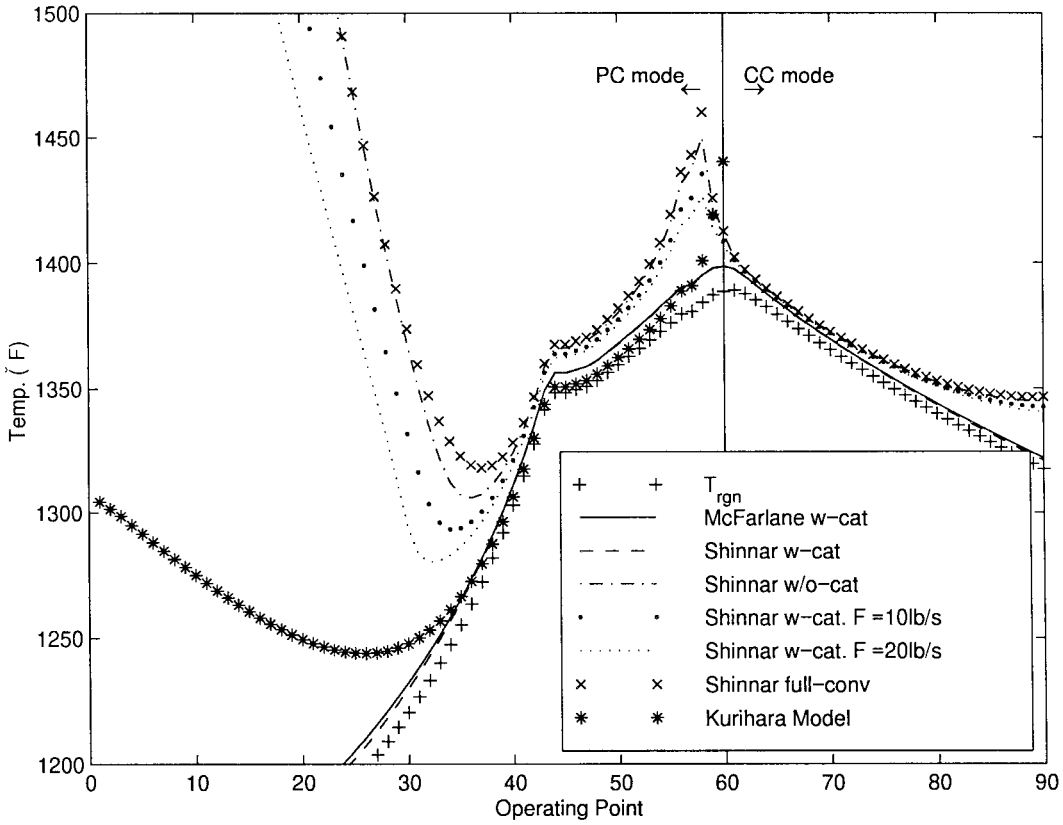

Figure B.2: Regenerator temperature and cyclone exit temperature over entire feasible operating range. $F_q = 1, T_{ris} = 1000°F$.

Note the following from Figure B.2:

- As mentioned before, the prediction of cyclone exit temperature using the rate expression from McFarlane et al. (1993) and the Arbel et al. (1995) rate ex-

pressions are very close. The two models therefore are consistent, at least in describing the homogeneous phase $CO \rightarrow CO_2$ combustion in the presence of catalyst.

- The temperature rise between the regenerator temperature and the cyclone exit gas temperature is significant only for low regenerator temperatures ($T_{rgn} < 1300°F$. Under these conditions, the rate of coke and CO burning in the dense bed is low, and there is significant quantities of both O_2 and CO in the cyclone (Figure B.3). Therefore, on removal of the catalyst, there is a high possibility of the flue gas igniting, and thereby raising the cyclone temperatures to unacceptable levels.

- (Hovd and Skogestad 1993, Ljungquist 1990) have adopted a simple empirical model describing the flue gas temperature as:

$$T_{fg} = T_{rgn} + 5555 \times \frac{f_{O_2,d}}{f_{tot,d}} \tag{B.6}$$

  Here, T_{fg} and T_{rgn} are in Kelvin (K) and $f_{i,d}$ indicates flow rate of component i in the regenerator dense bed in mol/s. Note that:

  - this empirical model is only valid in PC mode, where O_2 in the dense bed is limiting. In CC mode operation, this model would predict a large difference $T_{rgn} - T_{fg}$, which is not the case in practice since there is only ppm levels of CO in the cyclone, and hence negligible combustion.
  - T_{fg} predicted by this model also goes through a minimum (Figure B.2) although at a lower regenerator temperature than predicted by the Equation B.5.

- While there might be a significant difference between the cyclone flue gas temperature and the regenerator temperature, this should not necessarily cause concern if the regenerator temperatures are low. If the cyclones have a high

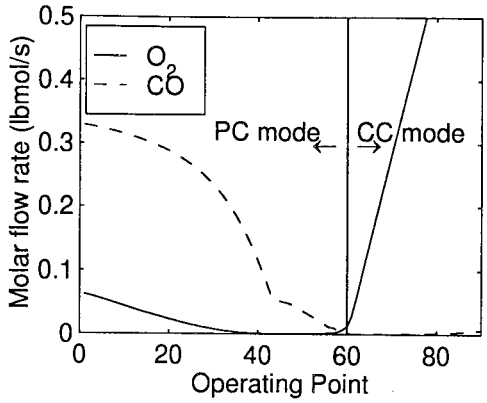

Figure B.3: Molar flow rate of O_2 and CO over the range of operating conditions considered. $F_q = 1, T_{ris} = 1000°F$.

enough temperature rating, the actual cyclone temperature might not be high enough to cause damage.

- It appears from the literature that operators often try to deliberately achieve a large temperature difference between the regenerator and cyclones, as it is thought to positively impact the overall FCC operation (Arbel et al. 1996). However, we do not find any justification for this practice from this analysis. In particular, it appears that a *small* difference in $T_{fg} - T_{rgn}$ is actually desirable since this indicates that essentially all the CO is combusted to CO_2 in the regenerator dense bed itself, indicating higher regeneration efficiencies in the regenerator! Moreover, from the physical setup of the cyclones downstream of the regenerator dense bed, it is unlikely that changes in the cyclone will propagate backwards to the regenerator, and hence affect the FCC operation.

- Two different rates of fines flow (10lb/s and 20lb/s) in the cyclone are also examined in Figure B.2. The heat capacity is assumed to be the same as for the catalyst particles. Because some of the enthalpy of combustion will be transferred to the fines, the increase in T_{cyc} should be less than if no fines are present. Moreover, the higher the rates of fines exiting the regenerator flue gas, the lower is the increase in T_{cyc}. This analysis indicates that the presence

of fines does not significantly aid in maintaining T_{cyc} close to T_{rgn}. Note that the fines flow rates considered are higher than the losses experienced in even the older FCCs (1950s), which were between 0.55lb/s and 1.5lb/s (Evans and Quinn 1993), and significantly higher than the fines loss rates typical in many present day units of $\leq 0.01 lb/s$.

- Afterburning in the cyclones appears to be of little concern for modern FCCUs that typically operate at higher regenerator temperatures $T_{rgn} > 1250°F$. This analysis suggests that older units where the regenerator temperatures were significantly lower, afterburning could have been a severe problem.

- It is assumed in the Arbel et al. (1995) model that there is complete (stoichiometric) conversion of the limiting component (either CO of O_2) in the cyclones. This simple assumption allows one to quickly calculate the flue gas exit temperature without requiring the kinetic parameters for the $CO \rightarrow CO_2$ combustion reaction. Figure B.2 shows that this assumption is in fact quite accurate in describing the combustion phenomenon in the cyclone.

From this analysis, we can conclude that:

- The temperature difference $\Delta T = T_{fg} - T_{rgn}$ is only significant for the "low" regenerator temperatures in PC mode operation - typically the practice in the past. However, at the higher regenerator temperatures currently common in modern FCC units, essentially all the $CO \rightarrow CO_2$ conversion occurs in the regenerator dense bed, and ΔT is low.

- All the models studied indicate that T_{fg} goes through a minimum for some regenerator temperature. The actual minimum T_{fg}, and the T_{rgn} at which it will occur is unit specific, and probably not accurately known.

Bibliography

Arbel, A., Huang, Z. P., Rinard, I. H., Shinnar, R. and Sapre, A. V.: 1995, Dynamic and Control of Fluidized Catalytic Crackers. 1. Modeling of the Current Generation of FCC's, *Ind. Eng. Chem. Res.* **34**(4), 1228 – 1243.

Arbel, A., Rinard, I. H. and Shinnar, R.: 1997, Dynamics and Control of Fluidized Catalytic Crackers. 4. The Impact of Design on Partial Control, *Technical report*, Chemical Engineering, City College of New York.

Arbel, A., Rinard, I. and Shinnar, R.: 1996, Dynamics and Control of fluidized Catalytic Crackers. 3. Designing the Control-System - Choice of Manipulated and Measured Variables for Partial Control, *Ind. Eng. Chem. Res.* **35**(7), 2215–2233.

Avidan, A. A. and Shinnar, R.: 1990, Development of Catalytic Cracking Technology. A Lesson in Chemical Reactor Design, *Ind. Eng. Chem. Res.* **29**, 931–942.

Balas, G. J., Doyle, J. C., Glover, K., Packard, A. K. and Smith, R. S. R.: 1991, *μ-Analysis and Synthesis Toolbox (μ-Tools) : MATLAB Functions for the Analysis and Design of Robust Control Systems*, The Mathworks, Inc., Natick, MA. Computer Software.

Braatz, R. D., Lee, J. H. and Morari, M.: 1996, Screening Plant Designs and Control-Structures for Uncertain Systems, *Comp. and Chem. Eng.* **20**(4), 463–468.

Chiu, M.-S. and Arkun, Y.: 1992, A Methodology for Sequential Design of Robust Decentralized Control Systems, *Automatica* **28**(5), 997–1001.

DeLasa, H. I., Errazu, A. F., Barreiro, F. and Solioz, S.: 1981, Analysis of Fluidized Bed Catalytic Cracking Regenerator Models in an Industrial Scale Unit, *Canadian Journal of Chemical Engineering* **59**, 549 – 553.

DeLasa, H. I. and Grace, J. R.: 1979, The Influence of the Freeboard Region in a Fluidized Bed Catalytic Cracking Regenerator, *AIChE Journal* **25**, 984 – 991.

Denn, M.: 1986, *Process Modeling*, Longman, New York.

Doedel, E. J.: 1986, *AUTO: Software for Continuation and Bifurcation Problems in Ordinary Differential Equations*, Concordia University: Montreal, Canada.

Doyle, J. C.: 1982, Analysis of Feedback Systems with Structured Uncertainties, *IEE Proceedings Part D* **129**, 242–250.

Edwards, W. and Kim, H.: 1988, Multiple Steady–States in FCC Unit Operations, *Chem. Eng. Sci.* **43**(8), 1825–1830.

Elnashaie, S. S. E. H. and Elshishini, S. S.: 1992, Digital Simulation of Industrial Fluid Catalytic Cracking Units - IV. Dynamic Behavior, *Chem. Eng. Sci.* **48**(3), 567–583.

Errazu, A. F., DeLasa, H. I. and Sarti, F.: 1979, A Fluidized Bed Catalytic Cracking Regenerator Model, Grid Effects, *Canadian Journal of Chemical Engineering* **57**, 191–197.

Evans, R. E. and Quinn, G. P.: 1993, Environmental Considerations Affecting FCC, *in* J. S. Magee and M. M. Mitchell Jr. (eds), *Fluid Catalytic Cracking: Science and Technology*, Vol. 76, Elsevier Science Publishers B.V., chapter 15, pp. 563–585.

Falti-Saravelou, O., Vasalos, I. A. and Dimogiorgas, G.: 1991, A Model for Fluidized Bed Simulation - II. Simulation of and Industrial Fluidized Catalytic Cracking Regenerator, *Comp. and Chem. Eng.* **15**(9), 647 – 656.

Felipe, L. I.: 1992, Dynamic Modeling of an Industrial Fluid Catalytic Cracking Unit, *European Symposium on Computer Aided Process Engineering - 1, Escape 1, Elsinore, Denmark*, pp. S139–S148.

Ford, W. D., Reineman, R. C., Vasalos, I. A. and Fahrig, R. J.: 1976, Modeling Catalytic Cracking Regenerators, *National Petroleum Refiners Association Annual Meeting*, National Petroleum Refiners Association.

Grosdidier, P., Mason, A., Aitolahti, A., Heinonen, P. and Vanhamåki, V.: 1993, FCC Unit Reactor-Regenerator Control, *Comp. and Chem. Eng.* **17**(2), 165–179.

Holt, B. R. and Morari, M.: 1985a, Design of Resilient Procesing Plants–VI. The Effect of Right-Half- Plane Zeros on Dynamic Resilience, *Chem. Eng. Sci.* **40**, 59–74.

Holt, B. R. and Morari, M.: 1985b, Design of Resilient Processing Plants - VI. The Effect of Right-Half-Plane Zeros on Dynamic Resilience, *Chem. Eng. Sci.* **40**(1), 59–74.

Hovd, M. and Skogestad, S.: 1993, Procedure for Regulatory Control Structure Selection with Application to the FCC Process, *AIChE Journal* **39**(12), 1938–1953.

Hovd, M. and Skogestad, S.: 1994, Pairing Criteria for Decentralized Control of Unstable Plants, *Ind. Eng. Chem. Res.* **33**, 2134–2139.

Huq, I. and Morari, M.: 1997a, Control Structure Selection for the Fluid Catalytic Cracking Process, *Technical report*, Automatic Control Lab, The Swiss Federal Institute of Technology.

Huq, I. and Morari, M.: 1997b, Decentralized Control of the Fluid Catalytic Cracking Process, *Technical report*, Automatic Control Lab, The Swiss Federal Institute of Technology.

Huq, I., Morari, M. and Sorensen, R. C.: 1995, Modifications to Model IV Fluid Catalytic Cracking Units to Improve Dynamic Performance, *AIChE Journal* **41**(6), 1481–1499.

Kurihara, H.: 1967, *Optimal Control of Fluid Catalytic Cracking Processes*, Ph.D. thesis, MIT.

Lee, E. and Groves Jr., F. R.: 1985, Mathematical Modeling of the Fluidized Bed Catalytic Cracking Plant, *Trans. Soc. Comp. Simul.* **2**(3), 219–236.

Lee, J., Braatz, R. D., Morari, M. and Packard, A.: 1995, Screening Tools for Robust-Control Structure Selection, *Automatica* **31**(2), 229–235.

Lee, W. and Weekman, V. W. J.: 1976, Advanced Control Practice in the Chemical Process Industry: A View from Industry, *AIChE Journal* **22**(1), 27–38.

Ljungquist, D.: 1990, *Online Estimation in Nonlinear State-space Models with Application to Catalytic Cracking*, Ph.D. thesis, Norwegian Institute of Technology.

Lundström, P., Skogestad, S. and Wang, Z.: 1991, Performance Weight Selection for H-infinity and μ-Control Methods, *Transanctions of the Institute of Measurement and Control* **13**(5), 241–252.

McFarlane, R. C., Reineman, R. C., Bartee, J. F. and Georgakis, C.: 1993, Dynamic Simulator for a Model IV Fluid Catalytic Cracking Unit, *Comp. and Chem. Eng.* **17**(3), 275–300.

Monge, J. J. and Georgakis, C.: 1987, Multivariable Control of Catalytic Cracking Processes, *Chem. Eng. Communications* **61**(1-6), 197–225.

Morari, M. and Zafiriou, E.: 1989, *Robust Process Control*, Prentice-Hall, Inc., Englewood Cliffs, N.J.

Morari, M., Zafiriou, E. and Holt, B. R.: 1987, Design of Resilient Processing Plants–X. Characterization of the Effect of RHP Zeros, *Chem. Eng. Sci.* **42**(10), 2425–2428.

Perry, R. H. and Green, D. W.: 1984, *Perry's Chemical Engineers' Handbook*, 6 edn, McGraw-Hill.

Ray, W. H.: 1981, *Advanced Process Control*, McGraw-Hill Chemical Engineering Series, 1 edn, McGraw-Hill Book Company.

Sadeghbeigi, R.: 1995, *Fluid Catalytic Cracking Handbook*, Gulf Publishing Company.

Shah, Y. T., Huling, G. P., Paraskos, J. A. and McKinney, J. D.: 1977, A Kinematic Model for an Adiabatic Transfer Line Catalytic Cracking Reactor, *Ind. Eng. Chem. Process Des. Dev.* **16**, 89–94.

Shinnar, R.: 1997, Personal Communication.

Skogestad, S. and Hovd, M.: 1990, Use of Frequency Dependent RGA for Control Structure Selection, *Proceedings of the American Control Conference, San Diego, CA.*

Skogestad, S. and Lundström, P.: 1990, Mu-Optimal LV-control of Distillation Columns, *Comp. and Chem. Eng.* **14**(4/5), 401.

Skogestad, S. and Morari, M.: 1987, Effect of Disturbance Directions on Closed Loop Performance, *Ind. Eng. Chem. Res.* **26**(10), 2029–2035.

Skogestad, S. and Morari, M.: 1989, Robust Performance of Decentralized Control Systems by Independent Designs, *Automatica* **25**(1), 119–125.

Skogestad, S., Morari, M. and Doyle, J. C.: 1988, Robust Control of Ill-Conditioned Plants: High Purity Distillation, *IEEE Trans. Aut. Control* **33**(12), 1092–1105.

Skogestad, S. and Postlethwaite, I.: 1996, *Multivariable Feedback Control*, John Wiley & Sons.

Sorensen, R. C.: 1993, Chevron Research and Technology Company, Richmond ,CA. *Personal Communications.*

Upson, L., Hemler, C. L. and Lomas, D. A.: 1993, Unit Design and Operational Control: Impact on Product Yields and Product Quality., *in* J. S. Magee and M. M. Mitchell Jr. (eds), *Fluid Catalytic Cracking: Science and Technology*, Vol. 76, Elsevier Science Publishers B.V., chapter 11, pp. 385–440.

Weisz, P. B.: 1966, Combustion of Carbonaceous Deposits within Porous Catalyst Particles III. The CO_2/CO Product Ratio, *Journal of Catalysis* **6**, 425–430.

Weisz, P. B. and Goodwin, R. D.: 1966, Combustion of Carbonaceous Deposits within Porous Catalyst Particles II. Intrinsic Burning Rate, *Journal of Catalysis* **6**, 227–236.

Wrench, R. E. and Glasgow, P.: 1992, FCC Hardware Options for the Modern Cat Cracker, *Ind. Eng. Chem. Process Des. Dev.* **291**(88), 1–8.

Zhou, K., Doyle, J. C. and Glover, K.: 1996, *Robust and Optimal Control*, Prentice Hall Inc., New Jersey.